THE UNIVERSITY OF QUEENSLAND

AUSTRALIA

Design, Synthesis and Evaluation of Peptides and Peptidomimetics Inhibiting the Bacterial DsbA-DsbB Interaction

Wilko Duprez

MBiolStruct, MBiotech

A thesis submitted for the degree of Doctor of Philosophy at

The University of Queensland in 2014

Institute for Molecular Bioscience

Abstract

The rapid development and dissemination of antibiotic resistance in pathogenic bacteria requires new strategies and new structural scaffolds of antimicrobial compounds to be investigated. A developing trend targets virulence factors rather than pathways essential for survival in an effort to neutralize pathogens while minimizing the risk of resistance. The thesis focuses on the design of new molecules from peptides to peptidomimetics aimed at disrupting the bacterial periplasmic oxidative system, a new antivirulence target.

This thesis initially describes in chapter I the recent emergence of peptidomimetics in antimicrobial treatments aimed at well-known mechanisms as well as novel targets. Peptidomimetics may be particularly efficient for disrupting protein-protein interactions and have been successful for instance in preventing post-translational modifications or the formation of pili machinery. The thesis also highlights the mechanism and context of the interaction between DsbA and DsbB, both primary factors in the periplasmic oxidative system of gram-negative bacteria and the target proteins of this PhD.

Developing inhibitors requires a solid screening pipeline of biophysical assays to measure binding parameters such as affinity, thermodynamics and kinetics. Chapter II highlights the building and optimization of such a pipeline by evaluating differential scanning fluorimetry, isothermal titration calorimetry, surface plasmon resonance, substrate oxidation assay and crystallography in order to characterize the designed peptide scaffolds.

Chapter III focuses on the structure-activity relationship studies of 31 manually synthesized peptide sequences screened through this pipeline. Based on peptide length scouting, alanine scanning and rational substitution of specific residues, a final heptameric peptide was found to bind *Escherichia coli* DsbA with a *K*d of 2.9 ± 0.3 µM. Moreover, the data suggest a probable disulfide bond formation between peptide and DsbA essential to the binding interface, while cysteine-free peptides present very weak affinity towards EcDsbA. This chapter generated a manuscript submitted to the *Journal of Medicinal Chemistry.*

In a slightly different strategy, Chapter IV evaluates this best heptamer peptide sequence against a newly characterized *Proteus Mirabilis* DsbA, a structurally related protein (59% similarity with *E. coli* DsbA) showing promise for co-crystallization. With the peptide showing the same affinity against wild type *E. coli* and *P. mirabilis* DsbA, a high-resolution (1.6 Å) co-crystal structure of the heptamer peptide bound to a cysteine mutant of *P. mirabilis* DsbA was solved. This structure shows the peptide binding to the *P. mirabilis* DsbA active site in a similar fashion to the native *E. coli* DsbA/DsbB interaction and differently from *E. coli* DsbA substrates. In-depth analysis of the high-resolution structure identifies two binding anchors, a H-bond-rich region and a hydrophobic pocket, which can be optimized for tighter affinities. This chapter generated a manuscript submitted to the *Journal of Biological Chemistry*.

Based on the peptide structure-activity relationship studies and the DsbA peptide complex structure reported in the two previous chapters, Chapter V describes the initial steps in designing novel peptidomimetic scaffolds. These molecules include cyclic peptides, irreversible peptide binders and a tripeptide scaffold designed to target a specific hydrophobic groove on both *E. coli* and *P. mirabilis* DsbA surface. The tripeptide scaffold was characterized through the screening pipeline, including an intensive co-crystallization optimization.

In summary, this thesis has employed a variety of assays and techniques to take a significant step towards the development of the first inhibitors targeting the oxidative folding system essential for bacterial virulence. Formation of a disulfide bond proved to be critical for ligand binding, and thus intense biochemical and structural investigation was executed to develop a potent inhibitory scaffold. This has lead to the characterization of the very first non-covalent peptide-DsbA crystal structure. The outcome of this research expands our understanding of the DsbA-DsbB interaction in different pathogenic bacteria and provides a peptide scaffold with high specificity as well as the optimization steps to be undertaken towards a potent and specific antivirulent peptidomimetic.

Declaration by author

This thesis is composed of my original work, and contains no material previously published or written by another person except where due reference has been made in the text. I have clearly stated the contribution by others to jointly-authored works that I have included in my thesis.

I have clearly stated the contribution of others to my thesis as a whole, including statistical assistance, survey design, data analysis, significant technical procedures, professional editorial advice, and any other original research work used or reported in my thesis. The content of my thesis is the result of work I have carried out since the commencement of my research higher degree candidature and does not include a substantial part of work that has been submitted to qualify for the award of any other degree or diploma in any university or other tertiary institution. I have clearly stated which parts of my thesis, if any, have been submitted to qualify for another award.

I acknowledge that an electronic copy of my thesis must be lodged with the University Library and, subject to the General Award Rules of The University of Queensland, immediately made available for research and study in accordance with the *Copyright Act 1968*.

I acknowledge that copyright of all material contained in my thesis resides with the copyright holder(s) of that material. Where appropriate I have obtained copyright permission from the copyright holder to reproduce material in this thesis.

Publications during candidature

1) **Emergence of peptidomimetics as antibacterial drug candidates**, W. Duprez, R. Reid, JL. Martin, DP. Fairlie.
In preparation. This review will be generated from Chapter I.
Proposed journal(s): European Journal of medicinal chemistry, Bioorganic and Medicinal Chemsitry, Trends in Molecular Medicine.

2) **Peptide inhibitors of the *Escherichia coli* DsbA/DsbB interface,** W. Duprez, M. Halili, F. Lindhal, R. Reid, DP Fairlie, JL Martin.
Manuscript submitted to the Journal of Medicinal Chemistry.

3) **Crystal Structure of the Dithiol Oxidase DsbA Enzyme From *Proteus Mirabilis* Bound Non-Covalently to an Active Site Peptide Ligand,** F. Kurth[#], W. Duprez[#], L. Premkumar, M. Schembri, DP. Fairlie, and JL. Martin.
[#] These authors contributed equally to this work.
Manuscript submitted to the Journal of Biological Chemistry

4) **Evaluation of an initial peptidomimetic scaffold targeting the *Escherichia coli* DsbA hydrophobic groove,** W. Duprez[#], P. Bachu[#], R. McMahon, S. Tay, M. Stoermer, DP Fairlie, JL Martin.
[#] These authors contributed equally to this work.
In preparation. This manuscript will be generated from Chapter V.
Proposed journal(s): PloS One.

5) **Comparative sequence, structure and redox analyses of Klebsiella pneumoniae DsbA show that anti-virulence target DsbA enzymes fall into different classes,** F. Kurth, K. Rimmer, L. Premkumar, B. Mohanty, W. Duprez, M. Halili, S. Shouldice, B. Heras, DP. Fairlie, MJ. Scanlon and JL. Martin. *PLoS One* (2013) Nov 14;8(11):e80210. doi:10.1371/journal.pone.0080210. eCollection 2013. Publication is available is the appendix A.

6) **Rv2969c, essential for optimal growth in Mycobacterium tuberculosis, is a DsbA-like enzyme that interacts with VKOR-derived peptides and has atypical features of DsbA-like disulfide oxidases**, L. Premkumar, B. Heras, W. Duprez, P. Walden, M. Halili, F. Kurth, DP. Fairlie, JL. Martin. *Acta Cryst*. (2013) D69, doi:10.1107/S0907444913017800. Publication is available is the appendix B.

7) **Membrane curvature protein exhibits interdomain flexibility and binds a small GTPase,** GJ.King, J. Stöckli, SH. Hu, B. Winnen, WG. Duprez, CC. Meoli, JR Junutula, RJ Jarrott, DE James, AE Whitten, JL Martin. *J Biol Chem*. 2012 Nov 30;287(49):40996-1006. doi: 10.1074/jbc.M112.349803. Epub 2012 Oct 10.

Two additional publications relevant to the thesis including significant contributions from the author are expected to be submitted in 2014.

Publications included in this thesis

Peptide inhibitors of the *Escherichia coli* DsbA/DsbB interface, W. Duprez, M. Halili, F. Lindhal, R. Reid, DP Fairlie, JL Martin **-** incorporated as Chapter 3.

Contributor	Statement of contribution
Wilko Duprez (Candidate)	Designed experiments (differential scanning fluorimetry, isothermal titration calorimetry) (50%) Performed experiments (95%) Wrote the paper (100%)
Dr Maria Halili	Designed experiments (substrate oxidation assay) (25%) Performed experiments (5%) Edited paper (10%)
Dr Fredrik Lindahl	Designed experiments (peptide synthesis) (25%) Edited paper (10%)
Dr Robert Reid	Edited paper (10%)
Prof. David P Fairlie	Edited paper (20%)
Prof. JL Martin	Supervising and main editor of the final draft (50%)

Crystal Structure of the Dithiol Oxidase DsbA Enzyme From *Proteus Mirabilis* Bound Non-Covalently to an Active Site Peptide Ligand, F. Kurth[#], W. Duprez[#], L. Premkumar, M. Schembri, DP. Fairlie, and JL. Martin. – incorporated as Chapter 4.

Contributor	Statement of contribution
Wilko Duprez (Candidate)	Peptide synthesis (100%) Peptide binding characterization (100%) Crystallization of PmDsbAC30S – peptide (50 %) Wrote the paper (50%)
Fabian Kurth (co-first author)	Biochemistry of native PmDsbA (100%) Crystallization and structure determination and refinement of native PmDsbA and PmDsbAC30S (100%) Crystallization of PmDsbAC30S – peptide (50 %) Structure determination of PmDsbAC30S-PWATCDS (50%) Wrote the paper (50%)
Dr Lakshmanane Premkumar	Structure determination and refinement of PmDsbAC30S-PWATCDS (50%) Assisted in draft editing (10%)
Prof. Mark Schembri	Assisted in draft editing (10%)
Prof. David P Fairlie	Assisted in draft editing (10%)
Prof. JL Martin	Supervising and main editor of the final draft (70%)

Contributions by others to the thesis

-*Dr Maria Halili*: setting up and optimization of the model substrate oxidation assay and tested one peptide in Chapter 3. Routine expression and purification of protein samples (DsbA and DsbB) for experiments described in chapters 2, 3, 4, and 5. Training and initial supervision of candidate for isothermal titration calorimetry.

-*Dr Fredrik Lindahl*: Training and initial supervision of the candidate in peptide synthesis as described in chapter 2, 3 and 4. Analysis and interpretation of the structure activity relationship data in chapter 3.

-*Mr Fabian Kurth*: optimization of protein purification protocol used in chapter 2, 3 and 5. Crystallization and structure determination of native PmDsbA and PmDsbAC30S mutant, biochemistry of native PmDsbA, crystallization and structure determination of the PmDsbAC30S complex as related in chapter 4.

-*Dr Prabhakar Bachu*: synthesis of non-natural residues and 10 peptidomimetic compounds as described in chapter 5.

-*Mrs Stephanie Tay*: Expression and purification of protein samples (DsbA and DsbB) for experiments described in chapters 2, 3, 4, and 5. Substrate oxidation assay for peptidomimetics in chapter 5.

-*Dr Roisin McMahon*: Differential scanning fluorimetry testing of peptidomimetics in chapter 5.

-*Dr Lakshmanane Premkumar*: training, supervision, troubleshooting and data interpretation in all experiments related to solving crystallographic structures and their analysis as related in chapter 2 and 4.

Statement of parts of the thesis submitted to qualify for the award of another degree

None.

Acknowledgements

First of all, I would like to thank Prof. Jenny Martin for initially offering me this position as part of her ARC Laureate Fellowship and for being an understanding and supportive supervisor all along this PhD. Thank you so much for your guidance and all your advice – it felt rewarding and exciting to do my PhD under your leadership.

Second, I would like to be particularly thanks Dr Amanda Carozzi, for her incredible dedication to the success of the PhD students from the institute.

For non-academic support, the first people I would never be able to thank enough are my parents for moral, financial and in general amazing support. So, to my mother, who foresaw my life accomplishment as *Doctor australianii* :

And to my father, whose help was priceless in the preparation of my most memorable speech in my scientific career so far.

To Jean-Yves, my travel companion, my comrade in arms, my brother in misfortune, for the most thrilling intellectual or adventurous challenges past and to come, and for sharing the most intense moments of my life for the past five years, from Mongolia to academic challenges. Your PhD is going to be alright.

To Fabian, my fellow lab member, for significantly improving my PhD inside and outside the lab. I'm glad to count you as a close friend.

To Alison, for her support, her patience, her understanding and her everyday sacrifices.

To Kylie Lovejoy, to whom I am not sure I will ever be able to return the numerous favors she did for me – among many others providing me a place to live in the difficult times, introducing me to amazing people, and in general to be Brisbane's unsurpassed R'n'R queen.

And finally, to the countless Brisbane bands that provided the live soundtrack of my PhD. Thanks for allowing me to spend my joy and frustrations alike on the dancefloor on the sound of true and heartfelt rock'n'roll.

Keywords

Oxidative folding, antivirulence, DsbA, DsbB, peptide, peptidomimetic, inhibitor.

Australian and New Zealand Standard Research Classifications (ANZSRC)

ANZSRC code: 030403 Characterisation of Biological Macromolecules 60%
ANZSRC code: 060112 Structural Biology (incl. Macromolecular Modelling) 20%
ANZSRC code: 030406 Proteins and Peptides 20%

Fields of Research (FoR) Classification

FoR code: 0304 Medicinal and Biomolecular Chemistry 80%
FoR code: 0601 Biochemistry and Cell Biology 20%

Table of contents

List of Figures

CHAPTER I

CHAPTER II

CHAPTER III

CHAPTER IV

CHAPTER V

CHAPTER VI

List of tables

CHAPTER I

CHAPTER II

CHAPTER III

CHAPTER IV

Abbreviations

AA	Amino acid
AMP	Antimicrobial peptide
BOP	Benzotriazol-1-yloxy-tris(dimethylamino)phosphonium hexafluorophosphate
CD	Circular dichroism
CDC	Center for Disease Control and prevention
DCM	Dichloromethane
DOTA	1,4,7,10-Tetraazacyclododecane-1,4,7,10-tetraacetic acid
DIPEA	Di-isopropylethylamine
DMF	Dimethyl formamide
DMSO	Dimethyl sulfoxide
DNA	Deoxyribonucleic acid
DsbA	Disulfide bond forming protein A
DsbB	Disulfide bond forming protein B
DSF	Differential scanning fluorimetry
DTT	Dithiothreitol
ECDC	European Center for Disease prevention and Control
EcDsbA	*Escherichia coli* Disulfide bond forming protein A
EcDsbB	*Escherichia coli* Disulfide bond forming protein B
EDC	1-Ethyl-3-(3-dimethylaminopropyl)carbodiimide
ELISA	Enzyme-linked imunosorbent assay
EMEA	Europan Medicine Agency
ESBL	Extended spectrum β-lactamase
Fmoc	Fluorenylmethyloxycarbonyl
HbTU	O-Benzotriazole-N,N,N',N'-tetramethyl-uronium-hexafluoro-phosphate
HPLC	High performance liquid chromatography
IDSA	Infectious Disease Society of America
MBHA	p-Methylbenzhydrylamine
MCA	Methyl coumarin
MDR	Multi drug resistant
MIC	Minimal inhibitory concentration
mRNA	messenger Ribonucleic acid
MR	Molecular replacement
Mtt	4-Methyltrityl
MRSA	Multidrug resistant *Staphylococcus Aureus*

NDM-1	New Delhi Metallo-ß-lactamase
NHS	N-Hydroxysuccinimide
NMR	Nuclear magnetic resonance
OAK	Oligoacyllysine
PDF	Protein deformylase
PDR	Pan Drug Resistant
PEG	Polyethylene glycol
PEM	Protein Epitope Mimetic
PmDsbA	*Proteus mirabilis* Disulfide Bond forming protein A
PPI	Protein-Protein Interaction
PyBOP	Otriazol-1-yl-oxytripyrrolidinophosphonium hexafluorophosphate
RT-PCR	Reverse Transcription Polymerase Chain Reaction
RU	Response Unit
SAR	Structure-Activity Relationship
SPPS	Solid Phase Peptide Synthesis
SPR	Surface Plasmon Resonance
TEV	Tobacco Etch Virus
TFA	Trifluoroacetic acid
TRX	Thioredoxin
TSA	Thermal Shift Assay
USA	United States of America
UTI	Urinary Tract Infection
XDR	eXtremely Drug Resistant

CHAPTER I

General Introduction

I.1 Current state of the antibiotic pipeline

The emergence of bacterial strains presenting resistance to most antibiotic treatments, including the most recently approved on the market, is now a widespread concern and identified as one of the major healthcare issues of the next decade (The Bacterial Challenge: time to react, 2010, ECDC/EMEA). The World Health Organization characterized this phenomenon as one of the three greatest threats to human health (*The 10 x '20 Initiative: pursuing a global commitment to develop 10 new antibacterial drugs by 2020*, 2010, IDSA). Antimicrobial resistance has become a major threat to human health across the globe, resulting in ≈25,000 deaths per year in developed regions of the world such as Europe with associated costs of > $2 billion in healthcare expenses and productivity (The Bacterial Challenge: time to react, 2010, ECDC/EMEA). In the United States of America (USA) alone, the Center for Disease Control and Prevention (CDC) reported more than 2 million infections annually by antimicrobial resistant pathogenic strains resulting in ≈25,000 deaths (Antibiotics Resistance Threats in the United States, 2013, 2013).

Antibiotic resistance has been observed and described since the early 1940's, when *Staphylococcus aureus* strains were found to be resistant to penicillin even before its large-scale use as a treatment (Plough, 1945, Miller & Bohnhoff, 1945). This was the starting point of a race between the introduction of new antibacterial drugs and the emergence of drug resistance by pathogenic strains (**Figure 1.1**).

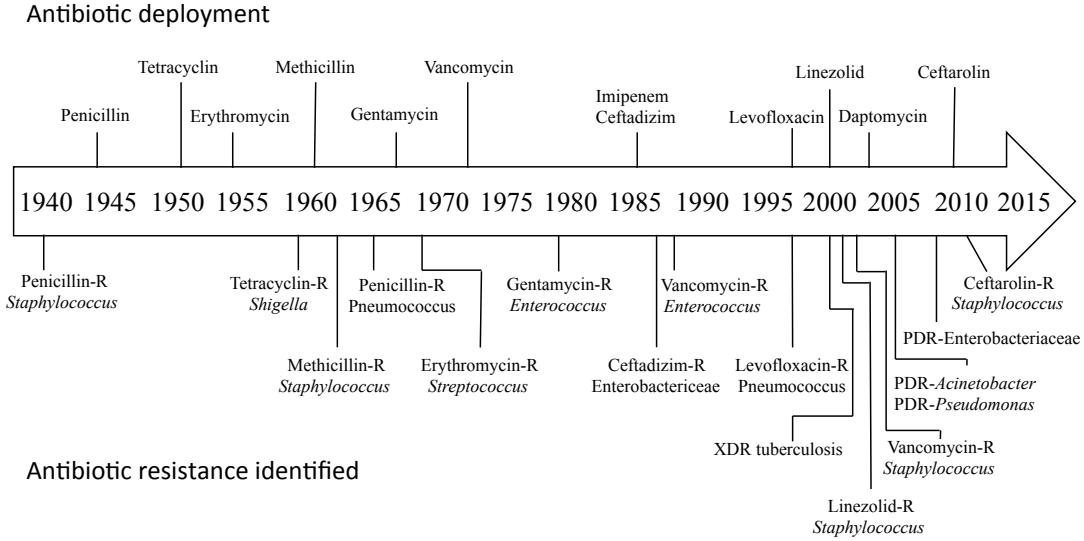

Figure 1.1. ***Timeline of the deployment and appearance of resistance against the major antibiotic classes.*** *XDR = Extremely Drug Resistant, PDR = Pan Drug Resistant. Modified from (Antibiotics Resistance Threats in the United States, 2013, 2013).*

The appearance and spread of resistance is enhanced by many factors: high global population growth, increased mobility, limited access to health facilities in many countries, misuse and overprescription of antibiotics (e.g. for treating viral infections for which they are ineffective), overuse (such as in animal feeding (Aarestrup, 2005)), low quality drugs (degraded and counterfeit antibiotics, (Okeke *et al.*, 1999)) and the habit of self prescription (Grigoryan *et al.*, 2010).

Multidrug-resistant (MDR) bacteria have been reported around the world, limiting the efficiency of medication against a large array of common diseases such as sepsis, skin, burn and urinary tract infections, leading to the term 'superbugs' being coined (Boucher *et al.*, 2009). These MDR strains are also qualified as extremely drug resistant (XDR) and in the case of resistance to the entire array of antimicrobial treatment as pan drug resistant (PDR). The Antimicrobial Availability Task Force at the Infectious Disease Society of America highlighted especially *Acinetobacter baumannii,* the *Aspergillus* species*,* the extended spectrum ß-lactamase (ESBL)–producing *Enterobacteriaceae,* the vancomycin-resistant *Enterococcus faecium, Pseudomonas aeruginosa,* and the methicillin-resistant *Staphylococcus aureus* (MRSA*)* as highest threats (Talbot *et al.*, 2006).

Two different mechanisms can be involved in resistance development: firstly non-specific intrinsic resistance is achieved through the expression of proteolytic enzymes (degrading antimicrobial compounds reaching the cytoplasm) and membrane efflux pumps (Li & Nikaido, 2009, Cox & Wright, 2013) expelling antibacterial molecules from the cytoplasm. Second, adaptive resistance involves the gain of long-term immunity towards specific molecular scaffolds through prolonged exposure by physically neutralizing the antibacterial drug or altering the therapeutic target (Rodriguez-Rojas *et al.*, 2013). In addition, inter-species transfer of newly gained drug resistance to other sensitive strains contributes to the rapid spread of MDR strains (Davies, 1994).

At the same time there has only been approval of six new antibiotic scaffolds over the past three decades: pseudomonic acid (mupirocin) in 1985 (Casewell & Hill, 1987), oxazolidinones in 2000 (Ford *et al.*, 2001), lipopeptides (daptomycin) in 2003 (Alder, 2005), pleuromutilin in 2007 (Novak & Shlaes, 2010), fidaxomicin in 2011 (Johnson & Wilcox, 2012) and bedaquiline in 2012 (Palomino & Martin, 2013). Resistance is already known for most of them (Shaw & Barbachyn, 2011, Thomas *et al.*, 2010, Li *et al.*, 2013, Miller *et al.*, 2013). Compared to the frequency of MDR strains discovered, this antibiotic pipeline is currently unable to cope with the rising demand for

new treatments. This has occurred despite the rapid development of new drug discovery technologies in the same period of time. It is partially caused by the limited profits to be expected from antibiotics due to the non-chronic nature of infection, the short duration of treatment and the increasing cost of drug development, estimated at more than $1.8 billion to take a lead molecule to the market (Paul *et al.*, 2010). New antimicrobial drugs revenue will also be limited because of health policies restraining antibiotic prescriptions to slow down generation of resistance. Overall, the quantity of antimicrobial drugs in the medical pipeline is in constant decrease (Spellberg *et al.*, 2004, Butler *et al.*, 2013)) along with pharmaceutical companies cancelling their antibacterial drug discovery programs.

Overall, progress towards new antibiotics that use different targets or different mechanisms of action to subvert resistance is slow, and there is a real threat of a worldwide spread of lethal drug-resistant bacteria. This was exemplified by the recent outbreak of the New Delhi Metallo-beta-lactamase 1 (NDM-1) pandemic strain presenting strong resistance against every medical treatment currently available (Deshpande *et al.*, 2010). The situation calls for innovation about designing new classes of antibiotics and limiting the resistance to medical treatments (Butler & Cooper, 2012). Large-scale initiatives are currently being undertaken to tackle the problem and fuel the antibiotic pipeline (Cooper & Shlaes, 2011). In this perspective, the purpose of my PhD is to investigate a novel drug target, DsbA, by designing inhibitors that could potentially lead to a new antimicrobial scaffold thwarting drug resistance.

I.2 EcDsbA as a novel target for antivirulence drug design

I.2.1 Background

The current struggle in the antibiotic pipeline with the shortage of new efficient antibacterial drugs not only requires the investigation of novel scaffolds but also the validation of new antimicrobial targets. One suggested approach is to inhibit the virulence system in bacteria to reduce selective pressure compared with targeting pathways essential for survival, hence potentially leading to a diminished mutation rate towards drug resistance (Rasko & Sperandio, 2010, Clatworthy *et al.*, 2007). Additionally, by specifically targeting virulence pathways, such a drug might not affect the host endogenous microbiota hence limiting side effects. Disulfide bond forming protein A (DsbA) has been highlighted as a key target in this endeavor against pathogenic Gram-negative bacteria (Heras *et al.*, 2009) and is described in the section below.

The process of oxidative folding, i.e. the catalysis of protein folding through disulfide bond formation, has been detected in most pathogenic members of the Enterobacteriaceae family and in other Gram-negative pathogenic species (Dutton *et al.*, 2008). In the archetypal model of oxidative folding, the machinery includes a soluble thioredoxin-fold protein, DsbA, and a membrane-bound partner, DsbB, located in the oxidizing environment of the intermembrane space, or periplasm (Wunderlich & Glockshuber, 1993, Bardwell *et al.*, 1991, Bardwell *et al.*, 1993, Martin *et al.*, 1993). DsbA is the primary oxidizing enzyme triggering the introduction of disulfide bonds into unfolded substrates freshly translocated into the periplasm (Bardwell *et al.*, 1991) while DsbB regenerates DsbA to its active oxidized form (**Figure 1.2**) (Regeimbal & Bardwell, 2002).

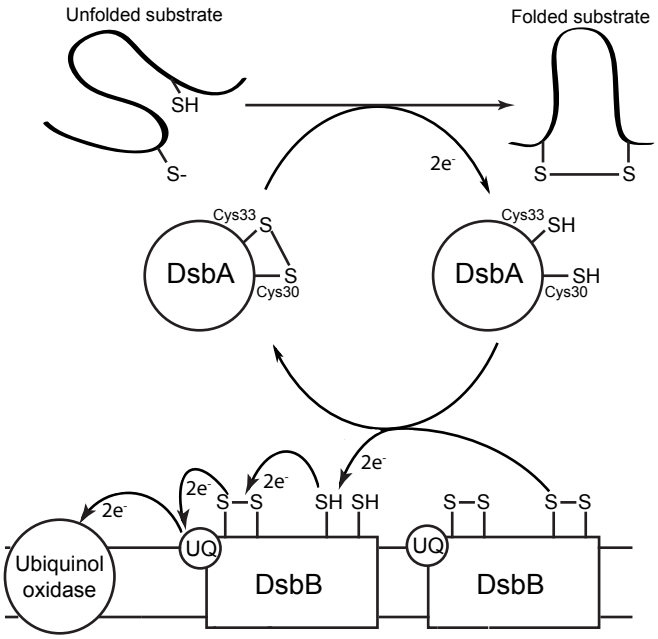

Figure 1.2. ***Perisplasmic oxidative folding mechanism***. *DsbA (in its oxidized form) is a powerful oxidase catalyzing the formation of a disulfide bond between two free cysteines in a substrate molecule, leading to a functional folded protein. DsbA in the reduced form transfers electrons to the transmembrane partner DsbB and is regenerated into the oxidized active form. These electrons are then transferred to a ubiquinone molecule (UQ) and transported to the respiratory system. Modified from (Inaba & Ito, 2008).*

The first DsbA protein was discovered in *Escherichia coli* in 1991 (Bardwell *et al.*, 1991) and the crystal structure solved in 1993 (Martin *et al.*, 1993). Since then, many homologues from a variety of pathogenic Gram-negative bacteria have been structurally and functionally characterized (Kurth *et al.*, 2013, Shouldice *et al.*, 2011). Importantly, many substrates of DsbA are essential for

virulence pathways (**Table 1.1**) (Heras *et al.*, 2009, Ha *et al.*, 2003): for example mutation of *Escherichia coli* DsbA (EcDsbA) prevents pili and flagella formation (Jacob-Dubuisson *et al.*, 1994, Hultgren *et al.*, 1993, Bringer *et al.*, 2007, Dailey & Berg, 1993), assembly of the type III secretion complex (Miki *et al.*, 2008), interaction with the host cell during infection (Vallance & Finlay, 2000, Bringer *et al.*, 2007), and the functional (but not structural) integrity of the bacterial membranes (Ruiz *et al.*, 2010). DsbA is also responsible for the correct folding of toxins, such as the enterolabile toxin in *E. coli* (Foreman *et al.*, 1995, Wulfing & Rappuoli, 1997), the cholera toxin in *Vibrio cholerae* (Peek & Taylor, 1992, Yu *et al.*, 1992) and pertussis toxin in *Bordetella pertussis* (Stenson & Weiss, 2002). Therefore, it was suggested that silencing DsbA enzymatic activity might ultimately lead to the disruption of virulence factor maturation and consequently impede infection (Heras *et al.*, 2009). To support this, a knock-out of *dsbA/dsbB* null uropathogenic *E. coli* (UPEC) cells are severely attenuated in a mouse infection model and unable to colonize the bladder though they remain viable (Totsika *et al.*, 2009b), fitting the expected phenotype of the antivirulence strategy.

Table 1.1. ***Selected substrates of DsbA involved in bacterial virulence. Modified from (Heras et al., 2009)***

Organism	DsbA substrate	Substrate function
Adhesion		
Uropathogenic *E. coli*	PapD	Molecular chaperone of P fimbriae
Enteropathogenic *E. coli*	BfpA	Major structural subunit of bundle-forming pili
Salmonella enterica	PefA	Major structural subunit of plasmid-encoded fimbriae
Toxin production and secretion		
Enterotoxigenic *E coli*	ST_8	Heat-stable enterotoxin
Enterotoxigenic *E. coli*	LT	Heat-labile enterotoxin
Bordetalla pertussis	S1 and S2	Pertussis toxin A and B subunits
Vibrio cholerae	Unknown	
Type III secretion system (T3SS)		
Enteropathogenic E. coli	EscC	Outer membrane secretin of T3SS
Salmonella enterica	SpiA	Outer membrane secretin of T3SS
Motility		
E. coli	Flgl	Flagellar P-ring motor protein
Outer membrane function		
E. coli	LptD	Lipopolysaccharide transporter

I.2.2 Escherichia coli DsbA, structure and mechanism

My project focuses primarily on developing inhibitors able to attenuate pathogenic strains of *E. coli*. From a potent scaffold against EcDsbA, derivatives could potentially be designed in the future targeting structurally similar DsbA enzymes from different pathogenic species or genus. Structurally, EcDsbA belongs to the thioredoxin related (TRX) protein family consisting of a classical thioredoxin domain with an inserted four α-helix domain (**Figure 1.3**) (Martin *et al.*, 1993). Residues 1 to 62 (β1-2, α1, β3) which harbor the catalytic site ^{30}CPHC^{33} and residues 139 to 189 (α6, β4-5, α7) which include the highly conserved *cis*-Pro loop region form the TRX domain, conferring the enzyme DsbA-like redox properties and its enzymatic reactivity (Charbonnier *et al.*, 1999). The α-helical domain comprises residues 63 to 138 (N-term α6, α2-5) and is embedded into the thioredoxin fold.

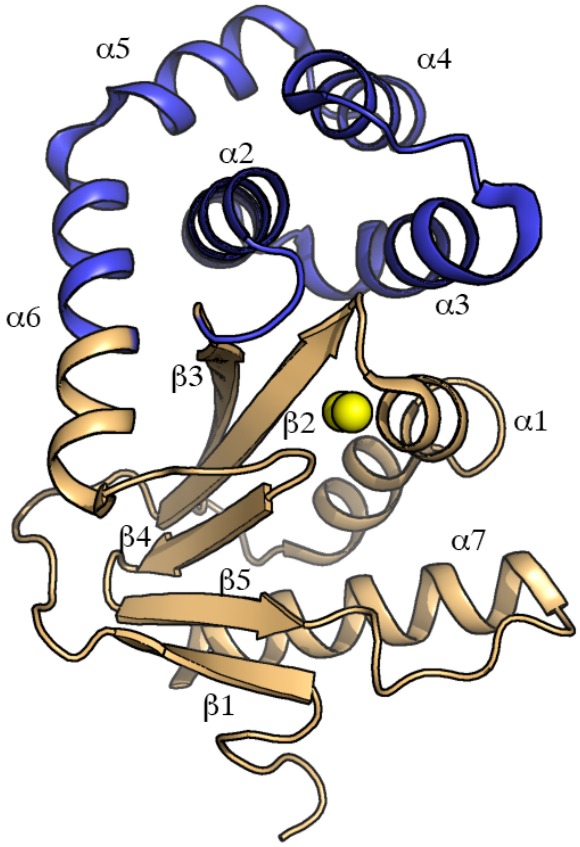

Figure 1.3. ***Crystal structure of oxidized EcDsbA.*** *The structure of EcDsbA (PDB code: 1DSB) is composed of a TRX domain (β1-5, α1, α6-7, in brown) and a α-helical domain (α2-5, in blue). The two thiolates from the catalytic cysteines Cys30 and Cys33 are shown as yellow spheres. The conserved cisPro loop region, contributing to the activity and stability of EcDsbA is located in the TRX domain between the α6 C-terminal end and β4, in close proximity to the catalytic cysteines.*

EcDsbA shares three typical properties with its homologues:

1) A CXXC motif, in this case ^{30}CPHC^{33}, includes the two active site cysteines essential for catalysis of redox reactions (Walker *et al.*, 1996). DsbA in its oxidized form presents an intramolecular disulfide bond between Cys30 and Cys33 that destabilizes the enzyme (Zapun *et al.*, 1993): the unfolding temperature of reduced EcDsbA is 8 K higher than that of the oxidized state (redEcDsbA: 350K, oxEcDsbA: 342 K Heras *et al.*, 2008)). Two residues varying according to the bacterial species (in *E. coli* Pro31 and His32) separate the catalytic cysteines and provide an electrostatic contribution to the enzyme stability (Guddat *et al.*, 1997). It was also shown that modification of these two intermediate residues shifts the pKa and the redox potential of DsbA (Kortemme *et al.*, 1996, Chivers *et al.*, 1997).

2) A highly acidic and nucleophilic cysteine, here Cys30, presents an uncommonly low pKa of 3.3 in EcDsbA (Huber-Wunderlich & Glockshuber, 1998) (with an average of 3.5 over the DsbA family). Cysteine residues in most proteins have a pKa around 8.3 (Karala *et al.*, 2010). This feature ensures that reduced Cys30 will always be in the anion thiolate form in physiological environment, thus able to perform nucleophilic attacks.

3) A highly oxidizing potential, -122 mV for EcDsbA (Huber-Wunderlich & Glockshuber, 1998), with the range for the DsbA protein family varying from -80 mV to -163 mV (Kurth *et al.*, 2013). In contrast, the redox potential of *E. coli* cytoplasmic thioredoxin Trx is much more reducing with a redox potential of -270 mV (Aslund *et al.*, 1997).

EcDsbA catalyzes the formation of a disulfide in unfolded substrates by using a bimolecular nucleophilic substitution reaction (Fernandes & Ramos, 2004, Inaba, Murakami*, et al.*, 2006, Frech *et al.*, 1996, Kadokura & Beckwith, 2009). A substrate thiolate group starts with a nucleophilic attack on oxidized EcDsbA Cys30, breaking the disulfide bond with EcDsbA Cys33 and leading to the formation of an intermolecular disulfide bond between enzyme and substrate (**Figure 1.4**). In the second phase, another substrate thiolate triggers nucleophilic attack on the first thiolate, forming a disulfide bond and folding the substrate while EcDsbA is released in its reduced and inactive form. The substrate binding site on EcDsbA can be considered as a therapeutic target, but since EcDsbA accepts hundreds of protein substrates the specificity and selectivity (and thus the interest in drug design) of this interaction is questionable.

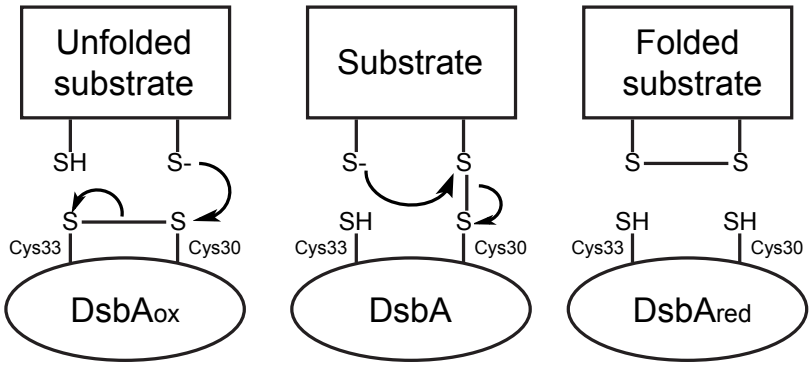

Figure 1.4. ***Nucleophilic substitution between EcDsbA and a substrate protein,*** *leading to the transfer of a disulfide bond to the substrate molecule. The nucleophilic attack of a substrate free cysteine thiolate functionality on EcDsbA Cys30 (left panel) leads to the formation of an intermolecular disulfide bond (center). Second nucleophilic attack from a neighboring free cysteine in the substrate triggers the release of EcDsbA in its reduced and inactivated form (right panel).*

Reduced EcDsbA with two free cysteines Cys30 and Cys33 then binds to the partner EcDsbB to regenerate the active oxidized form (**Figure 1.2**). EcDsbB has four transmembrane helices and mediates shuttling of EcDsbA between its reactive oxidized and inactive reduced state (Inaba, Murakami*, et al.*, 2006). EcDsbB, which shows strict binding specificity for EcDsbA, possesses two periplasmic loops (P1 and P2) each containing one pair of cysteines (P1 = C41/C44, P2 = C130/ C104) (Inaba, Murakami*, et al.*, 2006). Transfer of the disulfide bond to EcDsbA also occurs through a bimolecular nucleophilic substitution reaction: EcDsbA Cys30 starts a nucleophilic attack on oxidized EcDsbB Cys104, followed by nucleophilic attack of EcDsbA Cys33 onto Cys30, restoring the disulfide bond and releasing EcDsbA in the oxidized form. The additional electrons on EcDsbB Cys104 are transferred to a ubiquinone molecule through concerted disulfide bond exchange with EcDsbB Cys130, Cys41 and Cys44 (Inaba, Takahashi*, et al.*, 2006). The charged ubiquinone finally exchanges these electrons with the membrane bound respiratory system (**Figure 1.2**).

Both EcDsbA-EcDsbB and EcDsbB-ubiquinone interactions are promising targets for drug discovery, as their inhibition might force EcDsbA to remain in its reduced hence inactive state. The EcDsbB-ubiquinone interaction is not addressed in this thesis. However, the EcDsbA-EcDsbB interaction offers great potential: the interaction may be more specific than the EcDsbA substrate binding site, and the structure of the EcDsbA-EcDsbB complex has already been reported (Inaba, Murakami*, et al.*, 2006, Malojcic *et al.*, 2008, Inaba *et al.*, 2009b). To date no rational design of ligands towards DsbA has been reported (Shouldice *et al.*, 2011) and structural scaffolds able to inhibit EcDsbA activity remain to be identified. Moreover, the protein-protein interaction provides

an interesting starting point for the design of peptides and peptidomimetics. A structure-based drug design strategy based on the EcDsbA-EcDsbB interaction was the focus of my PhD project.

I.2.3 Characterization of the EcDsbB binding site on EcDsbA

The EcDsbB-binding site on the EcDsbA surface is well known: three different co-crystal structures of the EcDsbA-EcDsbB complexes have been solved in the past seven years (Inaba *et al.*, 2009a, Malojcic *et al.*, 2008, Inaba, Murakami*, et al.*, 2006). Due to the brevity of the transitional state between EcDsbA and EcDsbB (Inaba *et al.*, 2004, Inaba *et al.*, 2005), it was necessary to engineer a stable complex bound by a non-resolvable intermolecular disulfide bond using cysteine mutants of one or both proteins (EcDsbB-C130S and/or EcDsbA-C33A, **Figure 1.5**) (Guilhot *et al.*, 1995, Kishigami *et al.*, 1995).

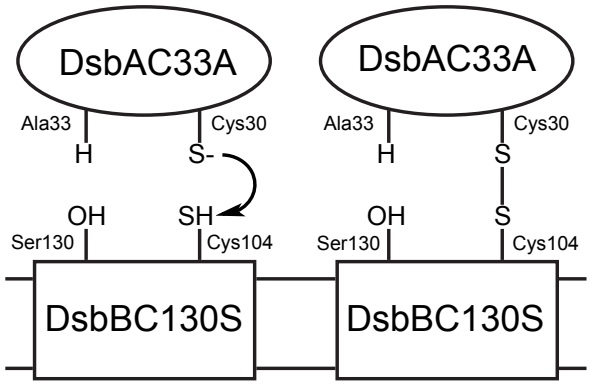

Figure 1.5. ***Formation of an irreversible DsbA/DsbB complex.*** *Mutations of the second cysteine in the catalytic dyad of DsbA (Cys33Ala) and/or DsbB (Cys130Ser) prevented the resolution of the intermolecular disulfide bond and thus impeded the release of EcDsbA in its active form. The complex formed from the mutants was stable and suitable for co-crystallization.*

In the 3.7 Å resolution structure of EcDsbA-EcDsbB (PDB ID: 2ZUP) the EcDsbB periplasmic loop P2 ^{98}PSPFATCDFMVR^{109} binds within a hydrophobic groove between EcDsbA helixes α1 and α7 formed by aromatic residues Phe36, Phe174 and Tyr178 and aliphatic residues Leu40 and Ile42 (**Figure 1.6**). This region had been predicted to interact with partner or substrate proteins prior to the complex crystal structure (Martin *et al.*, 1993). The EcDsbB P2 loop also interacts on the shallow surface of EcDsbA, next to the EcDsbA ^{30}CPHC^{33} catalytic motif triggering formation of a disulfide bond between EcDsbB Cys104 and EcDsbA Cys30, and also interacts with the *cis*Pro loop.

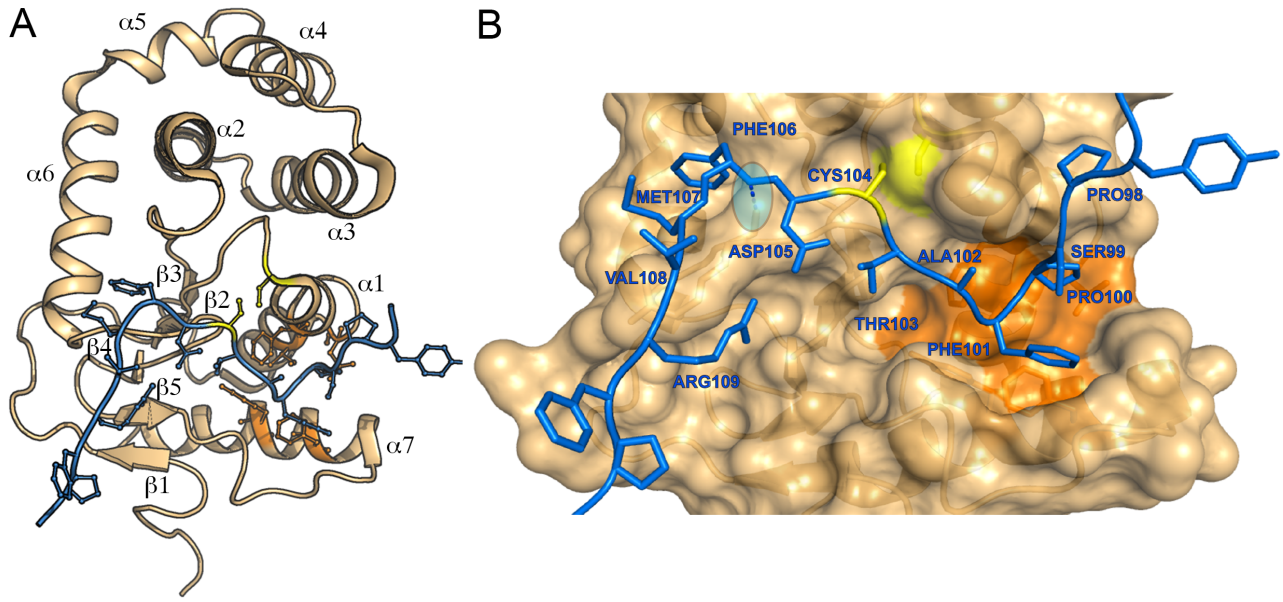

Figure 1. 6. ***Two representations of the EcDsbA$_{C33A}$ – EcDsbB$_{C130S}$ complex*** *from the 3.7 Å resolution crystal structure by Inaba et al. (Inaba, Murakami, et al., 2006).* ***A****. The model showed the EcDsbB periplasmic loop (in blue) to bind on the surface of EcDsbA (in light brown) making contacts with helices α1 and α7 and the cisPro loop.* ***B****. The EcDsbB periplasmic loop P2 (in blue with residues labeled) binds into the EcDsbA hydrophobic pocket (in orange). A disulfide bond linking EcDsbA Cys30 to EcDsbB Cys104 (both in yellow) covalently locks the two mutants and the EcDsbAC33A and EcDsbB C130S mutations prevent the mixed disulfide bond from being resolved. The predicted hydrogen bond between EcDsbA Arg148 and EcDsbA Phe106 is shown as a blue dashed line and highlighted in blue.*

NMR studies of the complex showed that additional contacts are made by EcDsbB residues ^{126}ASGDCA^{131} with the EcDsbA β3-α2 loop next to the ^{30}CPHC^{33} motif on the side opposite to the hydrophobic patch (Zhou *et al.*, 2008). EcDsbA Met64 is suspected to play a role in the separation between EcDsbB Cys104 and Cys130 for binding to EcDsbA Cys30; mutation of this residue to Gly or Ala leads to a significant decrease of the enzyme kinetics (Inaba *et al.*, 2009a). It is worth noting that the molecular mechanisms underlying the EcDsbA-DsbB interaction were interpreted based on a 3.7 Å crystal structure, therefore the initial working model might be slightly biaised. Submission of the EcDsbB-EcDsbA interface to the PDBsum server identifies interactions at the interface in addition to the EcDsbA Cys30 - EcDsbB Cys104 disulfide bond. Indeed, every residue from EcDsbB loop P2 sequence ^{98}PSPFATCDFMVR^{109} presents hydrophobic contacts with the EcDsbA surface (Shouldice *et al.*, 2011). A hydrogen bond is predicted between EcDsbB Phe106 backbone and EcDsbA Arg148 backbone on the *cis*Pro loop (**Figure 1.6**), suggesting there are more

interactions at play than the driving force of the disulfide bond that could be exploited for the development of a potent scaffold.

I.2.4. Analysis of the additional DsbA-ligand complex structures

A structure-based drug design strategy requires the analysis of the available DsbA-ligand crystal structures to provide additional information that can shed light on the ligand binding mode and specificity towards DsbA. The number of solved DsbA protein structures has rapidly increased within recent years, some of them including ligands. Two of these DsbA structures incorporate small molecules (Shouldice *et al.*, 2010, Kurz *et al.*, 2009, Crow *et al.*, 2009) and two were solved with peptides bound (Rinaldi *et al.*, 2009, Paxman *et al.*, 2009b) (**Figure 1.7**). The small molecules (glycerol and polyethylene glycol) present little interest for drug design purposes.

The recently characterized *Xyfella fastidiosa* DsbA was fortuitously cocrystallized (PDB ID: 2REM) with an octamer peptide ligand (Rinaldi *et al.*, 2009). Careful analysis reveals that the ligand binds within the hydrophobic pocket and close to the catalytic cysteine motif. Compared with the EcDsbA-EcDsbB structure, this polypeptide chain binds in a similar fashion to the EcDsbB P2 loop. However, the poor quality of the electronic density map only allowed fitting of an Ala-Ala-Ala-Ala-Ala-Gly-Gly-Ala polypeptide chain, giving little information about the specific interaction between peptide side chains and the DsbA surface.

In the second structure a known substrate peptide from autotransporter protein SigA was covalently linked by a thioether bond to EcDsbA Cys30 (PDB ID: 3DKS) (Paxman *et al.*, 2009b). The peptide of sequence PIPFL(Hse)QKD adopts a conformation very different from the EcDsbB loop. The SigA peptide interacts at the interface with the thioredoxin and the α-helical domains of EcDsbA, in particular with EcDsbA Phe29, Phe63, Met64 and Arg148, but no interactions are present between the SigA peptide and the hydrophobic groove (Paxman *et al.*, 2009b). Consequently, the binding mode differing from the EcDsbB loop presents limited interested in the design of inhibitors of the EcDsbA-EcDsbB interaction.

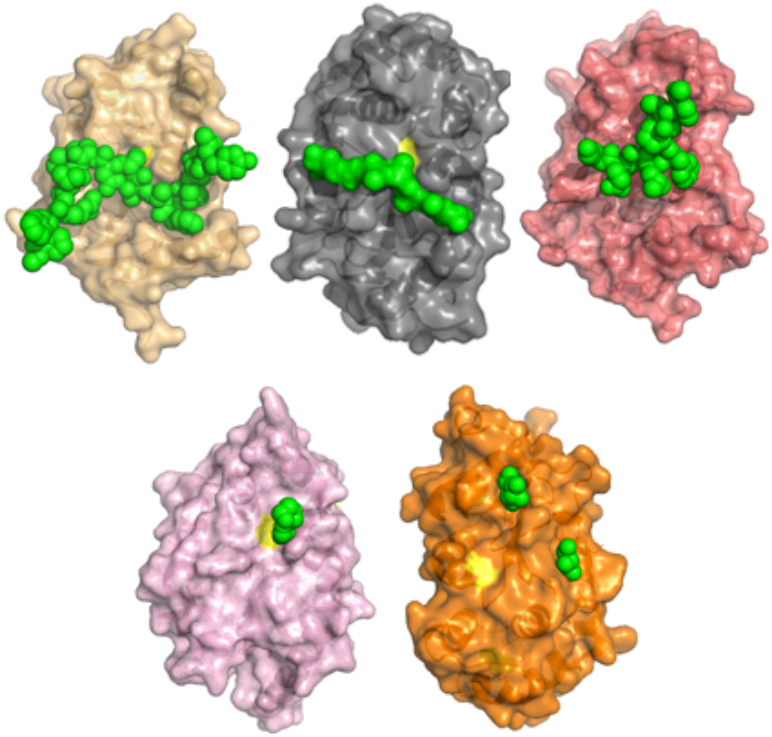

Figure 1.7. ***Surface representation of reported DsbA-ligand crystal structures.*** *Top left, EcDsbA in light brown with the EcDsbB loop in green. Top center, Xyfella fastidiosa DsbA in black with an unknown peptide sequence in green. Top right, EcDsbA in pink with a SigA substrate derivative peptide in green. Bottom left, Wolbachia pipientis αDsbA1 in pink with a bound polyethylene glycol molecule in green. Bottom right, Pseudomonas aeruginosa DsbA in orange with two glycerol molecules in green. Catalytic cysteines are shown in yellow. Besides EcDsbB, the only reported ligand binding to the DsbA hydrophobic pocket is the polypeptide chain interacting with XfDsbA, but the poor resolution prevented the accurate modeling of residues.*

Taken together, the best available structure from which to start designing peptidic inhibitors for the EcDsbB-binding site on EcDsbA is the 3.7 Å resolution EcDsbB-EcDsbA complex crystal structure itself. Although lacking a secondary structure, the disordered loop provided an amino acid sequence from which the initial ligands could be based, mimicking the binding properties to interact with EcDsbA. One approach is to use peptides that offer the possibility to reproduce the DsbB loop backbone and side chains. Moreover the development of peptides as drugs is an emerging field in the world of antibiotics and the recently acquired knowledge could prove useful to develop an inhibitor of the EcDsbA-EcDsbB interaction.

I.3 Peptides as antimicrobial drugs

The EcDsbB periplasmic loop P2 provides a suitable starting point for the design of peptide sequences targeting the binding of EcDsbA. My project was to identify and optimize such peptide sequences. These peptides would also present an ideal basis for the development of peptidomimetics, an emerging field of antimicrobial molecules. The purpose of antimicrobial peptidomimetics is to improve the overall efficiency of a peptide scaffold and novel strategies are meeting growing success as described in the section below. In this project the design of peptidomimetics could potentially lead to novel scaffolds that trigger significant inhibition of the EcDsbA folding activity.

I.3.1 Antimicrobial peptides (AMP)

A promising field of research for new antibiotics focuses on natural antimicrobial peptides (AMP), particularly from eukaryotic organisms. AMPs are typically amino acid chains up to 50 residues in length synthesized ribosomally (involving mRNA translation) rather than non-ribosomal 'natural products' antibiotics, and featuring bactericidal and/or fungicidal properties. AMPs were initially characterized in the 1980s and proved to be a vital component of many organisms' innate immune system (*Antimicrobial Sequences Database*). For detailed reviews on AMPs see (McPhee & Hancock, 2005, Powers & Hancock, 2003, Nguyen *et al.*, 2011).

The majority of AMPs act in an indiscriminate manner disrupting the bacterial and fungal membrane, hence differing from traditional antibiotics that have specific targets. The versatility of AMPs is very high, and the large reservoir of natural peptides available can lead to fruitful drug development though structure-activity relationship (SAR) studies. The amino acid sequence of membrane-disruptors is less relevant for antibacterial efficiency than the physicochemical properties, such as charge and hydrophobicity, which also regulate the specificity towards the bacterial membrane rather than the mammalian ones (Tossi *et al.*, 2000). All membrane disrupting mechanisms identified to date involve interactions between positive charges on the antibiotic ("cationic" peptide) and the negatively charged lipid of the outer membrane, together with a hydrophobic moiety to interact with the fatty acyl chains, ultimately leading to membrane degradation. Many structural groups of AMPs have been defined (**Figure 1.8**).

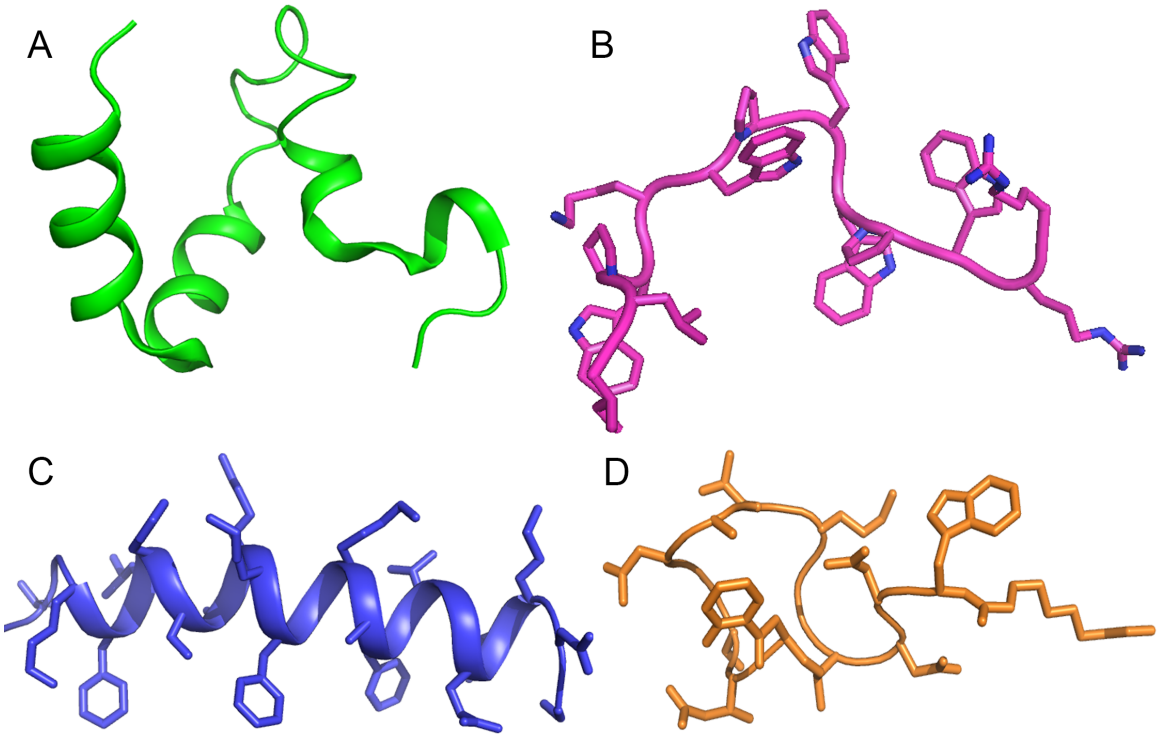

Figure 1.8. ***Selected examples of natural AMPs.*** ***A.*** *Structure of dermcidin (PDB code 2KSG), an AMP from human origin inducing membrane depolarization (Song et al., 2013).* ***B.*** *Structure of indolicidin (PDB code 1G89), a tryptophan-rich peptide from bovine origin triggering inner membrane polarization. (Falla et al., 1996)* ***C.*** *Structure of magainin 2 (PDB code 2MAG), an α-helical AMP of amphibian origin forming pores in the membrane leading to cell lysis (Imura et al., 2008).* ***D.*** *Structure of daptomycin, a cyclic AMP from bacterial origin that causes membrane aggregation and loss of membrane potential (Pogliano et al., 2012).*

For example, α-helical AMPs possess the ability to penetrate and span across the thickness of the lipid bilayer triggering the formation of pores or breaking off the membrane into micelles (Zasloff, 2002, Haney *et al.*, 2009, Holt & Killian, 2010). β-sheet AMPs, composed of β-hairpin peptides, are able to form β-barrels in lipid bilayers as well as β-sheets on their surface, also disrupting the membrane structure (Tang & Hong, 2009). Extended AMPs incorporate a high percentage of selected residues, usually Arg and Trp, and cause membrane leakage through formation of 'barrel-stave' pores in the lipid bilayer (Chan *et al.*, 2006).

Some natural peptides are also cyclized to link the termini and/or residue side chains together, thereby limiting conformational flexibility. These structural restraints offer advantages in stability and specificity. Indeed, cyclic peptides are not substrates for proteases. Moreover, stabilized pre-organized three-dimensional structure can result in high-affinity interactions with a target protein. Consequently, many cyclic peptides are membrane-inactive and instead target specific protein-

protein interactions (PPI) essential for bacterial viability. Many antibiotics already in clinical use are cyclic peptides, such as colistin, polymyxin b and daptomycin. Some antimicrobial peptides are polycyclic (two or more cycles) such as vancomycin, nisin and actinomycin D and are frequently used in the clinic (Baeriswyl & Heinis, 2013).

AMPs promised a solution to the microbial resistance issue (Peschel & Sahl, 2006): instead of local mutations bacteria would need to substantially alter the composition of the lipid membrane thus compromising other essential pathways (Zasloff, 2002, Schroder, 1999, Hancock & Chapple, 1999). However, this prediction about microbial resistance has since been criticized (Bell & Gouyon, 2003, Tzeng *et al.*, 2005, Kraus & Peschel, 2006, 2008). A very large number of AMPs have been identified but apart from a few exceptions presently on the market (Leader *et al.*, 2008) natural peptides offer little prospect as drug candidates for the following properties: 1) poor stability due to the sensitivity to proteases (with a lifetime of a few minutes in serum and tissues (Pollaro & Heinis, 2010)), 2) high sensitivity to pH and salts (Goldman *et al.*, 1997, Bals *et al.*, 1998, Rydlo *et al.*, 2006, Lee *et al.*, 1997), 3) their large size limiting large-scale manufacturing and 4) poor pharmacokinetics combined with high immunogenicity (Latham, 1999). These drawbacks have led to the generation of peptide analogues that can mimic AMP properties, so-called peptidomimetics.

I.3.2 Emergence of peptidomimetics

The term peptidomimetics embraces here any molecule derived from a peptide or a protein fragment, but not limited to the natural peptide backbone and the natural 20 α-amino acids. This includes *de novo* scaffolds, semi-synthetic peptides and even small molecules on which a peptide group was grafted. Here, I focus on artificial or synthetic modifications made to molecules of peptidic origin, and will not include natural products falling within this definition.

Apart from the large reservoir of natural AMPs to use as starting points, a certain advantage of peptidomimetics as drug candidates compared to natural peptides is that they enable a broad array of variations for stability, activity, solubility or bioavailability as well as various secondary structures (e.g. helices, ß-sheets, etc) based on simple modifications of the peptide backbone or specific side chains (also called multidimensional optimization (Satyanarayanajois & Hill, 2011)). Structure-activity relationship (SAR) studies lead to the emergence of new structural classes of peptidomimetics: for example β-peptides incorporate an additional carbon atom in the peptide

backbone and are able to fold into secondary structures such as helices and ß-sheet-like structures (**Figure 1.9**). The different class of peptoids presents residues with side chains attached to the nitrogen atom of the backbone amide functionality rather than the α-carbon. These simple transformations confer a far greater resistance to peptidases (Zuckermann *et al.*, 1994, Weinstock *et al.*, 2012).

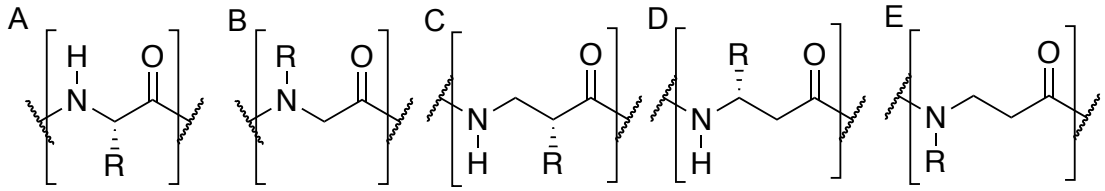

Figure 1.9. ***Selected examples of peptide backbone modifications providing resistance against peptidases. A.*** *'natural' α-amino acid.* ***B.*** *Peptoid.* ***C.*** *β^2-peptide.* ***D.*** *β^3-peptide.* ***E.*** *β-peptoid.*

Beside the ability of AMP peptidomimetics to bind bacterial membranes, peptidomimetics have the ability to mimic protein-protein interactions (PPI). Peptidomimetics can also adopt secondary structures such as ß-hairpins (Robinson, 2008), helices (Fischer *et al.*, 2010) and ß-sheets (Hammond *et al.*, 2006) to mimic recognition motifs specific to PPI (**Figure 1.10**).

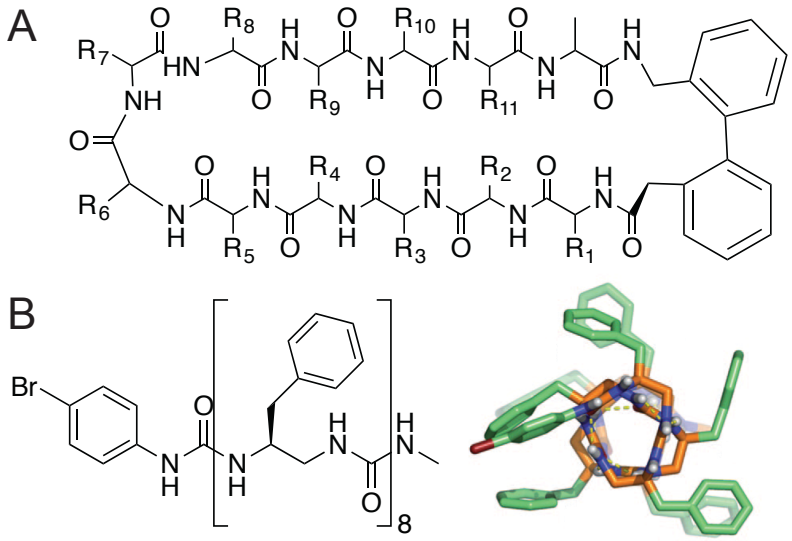

Figure 1.10. ***Selected examples of peptidomimetics adopting secondary structure motifs. A.*** *Structure of a ß-hairpin mimetic. To contrast, a 'natural' ß-hairpin peptide relies on disulfide bonds to adopt such a conformation.* ***B.*** *Sequence and tridimensional model of an α-helix mimetic. Reproduced and modified from (Fischer et al., 2010).*

Therefore, by developing inhibitors based on the structure of known partners, peptidomimetics might aim at novel targets not limited to the membrane. For drug design purposes, the possibility of conserving natural peptides antimicrobial activities with a much smaller molecular size also contributes to better druggability. Generally, small peptidomimetics (≤ 5 amino acids) fall into the set of Lipinski "rule of 5" (molecular weight ≤ 500 Da, LogP ≤ 5, ≤ 5 hydrogen donors, ≤ 10 hydrogen acceptors (Lipinski *et al.*, 2001)) adapted for antibiotics (O'Shea & Moser, 2008), and side chain variations offer convenient optimization options for them.

The following sections highlight innovations that peptidomimetics can offer to help fight the new MDR pathogenic strains. Rather than an exhaustive list of antimicrobial peptidomimetics produced to date, it illustrates some important advantages of using peptidomimetics as novel antimicrobial scaffolds through selected successful drug design approaches not limited to membrane disruptors (**Table 1.2**). Additional reviews about antimicrobial peptidomimetics are available elsewhere (Niu *et al.*, 2012, Ung & Winkler, 2011, Liskamp *et al.*, 2011, Giuliani & Rinaldi, 2011, Rotem & Mor, 2009, Chongsiriwatana *et al.*, 2008, Nguyen *et al.*, 2011, Ahn *et al.*, 2002, Vaara, 2009, Bragonzi, 2010, Hatahet & Ruddock, 2009, Patch & Barron, 2002). The examples below were selected to demonstrate the diversity in the mechanisms of action that are part of the peptidomimetic weaponry.

Table 1.2. ***Summary of the peptidomimetic targets and mechanisms approached in this chapter.***

Peptidomimetic	Gram +/-	Target specie(s)	Mechanism	Drug	Phase reached
PDF inhibitors	Both	*E. coli, M. tuberculosis, S. aureus, P. aeruginosa, E. faecium*	Binding peptide deformylase to prevent post translational protein maturation	BB-81384, LBM415	Ongoing Phase I
Oligoacyllysines (OAK)	Both	*E. coli, S. aureus, S. enterica, K. pneumoniae, P. aeruginosa, P. mirabilis*	Membrane depolarization, DNA binding,	/	/
ß-hairpin macrocycles	Gram -	*P. aeruginosa*	Membrane disruption	POL7080	Completed Phase I
Arylamides	Both	*E. coli, S. aureus, P. aeruginosa, K. pneumoniae*	Membrane permeabilization	PMX-30063 (Briladicin)	Completed Phase IIa
Pilicides	Gram -	*E. coli*	Inhibition of chaperones necessary for pili formation	/	/
EP inhibitors	Gram -	*P. aeruginosa*	Blocking efflux pumps	/	/
G6PS inhibitors	Both	*E. coli, S. aureus, B. subtilis*	Blocking cell wall synthesis	/	/

I.3.3 Improving potency and pharmacokinetics: bacterial peptide deformylase (PDF) inhibitors

Some traditional antibiotic scaffolds directly target the bacterial translation mechanism (such as the ribosome subunits 16S and 50S (Lambert, 2012)), but an alternative way to prevent proteins from functioning is to inhibit post-translational modifications (Hatahet & Ruddock, 2009). Peptidomimetics have been developed to bind the bacterial peptide deformylase (PDF) (Huntington *et al.*, 2000), an essential metalloenzyme present in most of the bacterial world and identified as a novel antimicrobial target (Mazel *et al.*, 1994, Meinnel & Blanquet, 1994, Sharma *et al.*, 2009). PDF specifically cleaves the N-terminal formyl moiety resulting from N-formylmethionine initiating ribosomal translation, hence allowing further maturation of the folding protein. The development of peptidomimetic BB-3497 that reached human clinical trials is a typical example of peptidomimetic design.

On the one hand, peptides and peptidomimetic molecules mimicking PDF substrates were screened using an activity assay to evaluate the simplest potent scaffold *in vitro* (Meinnel *et al.*, 1999). It resulted in dipeptide HS-CH_2-Nle-Arg-OCH_3 (**Figure 1.11A**) showing low micromolar affinity towards PDF *in vitro* (*K*d 2.5 ± 0.5 μM) but poor antibacterial activity. On the other hand, screening of a large library of small compounds for PDF inhibitors identified actinonine (Chen *et al.*, 2000) (**Figure 1.11B**) as a natural antibacterial agent. The antimicrobial activity of actinonine was recognized in the early 1960s but its mechanism of action was unknown then (Gordon *et al.*, 1962). Consequently, Clements et al. screened an in-house database of metalloenzyme inhibitors (Clements *et al.*, 2001) resulting in one peptidomimetic hit, BB-3497, sharing striking structural similarities with both natural substrates of PDF and actinonine (**Figure 1.11C**). BB-3497 featured minimal inhibitory concentrations (MIC, the lowest concentration of an antimicrobial necessary to completely impede bacterial growth) and bioavailability more potent than actinonine (against different strains of *E. coli* 0.125 μg/mL ≤ MIC ≤ 8 μg/mL). The crystal structure of the BB-3497-bound PDF was solved for SAR studies to further develop non-natural side chains on the peptidic backbone (Clements *et al.*, 2001). The knowledge of the structure allowed investigation of essential positions on the BB-3497 scaffold (**Figure 1.11D**), thereby allowing modification for peptidomimetics.

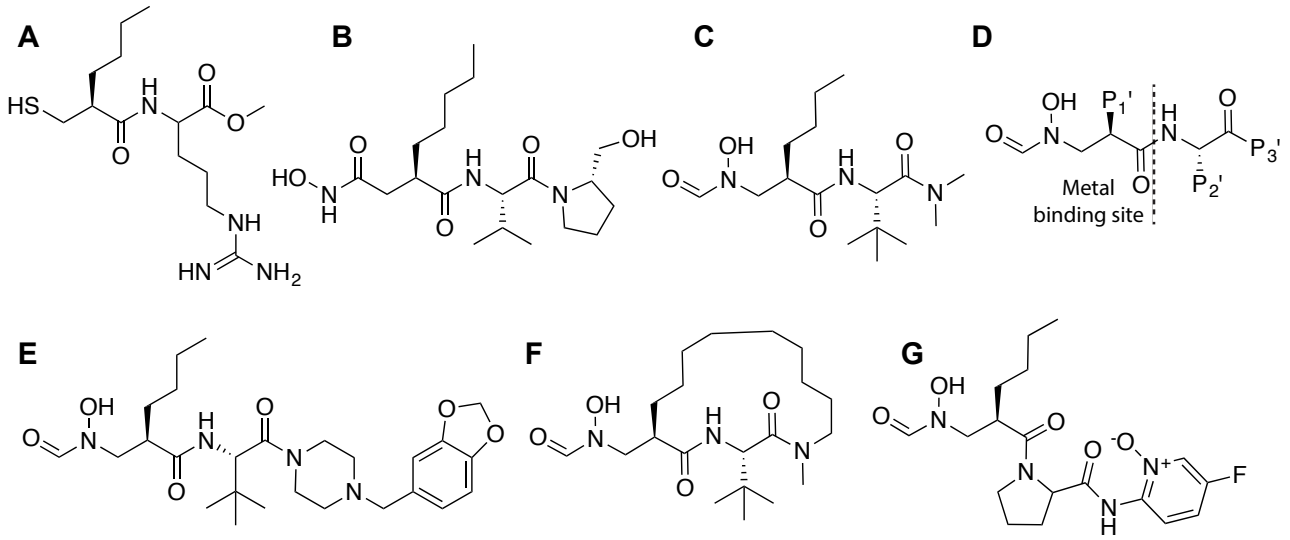

Figure 1.11. ***Peptidomimetic inhibitors of bacterial PDF.*** ***A.*** *dipeptide HS-CH_2-Nle-Arg-OCH_3 from peptide designed against PDF.* ***B.*** *Natural antimicrobial actinonine was identified as a PDF inhibitor through a step of library screening.* ***C.*** *The metalloenzyme inhibitor BB-3497 shares structural similarities with actinonine and HS-CH_2-Nle-Arg-OCH_3.* ***D****. Peptide scaffold on which peptidomimetic inhibitors of PDF are synthesized and tested.* ***E.*** *The 'hit' peptidomimetic BB-81834 derived from SAR (based on the scaffold in panel D) now in clinical trials.* ***F****. Macrocyclic scaffold based on BB-3497.* ***G****. Another PDF inhibitor LBM-415, also in clinical trials, presents similarities with BB-81834. Modified from (Meinnel et al., 1999, East et al., 2004, Azoulay-Dupuis et al., 2004, Anderegg & Jones, 2004, Clements et al., 2001, Chen et al., 2000).*

The N-formyl hydroxylamine functional group was replaced by similar metal binding groups (Smith *et al.*, 2002) found in other metalloenzyme inhibitors. The optimal distance between the metal-binding group and the peptide residues was investigated (Davies, Ayscough, Beckett, Bragg*, et al.*, 2003). The optimal side chains P1' (Davies, Ayscough, Beckett, Bragg*, et al.*, 2003), P2' and P3' (Davies, Ayscough, Beckett, Clements*, et al.*, 2003, East *et al.*, 2004) were identified, leading to the design of the peptidomimetic BB-81384 (**Figure 1.11E**). This compound had promising pharmacokinetics and oral bioavailability against a large array of bacterial strains including *Staphylococcus aureus* (Gross *et al.*, 2004, Azoulay-Dupuis *et al.*, 2004). Another standard peptidomimetic approach was also tested, using the cyclization of the side chains P2' and P3', resulting in an increase in potency and stability (**Figure 1.11F**) (Hu *et al.*, 2003, Nguyen *et al.*, 2004). A second peptidomimetic inhibitor, LBM415 (previously NVP-PDF 713), whose design process has not been disclosed, presented a remarkably similar scaffold (**Figure 1.11G**) and demonstrated high potency towards a wide spectrum of pathogens (Credito *et al.*, 2004, Ednie *et al.*, 2004, Anderegg *et al.*, 2003, Anderegg & Jones, 2004, Gordon *et al.*, 2003, Jones, Fritsche*, et al.*,

2004, Jones, Moet, *et al.*, 2004, Osborne *et al.*, 2009). Both BB-81384 and LBM415 are undergoing phase I clinical trials (Rolan *et al.*, 2011).

In this first case the design of peptidomimetics is suited for the fusion of two different approaches - small molecule screening and rational peptide design – leading to improved potency regarding natural products, such as actinonine, and better pharmacokinetics that allowed two lead peptidomimetic molecules to enter clinical trials.

I.3.4 Thwarting 'adaptive' resistance: β-peptides and peptoids

Peptides and peptidomimetics can be inactivated by peptidases, seriously limiting their stability in serum. This can be overcome through simple peptide backbone alterations, such as the introduction of an extra carbon atom between the α-carbon and the amide moiety (β-peptides), the linkage of the side chain on the amide nitrogen atom (α-peptoids) or a combination of both (β-peptoids). The effect of such backbone modifications goes beyond improved stability: recent studies suggest that such peptidomimetics evade traditional resistance mechanisms in MDR *E. coli* (Jahnsen *et al.*, 2012), increase antibacterial activity and lower hemolytic properties (Chongsiriwatana *et al.*, 2008).

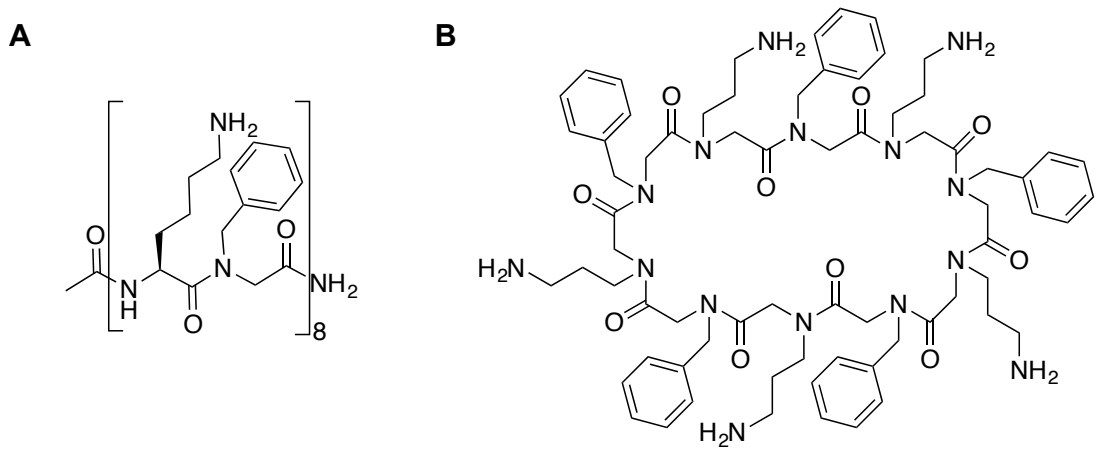

Figure 1.12. ***Examples of peptoid inhibitor alternatives of AMP sequences that evade AMP resistance in bacteria. A.*** *Example of an active alternate α-amino acid/peptoid residue scaffold, while the α-amino acid sequence is no longer potent due to bacterial resistance.* ***B.*** *An example of amphiphilic cyclic peptoid, combining alternate hydrophobic (Phe) and positively charged (Lys) residues. Modified from (Jahnsen et al., 2012, Huang et al., 2012)*

Pointing out that most peptidomimetic studies focus on side chain alterations specific to their mode of action, Jahnsen et al. analyzed backbone alterations on simple AMP mimetics (Jahnsen *et al.*, 2012). From Ac-(Lys-Phe)$_8$-NH$_2$ AMP sequence (with typical AMP features combining alternative cationic –Lys- and hydrophobic –Phe- components), they designed and synthesized hybrid peptidomimetics incorporating only α-peptoids, β-peptoids or β-aminoacids or replacing every second residue with α-aminoacids (**Figure 1.12A**). They subsequently tested their antibacterial efficiency against three MDR strains of *E. coli*, two MDR strains of *K. pneumoniae* and MRSA. The resulting data show clear evidence of improved antibacterial activities towards *E. coli* for the hybrid peptidomimetics compared to natural α-L-residue sequences. While the α-L-amino acid peptides and their α-D analogues have limited effects (MIC ≥ 128 μM), peptidomimetics especially α-aminoacid/α-peptoid hybrids showed great efficacy (2 μM ≤ MIC ≤ 8 μM) against all *E. coli* MDR and laboratory strains. Activities against *K. pneumoniae* and MRSA were however unchanged (MIC ≥ 128 μM), which the authors justified by the selectivity of the Lys-Phe sequence towards the *E. coli* membrane (Olsen *et al.*, 2010).

Barron et al. advanced that similar linear peptoids were able to act synergistically with AMPs, with both molecules using similar modes of actions (Chongsiriwatana *et al.*, 2011). Moreover, Huang et al. argued that cyclic analogues of linear peptoids (**Figure 1.12B**) further increased antibacterial activity compared to their linear versions (Huang *et al.*, 2012). A MRSA strain was found not to develop resistance against such a cyclic peptoid after 21 passages of bacteria.

These examples of peptoids show how small modifications to the backbone, independently of the side chains and thus possibly of the specificity of the antibiotic for its target, allow peptidomimetics to overcome existing resistance mechanisms, including those targeting the AMPs from which they were derived. Therefore, the combination of higher efficiency by optimization of the side chains and lower resistance by modification of the backbone could possibly lead to very potent antibacterial agents.

I.3.5 Tuning physicochemical properties and selectivity: oligoacyllysines

The secondary structure of AMPs has a crucial influence on antibacterial activity. For example, through the study of dermaseptin (a natural cationic AMP, **1.13A**) a higher helical content leads to higher antibacterial activity (potentially through easier spanning across the membrane bilayer), although it also reduces selectivity towards targeted cells (Shalev *et al.*, 2002). On the other hand, decreasing the hydrophobicity by truncating the AMP induced better selectivity between membrane types although coupled with reduced activity. According to these properties a structurally ordered dermaseptin analogue shaping as an amphipathic α-helix proved to be very potent against a broad spectrum of pathogens, but also possessed a very high hemolytic activity (Kustanovich *et al.*, 2002, Navon-Venezia *et al.*, 2002).

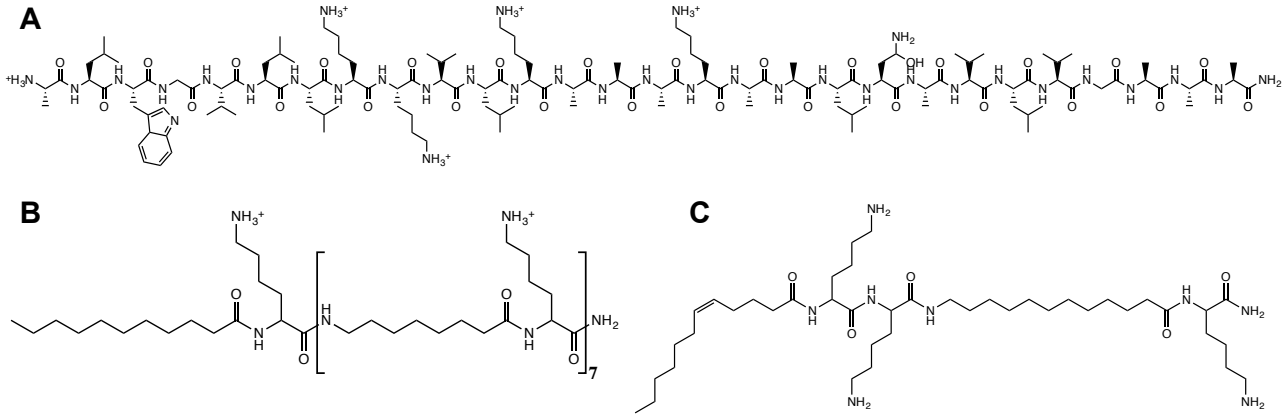

Figure 1.13. ***Oligoacyllysines (OAK) membrane-disrupting peptidomimetics.*** ***A.*** *Natural AMP dermaseptin, from amphibian origin.* ***B.*** *$C_{12}K\text{-}7\alpha_8$.* ***C.*** *C12(ω7)K-β12.* Modified from (Rotem & Mor, 2009, Epand *et al.*, 2008, Sarig *et al.*, 2010).

Mor et al. turned to a peptidomimetic approach to improve selectivity while retaining antibacterial activity, and obtained a significant enhancement by replacing long *N*-terminal sequences with acyl groups (Marynka *et al.*, 2007). Lysine-rich cationic peptidomimetics with acyl moieties were developed under the name of oligoacyllysines (OAKs). These offer the advantage of tuning the hydrophobicity of the peptidomimetic by varying acyl chain length for improved activity, while limiting formation of a secondary structure that could lead to lower selectivity and higher hemolytic activity. Thus, by screening physicochemical properties necessary for antibacterial activity, Mor et al. identified optimal parameters for minimal inhibitory concentrations against

different pathogens independently of the amino-acid sequence: for example a membrane disruptor against *E. coli* would require 50 % ± 2 % hydrophobicity and 6.5 ± 2 positive charges (Radzishevsky *et al.*, 2008). Hemolytic activity, however, was strongly linked to the presence of secondary structure. Disordered OAKs with butyl- and octyl- acyl moieties had hemolytic activities above 100 times the MIC hence presenting a certain advantage over natural dermaseptin (Radzishevsky *et al.*, 2007). To contrast, longer acyl chains (>11 carbon atoms) presented higher flexibility, spontaneous aggregation and formation of amphipathic structures perturbing the membrane of red blood cells.

The most potent OAK to date, $C_{12}K\text{-}7\alpha_8$ (MIC: 3.1 μg/mL against *E. coli*, **Figure 1.13B**) disrupts the cytoplasmic membrane (Rotem *et al.*, 2008, Epand *et al.*, 2008, Radzishevsky *et al.*, 2007) and has the ability to act synergistically with traditional antibiotics, raising the sensitivity of MDR bacteria (Livne *et al.*, 2010). Shorter peptidomimetics such as C12(ω7)K-β12 (**Figure 1.13C**) were also active, but the mode of action was different from longer OAKs with a bacteriostatic effect (Sarig *et al.*, 2010) unlike most AMPs which are bactericidal. In fact, a single broad-spectrum OAK might present several distinct antibacterial mechanisms, depending on the pathogen species and strain. Against two different strains of *E. coli*, C16(ω7)K-β12 (similar to C12(ω7)K-β12 but with 4 extra carbons on the N-terminal acyl chain) acted differently by triggering cell death through membrane depolarization or by impeding biosynthesis through directly binding DNA (Sarig *et al.*, 2011).

Different modes of action for different OAKs also imply that different bacterial resistance mechanisms were triggered. Against gram-negative pathogens, $C_{12}K\text{-}7\alpha_8$ was not affected by efflux pumps, while C12(ω7)K-β12 reportedly acted as a substrate of these pumps and its bacterial activity was consequently limited (Goldberg *et al.*, 2013). However, C12(ω7)K-β12 was still efficacious *in vitro* and *in vivo* against gram-negative bacteria when used synergistically with another antibiotic substrate of efflux pumps, such as erythromycin (Goldberg *et al.*, 2013). Finally, C12(ω7)K-β12 also restored sensitivity of selected MRSA strains when used in combination with traditional antibiotics (Kaneti *et al.*, 2013). A suggested mechanism for this restored sensitivity involved membrane depolarization by the OAK, thus facilitating entry of traditional compounds such as oxacillin. Importantly, this facilitated entry occurred without activation of membrane-bound proteins triggering antibiotic resistance pathways (in the case of oxacillin the β-lactamase receptor).

In summary, this drug design approach allowed exquisite optimization of the physicochemical properties from AMPs to bind bacterial membranes through the addition of acyl moieties to a poly-lysine chain. Moreover, shortening the length of the acyl side chains impeded formation of secondary structure and consequently hemolytic activity and toxicity. OAKs possess different modes of action depending on the targeted pathogenic species, therefore the horizontal transfer of DNA coding for OAK resistance might not transfer the resistance to other pathogenic strains. OAKs also show great promise when synergistically used with traditional scaffolds to restore antibacterial activity.

I.3.6 Mimicking ß-hairpin structures: lipposaccharide transport inhibitors

Peptidomimetic substitutes for a polypeptide sequence that can also mimic their secondary structure conformation can be valuable for targeting protein-protein interactions (PPI). Consequently, there has been a great deal of effort focused on turn, helix and strand mimetics. For example, antimicrobial β-hairpin mimetics have been developed through an approach called Protein Epitope Mimetic (PEM). Protegrin I, a mammalian broad-spectrum and membrane-disrupting AMP (Kokryakov *et al.*, 1993), presents a typical ß-hairpin motif though the formation of two disulfide bonds (**Figure 1.14A**). This scaffold was modified at the Swiss company Polyphor Ltd. into a macrocyclic peptidomimetic through the use of a stabilizing D-Pro-L-Pro motif (Shankaramma *et al.*, 2002, Robinson *et al.*, 2005) and optimized through iterative rounds of peptidomimetic library synthesis leading to the molecules POL7001 (**Figure 1.14B**) and POL7080 (structure not disclosed) (Srinivas *et al.*, 2010). A particular feature of these ß-hairpin mimetics is the much-improved resistance to proteolysis by substitution of the Lys/Arg residues by diaminobutyric acid. The resulting molecules showed significantly enhanced minimal inhibitory concentrations (MIC = 0.008 µg/mL) compared with the original AMP protegrin I (MIC = 0.5 µg/mL) (Steinberg *et al.*, 1997).

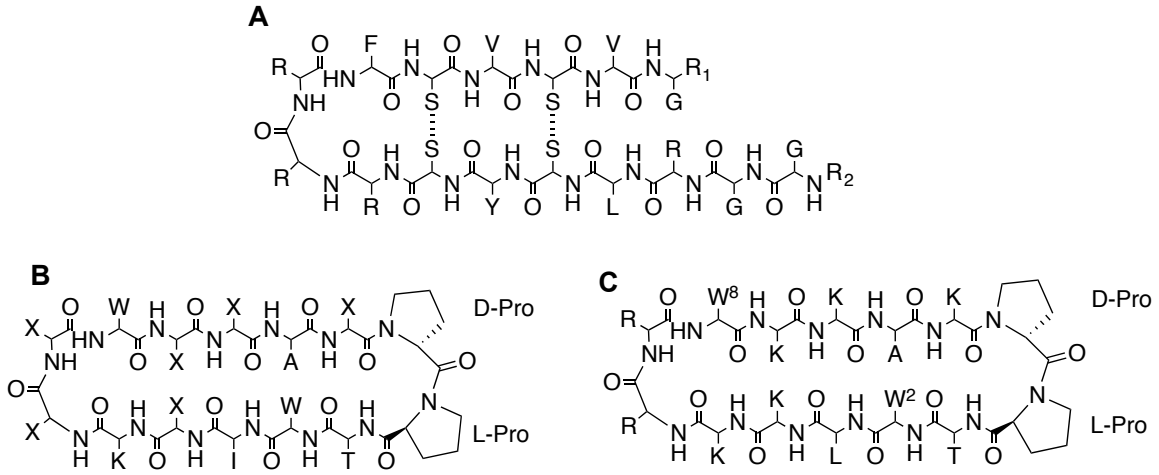

Figure 1.14. ***β-Hairpin peptidomimetics that bind to membrane lipopolysaccharides.*** ***A.*** *Natural AMP Protegrin-I forming a β-hairpin through the formation of two disulfide bridges.* ***B.*** *Structure of POL7001: the cyclic L-Pro-D-Pro motif stabilizes a structurally similar β-hairpin conformation to give a peptidomimetic scaffold with membrane disrupting activity.* ***C.*** *Structure of L27-11, showing that only W^2 and W^8 are essential for LptD binding. Consequently other residue positions might be improved to increase other properties such as stability or bioavaliability. Amino acids are represented by their one-letter-code and X = diaminobutyric acid. Modified from (Srinivas et al., 2010)*

A consequence of their ß-hairpin structures was a more focused targeting of *Pseudomonas* strains and the discovery of a novel target, LptD. Protegrin I forms pores in the bacterial membrane, whereas bacterial lysis is much slower when using ß-hairpin peptidomimetics. Sequencing of *Pseudomonas* strain genomes selected for resistance to POL7001 and POL7080 revealed mutations in the gene coding for LptD (Srinivas *et al.*, 2010), a membrane-bound protein involved in the assembly of lipopolysaccharides on the outer layer of the outer membrane of Gram-negative bacteria (Yuan *et al.*, 2013). To date the action of POL7001 and 7080 onto LptD remains unclear. For further investigation on the binding mechanism to LptD, a third peptidomimetic structure from the same series, L27-11 (**Figure 1.14C**) was analyzed by NMR spectroscopy and SAR by alanine scanning, proving that the β-hairpin conformation was essential for interaction with LptD (Schmidt *et al.*, 2013). Moreover, only two side chains (the indoles of tryptophan 2 and 8) were essential to retain strong antibacterial activity (Schmidt *et al.*, 2013), hence leaving 10 amino acid sidechains free for further improvements.

POL7001 and POL7080 demonstrated significant antibacterial activity *in vivo* with dose-dependent acceleration of infection clearance in mice (Srinivas *et al.*, 2010). POL7080 completed

phase I clinical trials in March 2013 for treating bacterial infections caused by *Pseudomonas aeruginosa* and Polyphor Ltd. was licensed to Roche in November 2013 for further clinical trials.

These macrocyclic peptidomimetics are able to retain a secondary structure from the original AMP that was essential for antibacterial activity, but stability was not the only parameter improved. The MIC was significantly lowered whereas the targeted pathogenic spectrum substantially narrowed to *Pseudomonas* strains. These ß-hairpin mimetics are aimed at a new membrane target, LptD, with a mode of action yet to be defined. Moreover, the recent finding that only two side chains are essential for this interaction allows a high level of scope for further modifications without altering the backbone that maintains the essential β-hairpin conformation.

I.3.7 Identifying a novel antibacterial mode of action: arylamides

Simple modifications such as β-peptides (Liu & DeGrado, 2001, Porter *et al.*, 2000) and self-assembling cyclic peptides (Fernandez-Lopez *et al.*, 2001) are sufficient to provide resistance against peptidases, while conserving broad-spectrum antibacterial efficacy. However, these are more costly to manufacture than simple peptides, especially when based around long peptide leads with multistep syntheses in large scale.

Tew et al. chose a peptidomimetic approach to develop short, less expensive and synthesis-friendly polymers based on natural AMPs that retain the antibacterial activity of longer peptides. From the common properties of cationic AMPs, an amphiphilic structure and a global positive charge, they developed a series of rigid arylamide polymers (Tew *et al.*, 2002). Computational analysis based on crystal structures and molecular dynamics were used to determine the optimal length and torsion angles of the initial scaffold (**Figure 1.15A**). This arylamide scaffold, here named Aryl1, was easy to synthesize, presented a hydrophilic side chain able to bind negatively charged membrane-bound lipids and a rigid hydrophobic core able to insert within the bilayer and induce lethal leaking. These arylamide peptidomimetics were effective against different pathogens (MIC < 25 μg/mL for several strains of *E. coli* for example), although they also exhibited high hemolytic activity. SAR studies aimed at reducing toxicity led to the discovery that selectivity of arylamides towards bacterial membranes depended mostly on the amphiphilicity of the compound but was not related to antimicrobial activity (Liu *et al.*, 2004).

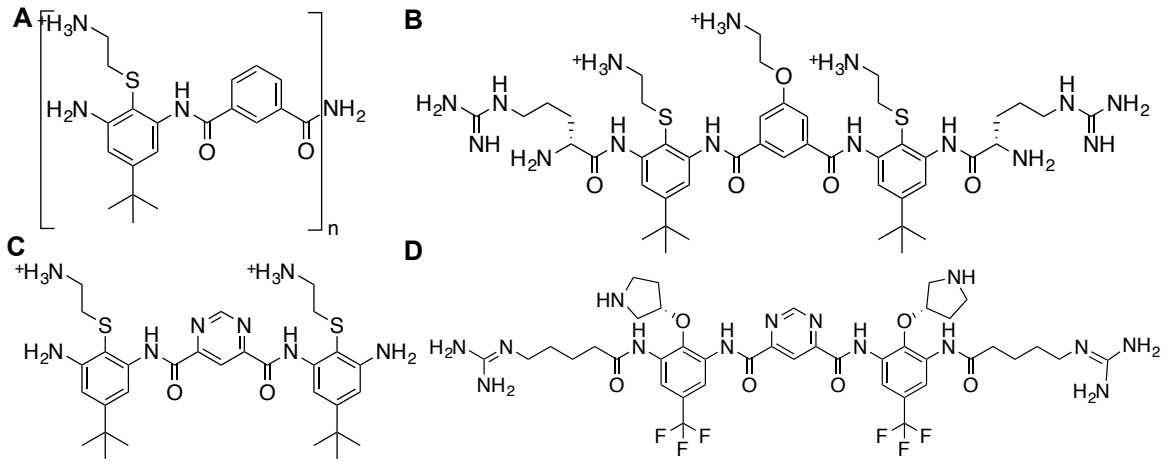

Figure 1.15. Arylamide peptidomimetics. ***A.*** *Aryl1: basic scaffold for polymeric arylamide-based AMP mimics.* ***B.*** *Aryl2: combination of hydrophobic (benzene rings and tert-butyl groups) and hydrophilic (arginine and aminoalkyl substituents) properties led to this highly selective and potent membrane disruptor.* ***C.*** *Rigidification of the scaffold here with pyrimidine moieties increased antibacterial activity by 10-fold compared to Aryl2-based compounds.* ***D.*** *PMX-30063, which achieved Phase IIa in clinical trials. Modified from (Tang et al., 2006, Liu et al., 2004, Tew et al., 2002)*

From this study, an extended arylamide (Aryl2, **Figure 1.15B**) was found to retain a similar bacterial activity to Aryl1 compounds, but with reduced hemolytic activity (500-fold lower than the bactericidal MIC) due to the arginine groups on each terminus and the aminoalkyl substituent on the central ring. Further studies linked antibacterial activity with the structural conformation; interestingly the more rigid core structure had more potent antibacterial activity (Choi *et al.*, 2009). For instance, introduction of pyrimidine moieties replacing the central benzene ring rigidified the backbone through additional intramolecular hydrogen bonds and induced a ten-fold improvement in antibacterial activity (compared to compounds based on Aryl2) with MIC 0.8 μg/mL (Tang *et al.*, 2006) against *E. coli* (**Figure 1.15C**). Preliminary infection models in mice showed the potency of another pyrimidine arylamer peptidomimetics to be almost comparable to vancomycin (Choi *et al.*, 2009). Moreover, bacteria did not develop effective resistance against selected lead compounds from the SAR after 17 passages (Scott *et al.*, 2008). This reinforced a controversial notion that it may be more difficult for bacteria to develop resistance to AMPs due to the absence of a specific target, and the requirement for a major change to the membrane composition (Zasloff, 2002).

An intriguing property was the strikingly different mode of action from those reported for natural AMPs. The lead peptidomimetic PMX30016 did not induce a significant physical disruption of the membrane, with NMR data suggesting that it penetrated into the membrane bilayer by

insertion between the lipid headgroup and the acyl chains (Su *et al.*, 2010). It was then thought to rotate to induce a change in the electric potential of the membrane, leading to dramatically increased permeabilization and cell death. Consistent with this hypothesis, two novel arylamide compounds from different SAR studies, PMX 10070 and PMX 10072, were shown to induce defects in the translocating mechanisms by dissipating the electrochemical potential across the membrane leading to a greater permeabilization to ions (Mensa *et al.*, 2011). Finally, the lead peptidomimetic PMX-30063 (**Figure 1.15D**) developed by the now defunct Polymedix company under the name Briladicin completed phase IIa clinical trials in early 2013, showing high antibacterial activity against MRSA.

By investigating a cheaper alternative to AMP synthesis, DeGrado et al. have developed peptidomimetic polymers that increased antibacterial activity and also identified a novel mode of action for AMPs. These discoveries led to a peptidomimetic that reached phase IIb clinical trials against MRSA. This success suggested that peptidomimetic development might generate stable AMP analogues with novel modes of action. The lack of resistance development against these arylamide peptidomimetics to date, possibly due to the novel mechanism, is a consequent milestone in the strategy that *de novo* peptidomimetics can provide better scaffolds to transform the actual antibiotic pipeline.

I.3.8 De novo scaffold: design of pilicides and curlicides

Inhibiting adherence of pathogenic bacteria to host cells is another potential way to fight infection (Stephens & Shapiro, 1997). The pili formation process has been highlighted as a mechanism to target in order to limit bacterial motility and pattern recognition on the surface of host cells (Waksman & Hultgren, 2009). Pili have also been demonstrated as essential for the formation of biofilms, involved in colonization of host tissues and medical devices and in antibiotic resistance (Anderson *et al.*, 2003). Pili formation involves thousands of proteins including two highly conserved adhesins PapG and FimH located at the very tip on the pilus (Kuehn *et al.*, 1993). Pili assembly requires translocation of these adhesins to the periplasm by two chaperones PapD and FlimC. Peptidomimetics are particularly suitable candidates for the inhibition of the specific PPI between adhesins and chaperones that can be a promising target for antibacterial development.

Initial screening of peptide binding using enzyme-linked immunoabsorbant assay (ELISA) and NMR revealed that the C-terminal sequence of PapG (^{307}MTMVLSFP^{314}, **Figure 1.16A**) inhibited PapG-PapD complex formation (Karlsson *et al.*, 1998). A 3.0 Å resolution PapD-PapG$^{307-314}$ complex crystal structure allowed the development of two peptidomimetic scaffolds using computational docking and surface plasmon resonance (Svensson *et al.*, 2001). The first scaffold retained a peptide backbone and had non-natural side chains (**Figure 1.16B**), whereas the second incorporated a 2-pyridinone scaffold (**Figure 1.16C**, Amino methylated 2-pyridinone - Patent # US7915417).

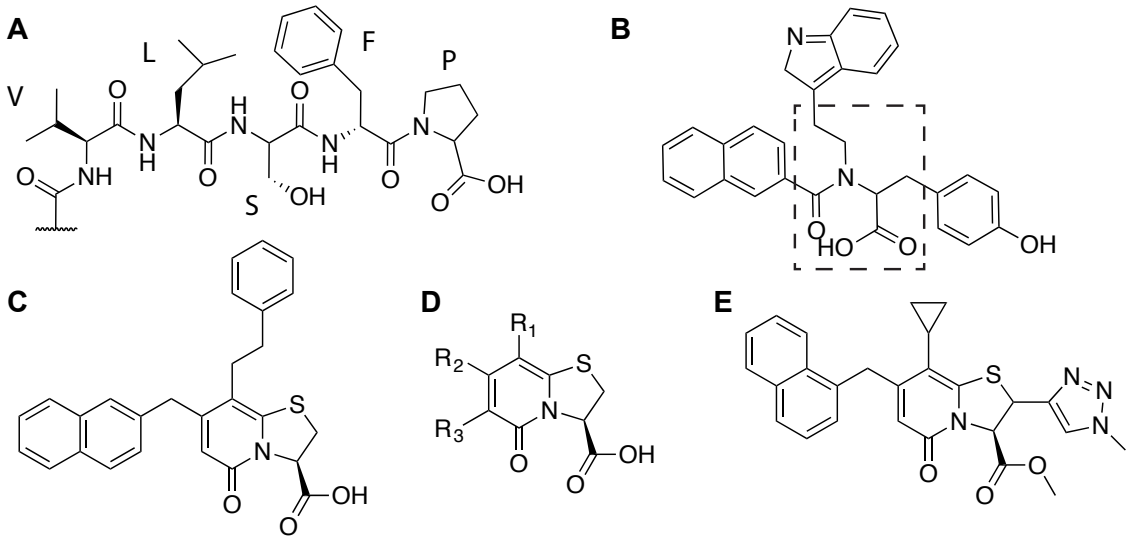

Figure 1.16. ***Structure of pilicide peptidomimetics from PapG C-terminal sequence. A.*** *Sequence VLSFP of the PapG C-terminal tail binding to PapD.* ***B.*** *First peptidomimetic design based on the PapG C-terminus, with the peptide backbone conserved (highlighted with the dashed square). The Pro314 ring was opened with indol and phenol moieties to improve binding to PapD.* ***C.*** *Second approach for peptidomimetics based on a 2-pyridinone scaffold binding to PapD.* ***D.*** *Core pyridinone scaffold for peptidomimetic development.* ***E.*** *Example of pyridinone peptidomimetic including a triazole function. Modified from (Bengtsson et al., 2012, Svensson et al., 2001, Karlsson et al., 1998, Pemberton et al., 2004).*

An innovative method for the high-throughput synthesis of 2-pyridinone scaffolds, allowed the exploration of different functional groups on the 2-pyridinone ring (**Figure 1.16D**). Position R1 and R2 favored aromatic groups and surface plasmon resonance evaluation suggested that position R2 played a large part in the specificity of binding to PapD (Chorell *et al.*, 2011, Emtenas *et al.*, 2002, Emtenas *et al.*, 2003). The importance of the pyridinone ring was illustrated by the dramatic loss of activity when the ring was opened (Berg *et al.*, 2008) or the sulfide replaced by amine or oxygen atoms (Berg *et al.*, 2008). However, adding aryl groups on the pyridone ring improved the

affinity of the compounds to give low micromolar potencies (Chorell *et al.*, 2010), as did incorporating other heterocycles such as triazoles (Bengtsson *et al.*, 2012) (**Figure 1.16E**). Likewise, the carboxylic acid scaffold on the pyridone ring, originating from mimicking the original peptides, was important for binding because replacing this group resulted in loss in activity (Aberg *et al.*, 2005). A new synthetic method allowed the exploitation of position R3 for refining solubility (Pemberton *et al.*, 2004) and bioavailability. Extensive work on position R3 to extend toward di- and tri- peptide mimetics resulted in an increased affinity towards PapD but a reduction in inhibition of pili formation (Berg *et al.*, 2006, Aberg & Almqvist, 2007).

Interestingly, NMR studies of peptidomimetics such as 6C and 6E showed three different binding locations on FlimC (Hedenstrom *et al.*, 2005), all leading to a defect in pili formation by preventing correct folding of the chaperone or by interfering directly with the protein-protein interaction with FimH. These compounds successfully inhibited pili and curli (another bacterial fiber (Barnhart & Chapman, 2006)) formation (Cegelski *et al.*, 2009, Chorell *et al.*, 2012). No clinical or *in vivo* data appear to have yet been released regarding therapeutic efficiency (Barber *et al.*, 2013).

These pilicides based on 2-pyridinone scaffolds demonstrate how peptidomimetics can be used for the design of an entirely *de novo* mode of action. Indeed, no natural product has ever been found to specifically inhibit the formation of pili and curli to date. The versatility of peptidomimetics allowed retention of the essential binding components from the initial protein sequence involved in the PPI and rational design allowed non-peptidic optimization of the backbone and the remaining positions on the 2-pyridinone scaffold.

I.3.9 Peptidomimetics with indirect antimicrobial activity: efflux pump inhibitors

Because of their ability to mimic PPI, peptidomimetics can also be used for limiting resistance mechanisms by recovering the sensitivity of MDR pathogenic strains to traditional antibiotic drugs. An interesting example is the development of peptidomimetics targeting the efflux pumps in *Pseudomonas aeruginosa*, largely responsible for antibiotic resistance by expelling compounds out of the cytoplasm (Livermore, 2002, Piddock, 2006, Schweizer, 2003). Neutralizing

efflux pumps has been identified as a promising approach to restore antibiotic activity (Mahamoud *et al.*, 2007).

A screening study by Renau et al. to discover a scaffold that restored fluoroquinolone activity, particularly for levofloxacin, singled out a phenylalanine-arginyl β-naphthylamide dipeptide (MC-207,110, **Figure 1.17A**) that was able to lower the MIC of levofloxacin (MIC = 2.5 µg/mL) (Renau *et al.*, 1999, Lomovskaya & Watkins, 2001). This property was shown against a large range of pathogenic strains, promising broad-spectrum activity for an antibiotic cocktail. Nevertheless, the initial investigation of a series of derived peptides suggested that instability in serum was a major issue. This was solved by the use of peptidomimetics composed of D-amino-acids and non-natural side chains (homophenylalanine for phenylalanine, ornithine instead of arginine) and by swapping side chain positions (MC-002-595, **Figure 1.17B**) (Renau *et al.*, 2001).

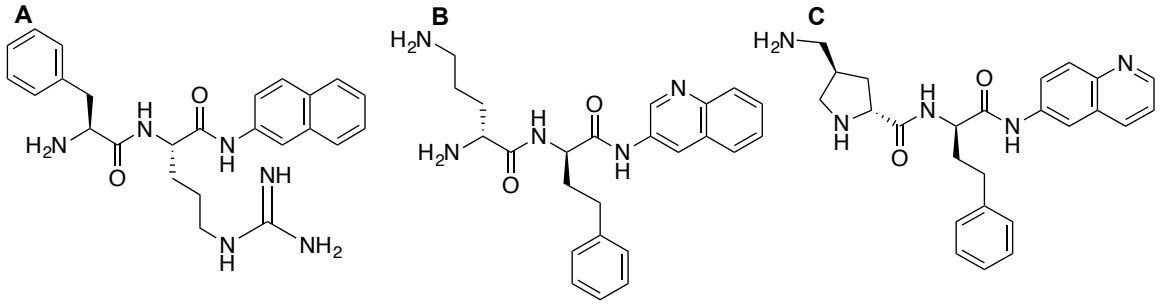

Figure 1.17. ***Peptidomimetic inhibitors of efflux pumps in Pseudomonas aeruginosa. A.*** *phenylalanine-arginyl β-naphthylamide dipeptide MC-207,110.* ***B.*** *Swapping side chain positions and replacing with non-natural residues such as ornithine for arginine and homophenylalanine for phenylalanine in MC-002,595 provided improved serum stability.* ***C.*** *Cyclization of the toxic ornithine function led to lower hemolytic activity for MC-04,124*. Modified from (Renau *et al.*, 2003, Renau *et al.*, 2001, Renau *et al.*, 1999)

Throughout animal studies, MC-002,595 proved to be stable but also highly toxic due to the presence of the ornithine group. Cyclization of the residue provided a peptidomimetic molecule with similar potency (5 µg/mL enhanced MIC of levoflaxin by 8-fold) and lower toxicity (MC04,124, **Figure 1.17C**) (Renau *et al.*, 2003). It was reported that these inhibitors behave as efflux pump substrates and trigger competitive binding with antibiotics. The efflux pumps expelled peptidomimetics and the traditional antibiotics remained in the cytoplasm and disrupted essential pathways (Lomovskaya & Bostian, 2006). A considerable advantage is that the efflux pump mechanism is not altered, thus unlikely to trigger adaptive resistance by modification of the pump mode of action. However, the relatively low affinity and specificity of the peptidomimetic to the

efflux pump led to the requirement for higher doses to produce substantial activity *in vivo*, thus resulting in higher toxicity. Consequently, this first series of efflux pump inhibitors did not enter clinical trials.

Efflux pump inhibitors are interesting examples of peptidomimetic compounds that do not have direct antimicrobial activity, but are used for their peptide-mimicking properties to compete against resistance mechanisms. If used in a cocktail with traditional antibiotics, they are expected to increase the duration of drug efficacy (Kourtesi *et al.*, 2013).

I.3.10 Improving membrane permeation and bioavailability: glucosamine-6-phosphate synthase inhibitors.

Peptides have high membrane permeation rates enabling access to different cellular compartments. In the case of glucosamine-6-phosphate synthase inhibitors, peptidomimetics helped improve permeation by allowing inhibitors to reach their targeted cellular compartment. Glucosamine-6-phosphate synthase is essential in the initial steps of the peptidoglycan synthesis, crucial for the bacterial cell wall (Milewski, 2002). Analogues of the glutamine substrate, such as N^3-(4-methoxyfumaroyl)-L-2,3-diaminopropanoic acid (FMDP, **Figure 1.18A**), have been reported as selective inhibitors *in vitro* (IC_{50} 15 μM, *Salmonella typhimurium*) (Andruszkiewicz *et al.*, 1986, Chmara *et al.*, 1986). It binds to the active site cysteine in the enzymatic substrate-binding site, but this potential is nullified in whole cells due to the very poor permeation. By combining FMDP with a transporter peptide, thus forming a peptidomimetic molecule, the FMDP-peptide molecule is transported into the cytoplasm via permeases, before release of the FMDP "warhead" through cleavage by a peptidase (Chmara *et al.*, 1998, Andruszkiewicz *et al.*, 1987). This way, FMDP dipeptides combining residues Met, Ala, Leu, Nva (norvaline) or Nle (norleucine) demonstrated MIC as low as 0.4 μg/mL (**Figure 1.18B** and **1.18C**) against whole bacterial cells (compared to no inhibition detected using FMDP alone) (Chmara *et al.*, 1998).

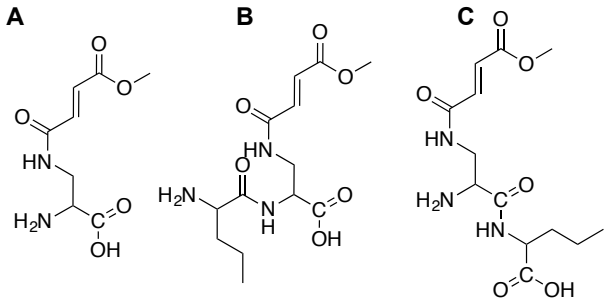

Figure 1.18*. Peptidomimetic inhibitors of glucosamine-6-phosphate synthase.** ***A. *N^3-(4-methoxyfumaroyl)-L-2,3-diaminopropanoic acid (FMDP) is an analogue of glucosamine-6-phosphate synthase substrates featuring inhibitory activity but unable to cross membranes.* ***B.*** *Graft of a norvaline residue onto FMDP allowed translocation into the cytoplasm through binding to the Opp permease and inducing in vivo antibacterial activity.* ***C.*** *Graft of the norvaline group onto the carboxylic acid end of FMDP also led to translocation but with substantially lower antibacterial activity.*

FMDP dipeptides possess inhibitory potential against various pathogenic species (*Escherichia coli, Staphylococcus aureus, Bacillus subtilis*). The position of the peptide residue was also vital, with a substantial increase in activity when linked to the N-terminus rather than the C-terminus of FMDP. Parallel progress in peptide transporters studies reported conformational features, such as backbone torsions and angles, necessary for recognition by permeases Dpp, Opp or Tpp. Molecular modelling of the different active FMDP dipeptides and comparison with typical permease peptide substrates directly correlated the antibacterial activity of a peptidomimetic with the proportion of features favorably recognized by transporter proteins, such as terminal charges, backbone torsion angles and chirality (Marshall *et al.*, 2003). A higher percentage of conformers matching these properties common to natural permease substrates resulted in higher antibacterial activity for the FMDP dipeptides. Moreover, the choice made for the peptide residue linked to FMDP, altering the backbone torsion of the peptidomimetic in different conformers, greatly influenced the permease responsible for transportation in the cytoplasm. The different lowest energy conformations of Tyr-FMDP, Lys-FMDP and Nva-FMDP influenced recognition and transportation by different permeases Dpp, Tpp and Opp, respectively.

This approach presented another alternative for the use of peptides for indirect improvement of antimicrobial potency. The data showed that the rational addition of a single amino acid could greatly facilitate transport of a small non-peptide inhibitor to the cytoplasm. Moreover, the choice of this single residue directly influenced the permeation mechanism through different conformations. This is a feature that could improve pharmacokinetics and bioavailability for a large array of inhibitors with limited membrane permeability.

I.4 Discussion

The DsbA/DsbB interaction, being part of a hub for the maturation of multiple virulence factors, is a promising and exciting new target for developing inhibitors limiting the appearance of resistance. However, while the disulfide bond exchange mechanism has been thoroughly described and reported in the literature, information about the structural features of the interaction itself are still scarce. The only structures available of the EcDsbA/EcDsbB complex presented a resolution of 3.7 Å, this limiting the possibilities for virtual tools that are usually a vital part of screening methods to identify inhibitory scaffolds and new ligands. Therefore, my PhD consisted in clarifying the mechanism underlying the interaction and to provide better structural insight. For this purpose, the design of peptides and peptidomimetics seemed an appropriate strategy to begin the EcDsbA inhibitor design program, and potentially develop molecules similar to AMPs.

Antimicrobial AMPs are a natural reservoir of antibacterial compounds – broad-spectrum and narrow-spectrum – that has not revealed its full potential yet, as new sequences and novel modes of action are still being identified. Nevertheless, from 2,000 described AMP molecules to date 10 peptides are undergoing clinical trials in different stages as of 2013 (Fox, 2013). Weaknesses of AMPs as drug candidates are now well known, including notably poor stability in serum and high toxicity, and the growing field of peptidomimetics is beginning to overcome some of these drawbacks. Far from only improving stability, selectivity and pharmacokinetics, peptidomimetics have also helped to discover new classes of antibiotics with scaffolds and modes of action quite different from the original AMPs, as exemplified above. The peptidomimetic concept also presents advantages for non-peptide antimicrobial compounds, with the example of glucosamine-6-phosphate synthase inhibitors now able to reach their cytoplasmic target and induce an antibacterial effect *in vivo*. To further broaden the possibilities, the development of non-antibacterial peptidomimetics targeting existing specific mechanisms such as efflux pump inhibitors might be fruitful when used to complement antibiotic cocktails to recover sensitivity in MDR pathogenic strains. Additionally, the development of peptidomimetics, contrary to the traditional antibiotic pipeline, has taken advantage of the tremendous technologic progress of the past few decades (high-throughput screening, computational docking and modelling, etc). The medical world might be lagging behind MDR strains in the race between treatments and drug resistance, but peptidomimetics might be the toolbox that will bring the antibiotic pipeline back on track.

The inhibition of the EcDsA-EcDsbB interaction is suitable to a peptidomimetic approach. The EcDsbA/EcDsbB complex is located in the periplasm, which is easily accessible by peptides and peptidomimetics. It is a specific protein-protein interaction that can possibly be mimicked best by a peptide providing similar properties in terms of charges, hydrophobicity and conformation as the EcDsbB loop. As described above, peptides present weaknesses that can be overcome by the transformation into peptidomimetics. Therefore, if an EcDsbB loop mimic peptide could benefit from the array of improvement available to peptidomimetics, it might be possible to develop a potent, stable and specific antivirulence scaffold inhibiting the bacterial oxidative folding.

I.5 Goals of this PhD

The overall aim of this PhD is to develop peptides and peptidomimetic ligands for the EcDsbB-binding site on the EcDsbA surface. The goal was to generate compounds competing with the EcDsbB periplasmic loop P2. The strategy behind this competition is to block the regeneration of EcDsbA in the oxidized active state, thus accumulating EcDsbA in a reduced state unable to fold virulence factors. Impeding this virulence pathway is predicted to lead to attenuated bacterial strains, unable to spread infection but still viable hence limiting drug resistance. To achieve this aim I had to develop robust tools to synthesize, screen and evaluate such peptides and peptidomimetics to design the most potent scaffold. Consequently, the specific aims of this PhD are:

(1) To assess and develop a robust *in vitro* screening pipeline including differential scanning fluorimetry, isothermal titration calorimetry, surface plasmon resonance and model substrate oxidation assays to characterize the binding affinity and DsbA inhibitory activity of synthesized molecules. This aim is addressed in chapter II.

(2) To create and enrich a database of peptide sequences binding to the *E. coli* EcDsbA groove ideally with a sub-micromolar affinity. This was to be done by identifying the key residues and properties to develop an optimal sequence. This aim is addressed in chapter III.

(3) To use biophysical methods such as soaking, cocrystallisation or NMR with the peptide/protein or peptidomimetic/protein complexes and solve the structures to characterize the interactions. This aim is addressed in chapter IV.

(4) To use these optimal peptide sequences to develop peptidomimetics that increase affinity, specificity, stability and bioavailability, potentially leading to a novel antibacterial scaffold. This aim is addressed in chapter V.

Finally, an overview of the outcome of this PhD is presented, along with discussion of the main data and future directions are suggested for the next steps to undertake in the development of an antivirulence drug.

CHAPTER II

Assembly and optimization of a screening pipeline to detect peptides that bind to EcDsbA

II.1 Overview of the screening pipeline

Rational drug discovery, in a similar fashion to traditional methods in drug design, requires a robust screening pipeline with which to evaluate the potency of new scaffolds towards the target of interest (Anderson, 2003, Mandal *et al.*, 2009). In the early stages of development, potential inhibitors can be ranked according to affinity, activity, and kinetic and thermodynamic specificities of binding (Keseru & Makara, 2006). Concurrent structural characterization through structural biology techniques such as crystallography and nuclear magnetic resonance (NMR) can shed light on the ligand binding mode and guide future optimization of the scaffold (Verlinde & Hol, 1994). Once a potent *in vitro* inhibitor scaffold has been identified, optimization focuses initially on the selectivity for the target and long-term stability, and later on potency, toxicity and bioavailability *in vivo*.

An important goal of my PhD was to set up robust binding assays that would enable the detection of the binding and the characterization of novel scaffolds. I opted not to include high-throughput screening of existing compound libraries but rather to focus on the rational design of peptides and peptidomimetics from existing biological and structural data. Therefore, a pipeline that enabled accurate detection of binding of compounds was favored over one that focused on a high rate of compound library screening. Ideally each tested compound would provide additional information, either biochemical or structural, that would inform the design of the next molecule in the series, enabling the iterative development of a final potent compound, or 'hit', suited to the inhibition of EcDsbA. As reported in the previous chapter, the starting point of this PhD was the 3.7 Å resolution EcDsbA-EcDsbB complex crystal structure (Inaba *et al.*, 2009a), using the EcDsbB loop bound to the EcDsbA groove to design the first peptide sequence. We hypothesized that this peptide would bind to EcDsbA and the optimization of the sequence would lead to a potent peptide or peptidomimetic with EcDsbA inhibitor activity that could be later tested *in vivo*.

The pipeline itself was designed to make use of the instrumentation available within the Institute for Molecular Bioscience. A flow chart for the ideal pipeline is shown (**Figure 2.1**).

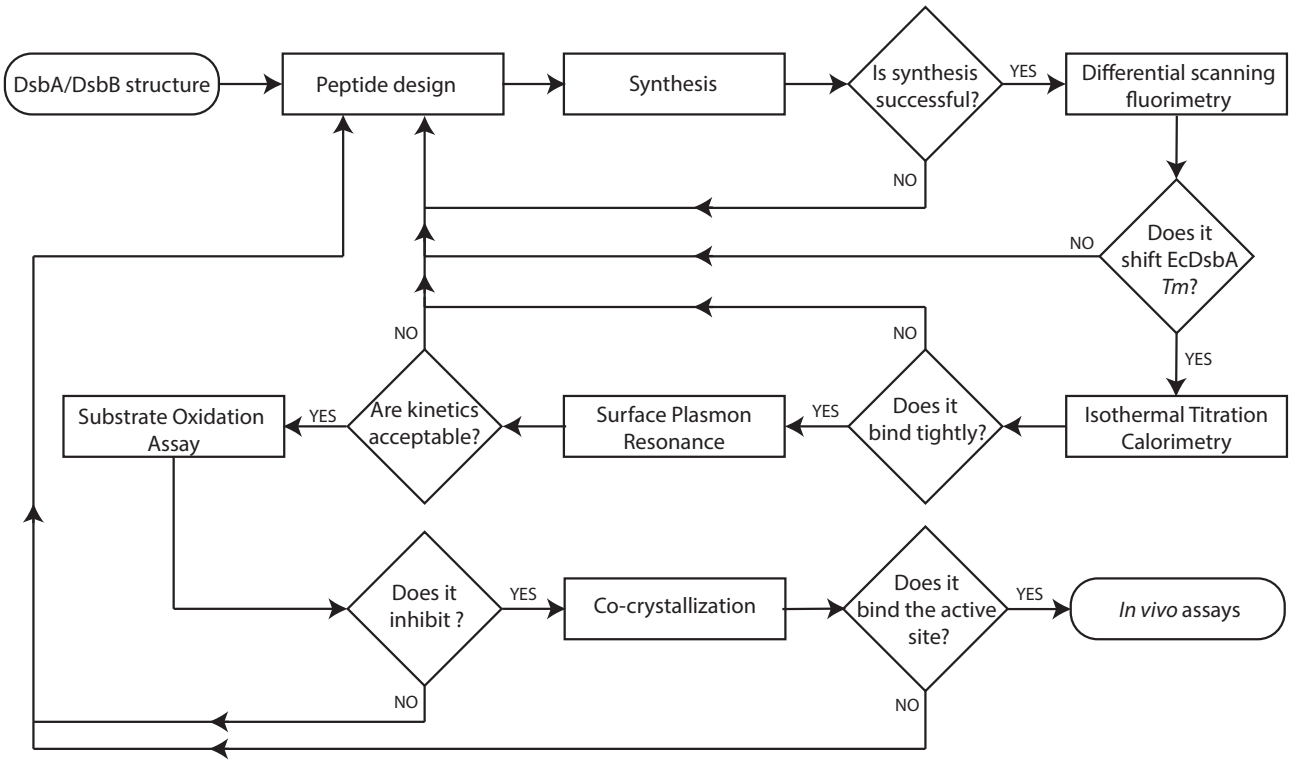

Figure 2.1. ***Flow chart of the screening pipeline for the design and evaluation of inhibitors of EcDsbA.*** *The pipeline includes three binding assays, one activity assay and structural biology experiments to characterize peptides in terms of binding affinity, thermodynamic and kinetic binding parameters, inhibitory activity and binding mode. Tm represents the melting temperature of EcDbsA.*

The design of the initial peptide sequence was based on available crystal structures. Virtual tools - such as docking experiments - were not included because of the difficulty of accurately predicting both the binding site on EcDsbA and the conformation of ≥7mer peptides due to the large number of rotatable bonds (Aloy & Russell, 2006, Gray, 2006). Only very recently specialized tools have been developed for peptide folding and docking (Raveh *et al.*, 2011, Audie & Swanson, 2013). Synthesis and purification of peptides were performed manually within the chemistry laboratory of co-supervisor Prof. David P. Fairlie. The first assay (differential scanning fluorimetry) was chosen because it is rapid and consumes small amounts of peptide and protein; it was intended to evaluate whether or not the peptide bound to EcDsbA by measuring changes in the EcDsbA melting temperature *Tm*. Non-binders, for which no significant shifts (< 0.2 ºC) in EcDsbA *Tm* were recorded, would not progress further. If concentration-dependent and significant shifts (> 0.2 ºC) were measured, then the peptide progressed through to the next step, Isothermal Titration Calorimetry (ITC). ITC provides an accurate measurement of the thermodynamics, including a *K*d value as well as enthalpy and entropy contributions. If the peptide had high affinity by ITC (*K*d <

50 μM) or improved affinity compared with previous molecules tested, surface plasmon resonance was to be used to confirm the affinity by an independent method and to provide kinetics of the binding reaction. If the kinetic rates were acceptable (10^3 $M^{-1}.s^{-1}$ < k_{on} < 10^9 $M^{-1}.s^{-1}$ and 10^{-6} s^{-1} < k_{off} < 1 s^{-1}, (Nunez *et al.*, 2012)), the peptide was then progressed through to an activity assay that monitored the oxidase activity of EcDsbA using a fluorescent synthetic substrate. Finally, if the peptide inhibited EcDsbA activity (IC_{50} < 50 μM), co-crystallization trials were set up to solve the structure of the EcDsbA-peptide complex in order to map the peptide binding site and provide structural information about the binding mode. If any peptides or peptidomimetics became a 'hit', then its potency was to be tested using *in vivo* assays, but this was beyond the scope of the work reported.

Overall, this pipeline provided two independent affinity measurements, as well as kinetic and thermodynamic characterization, assessment of inhibitory activity and structural characterization of binding conformations. This chapter reports my efforts to establish and optimize these screening methods; the outcomes of the design and characterization of DsbA peptidic inhibitors are presented in chapters III, IV and V.

II.2 Experimental details of materials and methods for subsequent chapters

II.2.1 DsbA expression and production

The expression and purification of EcDsbA and variants for the entire Martin lab use was jointly performed by myself, Dr Maria Halili, Mrs Stephanie Tay and Mr Fabian Kurth. Dr Stephen Shouldice engineered wild type EcDsbA and GST-tagged constructs. Mr Fabian Kurth developed the optimized expression and purification protocol used in this section.

Wild type *E. coli DsbA* (GenBank® accession number X80762), without the sequence coding for the predicted signal sequence was cloned into a modified pMCSG7 (Midwest Center for Structural Genomics) vector for cytoplasmic expression. The sequence includes an N-terminal His_6 affinity-tag followed by a linker region containing a Tobacco Etch Virus (TEV) protease cleavage site. The EcDsbAC30S variant was generated from the wild type construct by Mr Fabian Kurth using the QuikChange® protocol (Agilent Technologies). The following primers were used to introduce the point mutation, FW- GTTTTTCTCTTTCTTCAGCCCGCACTGCTATCAG and

REV- CTGATAGCAGTGCGGGCTGAAGAAAGAGAAAAAC. Transformed BL21(DE3)pLys cells containing plasmids for either EcDsbA or EcDsbAC30S were grown in auto-induction media (Studier, 2005) in Erlenmeyer flasks for 16-20 h at 30ºC with a stirring speed of 220 rpm. After an initial centrifugation (10,000 rpm for 10 minutes at 4ºC, rotor JLA 10.500, Beckman Coulter), the bacterial pellet was resuspended in 25 mM Tris, 150 mM NaCl, 1:1000 protease inhibitor cocktail (BioPioneer Inc) and DNase (Roche). Lysis was executed using a Cell Disruptor (TS-Series, Constant Systems LTD) applying a constant pressure of 25 Kpsi. Cell debris was removed by centrifugation (18,500 rpm for 30 min at 4ºC, rotor JM-25.5, Beckman Coulter). Purification by metal ion affinity chromatography using TALON resin (Clontech) was used to bind His-tag EcDsbA, which was then eluted with a solution of 25 mM Tris, 150 mM NaCl and 200 mM imidazole (**Figure 2.2A**). The His_6 affinity tag was removed by TEV cleavage using a 1:50 w/w ratio protein/TEV-protease incubated in a 50 ml tube overnight at 4ºC, leaving the EcDsbA with two additional amino acids (S–1 and N0) at the N-terminus. Removal of any remaining tagged EcDsbA and TEV was performed by reverse metal ion affinity chromatography using TALON resin.

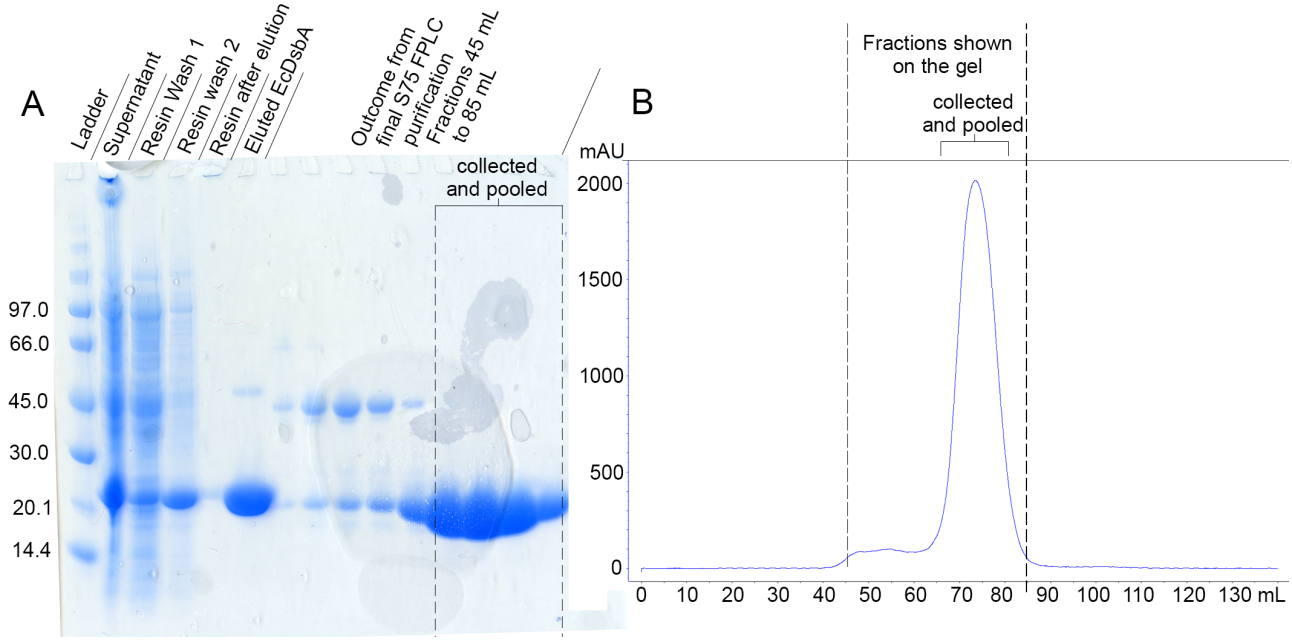

Figure 2.2. ***Purification profile of EcDsbA.*** ***A****. SDS-PAGE gel of samples collected during the purification process, leading to the collection of pure EcDsbA fractions for screening experiments. The bands oberseved at ≈42 kDa in five of the final FPLC fractions were likely EcDsbA dimers and were excluded from the final pooled fractions.* ***B****. Elution profile of EcDsbA during the final purification step using a FPLC Superdex 75 column. Fractions of 5 mL eluted from 45 mL to 85 mL between the dashed lines were injected into the gel in A and only fractions 65 mL to 85 mL were kept for binding experiments.*

A final size-exclusion chromatography step using a Superdex 75 16/60 column (GE Healthcare) injecting 5mL of concentrated protein in 25 mM Tris, 150 mM NaCl pH 7.4 that yielded high purity protein (≥ 95 %) verified by SDS-PAGE (**Figure 2.2B**). Protein was then concentrated and buffer exchanged into 25 mM HEPES, 150 mM NaCl pH 7.4. Quantitation was performed using a Nano-drop (thermo-Scientific) and revealed yields of 50-100mg of purified EcDsbA per liter of culture. EcDsbA was stored in 50 µL aliquots at 50 $mg.mL^{-1}$ at -80ºC. GST-EcDsbA was purified with the same protocol using a His-GST tagged construct, with the His-tag removed during purification.

Prior to all experiments, EcDsbA was fully oxidized or fully reduced by incubation with respectively 25-molar excess of copper(II)1,10-phenanthroline or dithiothreitol (DTT) for 60 minutes, followed by removal of the agent in a PD-10 desalting column (GE Healthcare). The redox state was confirmed by Ellman's assay (Aitken, 2009).

For substrate oxidation experiments *E. coli* DsbB (AAC74269) membrane extracts were prepared by Dr Halili as described previously (Bader *et al.*, 1998) and resuspended in phosphate buffered saline (PBS, 137 mM NaCl, 2.7 mM KCl, Na_2HPO_4 10 mM and KH_2PO_4, pH = 7.4) containing 10 % glycerol.

II.2.2 Peptide synthesis

Synthesis of all peptides reported in this thesis was performed using classic Solid Phase Peptide Synthesis (SPPS) on resin with Fmoc-protected (Fluoroenylmethyloxycarbonyl) amino acids (**Figure 2.3A**). Peptides were synthesized on rink-amide MBHA resin (p-methylbenzhydrylamine resin, ChemImpex International) with loading rates of 0.36 or 0.72 mmol/g. The resin initially presents an amine protected by a removable Fmoc protection group (**Figure 2.3B**).

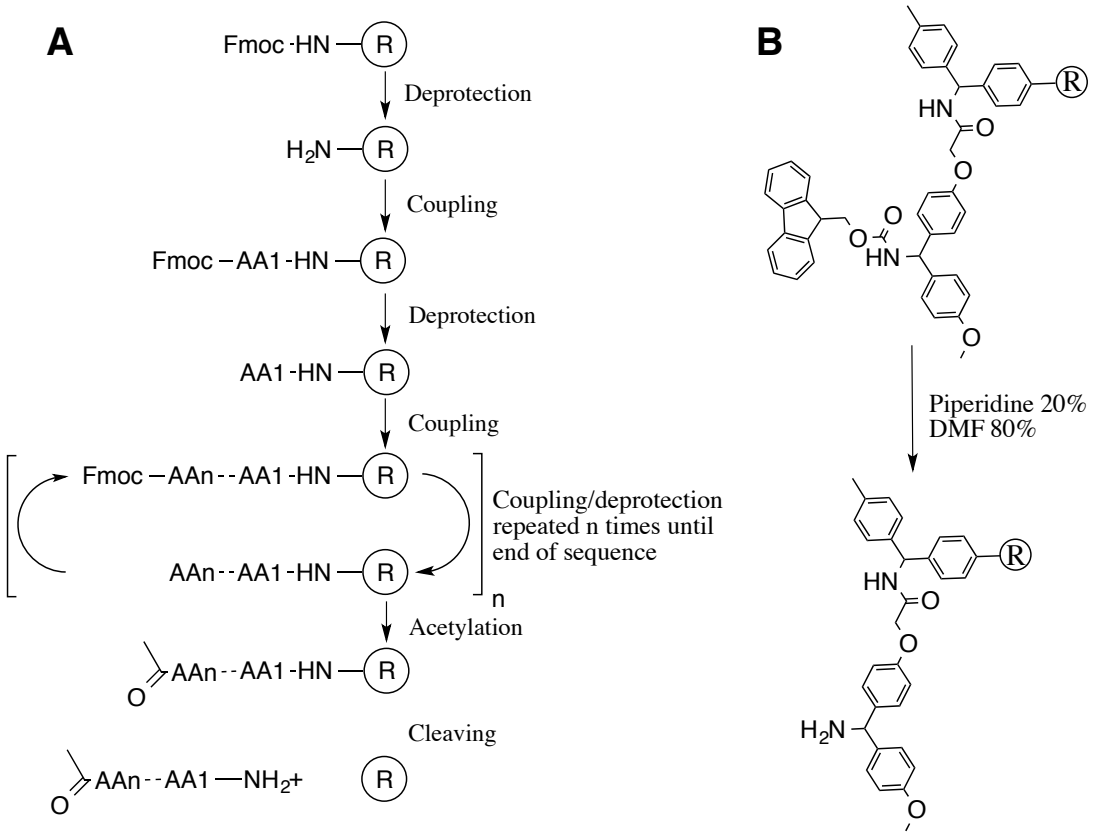

Figure 2.3. ***Schematic overview of the SPPS process.*** ***A****. Overview of the Fmoc-based solid phase peptide synthesis. Residues are coupled sequentially onto the resin with deprotection steps in between to remove the Fmoc group protecting the N-terminal amine, hence allowing the following residue's carboxylic acid to react. AAn = Amino Acid number n.* ***B.*** *Structure of the MBHA rink-amide resin, with the necessary removal of the Fmoc protection group to begin synthesis.*

After swelling the dry resin in Dimethylformamide (DMF, Rci Labscan) for 15 minutes, the Fmoc protection group was removed according to the mechanism shown in **Figure 2.4A** in the presence of an excess of piperidine. This step was performed twice (5 min incubation time) separated by thorough DMF washing. The resin was then activated and ready for the first amino acid (AA) coupling. The principle of solid-phase synthesis relies on the step-wise addition of AAs sequentially from the peptide C-terminus to the N-terminus. Each AA presents a free backbone carboxylic acid group able to react with the resin-linked AA terminal amine to form an amide bond. The N-terminal Fmoc group on the newly added residue prevents the sequential addition of the same AA on a single growing peptide linked on the resin; in this way only one residue is added at a time onto each growing peptide (**Figure 2.3A**). Similarly, side chains likely to react with a carboxylic acid or the activation reagents are also orthogonally protected. The Fmoc-protected residue to be coupled on the resin was activated by O-Benzotriazole-N,N,N',N'-tetramethyl-

uronium-hexafluoro-phosphate (HbTU, ChemImpex International) in the presence of an excess of a base, N,N-Diisopropylethylamine (DIPEA, Auspep) as shown in **Figure 2.4B**. After 5 minutes of activation the new residue was incubated with the resin for 30 minutes allowing binding to the N-terminal amine of the resin-linked sequence. This deprotection/coupling step was repeated for each residue until the sequence was complete. The peptide was then capped on the N-terminus with acetic acid, using the same coupling conditions as above. Incorporation of amino acids with non-natural side chains, such as L-homophenylalanine or L-homoserine, was performed using commercial reagents (all from ChemImpex International).

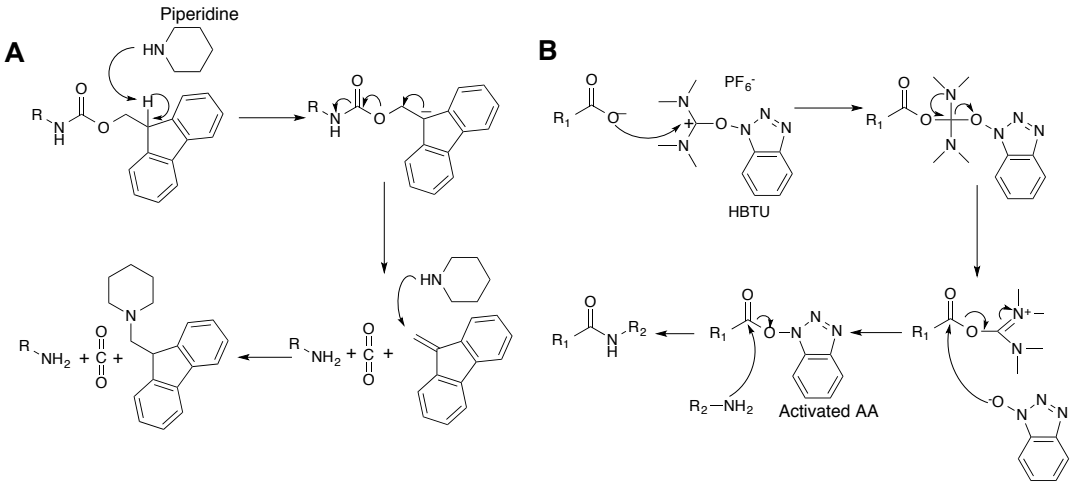

Figure 2.4. ***Reactions of the amino acid coupling steps. A.*** *General mechanism of Fmoc deprotection using an excess of piperidine, liberating the free amine for coupling with the available amino acid.* ***B.*** *Activation of an amino acid (R_1) by HbTU followed by coupling onto an already immobilized residue (R_2).*

The final sequence was cleaved from the resin using a 95:2.5:1.25:1.25 v/v mixture of trifluoroacetic acid (TFA), 1,2-ethanedithiol, triisopropylsilane (Sigma-Aldrich) and H_2O respectively, resulting in the amidation of the C-terminal end. Cleaved peptides were dried using N_2, washed with diethyl-ether (Ajax Finechem) and dissolved in an 80:20 v/v mix of acetonitrile/H_2O (RCI Labscan) before purification on reverse phase HPLC. Purification was executed on a Luna C18 column (250 x 21 mm, Phenomenex) using a 20-100% gradient 90:9.9:0.1 acetonitrile:H_2O:TFA over 12 minutes, until the peptide reached > 90% purity. Peptides were lyophilized and characterized by analytical UHPLC on a Shimadzu Nexera system using an Agilent Zorbax R-ODS III column (2.0 mm i.d x 75 mm 1.6 mm) and a 2020 LCMS, and their mass measured with a high-resolution QSTAR Elite mass spectrometer (Applied Biosystems). Peptide

powder stocks were stored at -20 ºC in vials wrapped with parafilm. Peptides were dissolved in 100 % DMSO to generate stock solutions between 200 mM and 500 mM according to the different screening assays.

Using this method, around a hundred unique peptides were manually synthesized during this PhD, targeting different DsbA proteins. By optimizing both the incubation and washing times I was able to synthesize a typical 10-residue peptide in the course of 48 hours, including cleavage and purification. With rare exceptions (i.e. because of very poor solubility), each of these peptides was tested in the screening pipeline, with the main outcomes presented in Chapter III. Peptides were also synthesized for collaborative projects in other studies on the DsbA proteins outlined in the Appendices B and C.

II.2.3 Differential scanning fluorimetry

Once a new peptide or peptidomimetic was synthesized, the primary purpose of the first screening assay was to quickly and cheaply assess if it could bind to EcDsbA. The Differential Scanning Fluorimetry (DSF, also called thermal shift assay or Thermofluor) is a well-studied technique that can detect ligand binding in a short timeframe (< 1 hour) (Niesen *et al.*, 2007, Lo *et al.*, 2004). DSF was initially developed to scout the stability of a protein in a broad range of different conditions (i.e. buffers, pH, metal ions, detergents, etc) (Ericsson *et al.*, 2006). The stability of a protein is related to its Gibbs free energy of unfolding ΔG_u: the higher ΔG_u, the more stable the protein (Schellman, 1997). According to the definition of Gibbs free energy ($\Delta G = \Delta H - T\Delta S$), ΔG is directly related to the temperature: the higher the temperature necessary to trigger protein unfolding ($\Delta G_u^{Tm} = 0$), the higher the ΔG_u associated with this protein and thus the higher its stability. Therefore, the melting temperature *Tm* of a protein, corresponding to the temperature at which $\Delta G_U = 0$ and half of the protein is unfolded, when measured under different conditions discriminates stabilizing factors from destabilizing factors. This principle can be extended to ligand screening; typically binding of a ligand to a macromolecule raises the overall free energy of a protein due to the solvation effect (Senisterra *et al.*, 2006) and hence the *Tm* of a complex is higher than the *Tm* of the native protein (Vedadi *et al.*, 2006). The difference between the complex *Tm* and the protein *Tm* is called the thermal shift (ΔTm). In this project, a positive ΔTm for EcDsbA in the presence of a peptide indicated that the peptide binds to EcDsbA, marking it for further testing in

the screening pipeline. To be significant, the Δ*Tm* in the presence of a ligand must be at least twice as large as the standard deviation of the native protein *Tm* (Kranz & Schalk-Hihi, 2011).

DSF measures the unfolding temperature using a fluorescent dye, typically SYPRO Orange (S-6650, Life Technologies). SYPRO Orange is quenched in aqueous solution but emits fluorescence when bound to hydrophobic residues. As the protein unfolds, the dye is able to access hydrophobic regions usually buried at the core of the macromolecule, hence triggering an increase in fluorescence that can be measured. Continuous fluorescent recording of a sample containing protein and dye along an incremental rise in temperature leads to the determination of the unfolding temperature from the resulting sigmoidal curve (**Figure 2.5**). The initial plateau of the curve is the background fluorescence of the quenched dye; the final plateau is reached when protein is entirely unfolded. It is usual to notice a decrease in fluorescence past the point of total unfolding caused by dye aggregation.

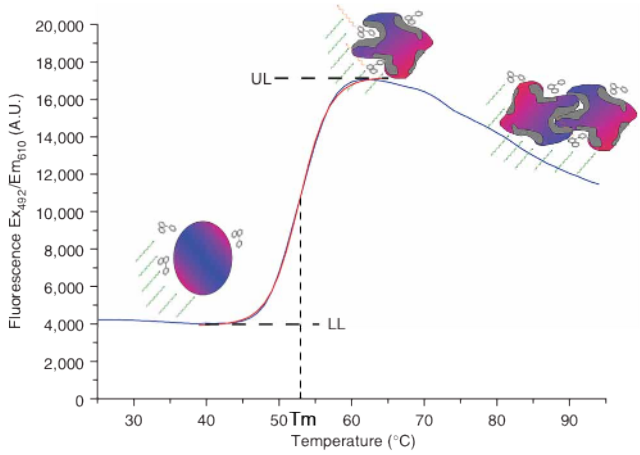

Figure 2.5. ***Protein unfolding monitored with a fluorescent dye.*** *The unfolding temperature Tm can be calculated from the inflection point of the sigmoidal section. LL = fluorescence lower limit, UL = fluorescence upper limit. Reproduced from Niesen et al. (Niesen et al., 2007).*

Experiments were initially performed in a Microamp Optical 384-well reaction plate (Applied Biosciences) on a 7900HT real-time PCR instrument with an excitation wavelength of 490 nm and an emission filter at 615 nm. RT-PCR systems offer the ability to increase temperature in a constant and monitored fashion although the Microamp instrument was not able to raise the temperature in incremental steps less than 1 ºC at a time, thus limiting the number of data points available to determine *Tm* values. Samples were set up in 5 technical replicates on the same plate in phosphate buffered saline (PBS) pH 7.4, with a final dye concentration of 5X (Life Technologies do not disclose the stock dye's molar concentration and list it only as a X5000 concentrate) in 20 μL

sample volume per well. A reference sample that did not contain any peptide but which contained an equivalent concentration of DMSO was included in every plate to measure the unfolding temperature of native EcDsbA. Negative controls consisted of a mix of dye and peptide at every concentration used in the assay, and dye by itself. Two separate plates were tested as replicates for each experiment.

Initial scouting of optimal DSMO concentration suggested that high concentrations of DMSO interfered with the dye, so I imposed an upper limit of 2 % DMSO v/v in any sample. On this instrument, EcDsbA concentration scouting showed that a concentration of 100 μM was necessary to obtain a strong fluorescent signal. Centrifuging the plate immediately prior to the fluorescent reading (2000 rpm, 60 sec, Beckmann Coulter rotor JS 5.3) was found to substantially increase signal intensity. Raw data were analyzed using Prism 6 (GraphPad) and fluorescence emission was fitted using the classic Boltzmann sigmoidal equation and the resulting inflection point was used as the unfolding temperature *Tm* value. Initial experiments revealed a high degree of variability between replicates from different plates, and no clear trend in Δ*Tm* values for different concentrations of a single peptide (**Figure 2.6A** and **2.6B**). Many peptides that gave significant binding in ITC experiments did not induce *Tm* shifts. Some peptides were also found to have a destabilizing effect upon EcDsbA inducing a reduction in *Tm* of up to 5 ºC. Differences in incubation times of EcDsbA with the peptide prior to the assay were shown to be partially responsible for this high degree of experiment to experiment variability; the longer the incubation (which were sometimes left overnight), the lower the shift. An incubation time of one hour appeared to favor larger Δ*Tm* shifts, but the high standard deviations between replicates precluded definitive conclusions.

DSF proved unreliable until the availability of a new state-of-the-art RT-PCR instrument, the VIAA7 (Life Technologies), offered the possibility for protocol improvement. The temperature ramp rate could be set to 0.05 ºC.sec^{-1} (instead of incremental 1 ºC steps) and the measured fluorescence signal intensity was improved by 20-fold using a 585 ± 15 nm emission filter. EcDsbA was diluted 5-fold to a final concentration of 20 μM and incubated for 1 h with different peptides at concentrations ranging from 125 μM to 4 mM in two-fold increments. Using this instrument, resulting Δ*Tm* values gave high reproducibility between replicates and concentration-dependent shifts (**Table 2.1**, **Figure 2.6C** and **2.6D**). It is relevant to note that the Δ*Tm* still increased beyond the peptide concentration that would saturate the EcDsbA molecules present in the samples; this phenomenon has been reported before, and is linked to an increase in the Gibbs free energy of the

system that arises from the interaction of free ligands in solution with the complexes, hence depending on the concentration of free ligands in the sample (Cimmperman *et al.*, 2008).

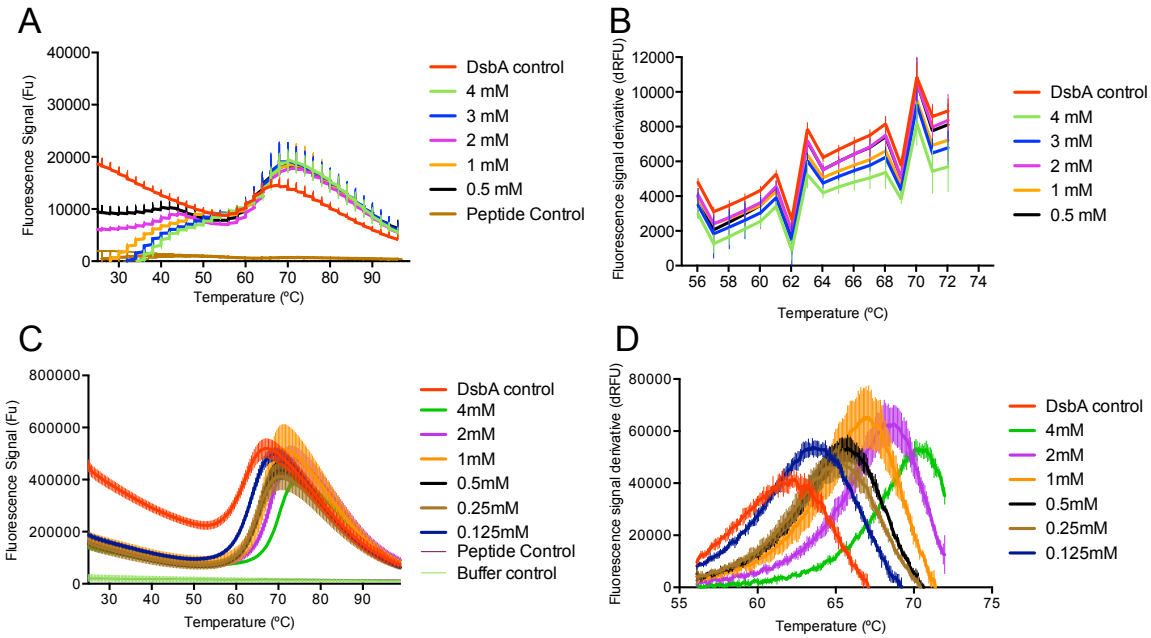

Figure 2.6. ***Example of positive thermal shift induced by the presence of peptide PWATCDS. A.*** *Raw fluorescence measurement of EcDsbA unfolding in presence of increasing concentrations of peptide PSPWATCDF using the 7900HT instrument. The unfolding temperature Tm is calculated from the inflection point of the sigmoidal curve but the signals were small and inaccurate.* ***B****. First derivative of the raw fluorescence signal in A. The unfolding temperature is also represented by a peak in the first derivative of the sigmoidal curve, but data are too poor to calculate a Tm value using this method.* ***C.*** *Raw fluorescence measurement of EcDsbA unfolding in presence of increasing concentrations of peptide PWATCDF using the VIAA-7 instrument, allowing determination of Tm.* ***D****. First derivatives of the raw fluorescence in C, with the unfolding temperature represented by the peak of each concentration curve. All curves are here represented with the standard deviation from 5 technical replicates.*

Table 2.1. ***Example of thermal shift using peptide PWATCDS*** *with concentrations ranging from 125 µM to 4 mM. ΔTm values are presented as mean and standard deviation from 5 technical replicates.*

	Peptide PWATCDS concentration					
	125 µM	250 µM	500 µM	1 mM	2 mM	4 mM
Δ*Tm* (ºC)	+1.7 ± 0.1	+ 3.3 ± 0.2	+3.7 ± 0.1	+5.0 ± 0.1	+6.9 ± 0.1	+9.8 ± 0.1

Overall, the differential scanning fluorimetry assay required significant optimization to enable it to be used reliably to identify peptides and peptidomimetics that alter the EcDsbA *Tm*. The breakthrough to achieving this was the use of a more sensitive instrument. The final protocol allowed testing a peptide at different concentrations and five technical replicates in a 2-hour timeframe including incubation and data analysis. If thermal shifts were detected, the next step was to evaluate the affinity of these ligands.

II.2.4 Isothermal Titration Calorimetry

Screening of inhibitors requires a robust assay to evaluate their affinity for the target and identify the best scaffolds, or 'hits', to progress further into potent and specific molecules. A label-free assay, isothermal titration calorimetry (ITC) provides an accurate measurement of the energy released or captured upon a binding interaction (Perozzo *et al.*, 2004, Leavitt & Freire, 2001). By titrating a target macromolecule with a binding ligand (here a peptide) one can directly deduce the binding affinity (*K*a), the enthalpy change (ΔH), and the molar stoichiometry (n) of the target-ligand interaction. The total Gibbs free energy (ΔG) and entropy contribution (ΔS) are mathematically calculated from these direct measurements using the Gibbs equations $\Delta G = - R*T*\ln(Ka)$ and $\Delta G = \Delta H - T\Delta S$. A titration experiment typically takes about two hours per ligand, and is thus poorly suited to high-throughput screening. However the robustness of the method and the usefulness of the thermodynamic information yielded (Ladbury, 2010, Holdgate, 2001) provide important details for a rational inhibitor design strategy such as this project.

ITC was initially performed using a manual MicroCal™ ITC200 instrument (GE Healthcare, USA). The sample cell was loaded with 200 µL of purified EcDsbA at 100 µM in 25 mM HEPES pH 7.4, 50 mM NaCl 0.8 % DMSO. The syringe was filled with purified peptide in the same buffer solution. Titrations were initially conducted at 25 °C using 12 consecutive injections of 2.8 µL with 180 s intervals and a stirring speed of 1000 rpm. In every experiment, an initial 0.5 µL of peptide was injected to avoid slow leakage of titrant that could interfere with the initial reading. Consequently, this initial data point was discarded for binding analysis. As a negative control, peptides were injected into a buffer solution lacking EcDsbA to measure the heat of dilution. The association constant ($K_a = 1/K_d$), enthalpy (ΔH) and entropy (ΔS) were calculated by fitting the data to a single-site binding model using the MicroCal™ Origin software (version 7.0552).

The first titrations with an EcDsbB derived peptide showed promising results, with a strong exothermic reaction indicated by a sharp decrease in the power supplied to the cell to keep the temperature constant (**Figure 2.7A**). However this phenomenon was only observed with freshly oxidized EcDsbA; titration of reduced EcDsbA by peptide sequences demonstrated insignificant energy release with no binding trends (**Figure 2.7B**) thus suggesting that the oxidation state of EcDsbA influenced peptide binding. Further discussion of these observations is presented in Chapter III, and unless stated otherwise all peptide sequences and peptidomimetic scaffolds in this PhD were tested in ITC against fully oxidized EcDsbA.

For all peptides the 1:1 binding model provided the most accurate curve fitting, suggesting that only one peptide binds to the EcDsbA surface. Due to differences in estimated concentrations between different peptide sequences, the initial stoichiometry factor *n* ranged from 1.0 to 1.6. The origin of these differences comes from peptide synthesis, where the final peptide powder stock might include 10 to 40% salts and solvent, leading to batch-to-batch variation in the actual concentration of peptide. To restrain the impact of this variation on the analysis and thermodynamic calculations, the peptide concentration input in the software (originally 4 mM) was adjusted for each peptide to achieve a calculated *n* value of 1.0 ± 0.05. The ITC parameters for optimal curve fitting are typically represented by a unitless c-value representing the ratio of the protein concentration over the dissociation constant *K*d, with a recommended range from 1 to 100. The calculated ITC c-values for the tested peptides varied from 2 to 50 therefore falling within the acceptable range. Each peptide was tested using three technical replicates, and the thermodynamic values were presented as mean and standard deviations from the separate analysis of each replicate.

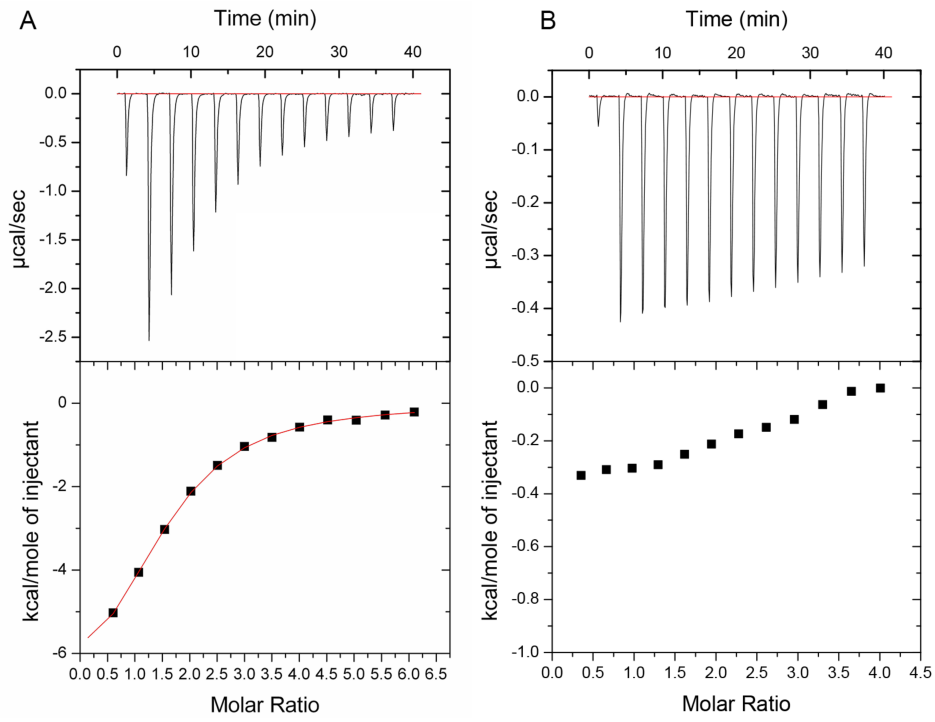

Figure 2.7. ***Examples of Isothermal Titration Calorimetry profiles. A.*** *Titration of oxidized EcDsbA with peptide PSPFATCD, leading to a strong exothermic reaction and saturation plateau.* ***B.*** *Titration of reduced EcDsbA by peptide PSPFATCDF, triggering a very low exothermic signal with no observed binding. Note the different scales in the energy release for each titration.*

Curve-fitting could be optimized with an initial plateau for the first injections, and the ITC protocol was extended to 19 injections of 2 µL as smaller injection volumes would delay the saturation of EcDsbA, for no improvement (**Figure 2.8A**). It suggested the binding of peptides to EcDsbA occurred in a very short timeframe.

The installation of the MicroCal™Auto-ITC200 (GE Healthcare), an automated version of the earlier instrument, enabled a significant increase in the throughput of tested peptides because it allowed for a 96-well plate format (**Figure 2.8**). However, this improvement was at a cost of greater consumption of peptide (almost two-fold) and of EcDsbA.

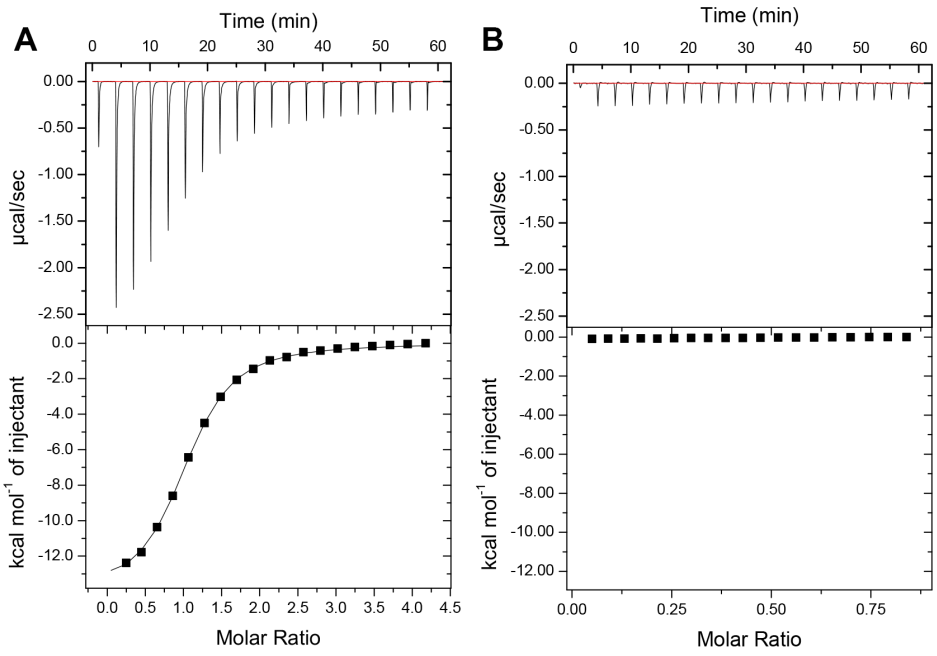

Figure 2.8. ***Example of successful ITC experiment titrating oxidized EcDsbA with peptide PWATCDS*** *using the automated ITC200 instrument.* ***A.*** *Titration of 4 mM PWATCDS into a solution of 100 µM EcDsbA.* ***B.*** *Negative control: titration of 4 mM PWATCDS into a buffer solution.*

In conclusion, the isothermal titration calorimetry assay proved to be reliable for the study of EcDsbA binders, providing essential thermodynamic information. The main drawback was the very high consumption of reagents, requiring larger-scale synthesis of peptides and production of purified protein. Nevertheless, a large number of peptides synthesized for this PhD were tested resulting in more than three hundred ITC titrations performed. The main outcome of these experiments is presented in Chapter III for EcDsbA, Chapter IV for PmDsbA and in the Appendix for KpDsbA and MtbDsbA.

II.2.5 Surface Plasmon Resonance

In the pipeline, the purpose of a surface plasmon resonance (SPR) experiment was to evaluate the kinetics of the peptide binding reaction to EcDsbA, and to provide a second affinity value independent of ITC. SPR is based on the alteration upon ligand binding of particle oscillations under a light beam (Homola *et al.*, 1999). A BIAcore T200, the most sensitive of the BIAcore instruments from GE Healthcare, was available at the IMB. Briefly, a sensor chip includes

four independent flow paths coated with a dextran matrix upon a gold nanolayer. The target molecule (the 'ligand') can be immobilized onto the dextran matrix through a broad range of chemical couplings (**Figure 2.9**) (Jason-Moller *et al.*, 2006). A light beam is directed towards the nanolayer on which polarized light will be reflected and the refractive angle measured by an optical detection unit. Injection of a molecule in solution (the 'analyte') triggers a mass change on the surface of the chip upon binding to the ligand, disturbing the gold nanolayer and shifting the local index of refraction. Measuring this shift under different concentrations of analyte provides the data used to calculate an affinity value (*K*d) and kinetic rates (Karlsson, 2004, Andersson *et al.*, 2006).

The BIAcore refractive index is highly influenced by the molecular mass of the interactants: a large analyte binding to a smaller ligand immobilized onto the chip surface will result in a higher mass change than the same interaction in the reverse orientation, hence yielding a higher shift in the refractive index and a higher response in response units (RU). Therefore in the case of EcDsbA and peptides, the recommended method was to immobilize the peptides and peptidomimetics (Mw 500 – 1500 Da) onto the chip (for example through capture using a streptavidin/biotin interaction) and inject EcDsbA (Mw 21170 Da) as analyte across the surface for each experiment. However, this approach requires individual labeling of every peptide for immobilization onto the chip. Moreover it also requires a high quantity of sensor chips as each flow path used for a specific peptide sequence cannot be reused, thus increasing the cost of the assay. Therefore, I initially decided to immobilize EcDsbA upon the chip and to inject peptides as analytes instead. The signal was expected to be low and therefore harder to detect, but if successful it would mean that an experimental series with all controls could be run on a single chip. This chip surface could be regenerated by peptide dissociation and with additional immobilization of EcDsbA when signal intensity decreased. A potential issue with this method was controlling the oxidation state of immobilized EcDsbA. Over a long period of time on the chip and through successive experiments the oxidation state of EcDsbA could change, with potential knock-on effects for peptide binding.

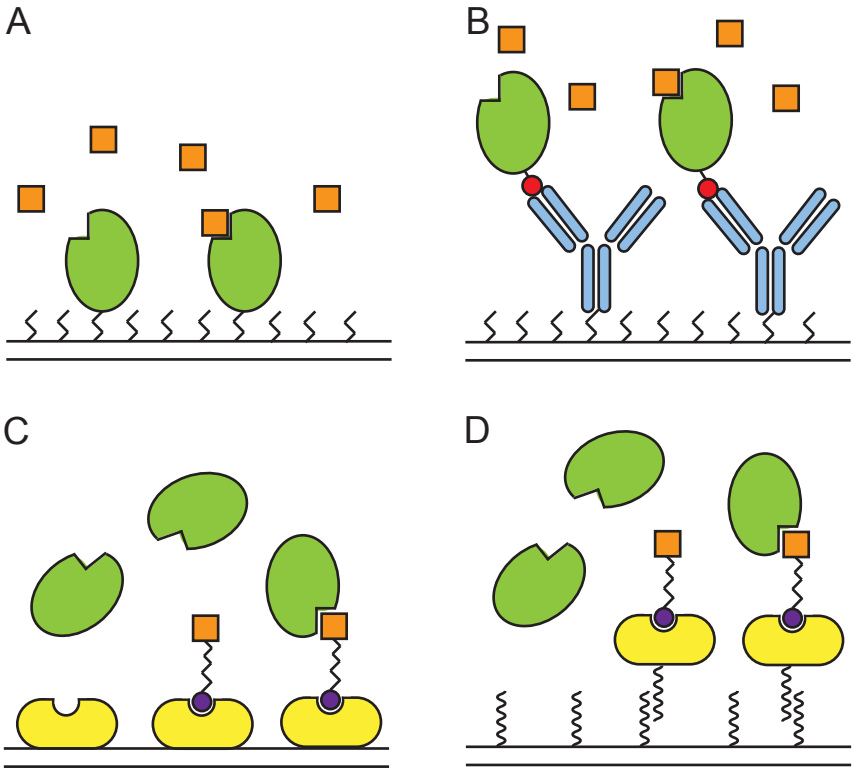

Figure 2.9. ***The different immobilization methods used in SPR for this project.*** ***A.*** *Direct immobilization of ligand EcDsbA (in green) onto the dextran-coated surface through amine coupling. The peptides (in orange) are injected as analytes and the mass change on the chip surface results in a shift in the refractive index.* ***B.*** *Capture of labeled EcDsbA with a 6xHis or GST tag (in red) by a monoclonal antibody (in blue) previously immobilized by amine coupling.* ***C.*** *Capture of a biotin-tagged (purple) peptide onto a chip coated with streptavidin (in yellow). The peptide acts as ligand and the analyte is the native EcDsbA, which should give a larger refractive shift because of the larger mass change on the surface upon binding. This technique however only allows one peptide tested per chip.* ***D.*** *Similar method to C except the streptavidin is captured through nucleotide strand complementarity beforehand. This method enables regeneration by breaking the DNA double strand, thus releasing the entire complex and allowing the use of the same chip for different peptides*

II.2.5.1 Initial optimization: EcDsbA immobilization

EcDsbA and peptides for use in the SPR assays were diluted into the running buffer HBS-EP (0.01 M HEPES pH 7.4, 0.15 M NaCl, 3 mM EDTA, 0.005% v/v Surfactant P20). Immobilization of EcDsbA could not be performed using standard thiol coupling onto a chip because the only two cysteines in the sequence are the two catalytic cysteines in the active site. Accordingly, the first attempts to immobilize EcDsbA onto a standard CM5 sensor chip (GE

Healthcare) utilized amine coupling between the activated surface and a free lysine residue of EcDsbA (**Figure 2.9A**). pH scouting of the immobilization buffer (sodium acetate 10mM, pH 4.0, 4.5 and 5.0) demonstrated that optimal binding of EcDsbA occurred at pH 4.0 with a steep binding curve that reached saturation at 6,000 RU (flow rate 10 µL.min^{-1}, contact time 60 sec, **Figure 2.10**). The surface was then regenerated with 10 mM glycine HCl pH 2.5 (flow rate 30 µL/min^{-1}, contact time 30 sec). No pH values lower than 4.0 were tested because the dextran matrix on the chip surface is required to be negatively charged (pH > 3.5).

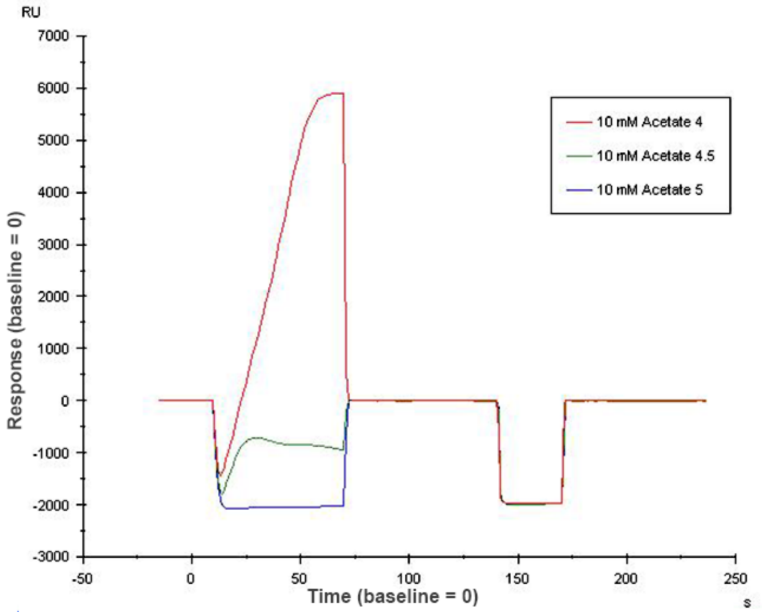

Figure 2.10. ***pH scouting for EcDsbA immobilization onto a BIAcore CM5 chip.*** *The first injection shows pH 4.0 (in red) to be optimal for EcDsbA binding while the second injection is a regeneration of the chip surface. At pH 5.0 (in blue) no binding is observed and at pH 4.5 (in green) saturation of the chip surface is not reached.*

An optimal response signal (R_{max}) for kinetics studies is between 50 and 100 response units (RU). A lower signal would be difficult to detect and a much greater response can result in misleading kinetics analysis. Knowing that the experimental response is usually lower than the theoretical equivalent due to nonspecific binding, the theoretical R_{max} (R_{maxT}) was set to 150 RU. This allows calculation of the theoretical level of EcDsbA immobilization required to detect binding kinetics with the following equation: $R_{maxT} = MW_{DsbA} * Rl * S / MW_{peptide}$, with Rl the immobilization level of EcDsbA in RU, and S the molar stoichiometry. Based on a 1:1 stoichiometry and the molecular weight of the EcDsbB peptide derivative PSPFATCD of 878.3 Da, I deduced that to achieve a 150 RU binding signal of PSPFATCD onto EcDsbA, the initial immobilization level of EcDsbA onto the chip had to be around 3,600 RU.

Immobilization of EcDsbA was achieved through activation of the chip dextran matrix with 1-ethyl-3-(3-dimethylaminopropyl)carbodiimide (EDC, GE Healthcare) and N-hydroxysuccinimide (NHS, GE Healthcare) following steps outlined in the BIAcore software wizard (GE Healthcare). EcDsbA (25 $\mu g.mL^{-1}$) was then injected onto the chip surface in pulses until the required immobilization level (here 3,600 RU) was reached (**Figure 2.11**). The remaining dextran matrix was then inactivated with ethanolamine to limit nonspecific binding in later experiments. Once EcDsbA had been immobilized and the baseline stabilized, different concentrations of peptide PSPFATCD (3 µM to 300 µM) were sequentially injected onto the chip, using different flow rates (10 $\mu L.min^{-1}$ to 30 $\mu L.min^{-1}$) to avoid the mass transport effect, and different contact times (60 to 180 seconds) in case of low association rates. However, no significant binding signal was observed. The best conditions gave less than 10% of the theoretical response R_{maxT}. Neither altering buffer pH (over a range of 4.0 - 9.0) nor saturating the chip with immobilized EcDsbA (with an immobilization response up to 8,000 RU) improved the binding signal. At this point it was suspected that the chosen immobilization method, by facilitating high density protein immobilization or favouring particular protein conformations, may have occluded access to the peptide-binding pocket. Consequently, alternative immobilization approaches were investigated.

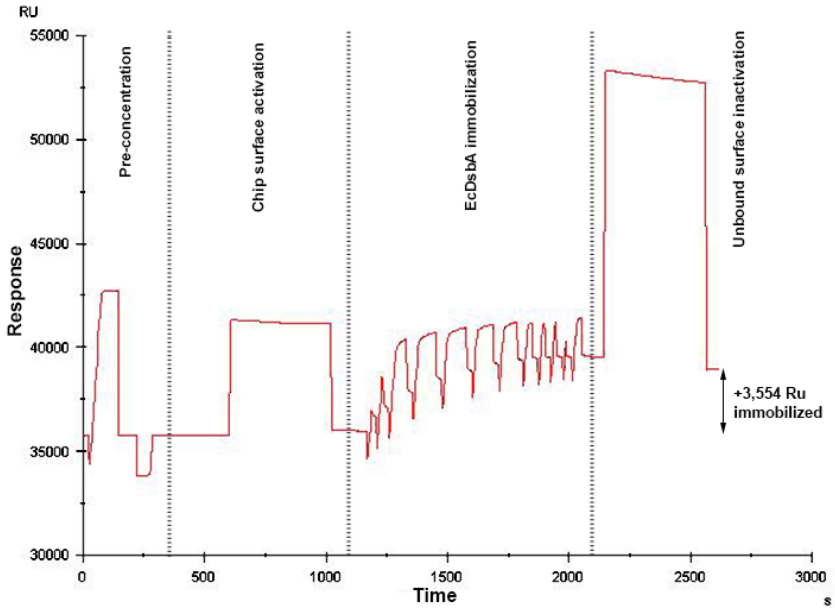

Figure 2.11. ***Example of EcDsbA immobilization by amine coupling onto a BIAcore CM5 chip.*** *Using consecutive pulses allowed reaching an immobilization level of 3,554 RU with a theoretical target of 3,600 RU. The pre-concentration loads the chip surface with ligand by electrostatic interactions, followed by dextran activation through injection of EDC and NHS preparations. EcDsbA is then injected in consecutive short pulses until the required immobilization is reached. Finally, the remaining active dextran matrix is blocked with ethanolamine to limit nonspecific binding of the analyte in the following experiments.*

II.2.5.2 EcDsbA capture approaches

To prevent covalent binding of EcDsbA upon the chip surface in a manner that might alter protein conformation and limit peptide binding, a 'capture' method of immobilization was used in which the ligand to be immobilized has a specific label captured by a high affinity antibody on the chip surface (**Figure 2.9B**). In this study, an N-terminal GST-tagged EcDsbA construct and a corresponding anti-GST tag polyclonal antibody (Life Technologies) were used. Native EcDsbA (immobilized via surface lysines as described above) and GST-EcDsbA (captured via the anti-GST antibody) were immobilized on different flow paths from the same chip along with controls to compare peptide binding between the two immobilization methods. The anti-GST tag antibody was immobilized through amine coupling at 30 $\mu g.mL^{-1}$ in sodium acetate 10 mM pH 4.0 reaching immobilization levels up to 12,000 R (**Figure 2.12A**). GST-EcDsbA was then injected on the chip with a capture response 1,800 RU at the highest GST-EcDsbA concentration (4 $mg.mL^{-1}$, flow rate 10 $\mu L.min^{-1}$, contact time 300 seconds, **Figure 2.12B**). To reach a similar density on the chip surface, native EcDsbA (1 $mg.mL^{-1}$) was immobilized on a different flow path with an immobilization level of 1,000 RU (the molecular mass of EcDsbA being half the GST-EcDbsA construct, the immobilization level had to be halfed for a similar density). However when peptide PSPFATCD was injected with concentrations ranging from 3 µM to 300 µM (flow rate 30 $\mu L.min^{-1}$, contact time 120 seconds and dissociation time 600 seconds) no significant binding was observed for either of the EcDsbA constructs (**Figure 2.13**).

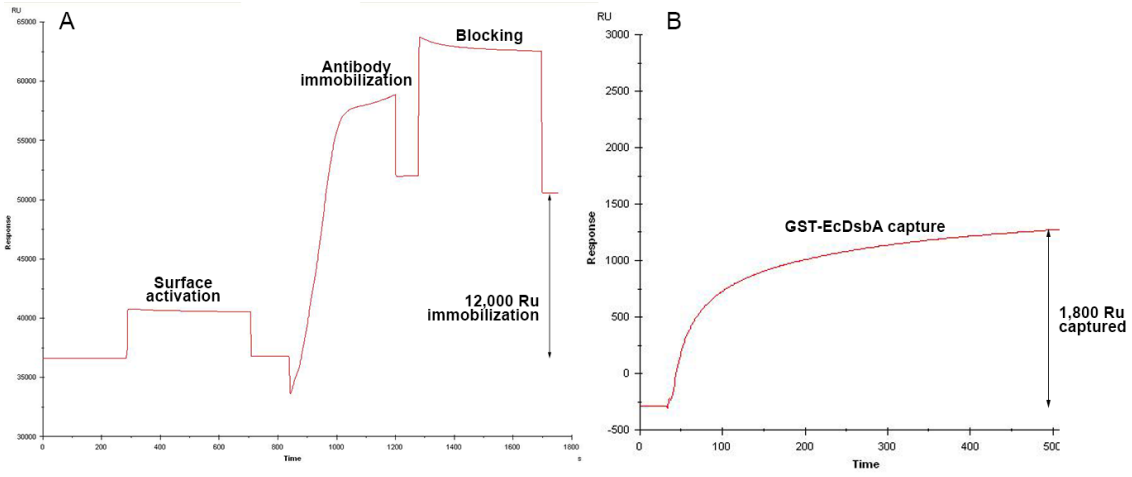

Figure 2.12. ***Immobilization of EcDsbA on a chip using the antibody capture method. A****. Immobilization by amine coupling of an anti GST antibody saturating the chip surface.* ***B****. The injection of GST-EcDsbA into the flow path led to irreversible capture by the antibody already present on the chip, here resulting in EcDsbA immobilization of 1,800 RU. In this way, EcDsbA did not undergo any chemical reaction for immobilization that could have modified the state of the protein.*

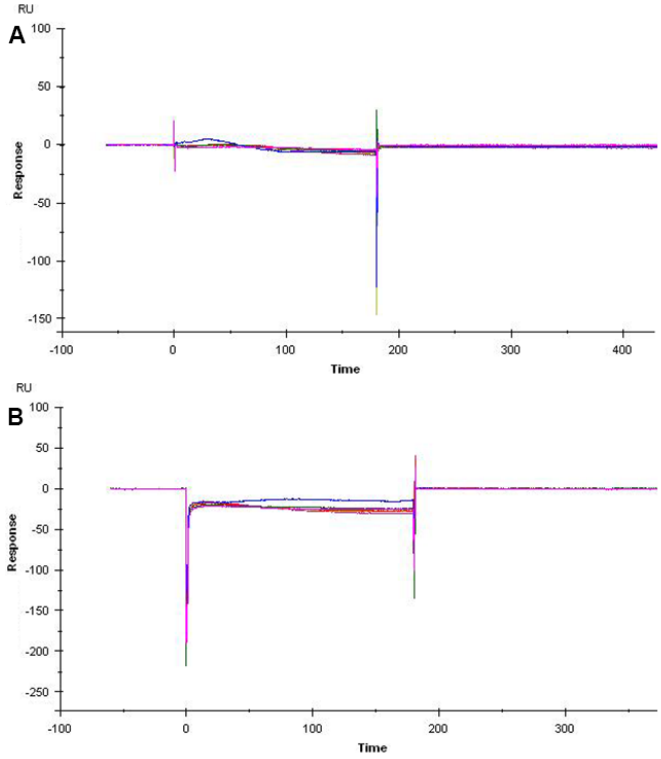

Figure 2.13. ***Absence of binding observed when injecting peptide PSPFATCD***. ***A*** *No response was observed with peptide concentrations ranging from 3 μM to 300 μM onto EcDsbA immobilized by amine coupling.* ***B***. *No significant binding was observed when injecting the peptide at similar concentrations of the flow path with antibody-captured GST-EcDsbA. The sharp peaks observed at the start and the end of the injections are a consequence of slight buffer mismatches between the sample buffer and the washing buffer.*

Three possible reasons for the absence of signal are: 1) the peptide could not access the EcDsbA binding site, 2) the EcDsbA peptide binding was modified by the immobilization/capture process or 3) the peptide bound to EcDsbA but the mass change and thus the refractive index was too low for the sensitivity of the BIAcore instrument. An approach to prevent the first two issues was to immobilize the peptide as a ligand on the chip and to use EcDsbA as an analyte. This alternative allowed the use of native EcDsbA in solution solving issues 1) and 2), and binding of the 21170 Da protein onto a 500-1500 Da peptide would lead to a high response signal, solving issue 3). The main drawback was the cost and handling of many chips as each flow path can only be used once for each peptide sequence, which becomes a costly exercise when screening a high number of peptides.

II.2.5.3 Peptide immobilization

To test the peptide immobilization approach, the sequence PSPWATCDF was biotinylated at the N- or the C- terminus with a spacer (EZ-Link Sulfo-NHS-LC-Biotin, Thermo Scientific) allowing flexibility and length for accessibility by EcDsbA on the chip surface (**Figure 2.9C**). These two peptides were injected on different flow paths of the same streptavidin-coated sensor chip (SA chip, GE Healthcare, 200 $\mu g.mL^{-1}$, flow rate 10 $\mu L.min^{-1}$, contact time 60 seconds) until surface saturation with an immobilization level of 420 RU for PSPWATCDF-biotin and 550 RU for biotin-PSPWATCDF was reached. For the binding measurements, EcDsbA was fully reduced or fully oxidized prior to the experiment using a molar excess of DTT or Cu(Phen) respectively. A PD-10 column (GE Healthcare) was used to remove the excess reducing or oxidising agent as well as buffer-exchanging EcDsbA into the HBS-EP running buffer (GE Healthcare). EcDsbA was then manually injected onto the peptide-coated chip at concentrations ranging from 0.5 $mg.mL^{-1}$ to 5 $mg.mL^{-1}$ (flow rate 5 $\mu L.min^{-1}$, contact time 120 seconds, dissociation time 120 seconds) and a concentration-dependent response was observed with a signal ranging from 100 RU to 1,300 RU (**Figure 2.14**). Unfortunately no negative controls (injection of EcDsbA on a flowpath with no peptide) were performed at this stage due to the shortage of free flow paths on the available chips.

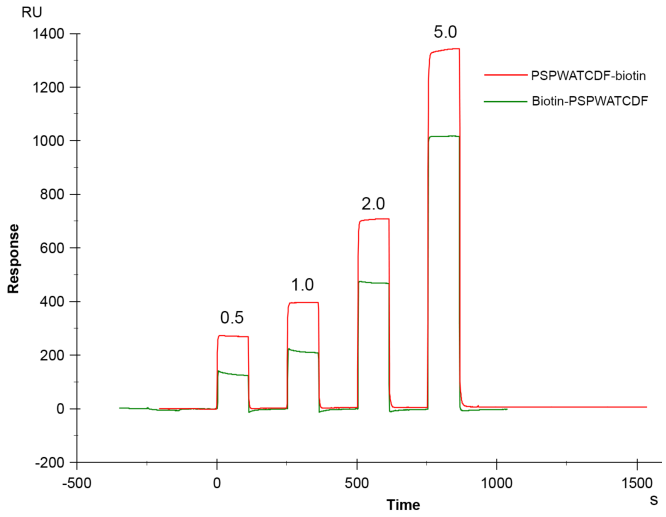

Figure 2.14. ***Oxidized EcDsbA binds in a concentration-dependent manner to PSPWATCDF*** *immobilized on the surface of the streptavidin coated chip via either an N- or C-terminal biotin tag. Above each injection is indicated the concentration of EcDsbA injected in* $mg.mL^{-1}$.

The sensorgram measured very high on-rate and off-rate, with EcDsbA binding and saturating the chip surface immediately after injection and dissociating very shortly after the end of

the injection. No residual EcDsbA remained on the chip with the signal immediately returning to baseline, and thus it was not necessary to include a regeneration step between injections. The sensorgrams suggested that EcDsbA (both oxidized and reduced) preferentially bound to the C-terminally biotinylated peptide (PSPWATCDF-biotin) with a response level 30% higher than biotin-PSPWATCDF, despite a lower density of immobilized peptide. Oxidized EcDsbA binding also triggered a higher signal than that of reduced EcDsbA.

A larger range of concentrations and a number of different peptide sequences needed to be tested but the requirement of a new chip per peptide substantially increased the cost and time efficiency of the assay. Recent progress in BIAcore technology from GE Healthcare provided a solution with the CAP sensor chip: the surface is coated with single-strand DNA on which a molecule composed of a streptavidin domain bound to the complementary DNA strand can bind at a high density. A biotin-labeled ligand (here a peptide) can then be immobilized on the streptavidin domain and experiments run with the analyte (here EcDsbA, **Figure 2.9D**). Afterwards the chip surface can be entirely regenerated by breaking the DNA double strand, thus freeing the chip for immobilizing another ligand (here another peptide sequence). This way, only a single chip is necessary to test a large number of peptides. This new CAP chip was tested, on which streptavidin was immobilized (CAP reagent, GE Healthcare, flow rate 2 $\mu L.min^{-1}$, contact time 300 sec) saturating the surface with a final immobilization level of 3,000 RU. The chip was then saturated with biotin-PSPWATCDF reaching an immobilization level of 64 RU (concentration 10 mM, flow rate 2 $\mu L.min^{-1}$, contact time 300 seconds, dissociation time 120 seconds). Successive injections of oxidized EcDsbA triggered concentration-dependent binding response from 30 RU at 0.25 $mg.mL^{-1}$ to 376 RU at 4 $mg.mL^{-1}$ in a similar fashion to that shown for the SA chip (**Figure 2.14**). As a negative control, the same solutions of oxidized EcDsbA were injected on flow paths only presenting the streptavidin reagent and no biotinylated peptide; a similar response was measured (**Table 2.2**). The data suggested that the observed binding of EcDsbA on the chip was non-specific and probably due to electrostatic interactions. This hypothesis explained the high on-rate and off-rate as EcDsbA was simply washed away at the end of the injection with no dissociation from specific binding to the ligand.

Table 2.2. ***Binding signals for EcDsbA injection on a CAP in presence and absence of peptides.*** *On one flow path biotin-PWATCDS peptide was immobilized on the streptavidin CAP reagent whereas on the second flow path only the CAP reagent was present. The binding responses (in RU) showed that EcDsbA bound to the chip the same way independently of the presence of peptide, suggesting a lack of specificity in the interaction with the chip. Due to the complexity of the chip, the experiment was executed in manual mode that does not provide clear graphic representation.*

	Injected EcDsbA concentration ($mg.mL^{-1}$)				
	0.25	0.5	1	2	4
Biotin-PWATCDS	+30	+58	+100	+192	+376
Negative control	+29	+60	+97	+190	+378

II.2.5.4 Discussion

The surface plasmon resonance assay transpired to be a major challenge to set up for EcDsbA. In all, four different methods of immobilization were investigated using a number of different labels, and the role of ligand and analyte swapped to overcome presumed steric hindrances and to amplify the change in the refractive index upon binding. Additionally flow, contact time, ligand and analyte concentrations, pH and running buffer composition were all scouted but no specific binding was observed between EcDsbA and peptides. The reasons behind the failure to detect specific binding are still unclear. One hypothesis is that immobilized EcDsbA undergoes a significant conformational change upon peptide binding thus modifying the refractive index of the protein in such a way that masks any shift due to specific peptide binding. However, such an explanation does not explain why EcDsbA when injected as an analyte seems to be unable to bind the immobilized peptide. Even with the long linker the peptide might be sterically hindered with the immobilization process substantially impeding binding by limiting the peptide flexibility. As a consequence of these issues and despite considerable efforts the SPR assay had to be abandoned and was removed from the peptide screening pipeline.

II.2.6 Model Substrate Oxidation Assay

DSF, ITC and SPR measure the affinity of EcDsbA towards the designed peptides but do not provide information about the inhibition of EcDsbA activity. Previous measurements of EcDsbA activity were performed by assessing the ability of EcDsbA to catalyze the reduction of insulin in the presence of DTT (Shouldice *et al.*, 2010, Heras *et al.*, 2010b, Heras *et al.*, 2008b).

Briefly, insulin possesses two intramolecular disulfide bonds between chains A and B and their reduction leads to the precipitation of the insoluble B chain, inducing an increase in turbidity that can be measured with a spectrophotometer at 650 nm (Holmgren, 1979). However this assay is not an optimal way to evaluate EcDsbA activity not least because it is based on a reaction (transfer of a disulfide bond from oxidized substrate to reduced EcDsbA) that is the reverse of that which EcDsbA catalyses *in vivo* (transfer of a disulfide bond from oxidized EcDsbA to a reduced substrate).

An assay has since been developed by Assoc. Prof. Martin Scanlon at the Monash Institute of Pharmaceutical Sciences to assess the activity of DsbA proteins by monitoring their ability to catalyse the folding of a synthetic substrate peptide (Vivian *et al.*, 2009). The peptide oxidation assay, hereafter referred to as the model substrate oxidation assay to avoid confusion between substrate peptide and inhibitor peptide, is based on a time-resolved fluorescence energy transfer phenomenon. The synthetic substrate peptide of EcDsbA of sequence CQQGFDGTQNSCK presents an N-terminal 1,4,7,10-Tetraazacyclododecane-1,4,7,10-tetraacetic acid (DOTA) group and a C-terminal methoxycoumarin amide (MCA) (Anaspec, **Figure 2.15**). The peptide is prepared in 2 mM stock in 100 mM imidazole pH 6.0 in the presence of 4mM of Europium^{3+} (Eu^{3+}) to form a chelate complex with the DOTA scaffold. Upon disulfide bond formation between the two cysteine residues, the coumarin group is brought close to the Eu^{3+}-DOTA fluorophore (**Figure 2.15**). Excitation of the coumarin moiety at 340 nm then leads to an energy transfer to the Eu^{3+}-DOTA fluorophore and an increase in fluorescence emission at 615 nm. Continuous reading of fluorescence, in the presence of EcDsbA allows measuring the rate of folding of the substrate peptide and thus EcDsbA activity. EcDsbB is also included in the reaction to regenerate oxidised EcDsbA, thus increasing the timeframe of the experiment and allowing study of the influence of a ligand on the EcDsbB-EcDsbA interaction. The presence of an inhibitor that blocks the substrate-EcDsbA, the EcDsbA-EcDsbB or the EcDsbB-ubiquinone interaction, would lead to a decrease in the substrate peptide folding rate and thus to a reduced fluorescence increase rate compared with EcDsbA activity in the absence of an inhibitor.

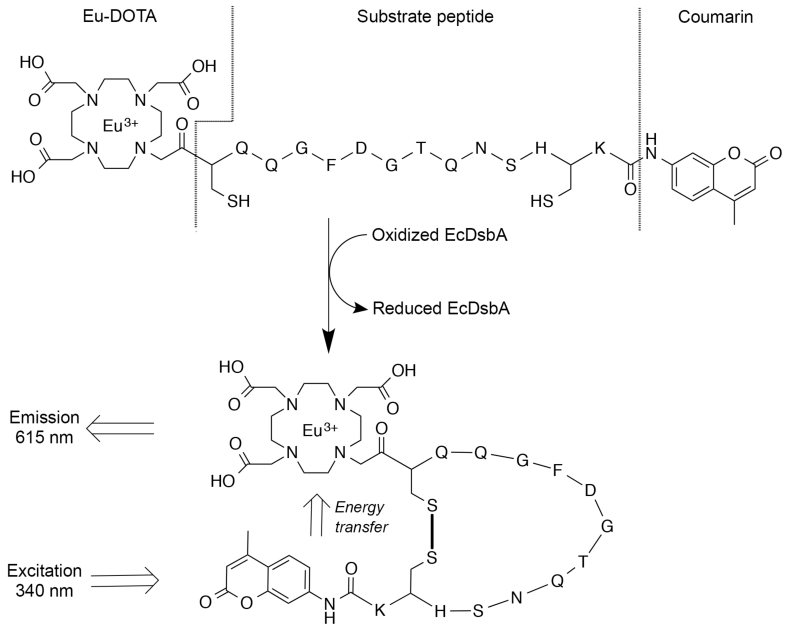

Figure 2.15. ***Model substrate oxidation mechanism.*** *Folding of the peptide by formation of a disulfide bond between the two cysteines by EcDsbA enables energy transfer from the spatially close coumarin moiety to the Eu-DOTA moiety. EcDsbA activity - and the inhibitory power of any molecule impeding its activity – can be assessed by following the emission fluorescence at 615 nm over time.*

The substrate oxidation assay was optimized in the laboratory at the IMB by Dr Maria Halili and I followed her procedure. Assays were performed in a white 384-well plate (Perkin Elmer OptiPlate-384, Part #: 6007290) in 50 mM MES, 50 mM NaCl and 2 mM EDTA at pH 5.5 buffer. Each sample well contained 80 nM EcDsbA, 1.6 µM EcDsbB in a membrane preparation (see section II.2.1), peptide or peptidomimetic at concentrations ranging between 64 nM to 1 mM, and 10 µM synthetic substrate (added last to initiate the reaction and fluorescence signal) in a final volume of 50 µL. A positive control did not include any peptide or peptidomimetic. The three negative controls included mixing the substrate peptide with respectively EcDsbB, EcDsbA or the inhibitory peptide alone. Plates were read using a Synergy H1 multimode plate reader (BioTek). First fluorescence background measurement was performed before adding the substrate peptide triggering the reaction. Once the synthetic substrate was added, fluorescence emission at 615 nm was measured every 75 seconds, which was the minimal timeframe for the instrument to read every well on the plate once, for a total length of 4 hours. Every reaction was performed in three technical replicates.

In the absence of inhibitors, the measured fluorescence increased rapidly, demonstrated by an initial steep curve. As the quantity of oxidized EcDsbB diminished, the rate of fluorescence signal showed an asymptotic behavior (**Figure 2.16A**, red curve) finally reaching absolute maximum fluorescence. In the presence of peptides the rate of fluorescence increase was substantially reduced from the beginning of the experiment, and the absolute maximum fluorescence was not reached within the experimental timeframe for the highest concentrations. The fluorescence rates were calculated based upon the first 15 minutes of the experiments before the asymptotic behavior. When plotted against the log of inhibitor concentrations, a dose-response sigmoidal curve can be fitted and an IC50 value calculated from the inflection point (**Figure 2.16B**).

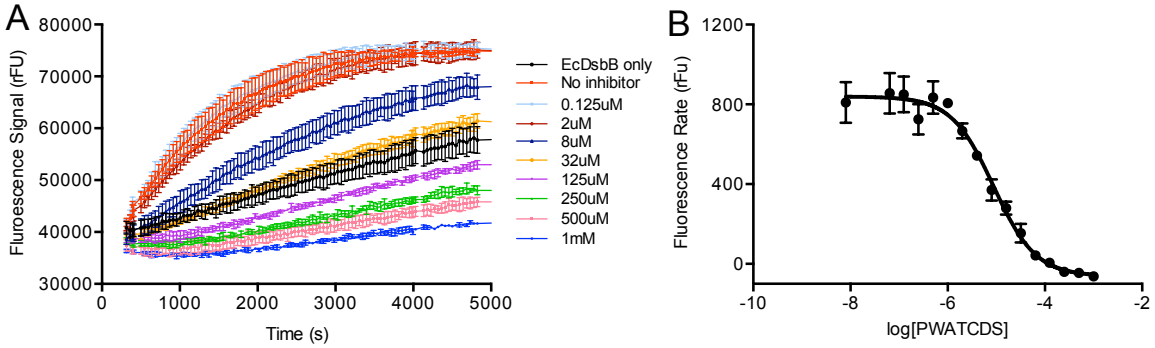

Figure 2. 16. ***Example of significant inhibition of the peptide folding*** *rate by peptide PWATCDS.* ***A.*** *Raw fluorescence measurements at 615 nm from wells containing increasing concentrations of PWATCDS from 64 nM to 1 mM. Lowest concentrations do not show any decrease in the rate of fluorescent signal increase compared to the positive control without peptide (red), while at the highest concentration (1 mM, in light blue) peptide folding is almost entirely prevented. Only half of the peptide concentrations tested in the assay is shown in this graph for clarity. Negative controls are not shown because their fluorescence is extremely low.* ***B.*** *Plotting the fluorescence increase rates against the log of the inhibitor concentration supports the fitting of a sigmoidal curve from which an IC50 can be calculated from the inflection point. Both graphs are presented with the standard deviation over three replicates.*

Overall, the model substrate oxidation assay was an efficient tool to detect inhibitory activity from peptides and peptidomimetics that satisfied the previous binding assays. Importantly this assay consumed low amounts of both peptides and EcDsbA and experiments for up to three compounds at a time could be run over half a day. However, a limitation of this particular assay is that it does not differentiate if the inhibitor competes for EcDsbA binding against the substrate, or against EcDsbB, or both.

II.2.7 Crystallography

Crystallography was an essential component of this PhD project to provide structural understanding of the targeted site. However, co-crystallizing and solving the structure of a complex is not without challenges. There are three major strategies to achieve crystal complexes: 1) co-expression of ligand and protein, 2) soaking of a ligand into a preformed protein crystal and 3) co-crystallization of a mixture of protein and ligand (Hassell *et al.*, 2007, Turnbull & Emsley, 2013, Danley, 2006, Schlichting, 2005). The first possibility was not envisaged due to the difficulty of co-expressing the peptide sequence along with EcDsbA.

Soaking is an attractive approach because the crystallization conditions of the protein alone are well known, although insertion of the ligand in the crystal depends on ligand size and conformation as well as crystal shape and the size of the solvent channels. In this technique, a ligand might not be able to access sites on the target that are available in solution. For co-crystallization, the binding of a ligand, especially one as large as a peptide, can lead to significant protein conformational changes hence altering the crystal forms initially screened for the protein alone (Hassell *et al.*, 2007). This can lead to the investigation and screening of entirely new crystallization conditions as well as the analysis of previously unreported crystal shapes for that protein. Moreover, the presence of a concentrated ligand was an additional consideration in the crystallization conditions, and ligand concentration might have to be scouted among other precipitants and additives. However this technique enables the possibility to saturate the protein with ligand thus resulting in a higher probability of finding a ligand molecule in the different protomers of the asymmetric unit of a crystal.

Both soaking and co-crystal approaches were performed and are described in this section for solving a high-resolution co-crystal structure of a DsbA in complex with a peptide from the pipeline. The most interesting structure solved during this PhD is analyzed and discussed in chapter IV. All crystallization trials were performed using the UQROCX (http://uqrocx.imb.uq.edu.au) diffraction facility. Diffraction data were collected at UQROCX and the Australian Synchrotron (http://www.synchrotron.org.au).

II.2.7.1 Soaking trials

Soaking crystals with ligands is a popular technique, as the crystallization conditions of the protein alone are already known. The usual process is to immerse pre-formed crystals into stabilizing solutions with different concentrations of the desired ligand for different periods of time. The ligand can then access the crystal solvent channels to reach the protein binding site. The soaking trials were performed under the supervision of Dr Begoña Heras. In this case, diamond-shaped crystals of EcDbsA were grown in 2 μL hanging drops containing 13%-18% PEG 8,000, 100 mM cacodylate, 8% glycerol and 1 mM $CuCl_2$. After 3 days, these crystals were transferred into 2 μL drops of a stabilizing solution (16% PEG 8,000, 100 mM cacodylate, 8% glycerol, 1 mM $CuCl_2$) and peptides (PSPFATCD and PSPWATCDFM) at concentrations from 2 mM to 15 mM (with DMSO concentration up to 3% from the DMSO 100% peptide stock solution). However this treatment led to blunted edges and visible cracks in the crystals within 2 hours and the entire dissolution of crystals within 4 hours. X-ray diffraction of these crystals at incubation times of two and three hours revealed a drastic loss of diffraction resolution (**Figure 2.17**).

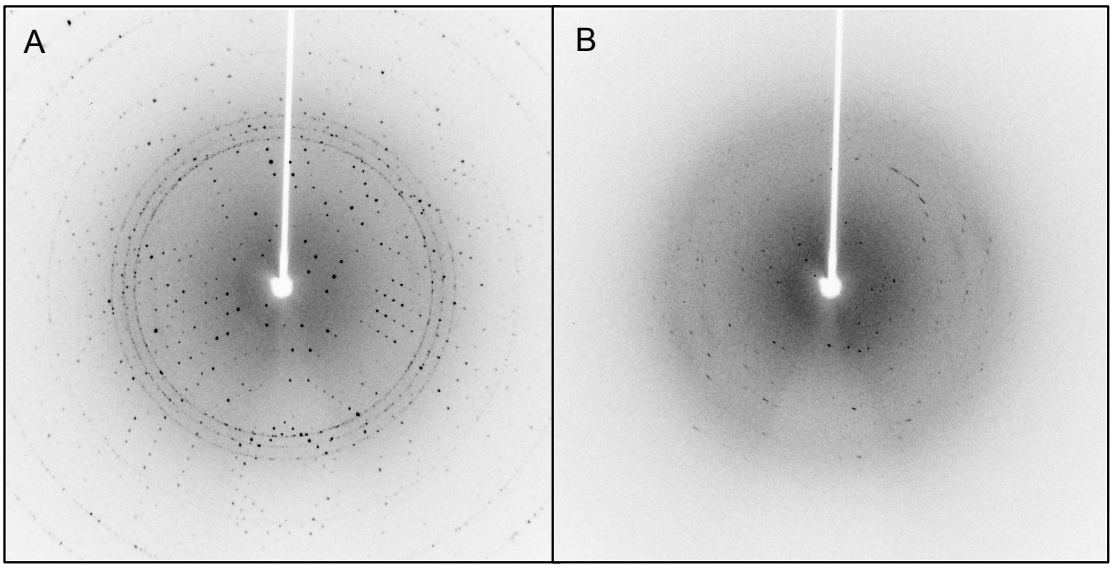

Figure 2.17. ***Diffraction patterns of EcDsbA crystals soaked with or without peptides. A****. Diffraction pattern with a resolution up to 1.7 Å of an EcDsbA crystal in stabilization solution for 2 hours.* ***B****. Diffraction pattern of an EcDsbA crystal grown with identical conditions as A, and incubated for 2 hours in a stabilizing solution including peptide PSPFATCD at 12 mM concentration.*

Interactions with EcDsbA (such as formation of an intermolecular disulfide bond with the catalytic cysteines) potentially accompanied with conformational change might have lead to the disruption of the crystal lattices on the crystal edges, ultimately leading to complete dissolution. This outcome suggested that soaking was not an appropriate technique in this case, even if it has been used successfully for smaller molecules (unpublished results), hence the co-crystallization approach was used for all subsequent experiments.

II.2.7.2 Co-crystallization

The co-crystallization approach requires the formation of a protein-ligand complex before setting the crystallization drops. This method has the advantage of allowing any conformational change on the protein caused by ligand binding to occur prior to the formation of lattice packing (in contrast to soaking techniques where the protein is already in a rigid lattice), but these conformational changes may also lead to alterations in the conditions required for crystallisation. Therefore, when an inhibitor peptide or peptidomimetic satisfied the screening pipeline and was incorporated into the co-crystallization trials, the EcDsbA-peptide complex was tested for crystallogenesis both using the known EcDsbA protein crystallization conditions (13%-18% PEG 8,000, 100 mM cacodylate, 8% glycerol, 1 mM $CuCl_2$), as well as commercial screens to find new conditions.

The EcDsbA-peptide crystals were obtained by mixing EcDsbA at a final concentration ranging from 30 $mg.mL^{-1}$ to 60 $mg.mL^{-1}$ (1.5 mM to 3 mM) with a molar excess of peptide at concentrations ranging from 5 mM to 30 mM in a solution of 10 mM HEPES pH 7.4 (with a final DMSO concentration of 2 %). The solutions were then incubated on ice for an hour to facilitate complex formation. Crystallization trials were set up in 96-well plates mixing 200 nL of EcDsbA-peptide complex with 200 nL of the crystallization condition using a Mosquito dispensing robot (TTP Labtech) and using the hanging drop vapor diffusion method. Trays were incubated and imaged at either 20 ºC or 8 ºC in a RockImager 1000 (Formulatrix). The commercial screening plates included Index, Peg/Ion and PegRX (Hampton Research), JCSG, Proplex, Morpheus and PACT (Molecular Dimensions), covering a broad array of common crystallization conditions (which implies a range of different solution compositions).

A substantial number of peptide sequences were tested for co-crystallization but crystallogenesis with EcDsbA proved difficult. The original EcDsbA crystallization conditions gave poor-looking crystals upon the addition of a peptide. Commercial screens led to several promising crystal hits (**Figure 2.18**) but diffraction revealed these either to be salt crystals or of poor diffraction quality. Conditions giving poorly diffracting crystals were optimized by varying pH, EcDsbA and peptide ratios and concentrations, and temperature. Promising conditions were also subject to further testing with an additive screen. Trays were also set up using solutions generated from ITC experiments; after successful titrations, EcDsbA-peptide complexes were retrieved from the ITC instrument, concentrated and directly used to set up crystallization drops. The possibility that the peptide was binding through the formation of an intermolecular bond with EcDsbA catalytic cysteine (see Chapter III) suggested the peptide might be turned over. To prevent such potential release of the peptide from EcDsbA, an EcDsbA mutant was engineered (see section II.2.1 of this chapter), substituting the catalytic Cys30 with Ser30 to prevent formation of any disulfide bond. Screening trays were set up with the EcDsbAC30S mutant to identify potential new 'hit' crystallization conditions, but only provided very poor and fragile crystals. Overall, the outcome of the co-crystallization attempts with EcDsbA was poor and no high-resolution co-crystal structures were solved.

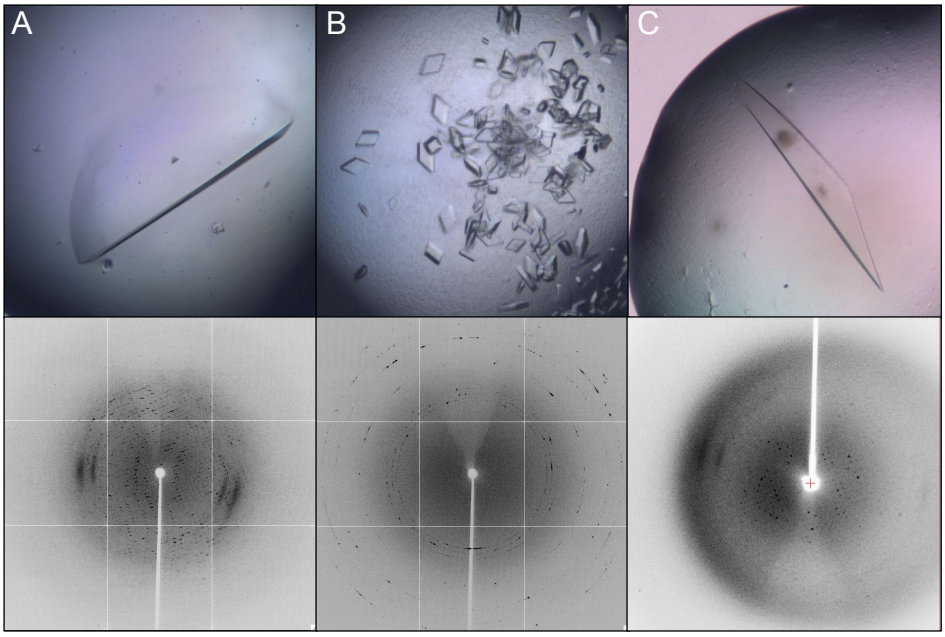

Figure 2.18. ***Examples of 'hit' co-crystallization conditions using EcDsbA and peptides. A.*** *EcDsbA – PSPWATCD crystal in sodium citrate dibasic 0.1 M, 22 % PEG 3,350 and n-octyl-6-D-glucoside 0.1 mM, which diffracted to low resolution (≥ 4.0 Å)* ***B.*** *EcDsbA – PSPWATCDF crystals in ammonium sulfate 2 M and citric acid 0.1 M, diffraction revealed the crystals to be salts.* ***C.*** *EcDsbA-PWATCDS crystal in Tris 0.1M pH 7.8, PEG 3,350 24% and sodium chloride 0.2M which gave anisotropic diffraction.*

An alternative protein was then trialled. The crystal structure of an EcDsbA homologue, *Proteus mirabilis* DsbA (or PmDsbA) had been solved within the lab by PhD student Fabian Kurth as part of another project investigating DsbA proteins in other pathogenic Gram-negative strains. PmDsbA shares many structural similarities with EcDsbA (see Chapter IV) and crystallization 'hits' in commercial plates were far more numerous than for EcDsbA. ITC showed that PmDsbA also bound the synthesized peptides with an affinity range similar to EcDsbA (see Chapter IV). Co-crystallization was therefore attempted using PmDsbA and a PmDsbAC30S mutant, giving a large number of crystal conditions (**Figure 2.19**).

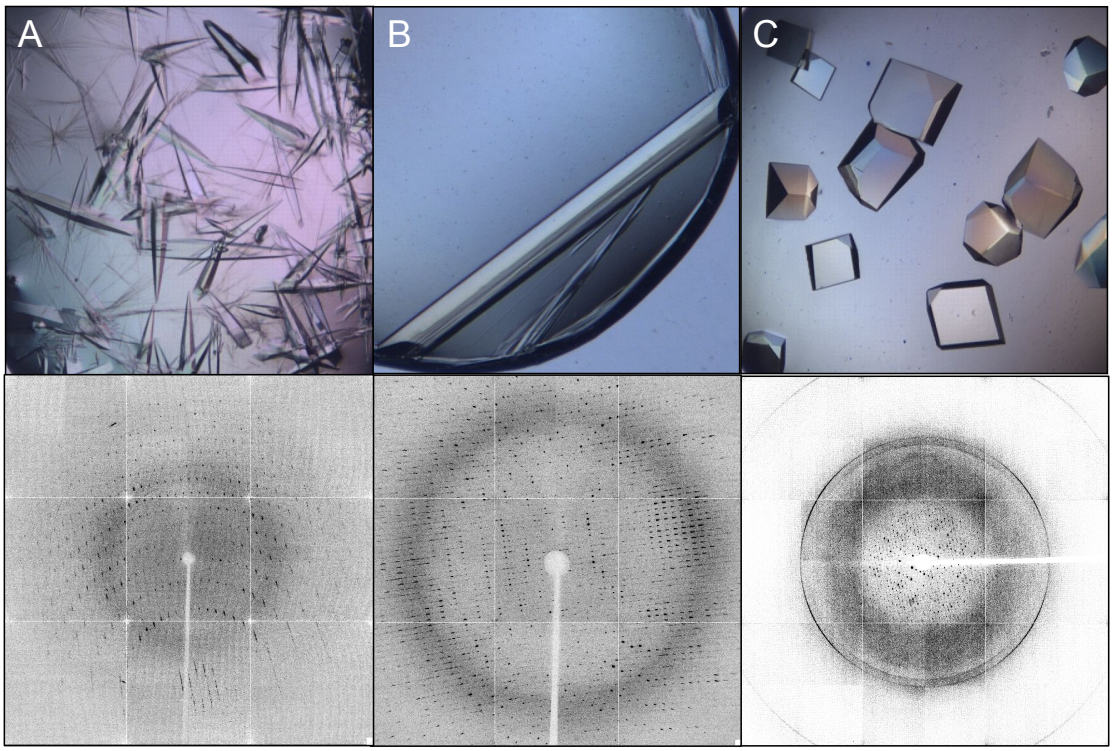

Figure 2.19. ***Examples of 'hit' co-crystallization conditions using PmDsbA and peptides. A.*** *PmDsbA-PSPWATCDF crystals in PEG 3,350 19.50% and Sodium Malonate 0.4 M. The solved 1.7 Å resolution structure did not include a peptide molecule.* ***B.*** *PmDsbAC30S-PWATCDS crystal in PEG 3,350 28% and potassium thiocyanate 0.6 M. This crystal provided the 1.6 Å co-crystal structure described in Chapter IV.* ***C.*** *PmDsbAC30S-PSPWATCDFMV crystal gave anisotropic diffraction.*

Crystallization trials were performed in collaboration with Fabian Kurth. Crystals that yielded a diffraction pattern with a resolution of 3 Å or higher during in-house screening at the UQ ROCX X-ray facility were subsequently tested at the Australian Synchrotron on beamlines MX1 or MX2. If the crystal diffracted to a resolution better or equal to 3 Å, diffraction images were

collected over 180º to 360º. Diffraction data were recorded with an ADSC Quantum 210r (MX1) or 315r (MX2) detector controlled by BLU-ICE (McPhillips *et al.*, 2002). Calculation of the density maps and refinements of the models were performed with the help and supervision of Dr Lakshmanane Premkumar. Reflections were indexed and integrated in Mosflm (Battye *et al.*, 2011) or XDS (Kabsch, 2010), analyzed in Pointless (Evans, 2006) and scaled in SCALA (Evans, 2006) from the CCP4 suite (Winn *et al.*, 2011). Molecular replacement (MR) was performed with PHASER (McCoy *et al.*, 2007) respectively using EcDsbA as a template (PDB code 1DSB) for EcDsbA co-crystals, PmDsbA (PDB code 4OCE) for PmDsbA co-crystals and PmDsbAC30S (PDB code 4OCF) for PmDsbAC30S cocrystals. Iterative refinement of the final structures were performed with Phenix.refine (Adams *et al.*, 2010) and Coot (Emsley *et al.*, 2010) with the details for the successful co-crystal structure described in Chapter IV.

Systematic co-crystallization of EcDsbA and PmDsbA with different peptides through a broad range of conditions was the most reagent- and time-consuming element in this research project. This step demonstrated a bottleneck in the pipeline, with the co-crystallization trays of more potent peptides being postponed while the previous molecules were still under co-crystallization optimization. However, this systematic approach provided the first reported high-resolution (1.6 Å) co-crystal structure of a DsbA with a non-covalently bound peptide, in this case PmDsbAC30S with peptide PWATCDS, which is the focus of Chapter IV.

II.3 Conclusion

From the initial ideal flowchart, the majority of the pipeline was successfully implemented; solid phase synthesis, DSF, ITC and model substrate oxidation assays were incorporated and used to synthesise and provide feedback on the characterization of peptides and peptidomimetics. Establishing a SPR assay was the major hurdle in this pipeline, and one that I was unable to overcome. Our collaborators have since reported similar difficulties in setting up an SPR assay for EcDsbA (M. Scanlon, personal communication). However, a potential solution has been found using a new EcDsbA construct using two 6xHis tags in tandem that optimizes the immobilization method. Using this construct specific binding of small molecules has been detected. The expression and purification of such a construct could be trialed for SPR analyses of specific binding from peptides and peptidomimetics. Systematic co-crystallization did not have the expected success due

to the strong influence of peptides upon the crystallization conditions but a high-resolution structure of a non-covalent DsbA-peptide structure was solved for the EcDsbA homologue from *P. mirabilis*.

Besides the assays presented within the pipeline, additional techniques could be envisaged to provide additional information on the peptide binding mode. STD NMR analysis of peptide binding could identify EcDsbA residues affected by the binding event hence provide additional information for the design of future peptides. Microscale thermophoresis offers an alternative in affinity measurement for molecules with a major entropy contribution in binding (for which ITC has a limited sensitivity). Microscale thermophoresis does not require immobilization of the protein or peptide (unlike SPR) and does not use thermodynamic measurements to calculate the affinity (unlike ITC). However, this assay would only provide a *K*d value and no thermodynamic or kinetic information. Finally mass spectrometry could be useful for detecting the formation of EcDsbA-peptides complexes and the formation of covalent adducts (for example if the peptide forms an irreversible disulfide bond).

In summary the pipeline I established (excluding the SPR component) is able to characterize a newly designed molecule in a timeframe of 5 days, from synthesis to the first co-crystallization plates, and the outcomes of these experiments are presented in chapters III, IV and V.

CHAPTER III

The following chapter is a manuscript submitted to the Journal of Medicinal Chemistry. Following the assembly of the screening pipeline as reported in Chapter II, a large number of peptides (based on the EcDsbA-EcDsbB interaction described in I.2.3) were synthesized and tested for binding and inhibition of the EcDsbA activity. A selection of 31 sequences was chosen to describe the interactions between these potential inhibitors and the EcDsbA binding site. The purpose of this structure-activity relationship (SAR) study is to identify the chemical moieties, residues and interactions essential for the binding and inhibition of EcDsbA. Peptides presenting weaknesses as druggable molecules (see Chapter I.3.1), the properties of the most advantageous peptide sequence (in terms of affinity, inhibition and ligand efficiency) will be used for the future design of peptidomimetic compounds. The supplementary information provided with the manuscript is available in Appendix C.

This manuscript is also the result of fruitful collaboration with other contributors: the substrate oxidation peptide protocol (see section II.2.6) was provided by Dr Halili, who performed the assay for one peptide sequence while I applied for the others. Dr Halili also contributed to the production of EcDsbA protein samples for this work and provided the EcDsbB membrane preparations necessary for the substrate oxidation assay. Peptides were all synthesized according to a protocol provided by Dr Lindahl (see section II.2.2) with his advice and expertise for optimal yields. The final manuscript was reviewed and critically revised by Dr Halili, Dr Lindahl, Dr Reid, Prof. DP Fairlie and Prof. JL Martin.

Peptide inhibitors of the *Escherichia coli* DsbA/DsbB interface

Wilko Duprez[1], Maria Halili[1], Fredrik Lindahl[1], Robert C. Reid[1], David P. Fairlie[1] and Jennifer L. Martin[1]**

[1]University of Queensland, Institute for Molecular Bioscience, Division of Chemistry and Structural Biology, Brisbane, Queensland 4072 Australia

* To whom correspondence should be addressed: j.martin@imb.uq.edu.au and d.fairlie@imb.uq.edu.au

Abstract

Antibacterials with novel modes of action are desperately needed to address the increasing problem of antibiotic resistance. One approach is to develop drugs that interfere with bacterial virulence. A master regulator of virulence in Gram-negative bacteria is the oxidative folding machinery comprising DsbA and DsbB. DsbA introduces disulfide bonds into folding protein substrates while its partner protein DsbB maintains DsbA in the active oxidized form. Using crystal structure information on the DsbA:DsbB complex we evaluated structure-activity relationships for 31 peptides using natural and unnatural amino acids, alanine substitutions and sequence length variation. Several peptides were found to bind oxidized DsbA (K_d 2.0 ± 0.3 μM) and inhibit its activity (IC_{50} 5.1 ± 1.1 μM). A cysteine was essential for interaction of the peptide with DsbA suggesting that future peptidomimetic inhibitors should be designed to exploit this thiol interaction. Such inhibitors could provide the basis for antivirulence agents with a novel mechanism of action.

Introduction

The rapid increase in antibiotic resistance (Boucher *et al.*, 2009) combined with only a trickle of new antibiotics (Zurenko *et al.*, 1997, Tally & DeBruin, 2000, Casewell & Hill, 1987, Novak & Shlaes, 2010) through the development pipeline has been described as a looming public health crisis (The Bacterial Challenge: time to react, 2010). One approach to generate new classes of antibacterial drugs is to target bacterial virulence traits rather than killing or inhibiting the growth of bacteria. This approach may induce less evolutionary pressure to develop resistance compared with current antibiotics (Clatworthy *et al.*, 2007). Moreover, targeting virulence might limit the detrimental impact of drugs on host flora (Rasko & Sperandio, 2010).

The Dsb periplasmic oxidative folding pathway of Gram-negative bacteria plays a master role in virulence (Heras *et al.*, 2009). This process is essential for assembly of host cell adhesins (Jacob-Dubuisson *et al.*, 1994), toxins (Wulfing & Rappuoli, 1997), type III secretion system systems (Miki *et al.*, 2008), and motility machines (Dailey & Berg, 1993) among others. Bacterial strains lacking Dsb enzymes are viable but non-pathogenic (Totsika *et al.*, 2009b), providing proof of principle that targeting this machinery may be a feasible antivirulence strategy. The archetypal system in *Escherichia coli K12* comprises two enzymes, DsbA and DsbB. The dithiol oxidase *E. coli* DsbA (EcDsbA) (Bardwell *et al.*, 1993, Bardwell *et al.*, 1991) introduces disulfide bonds between cysteine residues in protein substrates by thiol exchange (Dutton *et al.*, 2008) through a bimolecular nucleophilic reaction (**Figure 3.1**). EcDsbA is then re-oxidized by the membrane protein EcDsbB. The first step in re-oxidation is the formation of a mixed disulfide between EcDsbA Cys30 and EcDsbB Cys104 (located on a periplasmic loop of the EcDsbB membrane protein). This mixed disulfide is then subject to nucleophilic attack by EcDsbA Cys33 resulting in the release of oxidized EcDsbA (Kadokura & Beckwith, 2002). EcDsbB is highly specific for EcDsbA (Shouldice *et al.*, 2011).

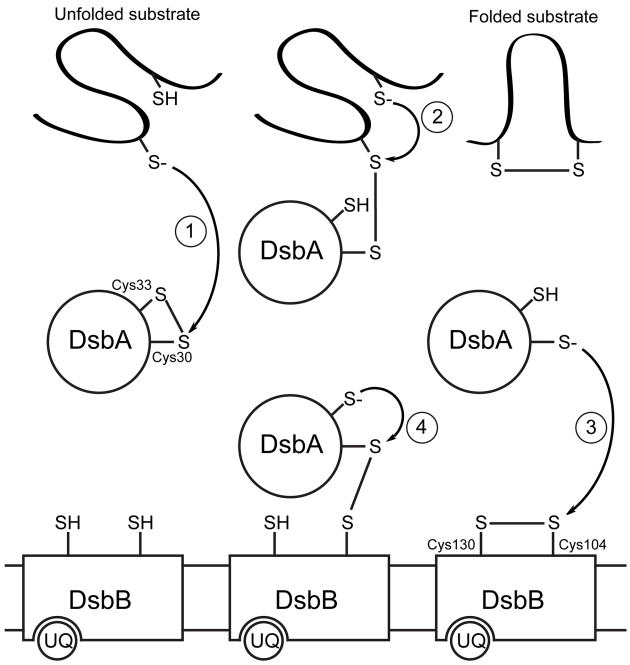

Figure 3.1. ***DsbA-induced disulfide bond transfer mechanism.*** *1. The nucleophilic attack of a substrate thiolate onto oxidized DsbA Cys30 leads to the formation of an intermolecular disulfide bond. 2. Nucleophilic attack on the disulfide by a second substrate thiolate induces substrate folding by formation of an intramolecular disulfide bond and releases DsbA in the inactive reduced state. 3. Reduced DsbA Cys30 forms a disulfide bond with membrane-bound oxidized DsbB Cys104. 4. Nucleophilic attack by DsbA Cys33 on Cys30 results in disulfide bond formation in the DsbA active site. The additional electrons on the DsbB loop are subsequently transferred to ubiquinone and ultimately to the respiratory system.*

The present study was aimed at discovering whether peptides derived from EcDsbB would inhibit EcDsbA and thus be useful as the basis for future development of antivirulence compounds. The goal was to identify peptides that inhibit DsbA activity by interfering with the DsbB binding surface. In our peptide design, we made use of information from low-resolution crystal structures defining the EcDsbA-EcDsbB interaction (Inaba *et al.*, 2009a, Malojcic *et al.*, 2008, Inaba, Murakami*, et al.*, 2006). The central interaction of the EcDsbB periplasmic P2 loop residues ^{98}PSPFATCDFMVR^{109} is the mixed disulfide formed between Cys104 of the EcDsbB P2 loop and EcDsbA Cys30 of the ^{30}CPHC^{33} active site motif. However, additional interactions are also present. Specifically, residues ^{98}PSPFAT^{103} interact with a hydrophobic groove on EcDsbA, which had been suggested previously as a potential peptide-binding groove (Martin *et al.*, 1993). The groove is formed from aromatic and aliphatic residues (Phe36, Leu40, Ile42, Phe174 Tyr178) of EcDsbA helices α1 and α6 (**Figure 3.2**). In addition, the EcDsbA *cis*Pro loop, a characteristic feature of the active sites of many thioredoxin-fold proteins (Qin *et al.*, 1996, Nikkola *et al.*, 1991), also participates in the interaction with EcDsbB through hydrogen bond formation with backbone atoms

of EcDsbA Arg148 and EcDsbB Phe106 (Figure 2). Taken together, the structural information suggested that interactions other than disulfide bond formation could be exploited for the development of an inhibitor scaffold targeting EcDsbA.

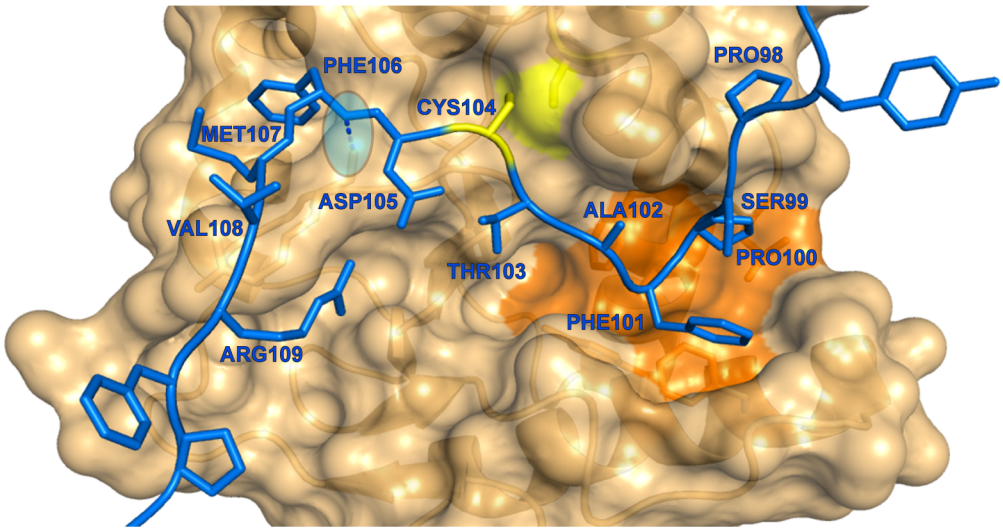

Figure 3.2. ***EcDsbB P2 loop - EcDsbA interface from the 3.7 Å resolution EcDsbA-EcDsbB crystal structure*** *by Inaba et al.(Inaba et al., 2009b) (PDB code 2ZUP). The EcDsbB loop is shown in blue with interacting residues at the interface labeled. The surface of EcDsbA is shown in beige with the hydrophobic pocket identified in orange. Both cysteines involved in a disulfide bond are shown in yellow. The predicted hydrogen bond between EcDsbB Phe106 and EcDsbA Arg148 is shown as a blue dashed line and its location highlighted in light blue.*

The EcDsbA-EcDsbB crystal structure was used to determine the initial synthetic peptide for these studies which corresponded to the sequence of the EcDsbB P2 loop that binds EcDsbA (Figure 2). A screening pipeline comprising thermal shift, isothermal titration calorimetry, and substrate oxidation assays was established to measure binding affinity for EcDsbA and inhibitor characteristics of a series of synthetic peptides. Structure-activity relationships for 31 synthetic peptides were assessed by varying length, using non-native amino acids, and by substituting side chains with alanine to identify critical components for activity.

Results

EcDsbB-derived peptides bind to oxidized EcDsbA

The sequence of peptide **1** was identified from the low-resolution crystal structure of the EcDsbA-EcDsbB crystal structure (Inaba *et al.*, 2009a) (PDB code 2ZUP) and corresponds to residues ^{98}PSPFATCDF^{106} of the EcDsbB periplasmic loop P2 that interact with EcDsbA. We first assessed the ability of this synthetic 9-residue peptide to interact with EcDsbA using a thermal shift assay that required small quantities of protein and peptide and which can be performed rapidly. The free energy contribution of peptide binding increases the Gibbs free energy of protein unfolding, which is measured as an increase in the protein melting temperature, *Tm* (Kranz & Schalk-Hihi, 2011). Peptide **1** was found to markedly affect the EcDsbA melting temperature (**Figure 3.3** and **S1**), with Δ*Tm* 1.5 ± 0.1 ºC at the lowest concentration used ([PSPFATCDF] 125 μM) and 7.5 ± 0.1 ºC at the highest concentration ([PSPFATCDF] 4 mM) (**Table 3.1**). These results suggested that this short synthetic peptide sequence, corresponding to a single loop fragment of EcDsbB, did indeed have significant binding affinity for EcDsbA.

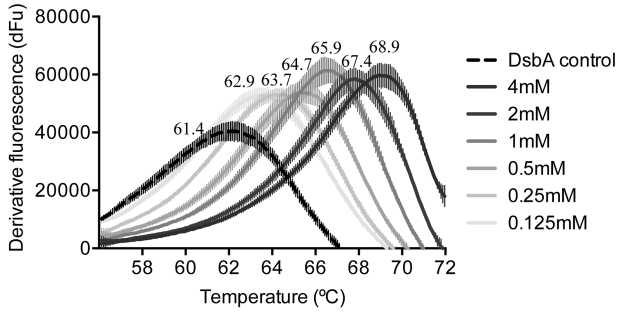

Figure 3.3. ***PSPFATCDF binds to EcDsbA.*** *Sigmoidal curves can be fitted onto unfolding fluorescence readings where an inflexion point indicates Tm (see Supplementary figure S1). Tm is here shown as a peak in the first derivative of the sigmoidal curve for each peptide concentration. Tm values are determined from fitting the sigmoidal curve between 56°C and 72°C and values are shown here above the derivative curves according to each peptide concentration.*

Table 3.1. ***Shifts in EcDsbA melting temperature*** *observed in thermal shift assay for peptides* ***1, 23*** *and* ***31****.*

		Peptide Concentration						
		0 μM	125 μM	250 μM	500 μM	1 mM	2 mM	4 mM
Nº	Peptide	Tm[A]	ΔTm[A]	ΔTm	ΔTm	ΔTm	ΔTm	ΔTm
1	PSPFATCDF	61.4 ± 0.1	+1.5 ± 0.1	+2.3 ± 0.1	+3.4 ± 0.1	+4.5 ± 0.1	+6.0 ± 0.1	+7.5 ± 0.1
23	PWATCDS	61.4 ± 0.1	+1.7 ± 0.1	+ 3.3 ± 0.2	+3.7 ± 0.1	+5.0 ± 0.1	+6.9 ± 0.1	+9.8 ± 0.1
31	PWATSDS	61.4 ± 0.1	+0.1 ± 0.1	+ 0.2 ± 0.2	+0.2 ± 0.3	+0.6 ± 0.1	+1.5 ± 0.1	+2.9 ± 0.1

[A]Tm (ºC) represents the unfolding temperature and ΔTm (ºC) is the difference between the Tm for EcDsbA in the presence and absence of the peptide.

To investigate binding further, isothermal titration calorimetry (ITC) was used to assess the affinity and thermodynamics of the interaction. ITC profiles of PSPFATCDF binding to oxidized EcDsbA revealed an exothermic reaction with a significant release of energy (2.4 μcal.sec^{-1}) for the first injection (Figure S2). The absence of an initial plateau, despite varying the peptide concentration, protein concentration and injection volumes (not shown), suggested a very fast on-rate (k_{on}) for the peptide binding to EcDsbA. The ITC profile is typical of a 1:1 stoichiometry, and we therefore concluded that one peptide molecule bound to one molecule of EcDsbA and curve-fitting analysis parameters were configured appropriately. Using these parameters, peptide **1** had a K_d 4.0 ± 1.5 μM for EcDsbA, with a strong enthalpic component to binding (ΔH = -9.9 ± 0.1 kcal.mol^{-1}) and a relatively unfavorable entropy (ΔS = -8.3 ± 2.9 cal.mol^{-1}.deg^{-1}) (**Table 3.2**), an observation that is common for binding of linear peptides (Temussi *et al.*, 1989). This binding affinity equates to a Binding Efficiency Index (BEI) of 5.3 (BEI is used to assess the interaction quality as the mass of the ligand changes (Abad-Zapatero & Metz, 2005) with higher values being better; see materials and methods). ITC did not detect binding of peptide **1** to reduced EcDsbA (where the CXXC active site was in the dithiol form) (Figure S2). All subsequent peptide binding assays were performed using oxidized EcDsbA. Peptide **2**, PSPFATCD, which differed from **1** only in the removal of the C-terminal Phe9 residue, had a 4-fold lower affinity for EcDsbA (K_d 16.2 ± 1.8 μM, Table 2) but a slightly increased BEI of 5.5. The reduced enthalpy of binding of octapeptide **2** compared with nonapeptide **1** is likely a consequence of the loss of a hydrogen bond between the backbone atoms of the additional C-terminal Phe9 in peptide **1** with EcDsbA Arg148(Shouldice *et al.*, 2011) of the *cis*Pro loop (see **Figure 3.2**).

Table 3.2. ***Isothermal titration calorimetry analysis of peptides 1 to 31*** *binding oxidized EcDsbA.*

N°	Sequence	N	**Kd (µM)**	ΔH (kcal/mol)	ΔS (cal/mol/°)	ΔG (kcal/mol)	Mw (Da)	BEI
1	PSPFATCDF	1.0 ± 0.1	**4.0 ± 1.5**	-9.9 ± 1.1	-8.3 ± 2.9	-7.4 ± 0.2	1025	5.3
2	PSPFATCD	1.1 ± 0.1	**16.2 ± 1.8**	-8.4 ± 0.1	-6.1 ± 0.5	-6.5 ± 0.1	878	5.5
3	PSP**W**ATCDF	1.1 ± 0.1	**2.9 ± 0.3**	-11.1 ± 0.2	-12.1 ± 0.4	-7.6 ± 0.1	1064	5.2
4	PSP**W**ATCD	1.0 ± 0.1	**10.7 ± 0.7**	-11.8 ± 0.2	-17.0 ± 0.5	-6.8 ± 0.2	917	5.4
5	PSP**W**ATC	1.1 ± 0.1	**18.0 ± 0.7**	-8.6 ± 0.2	-7.2 ± 0.6	-6.5 ± 0.1	802	5.9
6	PSP**hf**ATC	1.0 ± 0.1	**14.9 ± 2.2**	-9.1 ± 0.8	-8.4 ± 2.8	-6.6 ± 0.1	776	6.2
7	PSP**1dip**ATC	1.1 ± 0.1	**9.7 ± 1.8**	-8.7 ± 0.7	-6.5 ± 2.3	-6.8 ± 0.1	838	6.0
8	PS**pip**WATC	1.1 ± 0.1	**12.0 ± 2.6**	-8.6 ± 0.7	-6.2 ±2.4	-6.7 ± 0.2	815	6.0
9	PS**thiq**WATC	1.0 ± 0.1	**13.1 ± 3.0**	-11.1 ± 0.9	-15.6 ± 3.5	-6.5 ± 0.5	866	5.7
10	**A**SPWATCDF	1.1 ± 0.1	**2.7 ± 1.0**	-11.6 ± 1.5	-13.5 ± 4.1	-7.6 ± 0.3	1038	5.4
11	P**A**PWATCDF	1.0 ± 0.1	**2.8 ± 0.2**	-9.5 ± 0.9	-6.4 ± 2.9	-7.6 ± 0.1	1048	5.3
12	PS**A**WATCDF	1.0 ± 0.1	**5.5 ± 1.5**	-8.5 ± 0.3	-4.5 ± 0.3	-7.2 ± 0.2	1038	5.1
13	PSP**A**ATCDF	1.0 ± 0.1	**5.8 ± 0.8**	-11.7 ± 0.6	-15.4 ± 2.2	-7.4 ± 0.2	949	5.5
14	PSPWA**A**CDF	1.1 ± 0.1	**11.3 ± 2.3**	-7.4 ± 0.5	-2.3 ± 1.6	-6.7 ± 0.1	1034	4.8
15	PSPWAT**A**DF	N/A					1032	
16	PSPWATC**A**F	1.0 ± 0.1	**3.1 ± 1.1**	-13.0 ± 0.5	-18.3 ± 1.7	-7.6 ± 0.3	1020	5.4
17	PSPWATCD**A**	1.0 ± 0.1	**4.4 ± 0.7**	-14.9 ± 1.3	-25.7 ± 4.6	-7.3 ± 0.1	988	5.4
18	PSP**W**ATCDFMV	1.0 ± 0.1	**2.5 ± 0.7**	-12.5 ± 0.4	-16.1 ± 1.9	-7.7 ± 0.2	1295	4.3
19	PSP**W**ATCDFM	1.2 ± 0.1	**2.0 ± 0.3**	-12.6 ± 1.8	-16.2 ± 6.0	-7.8 ± 0.1	1195	4.8
20	SP**W**ATCDF	1.0 ± 0.1	**2.2 ± 0.1**	-15.6 ± 0.8	-26.7 ± 2.7	-7.6 ± 0.2	967	5.8
21	P**W**ATCDF	1.0 ± 0.1	**3.0 ± 0.1**	-14.3 ± 0.5	-22.6 ± 2.8	-7.5 ± 0.3	880	6.3
22	P**W**ATCD**S**	1.0 ± 0.1	**5.7 ± 0.4**	-13.6 ± 0.1	-21.6 ± 3.5	-7.1 ± 0.1	820	6.4
23	P**hF**ATCD**S**	1.0 ± 0.1	**8.3 ± 0.4**	-11.8 ± 0.3	-16.2 ± 0.9	-6.9 ± 0.1	795	6.4
24	PSP**W**AT**S**DF	N/A					1048	
25	PSP**W**AT**hs**	N/A					801	
26	PSP**W**AT**N**	N/A					813	
27	PSP**W**AT**V**DF	N/A					1060	
28	PSP**W**AT**I**DF	N/A					1074	
29	PSP**W**AT**nve**	N/A					799	
30	PSP**W**AT**M**	N/A					830	
31	P**W**AT**S**D**S**	N/A					804	

Calculated values are stoichiometry (N), affinity (Kd), enthalpy change (ΔH) and entropy change (ΔS). Total free energy (ΔG) is calculated according to the equation ΔG = ΔH – TΔS, with T the temperature set up for the ITC experiment. The Binding Efficiency Index (BEI) is calculated with the following equation: BEI = -pKd / Mw, where Mw is the molecular weight of the ligand in kDa. In bold are shown residues differing from the original EcDsbB peptide sequence. N/A indicates weak binding preventing analysis. hf = homophenylalanine, 1dip = Ala-1-Diphenol, pip = pipecolic acid, thiq = tetrahydroisoquinolone, hs = Homoserine and nve = Norvaline.

Modification of residues that interact with the EcDsbA hydrophobic groove

An attractive starting point for optimization of peptide ligands is the Phe4 residue of nonapeptide **1** (PSP**F**ATCDF), the residue equivalent to EcDsbB Phe101. In the crystal structure of the EcDsbA-EcDsbB complex, Phe101 is buried in a hydrophobic pocket within the groove of EcDsbA (**Figure 3.2**). The binding interactions for this residue are exclusively hydrophobic, suggesting that a bulkier hydrophobic side chain might increase interactions with EcDsbA (residues Phe36 and Phe174). We investigated the effect of modifying this side chain. When Phe4 was substituted with the bulkier residue Trp (PSP**W**ATCDF, peptide **3**), a slightly improved affinity was observed (K_d 2.9 ± 0.3 μM) (Table 2) but this corresponded to a reduced BEI value (5.2). The same replacement in peptide **2** (*ie* PSP**W**ATCD, peptide **4**) gave an improvement in binding affinity (K_d 10.7 ± 0.7 μM) and a similar BEI (5.4).

To circumvent difficulties encountered during the synthesis of peptides **6** to **9** containing unnatural amino acid residues (**Figure 3.4**), the C-terminus was truncated by not including residues Asp8 and Phe9. The reference compound for this series was heptapeptide **5**, PSPWATC, which is related to peptide **1** by the removal of these two C-terminal residues and by using Trp in place of Phe4. Peptide **5** had a slightly reduced K_d (18.0 ± 0.7 μM) compared to peptides **1** and **4**, but this lower affinity was offset by the smaller size of peptide **5**, so that it had an improved BEI (5.9) towards oxidized EcDsbA. The binding of peptide **5** was associated with a lower enthalpy contribution (ΔH -8.6 ± 0.2 kcal.mol^{-1}) and a more favorable entropy change (ΔS -7.2 ± 0.6 cal.mol^{-1}.deg^{-1}) in comparison to peptides **1** and **4**.

Next, the Phe4 residue was replaced with the unnatural amino acid homophenylalanine (PSP(**hF**)ATC, peptide **6,** Figure 4). Compared with peptide **5** (PSPWATC), the hPhe substitution improved the affinity to a small degree (K_d 14.9 ± 2.2 μM, Table 2) and also improved the thermodynamics (ΔH -9.1 ± 0.8 kcal.mol^{-1}, ΔS -8.4 ± 2.8 cal.mol^{-1}.deg^{-1}). Importantly, the longer side chain resulted in an improved BEI (6.2 compared with 5.9). Alternative substitution at the 4 position with a diphenylmethyl group (peptide **7,** Figure 4) increased the bulk of the side chain and improved affinity for EcDsbA almost two-fold (K_d 9.7 ± 1.8 μM, Table 2) relative to peptide **5** (PSPWATC). However, the larger side chain translated into only a small improvement in BEI (6.0). Overall, the phenylethyl side chain at position 4 was a slightly better option than the diphenylmethyl group, though for further exploration of peptide SAR the natural amino acid Trp was maintained at this position.

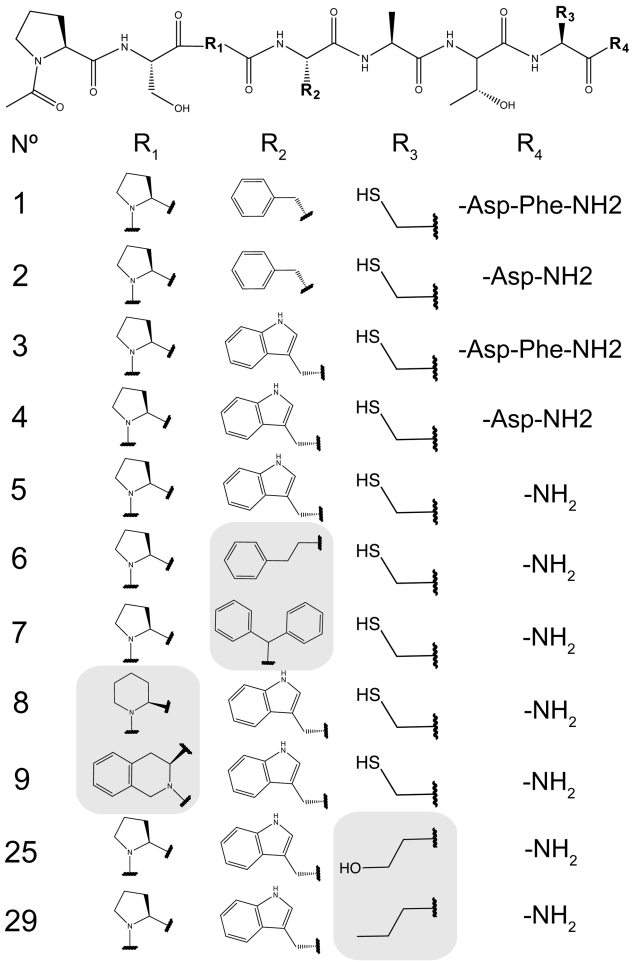

Figure 3.4. ***Structure of the peptide scaffold of PSPFATCDF*** *(peptide 1) and the modified positions in selected subsequent peptides. Non-natural side chains are highlighted in grey.*

We next sought to investigate the effect of substituting Pro3, the residue preceding Trp4 in peptide **5** that corresponds to Pro100 in EcDsbB and which binds in the same hydrophobic groove of EcDsbA as Phe101. Pro3 was replaced by two non-native residues pipecolic acid (**Pip**) and tetrahydroisoquinoline-3-carboxylic acid (**Thiq**) (peptides **8** and peptide **9** respectively, Figure 4) to probe the space available in the groove. Both PS(**Pip**)WATC (peptide **8**) and PS(**Thiq**)WATC (peptide **9**) gave a moderate improvement in affinity (K_d 13.1 ± 3.0 μM and 12.0 ± 2.6 μM, respectively) over peptide **5**, however their BEI values indicated no overall improvement in the quality of the interaction (5.9, 6.0, and 5.7, respectively for peptides **5**, **8** and **9**). Moreover the binding entropy for peptide **9** (ΔS -15.6 ± 3.5 cal.mol^{-1}.deg^{-1}) suggested an unfavorable binding conformation.

Alanine substitution and importance of Cys in peptide binding

The limited improvement in BEI observed upon substituting Pro3 and Trp4, residues corresponding to Pro100 and Phe101 in EcDsbB, suggested that other residues of the peptide might

contribute to EcDsbA binding. We therefore performed a focused alanine scan with the aim of identifying residues that were critical for interaction. We evaluated the 9-residue peptide PSPWATCDF (peptide **3**, BEI 5.2), substituting each residue in turn with alanine. Using the BEI values as a guide, we found that peptides **10** (Pro1Ala) and **11** (Ser2Ala) had slightly improved BEI values, indicating that their sidechains probably contributed little to the binding interaction. Peptide **12** (Pro3Ala, BEI 5.1) had a slightly reduced BEI value indicating a loss in binding relative to Pro3. This is supported by the EcDsbA-EcDsbB crystal structure showing that the corresponding Pro100 of EcDsbB interacts with the EcDsbA hydrophobic groove. Interestingly, peptide **13** (Trp4Ala) had a similar BEI of 5.5 compared with peptide **1**. However, the binding thermodynamics were strongly affected, the entropy contribution being more unfavorable (ΔS -15.4 ± 2.2 cal.mol^{-1}.deg^{-1}), suggesting that this peptide adopted a conformation with little shape complementarity for EcDsbA. Peptide **14** (Thr6Ala) exhibited a large reduction in BEI (**Table 3.2**) compared with **3,** suggesting that this sidechain should be retained. The reduction in affinity of peptide **13 (**PSPWA**A**CDF) for EcDsbA was surprising given that the EcDsbA-EcDsbB crystal structure showed the EcDsbB Thr103 side chain oriented away from EcDsbA. Therefore, the role of Thr6 in the binding mechanism remained unclear.

Replacement of the C-terminal residues Asp8 and Phe9 with alanine (peptides **16** and **17**) resulted in an increase of the BEI value (5.4), indicating that these side chains contribute little to the binding interaction. Indeed, removal of these two residues (peptide **5**) improved the BEI considerably (5.9), although the crystal structure suggested the presence of hydrogen bond formation between the backbone atoms of the corresponding EcDsbB Phe106 residue and the EcDsbA *cis*Pro loop, as well as π-stacking interactions between EcDsbB Phe106 and EcDsbA Phe63. The entropic contribution to the interaction of peptides **16** and **17** was very unfavorable (ΔS -18.3 ± 1.7 cal.mol^{-1}.deg^{-1}and -25.7 ± 4.6 cal.mol^{-1}.deg^{-1}, respectively) suggesting that the corresponding residues Asp105 and Phe106 may play a role in pre-ordering the loop conformation in EcDsbB for binding to EcDsbA.

Replacement of Cys7 with alanine (peptide **15**, PSPWAT**A**DF) abolished binding as determined by ITC. This suggested that nucleophilic attack of EcDsbA Cys30 by the peptide to form a mixed disulfide bond is critical for interaction of this synthetic peptide series corresponding to the EcDsbB loop residues 98-106. This result indicated that the peptides form a covalent interaction with EcDsbA. This is consistent with the activity of EcDsbA enzyme to interact with reduced proteins and is supported by the data described above showing that peptide **1**

(PSPFATCDF) binds to oxidized EcDsbA (forming a mixed disulfide) and weakly, if at all, to reduced EcDsbA.

In summary, the alanine substitution experiments showed that Cys7 was critical and that the Trp4 and Thr6 side-chains were most important for interacting with EcDsbA.

Effect of peptide length

We explored the effect of peptide length to identify residues that could be truncated without impacting greatly on affinity. For this purpose, a series of seven peptides with sequence lengths ranging from 6 to 11 residues was generated. Peptides **18** (PSPWATCDF**MV**) and **19** (PSPWATCDF**M**) included residues that correspond to residues Met107 and Val108 in DsbB that made hydrophobic interactions with EcDsbA in the crystal structure complexes with EcDsbB (Inaba *et al.*, 2009a, Inaba, Murakami*, et al.*, 2006, Malojcic *et al.*, 2008). However, both peptides had considerably lower BEI values than peptide **3** (PSPWATCDF) indicating that these additional residues were dispensable (**Table 3.2**). As described above, an addition of phenylalanine to peptide **4** (PSPWATCD) giving peptide **3** (PSPWATCDF) also reduced the BEI value. However, Phe9 in peptide **3** corresponds to Phe106 of DsbB which forms a backbone hydrogen bond with Arg148 of the *cis*Pro loop of EcDsbA in the crystal structure. Therefore, we investigated the effect of reducing the side chain size of this residue (below). Similarly, the addition of aspartate to peptide **5** (PSPWATC) giving peptide **4** (PSPWATCD) was associated with an increase in affinity (K_d 18.0 ± 0.7 μM to 10.7 ± 0.7 μM) but a decreased BEI value (5.9 to 5.4). In the crystal structure, EcDsbB Asp105 appears to form a salt bridge with EcDsbB Arg109 and a hydrogen bond to EcDsbB Thr103. These intramolecular interactions may structurally organize the EcDsbB loop although this wasn't apparent in the entropy changes observed for the shorter peptides.

We next investigated N-terminal truncation. In the 3.7 Å resolution crystal structure both Pro98 and Ser99 of EcDsbB are located outside of the hydrophobic groove and make few if any contacts with EcDsbA (Shouldice *et al.*, 2011). Removing the corresponding Pro**1** from peptide **3** gave peptide **20** (SPWATCDF) with similar binding affinity (K_d 2.2 ± 0.1 μM, **Table 3.2**), an improved BEI (5.8 compared with 5.2), and increased enthalpy (ΔH -15.6 ± 0.8 kcal.mol^{-1}) but more unfavourable entropy (ΔS -26.7 ± 2.7 cal.mol^{-1}.deg^{-1}). Removing both Pro1 and Ser2 to give peptide **21** (PWATCDF) gave similar binding affinity and thermodynamic properties to peptide **20**, and a further increase in BEI to 6.3. However, peptide **21** had low water solubility. To address this, Phe7 was replaced with Ser7 to give peptide **22** in an attempt to increase solubility without affecting

affinity. This peptide had the highest BEI value of all peptides in this study (6.4) and much improved aqueous solubility. Combining the two peptide sequences with the best BEI (peptide **8** and **22**) gave peptide **23** (P(**hF)**ATCD**S**) which showed a slightly lower affinity (*K*d 8.3 ± 0.4 μM) but a similar BEI (6.4) with a decreased enthalpy (ΔH -11.8 ± 0.3 kcal.mol^{-1}) and more favorable entropy (ΔS -16.2 ± 0.9 cal.mol^{-1}.deg^{-1}).

Overall, peptides with the most favorable affinity/length ratio and best solubility were the 7-residue peptides **22** and **23**, PWATCDS (K_d 5.7 ± 0.1 μM) and P(hF)ATCDS (*K*d 8.3 ± 0.4 μM). In comparison with peptide **1** (PSPFATCDF), these two peptides increased BEI from 5.3 to 6.4.

Evaluation of peptides lacking a cysteine

The formation of a covalent disulfide bond between peptide Cys7 and EcDsbA Cys30 may not be desirable in viable drug-like antivirulence agents targeting EcDsbA. We then investigated whether non-covalent binding of a peptide to EcDsbA could be achieved by replacing the cysteine side chain. A logical substitution for the Cys7 thiol side chain is the hydroxyl side chain of Ser7 (PSPWAT**S**DF, peptide **24**), due to its similar size and the potential to form hydrogen bonds through its hydroxyl group with the *cis*Pro loop. However peptide **24** bound weakly, if at all, to EcDsbA based upon ITC measurements (**Table 3.2**). To investigate the possibility that the hydroxyl side chain of Ser7 may be too short to form hydrogen bonds with EcDsbA, peptide **25** was synthesized with a homoserine (**Figure 3.4**) at position 7 (PSPWAT**hS**). Again, there was no evidence of binding using ITC. Similarly, replacement of Cys7 with Asn7 (PSPWAT**N**, peptide **26**) resulted in no detectable binding. We then sought to replace Cys7 with hydrophobic residues Val7, Ile7, Norvaline7 and Met7 (PSPWAT**V**DF, **27**; PSPWAT**I**DF, **28**; PSPWAT(**Nve**), **29**; PSPWAT**M**, **30**) to potentially capture interactions with the hydrophobic surface of EcDsbA. Once again these peptides gave no detectable binding with EcDsbA (**Table 3.2**).

ITC is best used for detecting enthalpy-driven binding rather than lower energy hydrophobic interactions. We therefore attempted to detect binding of the Cys-replacement peptides using thermal shift. For this analysis, we chose the peptide with the highest BEI, PWATCDS (peptide **22**, BEI 6.4) as the reference, and then synthesized the Cys5Ser substituted peptide PWAT**S**DS (peptide **31**). As expected, we were unable to detect binding of peptide **31** to EcDsbA using ITC (**Table 3.2**). We did, however, detect evidence of binding in the thermal shift assay. The reference cysteine-containing peptide **22**, PWATCDS, induced significant shifts in the unfolding temperature T_m of EcDsbA of +1.7 ± 0.1 ºC at 125 μM and up to +9.8 ± 0.1 ºC at 4mM peptide **22** (**Table 3.1**). For

peptide **31**, where the cysteine was replaced with serine, we also detected statistically significant shifts in T_m though at higher peptide concentrations (DT_m 0.6 ± 0.1 ºC at 1 mM peptide **31** to 2.9 ± 0.1 ºC at 4 mM peptide **31**). These findings suggest that peptide **31** lacking a cysteine binds to oxidized EcDsbA with millimolar affinity.

EcDsbB-derived peptides inhibit the oxidase activity of EcDsbA

ITC and thermal shift both indicated that the peptides bound to EcDsbA. To address whether they inhibited EcDsbA activity, we made use of an enzyme inhibitor assay that measures disulfide bond catalysis. In this assay, oxidation of cysteines in a model substrate was detected as increased fluorescence as two chromophores moved into close proximity after folding. The aim was to determine whether EcDsbA activity in this assay was inhibited in the presence of the DsbB-derived peptides.

The tightest-binding cysteine-containing peptides all inhibited EcDsbA activity with IC_{50} values similar to their K_d values. For example, peptide **1** (PSPFATCDF, K_d 4.0 μM) yielded an IC_{50} value of 6.7 ± 1.1 μM (**Figure 3.5A** and **3.5B**). Peptide **3** (PSPWATCDF, K_d 2.9 μM) gave IC_{50} 5.1 ± 1.1 μM. The shorter peptides **22** (PWATCDS, K_d 5.7 ± 0.4 μM) and **23** (P(hF)ATCDS, K_d = 8.3 ± 0.4 μM) resulted in IC_{50} values of 8.8 μM and 19.2 μM, respectively. Peptide **31** lacking a cysteine (PWATSDS) (Figure 5C) did not exhibit any measurable effect on EcDsbA activity, even at the highest concentrations tested. These results demonstrated that although peptide **31** bound to EcDsbA, it did not compete effectively with EcDsbB or the synthetic substrate to block enzyme activity.

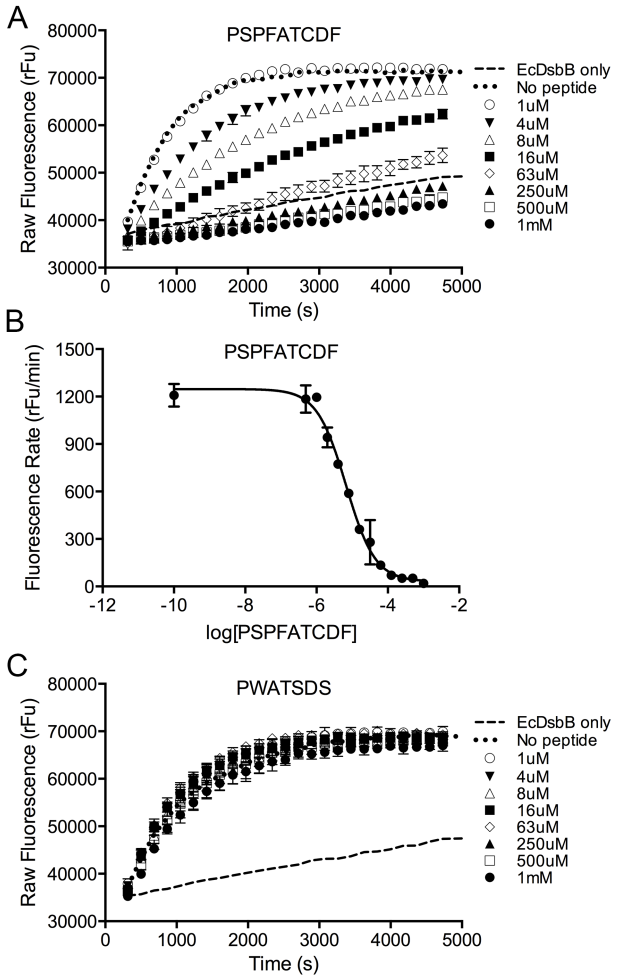

Figure 3.5. ***Inhibition of EcDsbA activity.*** ***A.*** *Raw fluorescence measurement for the peptide oxidation assay in the presence of increasing concentrations of PSPFATCDF (peptide* ***1****).* ***B.*** *Average increase in fluorescence over the first 15 minutes of the reaction plotted against the log of PSPFATCDF concentration. Sigmoidal curve-fitting allows the estimation of an* IC_{50} *of 6.7 ± 1.1 µM.* ***C.*** *Raw fluorescence measurement for the peptide oxidation assay in the presence of increasing concentrations of PWATSDS (peptide* ***31****) lacking a cysteine. No significant inhibition was detected. On both panels A and C 12 peptide concentrations between 0.5 µM and 1 mM were tested but only 8 are displayed for clarity.*

Discussion

Inhibitors of the enzyme DsbA have potential as a new class of antivirulence drugs to treat bacterial infections(Heras *et al.*, 2009). We have focused here on identifying peptides that bound to DsbA, using information from the crystal structure of the EcDsbA:EcDsbB complex as the starting point. Peptides have limitations as drugs but are valuable starting points in drug design, and substantial progress has been made towards improving their stability, resistance to peptidases/proteases, cell permeability and bioavailability (Nguyen *et al.*, 2011, Liskamp *et al.*, 2011, Vaara, 2009, Rotem & Mor, 2009) through modifications that generate peptidomimetics.

The reference point was a 9-residue peptide PSPFATCDF corresponding to residues 98-106 from the EcDsbB periplasmic loop. This peptide **1** interacted with oxidized EcDsbA with a K_d value of 4.0 ± 1.5 μM. A total of 30 peptide derivatives were assessed in comparison to this reference peptide in terms of enhanced affinity and BEI values. This led to peptide sequences PWATCDS (K_d 5.7 ± 0.4 μM) and P(hF)ATCDS (K_d 8.3 ± 0.4 μM) both having the best BEI value of 6.4.

Alanine substitution revealed that Cys104 of the peptide was critical for binding to EcDsbA. The cysteine-containing peptides interacted strongly with oxidized EcDsbA, but not with the reduced form of the enzyme, and inhibited the activity of EcDsbA in an *in vitro* assay. Peptides lacking a cysteine interacted weakly with EcDsbA and did not inhibit EcDsbA activity. These findings support the notion that disulfide bond formation occurs between EcDsbA Cys30 and peptide Cys104.

Three scenarios are possible for the cysteine peptide interaction with EcDsbA. First, the peptides may bind irreversibly to EcDsbA, acting as “suicide” ligands through formation of an unresolved mixed disulfide bond with EcDsbA. If so, inhibition of the oxidation assay would result from progressive inactivation of EcDsbA rather than competitive binding with the substrate. A second possibility is that after formation of a mixed disulfide between the peptide and EcDsbA, the Cys7 of a second peptide attacks the disulfide to form a disulfide-bonded dimer peptide thereby releasing EcDsbA in the reduced inactive state. This scenario reflects the catalytic mechanism of the enzyme (Kadokura & Beckwith, 2009, Frech *et al.*, 1996) (Figure 1) but is unlikely because only one peak was observed in the thermal shift assay, rather than two peaks indicative of the different T_m values for oxidized and reduced EcDsbA. A third possibility is that the mixed disulfide is resolved by nucleophilic attack of EcDsbA Cys33 on EcDsbA Cys30, releasing the peptide and

restoring EcDsbA in its oxidized state. This scenario would qualify the peptides as reversible binders.

The finding that the peptide cysteine is essential for strong interaction with EcDsbA suggests the potential for the development of "suicide" inhibitors that bind irreversibly to the enzyme. For example, α-difluoromethylornithine forms a covalent pyrrole adduct to the mammalian ornithine decarboxylase through alkylation of the active site Cys360(Poulin *et al.*, 1992) and dipeptide diazoketones with Michael acceptor C-termini are inhibitors of cathepsin C that target the active site Cys234(Laine & Busch-Petersen, 2010). Many irreversible cysteine protease inhibitors have been reported(Powers *et al.*, 2002) that target the active site cysteine and have been carried through to clinical trials(Abbenante & Fairlie, 2005).

Similar approaches could be considered to generate peptidic inhibitors targeting EcDsbA Cys30 and Cys33. A 'warhead' targeting the more accessible catalytic Cys30 could be linked to a peptidic scaffold such as those described here. For example, a halomethyl ketone or an epoxide group incorporated in the peptide could generate a thioether covalent adduct to EcDsbA Cys30. Alternatively azapeptides could acylate EcDsbA through nucleophilic attack by Cys30 on the carbonyl group of the aza-amino acid. A nitrile functionality on the peptide in place of the cysteine might lead to formation of a covalent thioimidate adduct. However, the challenge would be to design peptides with exquisite specificity towards EcDsbA.

In summary, this SAR study has provided the first evidence that peptides designed to target EcDsbA can bind and inhibit activity of the enzyme. A cysteine residue in the peptide was essential for activity, highlighting the possibility that a covalent interaction occurs between the peptide and the EcDsbA catalytic cysteine. The generation of more potent and selective irreversible inhibitors based on this peptide scaffold could lead to a new class of antivirulence drugs to treat antibiotic resistant infections.

Material and methods

Protein expression and purification

Wild type *E. coli DsbA* (GenBank® accession number X80762), without the sequence coding for the predicted signal sequence was cloned into a modified pMCSG7 (Midwest Center for Structural Genomics) vector for cytoplasmic expression. The sequence includes an N-terminal His_6 affinity-tag followed by a linker region containing a Tobacco Etch Virus (TEV) protease cleavage site. EcDsbA was expressed in the cytoplasm of *E. coli* BL21 (DE3) pLysS strain grown in auto-induction media(Studier, 2005) (1L) in erlenmeyer flasks for 16-20 h at 30ºC with a stirring speed of 220 rpm. After an initial centrifugation (10,000 rpm for 10 minutes at 4ºC, rotor JLA 10.500, Beckman Coulter, Brea, CA), the bacterial pellet was resuspended in 25 mM Tris, 150 mM NaCl, 1:1000 protease inhibitor cocktail (BioPioneer Inc., San Diego, CA) and DNase (Roche, Australia). Lysis was executed using a Cell Disruptor (TS-Series, Constant Systems LTD., UK) applying a constant pressure of 25 Kpsi. Cell debris was removed by centrifugation (18 500 rpm for 30 min at 4ºC, rotor JM-25.5, Beckman Coulter, Brea, CA). Purification by metal ion affinity chromatography using TALON resin (Clontech, Australia) was used to bind His-tag EcDsbA, consequently eluted with a solution of 25 mM Tris, 150 mM NaCl and 200 mM imidazole. The His_6 affinity tag was removed by TEV cleavage using a 1:50 ratio (protein/TEV-protease, in $mg.ml^{-1}$) incubated in a 50 ml tube overnight at 4ºC, leading to two additional non-native residues Ser and Asn at the N-terminus of EcDsbA. Removal of the remaining tagged EcDsbA and TEV was performed by reverse metal ion affinity chromatography using TALON resin. Final size-exclusion chromatography step using a Superdex 75 16/60 column (GE Healthcare, USA) injecting 5mL of concentrated protein in 25 mM Tris, 150 mM NaCl pH 7.4 yielded high purity protein (≥ 95 %) verified by SDS-PAGE. Protein was then concentrated and buffer exchanged into 25 mM HPES, 150 mM NaCl pH 7.4. Quantitation using a Nano-drop (thermo-Scientific) revealed a final yield of 50 mg of pure EcDsbA per liter of culture. EcDsbA was stored in 50 µL aliquots at 50 $mg.mL^{-1}$ at -80ºC. Prior to experiments EcDsbA was fully oxidized or fully reduced using a 25-molar excess of copper(II)1,10-phenanthroline or dithiothreitol (DTT), respectively, followed by removal of the agent in a PD-10 desalting column (GE Healthcare) and the redox state confirmed by Ellman assay (Aitken, 2009).

E. coli membrane preparations containing over-expressed EcDsbB (GenBank® accession number AAC74269) were produced as previously reported(Bader *et al.*, 1998), and resuspended in PBS buffer containing 10% glycerol.

Peptide synthesis

Peptide synthesis was conducted using standard Fmoc-protected amino acids in solid-phase peptide synthesis (SPPS) on rink-amide MBHA resin (p-methylbenzhydrylamine resin, ChemImpex International, USA). AA (Amino-acids) were loaded after 5 minutes of preactivation using 4 eq of HBTU (O-Benzotriazole-N,N,N',N'-tetramethyl-uronium-hexafluoro-phosphate, ChemImpex International, USA) 500 mM and 5 eq of DIPEA (N,N-Diisopropylethylamine, Auspep, Australia) before coupling to the deprotected resin for 60 min. Fmoc removal was performed using a 80/20 v/v mix of dimethylformamide/piperidine (Rci Labscan, Thailand / Auspep, Australia) for 2 x 5 min. Peptides **6, 7, 8, 9, 23, 25** and **29** were synthesized using their respective unnatural AA Fmoc-L-homophenylalanine, Fmoc-3,3-diphenyl-L-alanine, Fmoc-L-pipecolic acid, Fmoc-L-1,2,3,4-tetrahydroisoquinoline-1-carboxylic acid, Fmoc-O-trityl-L-homoserine and Fmoc-L-norvaline (all Chem Impex International, USA). After final AA coupling all peptides were N-capped by acetylation. Peptides were released using a cleavage mixture (95/2.5/1.25/1.25 v/v mix of respectively Trifluoroacetic acid / Ethanedithiol / Triisopropylsilane / H_2O, Sigma-Aldrich, USA) resulting in a C-terminal amide group. Cleaved peptides were dried using N_2, precipitated with diethyl ether (Ajax Finechem, Australia) and dissolved into a 80/20 v/v mix of acetonitrile/H_2O (RCI Labscan, Thailand) before purification by reversed phase HPLC (Waters). Purification was executed on a Luna C18 column ((250 x 21 mm, Phenomenex, USA) using a 20-100% gradient 90/9.9/0.1 acetonitrile/H_2O/TFA in 12 minutes until peptide reached > 95% purity. Peptides were lyophilized and characterised by analytical UHPLC on a Shimadzu Nexre using an Agilent Zorbax R-ODS III column (2.0 mm i.d x 75 mm 1.6 mm) and mass measured with a LCMS 2020 (Shimadzu) and a high-resolution QSTAR Elite mass spectrometer (Applied Biosystems). Retention times and m/z ratios are available in Figure S3 and HPLC profiles of the most active peptides 6, 21, 22 and 23 are available in the supplementary information (Figures S4 and S5).

Thermal Shift Assay

EcDsbA was diluted to a final concentration of 20 µM in phosphate buffered saline (PBS) pH 7.4 and incubated for 1 h with peptides PSPFATCDF, PWATCDS and PWATSDS at concentrations ranging from 125 µM to 4 mM in two-fold increments. SYPRO® orange (S-6650, Life Technologies Australia, Australia) was added at a final 5X concentration (from a X5000 stock provided by Life Technologies) to a final volume of 20 µL per sample. Controls were set up in the absence of peptide (positive control) or EcDsbA (negative control). The assay was conducted in a translucent Microamp Optical 384-well reaction plate (Applied Biosciences) with 5 replicates per

condition. Plates were sealed with optically clear seal and centrifuged immediately prior to use. Fluorescence emission was monitored throughout the course of an incremental temperature ramp from 25 °C to 95 °C (ramp rate = 0.05 °C.sec^{-1}) using a VIAA7 Real-Time PCR instrument (Life Technologies Australia, Australia) with a 585 ± 15 nm emission filter. Raw data were analyzed using Prism 6 (GraphPad, CA, USA). Fluorescence emission was fitted using the classic Boltzmann sigmoidal equation and the resulting inflexion point was used as the unfolding temperature *Tm* value. To calculate Δ*Tm* (shift in unfolding temperatures), *Tm* values for EcDsbA were subtracted from *Tm* values of EcDsbA-peptide complexes. In table 1, shifts are presented as mean and standard deviation from the 5 replicates per experiment. Δ*Tm* is significant when it is larger than twice the standard deviation of the native protein *Tm(Kranz & Schalk-Hihi, 2011)*.

Isothermal Titration Calorimetry (ITC)

ITC was performed using a MicroCal™ Auto-iTC200 instrument (GE Healthcare, USA). The sample cell was loaded with 200 µL of purified EcDsbA (fully oxidized or reduced beforehand) at 100 µM in 25 mM HEPES pH 7.4, 50 mM NaCl 0.8 % DMSO. The syringe was filled with purified peptide in the same buffer solution. Titrations were conducted at 25 °C using 19 consecutive injections of 2 µL or 15 injections of 2.6 µL with 180 s intervals and a stirring speed of 1000 rpm. In every experiment, an initial 0.5 µL of peptide was injected to avoid slow leakage of titrant which can interfere with the initial reading. Consequently, this initial data point was discarded for binding analysis. The association constant ($K_a = 1/K_d$), enthalpy (ΔH) and entropy (ΔS) were calculated by fitting the data to a single-site binding model using the MicroCal™ Origin software (Origin 7.0 SR4 v7.0552 beta) and adjusting the peptide concentration to give a stoichiometry parameter of ~1.0. Every peptide was tested in triplicate and the values given represent mean and standard deviation from these triplicate analyses.

A ligand efficiency measurement Binding Efficiency Index (BEI) was used to compare the quality of binding. BEI is defined by both the measured binding affinity of a ligand for its target and the molecular weight of the ligand (Abad-Zapatero & Metz, 2005). The BEI is calculated as follows, with the dissociation constant Kd in M and the molecular weight Mw in kDa:

$$BEI = \frac{-\log (Kd)}{Mw}$$

The BEI value of an idealized ligand of molecular weight 0.333 kDa (which is the mean value of the molecular weight of marketed drugs (Vieth *et al.*, 2004)) and affinity *K*d 1 nM is 27.

Model Substrate Oxidation Assay

The ability of the peptides to inhibit the activity of EcDsbA was evaluated using a model substrate oxidation assay(Kurth *et al.*, 2013). Briefly, a synthetic peptide substrate of EcDsbA (CQQGFDGTQNSCK) with an *N*-terminal europium-DOTA (1,4,7,10-tetraazacyclododecane-1,4,7,10-tetraacetic acid), a *C*-terminal methylcoumarin and two cysteine residues (AnaSpec, USA) does not fluoresce in the reduced state. Introduction of a disulfide bond by DsbA brings the europium-DOTA and coumarin moieties into close proximity triggering an energy transfer and a measurable signal upon excitation and allowing fluorescence emission to be monitored at 615 nm. Inhibition of EcDsbA activity is assessed as a reduction in the fluorescence rate in the presence of the peptide, corresponding to a decrease in substrate oxidation. Lyophilized synthetic substrate peptide was dissolved in 100 mM imidazole pH 6.0 at a final concentration of 2 mM. 100 mM of europium trifluoromethanesulfonate (Sigma Aldrich, Australia) was added to the synthetic substrate peptide at a molar ratio of 2:1 and incubated for 5 min at room temperature to allow europium chelation. Assays were performed using a Synergy H1 multimode plate reader (BioTek, USA) as described previously(Walden *et al.*, 2012). The time-resolved fluorescence of substrate peptide folding (excitation λ = 340 nm and emission λ = 615 nm) was measured in a white 384-well plate (Perkin Elmer OptiPlate-384, Part #: 6007290) in 50 mM MES, 50 mM NaCl and 2 mM EDTA at pH 5.5 buffer. Total reaction volume was 50 µL solution in each well including 80 nM EcDsbA, 1.6 µM EcDsbB, peptide **1, 3, 22, 23** or **31** at concentrations ranging from 0.5 µM to 5 µM and 10 µM substrate peptide was added last to initiate the reaction. Samples containing buffer only, EcDsbA without peptide inhibitor, or peptide inhibitor without EcDsbA were used as controls. Data were measured for three replicates and values for the mean and standard deviation reported. Fitting of a sigmoidal dose-response curve with peptide concentrations in a logarithmic scale allows to calculate an IC50 value from the inflexion point. To allow plotting of the positive control (EcDsbA only), the peptide concentration is considered negligible (10^{-10} M) rather than 0.

Supporting information available

Additional figures for the thermal shift and isothermal titration calorimetry assays as well as peptide characterization data are included into the supporting information. This material is available free of charge via the Internet at http://pubs.acs.org.

AUTHOR INFORMATION

Corresponding Author

*To whom correspondence should be addressed: Jennifer L. Martin (j.martin@imb.uq.edu.au) and David P. Fairlie (d.fairlie@imb.uq.edu.au)

Funding Sources

This work was supported by an Australian Research Council (ARC) Laureate Fellowship (FL0992138) to JLM. JLM is also an Honorary NHMRC Research Fellow (455829). DPF is an NHMRC Senior Principal Research Fellow (1027369) and was an ARC Federation Fellow (FF0668733) during these studies.

Acknowledgements

We are grateful to Stephanie Tay for providing DsbB membrane preparations for the oxidation assay, Fabian Kurth for optimising production of DsbA and Annika Yau, Shiao Chow and Sheila Barbero for their help in high-resolution mass spectrometry experiments. We thank Brett Collins and Matt Cooper for helpful discussions on ITC analysis and antibacterial research, respectively.

CHAPTER IV

The following chapter is a manuscript submitted to the Journal of Biological Chemistry. The structure-activity relationship study in Chapter III highlighted the difficulties in describing the set of interactions necessary for the specificity of the EcDsbA-EcDsbB or the EcDsbA-peptide binding mode. The systematic substitution of side chains located in the hydrophobic pocket did not alter the affinity while the only critical residue for binding was the cysteine. The formation of a disulfide bond between peptide and EcDsbA is the favored explanation for the formation of an EcDsbA-peptide complex. To progress further in designing potent inhibitors of EcDsbA, high-resolution structural information was highly required. This manuscript describes the efforts provided in obtaining and solving the crystal structure of a peptide non-covalently bound to a DsbA protein from a different organism, *Proteus mirabilis*, which proved much easier to crystallize than EcDsbA. This resulted in a 1.6 Å resolution PmDsbAC30S-PWATCDS peptide structure. The structural information observed from the complex structure would be invaluable to the future design of peptidomimetic molecules.

This manuscript resulted from collaboration with Mr Fabian Kurth, sharing the co-first authorship. The biochemistry and crystal structure characterization of native PmDsbA was performed by Mr Kurth as part of his own PhD project, whereas I performed all assays linked to peptide binding and characterization. The co-crystallization and structure characterization of a PmDsbA mutant with the best peptide sequence from chapter III (PWATCDS) is the result of an equal effort from Mr Kurth and myself, under the supervision of Dr Premkumar. The final manuscript was reviewed and critically revised by Dr Premkumar, Prof. Schembri, Prof. DP Fairlie and Prof. JL Martin.

Crystal Structure of the Dithiol Oxidase DsbA Enzyme From *Proteus Mirabilis* Bound Non-Covalently to an Active Site Peptide Ligand

Fabian Kurth[a*], Wilko Duprez [a*], Lakshmanane Premkumar[a], Mark A. Schembri[b], David P. Fairlie[a], and Jennifer L. Martin[a#]

[a]Institute for Molecular Bioscience, Division of Chemistry and Structural Biology and
[b]Australian Infectious Diseases Research Centre, School of Chemistry and Molecular Biosciences
University of Queensland, St Lucia, QLD, 4067, Australia

[*]These authors contributed equally
[#]To whom correspondence should be addressed: Jennifer L. Martin (j.martin@imb.uq.edu.au)

Running title: DsbA:peptide interactions as the basis for novel antimicrobials

Background: DsbA enzymes assemble bacterial virulence factors and are targets for a new drug class.
Results: *Proteus mirabilis* DsbA was characterized and its structure determined.
Conclusion: The crystal structure for this DsbA with a non-covalently bound active site peptide provides a basis for future inhibitor design.
Significance: New drugs to treat superbugs are urgently needed. DsbA inhibitors could have antivirulence activity against bacterial pathogens.

Keywords: Oxidative folding; thioredoxin fold; dithiol oxidase; virulence; crystal structure; structural biology; protein:peptide complex; peptide interactions; enzyme structure; enzyme catalysis

The disulfide bond forming DsbA enzymes and their DsbB interaction partners are attractive targets for development of antivirulence drugs because both are essential for virulence factor assembly in Gram-negative pathogens. Here we characterize PmDsbA from *Proteus mirabilis*, a bacterial pathogen increasingly associated with multidrug resistance. PmDsbA exhibits the characteristic properties of a DsbA, including an oxidizing potential, destabilizing disulfide, acidic active site cysteine, and dithiol oxidase catalytic activity. We also evaluated a peptide PWATCDS derived from the partner protein DsbB and showed by thermal shift and ITC that it binds to PmDsbA. The crystal structures of PmDsbA, and the active site variant PmDsbAC30S were determined to high resolution. Analysis of these structures allows categorization of PmDsbA into the DsbA class exemplified by the archetypal *Escherichia coli* DsbA enzyme. Other members of this DsbA subclass include enzymes from *Salmonella enterica* subtype Typhimurium and *Klebsiella pneumoniae*. A third crystal structure of PmDsbAC30S in complex with the PWATCDS peptide reveals non-covalent binding to this variant, potentially providing a platform for future peptidomimetic design.

Introduction

Proteus mirabilis is a significant Gram-negative extra-intestinal human pathogen that belongs to the *Enterobacteriaceae* family, which also includes other important pathogens such as *Escherichia coli*, *Klebsiella pneumonia,* and *Enterobacter cloacae*. Together, the *Enterobacteriaceae* account for the vast majority of community-acquired and nosocomial urinary tract infections (UTIs) (Guay, 2008, Ronald, 2003). *P. mirabilis* is a frequent cause of both complicated and catheter- associated UTIs (Jacobsen *et al.*, 2008, Jacobsen & Shirtliff, 2011). Multidrug resistant strains of clinical pathogenic *P. mirabilis* have been reported for several decades (Guay, 2008). For example clinical isolates of *P. mirabilis* resistant to streptomycin, tetracycline, kanamycin, chloramphenicol and polymyxin B were described in the 1960s (Coetzee & Sacks, 1960, Sabath, 1969) and reports of antibiotic resistance have increased since then (Pearson *et al.*, 2008, Hitchings, 1973, Wellington *et al.*, 2013, Wang *et al.*, 2009, Elsea *et al.*, 1992, Tibbetts *et al.*, 2008, Mehtar *et al.*, 1991, Franklin & Rownd, 1973, Coetzee, 1975, Zhao & Hu, 2013).

DsbA enzymes from Gram-negative bacteria are targets for the development of anti-virulence drugs that could represent an entirely new class of antimicrobial agents (Heras *et al.*, 2009, Kurth *et al.*, 2013). Drugs that target bacterial virulence could minimize the selective pressure that generates antibiotic resistance and simultaneously preserve the endogenous host microbiome (Rasko & Sperandio, 2010). DsbA is a key target for such drugs because it is essential for the

correct folding or assembly of multiple virulence factors, including toxins, fimbrial adhesins, flagella, and type II and type III secretion systems (Heras *et al.*, 2009). The mutation of *dsbA* results in the attenuation of virulence factor production in multiple pathogens (Heras *et al.*, 2009) some examples include *Proteus mirabilis* (Burall *et al.*, 2004), uropathogenic *E. coli* (Totsika *et al.*, 2009a) and *Burkholderia pseudomallei* (Ireland *et al.*, 2014), *Vibrio cholerae* (Peek & Taylor, 1992), *Shigella flexneri* (Yu, 1998) and *Salmonella enterica* serovar Typhimurium (Lin *et al.*, 2008).

DsbA enzymes are thioredoxin fold proteins (Martin *et al.*, 1993) localized to the periplasm of Gram-negative bacteria where they catalyze oxidative folding (Bardwell *et al.*, 1991). This reaction involves the transfer of a disulfide bond from the active site ^{30}CXXC^{33} motif of DsbA to cysteine thiols in newly translocated proteins (Shouldice *et al.*, 2011). Through this disulfide-exchange reaction, the active site cysteines of DsbA become reduced. The enzymatic cycle is completed through oxidation of DsbA by the inner membrane partner protein, DsbB (Inaba, Murakami*, et al.*, 2006). DsbA from *E. coli* (EcDsbA) is a highly promiscuous enzyme, that catalyzes disulfide bond formation in many cysteine-containing proteins (Shouldice *et al.*, 2011). In contrast, EcDsbB has a very strict binding specificity for EcDsbA (Inaba, Murakami*, et al.*, 2006). The interaction between EcDsbA and EcDsbB involves the formation of a mixed disulfide between Cys30 of the ^{30}CXXC^{33} motif of EcDsbA and Cys104 of EcDsbB in the P2 periplasmic loop, which has the sequence ^{98}PSPFATCDF^{106} (Inaba *et al.*, 2009b). The crystal structure of the complex between EcDsbA and EcDsbB also revealed non-covalent binding of EcDsbB P2 loop residues to the EcDsbA hydrophobic groove (Inaba *et al.*, 2009a). The P2 periplasmic loop sequence of *P. mirabilis* DsbB (PmDsbB) is identical to that of EcDsbB, suggesting a similar interaction occurs between PmDsbA and PmDsbB.

Here we characterize PmDsbA from *P. mirabilis*, which shares 59% sequence identity with EcDsbA. We confirm that its redox and enzymatic properties classify it as a *bona fide* DsbA enzyme. We demonstrate that the heptapeptide PWATCDS, derived from the DsbB P2 loop sequence, binds to wild type PmDsbA and to a C30S active site variant (PmDsbAC30S). We report high-resolution crystal structures of PmDsbA and PmDsbAC30S. We also report the crystal structure of the PmDsbAC30S:PWATCDS complex, which represents to our knowledge the first reported example of peptide bound non-covalently to a DsbA structure. This structure can provide the basis for future drug design efforts to generate anti-virulence agents targeting *Enterobacteriaceae* DsbAs.

Experimental procedures

Protein production and molecular biology – Codon-optimized wild type *P. mirabilis dsbA* (GenBank® accession number CAR45574), lacking the sequence coding for the predicted signal peptide (amino acids 1-19), was cloned into a modified pMCSG7 (Eschenfeldt *et al.*, 2009) vector using ligation-independent cloning. The cytoplasmic expressed PmDsbA contained an N-terminal His_6 affinity-tag followed by a linker region including a Tobacco Etch Virus (TEV) protease cleavage site. The PmDsbAC30S variant was generated from the wild type construct using QuikChange® (Agilent Technologies). The following primers were used to introduce the point mutation, FW-GAATTTTTCTCATTTTATTCTCCGCATTGTTACC and REV-GGTAACAATGCGGAGAATAAAATGAGAAAAATTC. Transformed BL21(DE3)pLys cells containing plasmids for either PmDsbA or PmDsbAC30S were grown (1 L) at 30 °C in 2.5 L baffled shaker flasks for 16-20 h using autoinduction media (Studier, 2005). Cells were resuspended in 25 mM Tris, 150 mM NaCl (10 g cells per 100 mL buffer) and protease inhibitor cocktail (diluted 1 in 1000 into the lysate) (BioPioneer Inc., San Diego, CA) and DNase (1300 U per 100 mL Lysate) (Roche, Australia) added. Lysis was performed in a Cell Disruptor (TS-Series, Constant Systems LTD., UK) applying a single run with a constant pressure of 25 Kpsi. Cell debris was removed by centrifugation (18500 rpm, 30 min, 4 ºC, rotor JM-25.5, Beckman Coulter, Brea, CA). The proteins were further purified by immobilized metal ion affinity chromatography (IMAC) using 12 mL / 1 L cells of equilibrated Talon (Clontech, Australia) and eluted with 25 mM Tris, 150 mM NaCl, 200 mM imidazole after incubation of 30 min at RT. Total protein amount was determined at 280 nm with a NanoDrop™ 2000c (Thermo Fisher Scientific, USA). The His_6 affinity tag was removed by tobacco etch virus protease (TEV) cleavage using a 50:1 (w/w) ratio (protein/TEV-protease) incubated in a 50 mL falcon tube including 1 mM β-mercaptoethanol for 2 h on a rotary mixer at room temperature. After cleavage, the PmDsbA proteins had an additional two non-native residues ($Ser^{-2}Asn^{-1}$) at the N-terminus. To remove imidazole, the mixture was rapidly buffer-exchanged into 25 mM Tris, 150 mM NaCl using a Sephadex G-25 fine 16/60 column connected to an ÄKTA system (GE Healthcare, USA). The His_6-tagged TEV protease was removed by reverse IMAC using Talon resin (0.5 mL resin / 2 mg TEV protease) (Clontech, Australia) and the PmDsbA proteins were recovered in the flow through. The final step of purification was performed using a Superdex S75 gel-filtration column (GE Healthcare, USA). Peak fractions were then combined and the protein was oxidized using copper(II) 1,10-phenanthroline at 1.7 mM final concentration or reduced using DTT at 25x molar excess. To remove oxidizing or reducing agent, the mixture was then buffer-exchanged into 10 mM HEPES pH 7.4 using a Sephadex G-25 fine 16/60 column. Finally, the protein was concentrated to 100 mg/mL using Amicon Ultra filter

devices with a 10-kDa cutoff (Millipore, USA). Yield was generally 120-150 mg per L culture. Protein quality was assessed by SDS-PAGE (NuPAGE® system, 4-12% Bis-Tris gel, Invitrogen, Australia). Molar protein concentrations were determined from calculated extinction coefficients derived from ProtParam (Gasteiger E., 2005).

Purified EcDsbA (GenBank® accession number CAA56736) and EcDsbC (GenBank® accession number AAA83074), lacking the periplasmic leader signal were expressed and purified as described above for PmDsbA. Yields were generally 120 mg and 80 mg per L culture, respectively. *E. coli* membrane extracts containing over-expressed EcDsbB (GenBank® accession number AAC74269) were prepared as described previously (Bader *et al.*, 1998), and resuspended in PBS buffer containing 10% glycerol.

EcDsbA complementation – E. coli Δ*dsbA* (JCB817) and Δ*dsbA*/Δ*dsbB* (JCB818) non-motile strains were used for motility assays as described previously (Shouldice *et al.*, 2010). The gene sequence coding for mature PmDsbA (lacking the periplasmic signal sequence) was cloned into pBAD33 under an arabinose inducible promoter with an N-terminal EcDsbA signal sequence (Guzman *et al.*, 1995). As a positive control, EcDsbA was expressed within the same pBAD33 vector background. $2x10^6$ non-motile *E. coli* Δ*dsbA* (JCB817) and Δ*dsbA*/Δ*dsbB* (JCB818) double-mutant (JCB818) (Bardwell *et al.*, 1991) cells harboring pBAD33(EcDsbA) or pBAD33(PmDsbA) were spotted onto the center of a soft M63 minimal agar plate containing 40 mg/mL of each amino acid (except L-cysteine) and 0.1% arabinose. Plates were incubated at 37 ºC and cell motility was monitored after 4-5 h using a Molecular Imager® Gel Doc™ system from BIO-RAD (CA 94547, USA). Complementation experiments were performed as biological triplicates.

Cysteine Thiol Oxidation Assay – A synthetic peptide substrate of EcDsbA (CQQGFDGTQNSCK) with a europium DOTA (1,4,7,10-tetraazacyclododecane-1,4,7,10-tetraacetic acid) group amide-coupled to the N-terminus and a methylcoumarin amide-coupled to the ε-amino group of the C-terminal lysine was purchased from AnaSpec (Fremont, CA) and prepared as previously reported (Vivian *et al.*, 2009).

Assays were performed using a Synergy H1 multimode plate reader (BioTek, USA) as described previously (Walden *et al.*, 2012). In brief, fluorescence (excitation λ = 340 nm and emission λ = 615 nm) corresponding to disulfide formation in the substrate peptide was measured in a white 384-well plate (Perkin Elmer OptiPlate-384, Part #: 6007290) in 50 mM MES, 50 mM NaCl and 2 mM EDTA at pH 5.5 buffer. Total reaction volume in each well was 50 μL, containing

40, 80 or 160 nM PmDsbA or EcDsbA, 1.6 μM EcDsbB membrane and 8 μM peptide substrate (added last to initiate the reaction). Samples containing DsbA proteins, EcDsbB and buffer were used as controls. For every biological replicate (3 in total), the values derived from three technical replicates were averaged. The slope (reaction rate) for each sample was calculated for the first 8 min of reaction. The reaction rates were plotted including the S.D. calculated combining data of three biological replicates.

Thermal Stability of PmDsbA– Temperature-induced unfolding of native PmDsbA was recorded by far-UV circular dichroism as previously reported for other DsbA enzymes (Heras *et al.*, 2008a) using a Jasco J-810 spectropolarimeter (Jasco, USA). The initial redox state of PmDsbA was confirmed by Ellman's assay (Ellman, 1959). The maximum difference in CD signal was determined by subtraction of the CD-spectra of the folded protein (25 ºC) from the unfolded (95 °C) protein, for the oxidized and the reduced forms of the protein. Unfolding of oxidized PmDsbA (210 nm) and reduced PmDsbA (213 nm) was monitored in a 1-mm quartz cuvette using a heating rate of 1 ºC/min from 25 ºC to 95 ºC. Measurements were carried out using 10 μM protein in a buffer containing 100 mM NaH_2PO_4 / Na_2HPO_4, 1 mM EDTA, pH 7.0. To ensure PmDsbA remained reduced throughout the entire measurement, reduced samples contained 0.75 mM DTT. Data were fitted to a two-state unfolding model and errors calculated using Prism 6 (GraphPad, CA, USA) as described previously (Kurz *et al.*, 2009)

Redox properties of PmDsbA – The standard redox potential of PmDsbA was measured utilizing the intrinsic fluorescence of tryptophan residues in PmDsbA, similar to the method used for EcDsbA (Wunderlich & Glockshuber, 1993). In brief, oxidized PmDsbA was equilibrated for 3 h at 25 ºC in degassed 100 mM NaH_2PO_4 / Na_2HPO_4, pH 7.0, 1 mM EDTA, 298K containing 1 mM oxidized glutathione (GSSG) and a range of reduced glutathione (GSH) concentrations (0–2000 μM). 200 μL of PmDsbA from each redox condition was dispensed into a 96-well plate (TPP AG, Switzerland #92096) and tryptophan fluorescence measured (excitation wavelength 280 nm, emission 332 nm) using a Synergy H1 microplate reader and Gen5 2.0 software (Biotek, USA). Data were analyzed in Prism 6 (GraphPad, CA, USA) and the redox potential calculated as described previously for EcDsbA (Wunderlich & Glockshuber, 1993).

Determination of Cys30 pKa – Absorbance at 240 nm of the catalytic thiolate anion is pH-dependent allowing the equilibrium between protonated and deprotonated Cys30 to be measured (Nelson & Creighton, 1994) using a UV/VIS spectrophotometer (CARY 50, Agilent Technologies).

Absorbance at 240 nm and 280 nm were measured over pH values starting at 6.5 and decreasing to 2.0, in 0.25 pH unit increments. Samples contained either oxidized or reduced PmDsbA (40 μM) in composite buffer (10 mM Tris, 10 mM sodium citrate, 10 mM K_2HPO_4, 10 mM KH_2PO_4, 200 mM KCl, and 1 mM EDTA) at 22 ºC. The pK_a value was calculated from the fitted curves using the Henderson Hasselbalch equation ($pH = pK_a - \log([A_{240}/A_{280}]_{red} / [A_{240}/A_{280}]_{ox})$). Average and standard deviation from the mean derived from triplicate measurements are plotted.

Disulfide Reductase Activity – DsbA enzymes can reduce the intermolecular disulfide bonds between insulin chains A and B under mild reducing conditions (Bardwell *et al.*, 1991). Disulfide bond reduction of insulin can be followed spectrophotometrically at λ = 650 nm (OD_{650nm}). The OD_{650nm} value gives a measure of turbidity, which occurs as a result of the increase in production of insoluble B-chain of insulin (Holmgren, 1979). Samples were prepared in 1-cm cuvettes containing 10 μM of protein (PmDsbA, EcDsbA or EcDsbC), 0.33 mM DTT and 2 mM EDTA in 100 mM NaH_2PO_4 / Na_2HPO_4 pH 7.0. Catalysis was initiated by the addition of 0.131 mM insulin (I0516, Sigma-Aldrich, Australia) to the mixture. The assay was repeated three times and the mean values are plotted including the standard deviations of the measurement at each time point.

Peptide Synthesis – Peptides were synthesized using solid-phase peptide synthesis (SPPS) on rink-amide (4-methyl)benzhydrylamine (MBHA) resin (ChemImpex International, Wood Dale USA) with a loading of 0.65 mmol/g. De-protection of the resin and amino acids was performed using an 80 / 20 v/v mix of dimethylformamide/piperidine (Rci Labscan, Bangkok Thailand / Auspep, Australia) for 2 x 5 min. L-aminoacids (ChemImpex International, Wood Dale USA) were activated using 4 resin equivalents (eq) and 4 eq of HbtU (O-Benzotriazole-N,N,N',N'-tetramethyl-uronium-hexafluoro-phosphate, ChemImpex International, Wood Dale USA) 500 mM and 5 eq of DIPEA (N,N-Diisopropylethylamine, Auspep, Australia) for 5 min before coupling to the de-protected resin for 60 min. After final coupling, all peptides were acetylated at the N-terminus using 4 eq of acetic acid (Chem Supply, Australia), 4 eq of HbtU and 5 eq of DIPEA (Auspep, Australia) for 30 min. Cleaving was executed using a 95/2.5/1.25/1.25 v/v mix of trifluoroacetic acid (TFA)/ethane-dithiol (EDT)/triisopropylsilane (TIPS)/water (H_2O) (chemicals from Sigma-Aldrich, Saint Louis USA). Cleaved peptides resulted in an amidated C-terminus from the resin rink amide and were dried using N_2 gas, washed with diethyl ether (DEE, Ajax Finechem, Sydney Australia) and dissolved in a 80/20 v/v mix of acetonitrile/H_2O (RCI Labscan, Bangkok Thailand) before purification on HPLC. Purification was executed on a C18 column (Phenomenex, Torrance USA) using a gradient from 20% to 80% of acetonitrile and TFA 0.1%. Fractions were analyzed by mass spectrometry

(Waters Micromass LCT, Milford USA) and the purified peptide was lyophilized using a freeze drier (Christ, Osterode am Harz, Germany).

Peptide-Induced Thermal Shift Measurements – 25 µM of PmDsbA in phosphate buffered saline (PBS) pH 7.4 was incubated with peptide PWATCDS at concentrations ranging from 125 µM to 4 mM for 1 h. Then Sypro orange (S-6650, Life Technologies, Australia) was added to a 5X final concentration (stock concentration 5000X). Controls contained either no peptide, no DsbA or the dye alone. Measurements were conducted in a white 384-well plate (Perkin Elmer OptiPlate-384, Part #: 6007290) with 5 replicates. Fluorescence emission from Sypro Orange binding to unfolded protein was measured following a temperature time course increasing from 25°C to 95°C (heat rate = 0.05 °C/sec) using a VIAA7 Real-Time PCR system (Life Technologies, Australia) with a l = 585 ± 15 nm wavelength filter. Raw data were analyzed using Prism 6 (GraphPad, CA, USA). Fluorescence emission was fitted to a classic Boltzmann sigmoidal curve, and the inflexion point was used as the melting temperature, *Tm*. To determine Δ*Tm* (the shift in melting temperature in the presence of peptide), the *Tm* value for the wild type protein was subtracted from the *Tm* value for PmDsbA-PWATCDS and the *Tm* value for the variant PmDsbAC30S was subtracted from the *Tm* value for PmDsbAC30S-PWATCDS. Δ*Tm* values are presented as the mean and standard deviation from 5 replicates. A significant Δ*Tm* is considered to be greater than two times the standard deviation of the *Tm* value for the protein in the absence of ligand (Kranz & Schalk-Hihi, 2011).

Isothermal Titration Calorimetry – Evaluation of affinity and thermodynamics of binding between PWATCDS and PmDsbA or PmDsbAC30S were assessed by Isothermal Titration Calorimetry (ITC) using an Auto-iTC$_{200}$ instrument (MicroCal™, GE Healthcare, USA). The sample cell was loaded with 200 µL of purified protein (oxidized PmDsbA or untreated PmDsbAC30S) at 100 µM concentration in 25 mM HEPES pH 7.4, 50 mM NaCl 0.8% DMSO (ITC buffer). The syringe was filled with purified peptide PWATCDS in ITC buffer at a concentration of 4 mM. Titrations were conducted at 25 °C using 19 consecutive injections of 2 µL each delayed by 180 seconds with a stirring speed of 1000 rpm. In every experiment an initial 0.5 µL of peptide was injected to avoid slow leakage of titrant and this data point was discarded for binding analysis. As a control for background noise, titration of PWATCDS into a solution containing ITC buffer only was performed. The association constant ($K_a = 1/K_d$), free energy (ΔG) and enthalpy change (ΔH) were calculated by fitting the data to a single-site binding model using the MicroCal™ Origin software (Origin 7.0 SR4 v7.0552 beta) and correcting peptide concentrations to adjust the stoichiometry parameter close to 1.0. Entropy change (ΔS) was deduced from the standard free energy equation

$\Delta G = \Delta H - T\Delta S$. Parameters reported include the mean and standard deviation across three replicates. The calculated c-value for these measurements is 12.

Crystallization, structure determination and structural analysis – Crystallization screening was performed at the UQ ROCX diffraction facility (http://uqrocx.imb.uq.edu.au). Protein crystallization trials were performed in 96-well plates using the hanging drop vapor diffusion method at 8 ºC or 20 ºC. In general, purified protein (200 nL) was mixed with crystallization solution (200 nL) using a Mosquito crystallization robot (TTP Labtech, UK), and trays were incubated and imaged in a RockImager 1000 (Formulatrix, USA). Wild type PmDsbA was crystallized by mixing 0.5 µL of 3 mM (60 mg/mL) purified PmDsbA including 10 mM of PSPWATCDF peptide (1:3 protein:peptide ratio) dissolved in DMSO (final concentration = 2% DMSO) with 0.5 µL of an optimized crystallization condition consisting of PEG3350 15% and 0.4 M sodium malonate pH 5.0. The presence of the peptide permitted crystallization but no density was evident for the peptide in the phased data; the final refined structure from this condition is referred to as native PmDsbA. Crystals were harvested in cryo solution (PEG3350 25%, 0.4 M sodium malonate pH 5.0, 20% PEG400) and immediately flash frozen in liquid nitrogen.

PmDsbAC30S crystals appeared overnight at 8 ºC in 0.2 M KSCN, PEG3350 23% and 30 mg/mL of protein and 15 mM of PWATCDS (both final concentrations); again the presence of peptide permitted crystallization but there was no evidence of peptide binding in the electron density maps. The cryo solution used was 0.2 M KSCN, PEG3350 25% and 20% PEG400. The structure of the protein derived from this condition is referred to as PmDsbAC30S.

PmDsbAC30S:PWATCDS co-crystals grew at 20 ºC using a 12-fold molar excess of peptide (30 mM) over protein (60 mg/mL), with the two components incubated on ice for 1 h prior to crystallization. The protein:peptide solution was then mixed with crystallization solution, which contained 0.2 M KSCN, 22% PEG3350, 0.2 M non-detergent sulfobetaine (NDSB-221). Differences in crystallization conditions in comparison to PmDsbC30S, included the use of NDSB-221 and incubation of plates at 20 ºC. Crystals were flash frozen in cryo solution consisting of PEG3350 30%, 0.3 M KSCN and PEG400 20%.

Diffraction data for all three crystal structures were measured at the Australian Synchrotron MX2 beamline at a wavelength of 0.9537 Å, and recorded with an ADSC Quantum 315r detector controlled by BLU-ICE (McPhillips *et al.*, 2002). Reflections were indexed and integrated in

Mosflm (Battye *et al.*, 2011) or XDS (Kabsch, 2010), analyzed in Pointless (Evans, 2006) and scaled in SCALA (Evans, 2006) from the CCP4 suite. (Winn *et al.*, 2011). Phases for PmDsbA were obtained by molecular replacement (MR) using PHASER (McCoy *et al.*, 2007) with EcDsbA as a template (PDB code 1FVK, sequence identity 59%). PmDsbAC30S: PWATCDS were solved using the wild type PmDsbA structure as the template. Initial electron density maps from PHASER were improved by cycles of iterative refitting of the model by using the program COOT (Emsley *et al.*, 2010) and PHENIX.refine (Adams *et al.*, 2010). The refinement of the complex structure was stalled at R-factor/R-free: 30% / 33%. Phenix.xtriage analysis indicated that the diffraction data was twinned with a twinning fraction of 0.49. The twin target function implemented in PHENIX was applied in further refinement cycles with the twinning operator -h+k, k, -l. The final R-factor/R-free was 17.2% / 19.9%. For PmDsbAC30S:PWATCDS, density corresponding to bound peptide was modeled for all seven residues including N-terminal acetylation and C-terminal amidation. In addition, a malonate anion was modeled into the crystal structure of PmDsbA and four SCN molecules were modeled into the PmDsbAC30S:PWATCDS crystal structure with one pair in each protomers A and C. One thiocyanate molecule is buried between α1 and β2 of protomers A/C, while the second molecule binds between *Pro* and PmDsbAC30S helix α1, possibly forming a weak hydrogen bond with the *Pro* backbone carbonyl (distance N:O = 3.4 Å). Thiocyanate molecules do not appear to influence peptide binding, since the peptide binding site and conformation is identical in protomer B which lacks a bound thiocyanate.

Data processing and refinement statistics for all three crystal structures are provided in **Table 4.1.** Molecular figures were generated using PyMOL (The PyMOL Molecular Graphics System, Version 1.6.0.0 Schrödinger, LLC) and figures of the electrostatic potential were generated using APBS (Baker *et al.*, 2001). RMSD calculations and structural alignments were conducted in PyMOL and FATCAT (Ye & Godzik, 2003). Interaction analyses were conducted with the program COOT (Emsley *et al.*, 2010) and the PDBePISA (Krissinel & Henrick, 2007) and Cocomaps servers (Vangone *et al.*, 2011).

Table 4.1. ***X-ray data collection and refinement statistics***

Data collection	**PmDsbA (4OCE)**	**PmDsbAC30S (4OCF)**	**PmDsbAC30S: PWATCDS (4OD7)**
Wavelength (Å)	0.95369	0.95369	0.95370
Resolution range (Å)	42.64 - 1.77	57.22 - 1.98	64.13 – 1.60
Highest resolution shell (Å)	1.77 - 1.86	1.98 – 2.09	1.60 – 1.68
Space group	$P\ 4_32_12$	$P2_1$	$P3_2$
Unit cell dimensions			
a (Å)	37.8	37.9	74.06
b (Å)	37.8	80.2	74.06
c (Å)	298.4	114.4	93.27
α, β, γ (º)	90, 90, 90	90, 91, 90	90, 90, 120
Total reflections	303398	176891	839517
Unique reflections	22817	47865	74969
Multiplicity	13.3 (13.6)[a]	3.7 (3.6)[a]	11.2 (10.2)[a]
Completeness (%)	100 (100)	99.7 (98.9)	98.6 (93.9)
Mean <I>/<σI>	16.1 (4.8)	14.3 (8.4)	16.3 (2.4)
R_{merge}[a]	0.127 (0.587)	0.073 (0.155)	0.080 (0.973)
$R_{p.i.m.}$	0.035 (0.157)	0.044 (0.095)	0.026 (0.327)
Refinement statistics			
R_{free} (%)	16.9 (21.9)	21.1 (24.0)	19.9 (29.2)
R_{work} (%)	14.8 (17.3)	15.2 (15.2)	17.2 (30.3)
Unique reflections	22686	47846	74969
Number of non-H atoms			
Protein	1492	5841	4506
Water	268	749	542
Protein residues	189	810	561
RMSD Bond lengths (Å)	0.009	0.012	0.017
RMSD Bond angles (º)	1.152	1.240	1.555
Ramachandran			
Favoured (%)	98.4	98.5	98.9
Outliers (%)	0	0	0
Average B-factor ($Å^2$)	14.6	12.8	25.7
Wilson B-factor ($Å^2$)	16.0	10.3	22.1
Molprobity[b]			
Clashscore (percentile)	1.03 [100th, (839)]	2.32 [100th, (714)]	4.25 [97th, (699)]
Score (percentile)	0.80 [100th, (11193)]		1.21 [98th,(6780)]

[a] The values in parentheses refer to the highest resolution shell
[b] 100th Molprobity (Chen *et al.*, 2010) percentile is the best among the structures of comparable resolution.

Results

PmDsbA catalyzes disulfide formation in vitro and in vivo – DsbA enzymes catalyze oxidative folding, or the introduction of disulfide bonds into proteins. To assess whether PmDsbA has dithiol oxidase activity we assessed its activity in an *in vitro* peptide oxidation assay. A europium labeled peptide (CQQGFDGTQNSCK) fluoresces when the two cysteines are oxidized, but not when the cysteines are reduced (Vivian *et al.*, 2009). We found that PmDsbA, like EcDsbA, catalyzed peptide thiol oxidation as evident by an increase in the reaction rate comparing three different concentrations of both enzymes (**Figure 4.1A**). The reaction rate reflects the kinetics of the peptide turnover within the first 8 min of catalysis. At the same enzyme concentrations PmDsbA catalysis was a little slower than that of EcDsbA. This slightly reduced activity may reflect the use of a peptide derived from an EcDsbA substrate. Nonetheless, the results establish that PmDsbA catalyses dithiol oxidation in a model substrate.

We also assessed the ability of PmDsbA to complement EcDsbA *in vivo*. *E. coli* strains deficient in the P-ring protein FlgI fail to assemble functional flagella (Ohnishi *et al.*, 1987). Moreover, *E. coli* strains lacking EcDsbA, EcDsbB or both, have the same phenotype (Dailey & Berg, 1993) because FlgI requires a disulfide bond to function. The non-motile strains *E. coli* Δ*dsbA* (JCB817) and Δ*dsbA* / Δ*dsbB* (JCB818) were therefore used for *in vivo* DsbA complementation experiments. When EcDsbA or PmDsbA were expressed in JCB817 following arabinose induction, full rescue of motility was observed in JCB817 (**Figure 4.1B**). However cells from the double knockout (JCB818) remained non-motile for both PmDsbA and EcDsbA. These results demonstrate that PmDsbA can replace EcDsbA functionally *in vivo* in the context of flagella assembly. Since EcDsbB was also essential for complementation in this experiment, the results confirm that PmDsbA and EcDsbB can form a functionally competent system. This was expected since the P2 loop sequence from PmDsbB is identical to that of EcDsbB. Furthermore, the *P. mirabilis* FlgI homologue shares 74% sequence identity with EcFlgI including two conserved cysteine residues.

PmDsbA shares the same characteristic redox properties as EcDsbA – DsbA enzymes exhibit unique properties that contribute to their ability to catalyze disulfide bond formation (Pogliano *et al.*, 1997, Shouldice *et al.*, 2011). We next established whether these characteristics are shared by PmDsbA. First, we investigated the relative thermostability of the oxidized and reduced forms of the enzyme. In most DsbAs, the reduced form of the CXXC active site is more stable than the

oxidized form. For instance, the melting temperature of reduced EcDsbA is almost 10 K higher than that of the oxidized form (Heras *et al.*, 2008b). Similarly, we found that reduced PmDsbA (T_m^{red} 348.4 ± 0.1 K) is 10 K more stable than oxidized PmDsbA (T_m^{ox} 338.4 ± 0.2 K) (**Figure 4.1C**).

DsbAs are also highly oxidizing. The redox potential of EcDsbA is -122 mV (Wunderlich & Glockshuber, 1993) and the range of values reported for other DsbAs varies from -80 mV for NmDsbA1 (Vivian *et al.*, 2009) to -163 mV for WpDsbA (Kurz *et al.*, 2009). Nevertheless, closely related (> 80% sequence identity) homologues of EcDsbA such as SeDsbA and KpDsbA have redox potential values very similar to that of EcDsbA (-126 mV, -116 mV respectively). We determined the redox potential of PmDsbA to be -129 mV (**Figure 4.1D**), which is consistent with those of other *Enterobacteriaceae* DsbAs.

The oxidizing nature of DsbA proteins is thought to be a consequence of the highly acidic cysteine in the **C**XXC active site motif. The pK_a of 3.3 for this nucleophilic cysteine Cys30 for EcDsbA is unusually low for a cysteine (pK_a 9.0) (Huber-Wunderlich & Glockshuber, 1998). Values reported for other DsbAs vary from 3.0 (NmDsbA1) (Lafaye *et al.*, 2009) to 5.1 (VcDsbA) (Ruddock *et al.*, 1996). We measured the pK_a of the equivalent cysteine in PmDsbA, by pH-dependent specific absorbance at λ = 240 nm, and determined the value to be 4.0 (**Figure 4.1E**). Thus, the nucleophilic cysteine of PmDsbA, like that of other DsbAs, is likely to be in the thiolate form at physiological pH when the enzyme is reduced.

Although DsbA proteins are dithiol oxidases they can catalyse disulfide reduction in the presence of mild reducing agents such as DTT. Typically, insulin is used as a substrate to study *in vitro* disulfide bond reduction. The two chains of insulin are linked by three disulfide bonds, which can be rapidly reduced by disulfide reductases such as the disulfide isomerase EcDsbC. This reduction leads to separation of the insulin A and B chains, and precipitation of the insoluble B chain. Reduction can be followed by measuring the increase in turbidity of the solution over time. We found that PmDsbA is able to reduce the disulfide bonds of insulin as rapidly as EcDsbA (**Figure 4.1F**), but more slowly than the specialist reductant EcDsbC.

In summary, the redox properties of PmDsbA reported here place it in the same class as EcDsbA and other *Enterobacteriaceae* DsbAs such as *Salmonella enterica* DsbA (SeDsbA) and *Klebsiella pneumoniae* DsbA (KpDsbA) (Kurth *et al.*, 2013).

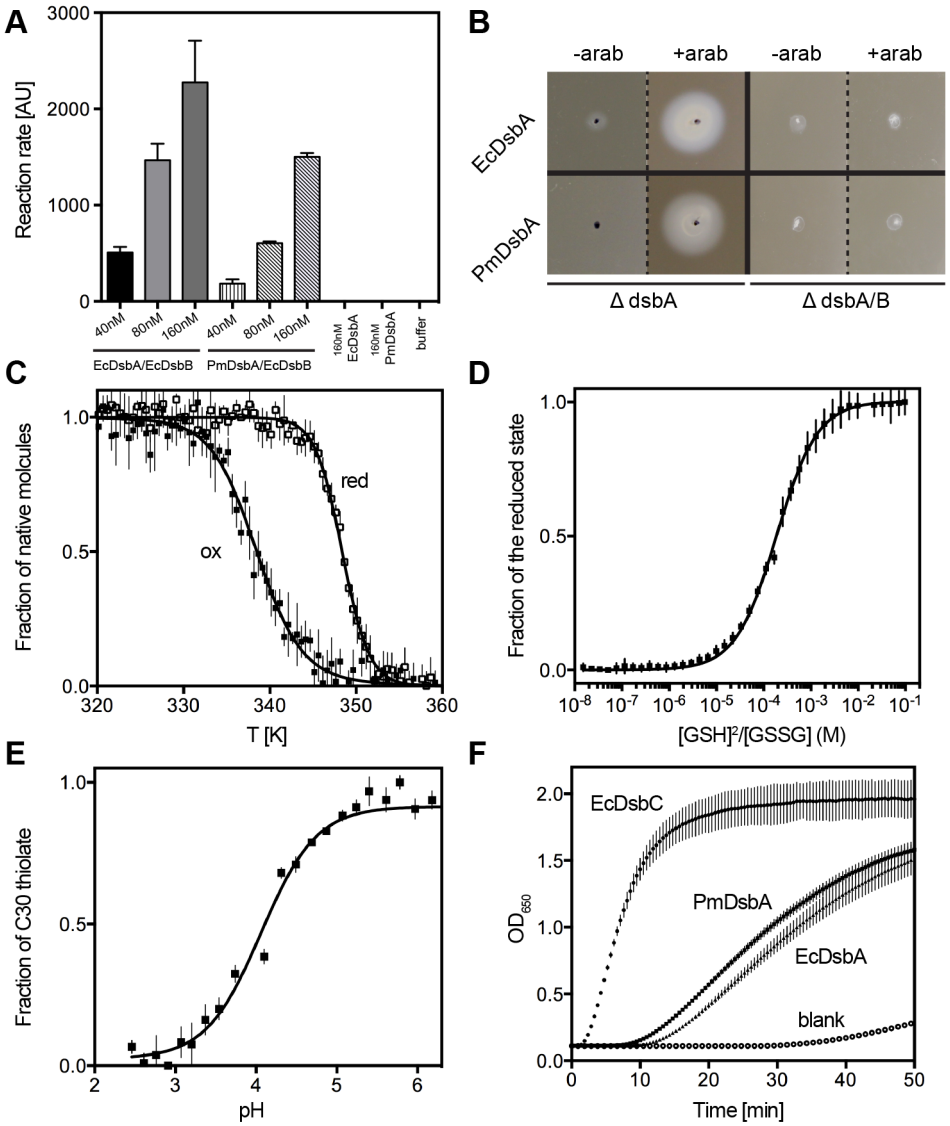

Figure 4.1. ***Redox Properties of PmDsbA.*** ***A.*** *In vitro disulfide catalysis. Plot shows increase in reaction rates as a consequence of peptide disulfide formation catalyzed by EcDsbA or PmDsbA in the presence of EcDsbB. Rates reflect the kinetics of the catalysis within the first 8 min. As controls rates derived from DsbA proteins / buffer alone are displayed in the right.* ***B.*** *In vivo disulfide catalysis. ΔdsbA knock-out or ΔdsbA/B double knock-out cells are non-motile due to their inability to fold FlgI. Expression of PmDsbA or EcDsbA restores motility in ΔdsbA, but not in ΔdsbA/B.* ***C.*** *Thermal melting curves of oxidized and reduced PmDsbA shows that reduced PmDsbA (T_m^{red} 348.4 ± 0.1 K) is more stable than its oxidized counterpart (T_m^{ox} 338.4 ± 0.2 K).* ***D.*** *Measurement of PmDsbA redox potential. PmDsbA was equilibrated in glutathione (GSSG/GSH) redox buffers to measure the equilibrium constant K_{eq} (187. 5 ± 6 μM) which corresponds to a redox potential of -129 mV.* ***E.*** *Absorbance of the catalytic thiolate anion is pH-dependent and this property was used to determine that the pK_a of PmDsbA Cys30 is 4.0* ***F.*** *Disulfide reductase activity measured by following OD_{650nm}. PmDsbA has activity similar to that of EcDsbA, and much lower than that of the isomerase EcDsbC. For panels A and C-F, data are shown as mean and standard deviation from three replicates.*

PWATCDS binding to PmDsbA and PmDsbAC30S – We were interested to understand how peptides interact with PmDsbA, as the basis for future peptidomimetic inhibitor development. The low resolution crystal structures and the NMR characterization of the EcDsbB:EcDsbA complex revealed that the EcDsbB periplasmic loop P2 forms a mixed disulfide with the nucleophilic cysteine of EcDsbA and binds to a hydrophobic groove near the active site (Inaba *et al.*, 2009a, Inaba, Murakami*, et al.*, 2006, Malojcic *et al.*, 2008, Sperling *et al.*, 2013). The peptide sequence of the EcDsbB P2 loop ^{98}PSPFATCDF^{106} is conserved in PmDsbB (^{99}PSPFATCDF^{107}) suggesting that a similar interaction occurs between PmDsbA and PmDsbB. From the sequence of this P2 loop peptide, we developed a shorter, modified peptide PWATCDS optimized for solubility and binding affinity with EcDsbA (details of design reported elsewhere). Briefly, from an initial peptide of sequence PSPFATCDF an alanine scanning, peptide length scouting and substitution of specific residues showed that the PWATCDS sequence had the optimal affinity-to-mass ratio (or binding efficiency) to bind oxidized EcDsbA. Moreover, PWATCDS was shown to limit EcDsbA substrate folding activity in a competition assay. We hypothesized that this peptide would also interact with PmDsbA, and therefore evaluated its binding using two complementary methods, thermal shift and isothermal titration calorimetry (ITC).

Tm values for PmDsbA and PmDsbAC30S (a variant in which the nucleophilic cysteine was replaced by serine) were measured in the presence and absence of the peptide PWATCDS, with varying peptide concentrations. *Tm* values of +2.0, +4.1 and +5.0 K were observed at peptide concentrations of 1, 2 and 4 mM respectively (**Figure 4.2A**), suggesting that PWATCDS binds to PmDsbA. These data show that the *Tm* shift continued with increasing peptide concentration beyond saturation, as is commonly observed in this assay (Cimmperman *et al.*, 2008). When the variant PmDsbAC30S was used, thermal shifts (ΔTm > + 0.3 K) were detectable at concentrations of PWATCDS ranging from 250 µM to 4 mM. However the maximum ΔTm at 4 mM was significantly lower than that at the same concentration for PmDsbA (ΔTm +1.5 K, compared with 5.0 K, respectively) (**Figure 4.2A**). This difference in ΔTm suggests the possibility of different binding modes.

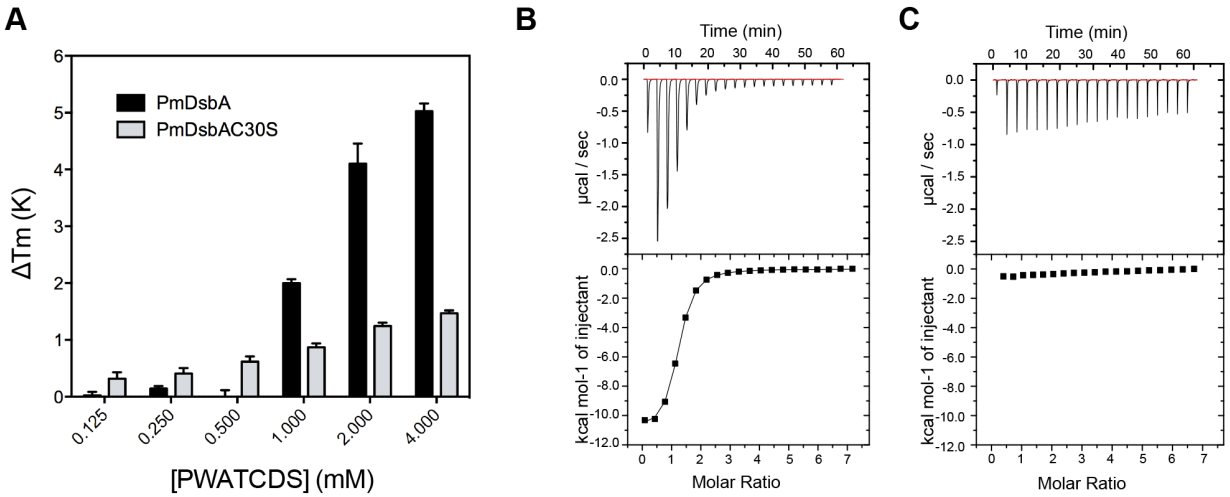

Figure 4.2. ***Peptide PWATCDS interacts with PmDsbA. A.*** *Values of ΔTm upon addition of increasing PWATCDS peptide for PmDsbA and PmDsbAC30S. Data are shown as mean and standard deviation from 5 replicates.* ***B.*** *ITC data titrating PWATCDS into PmDsbA. The reaction is exothermic suggesting a dominant enthalpic contribution to binding.* ***C.*** *ITC data titrating PWATDCS into PmDsbAC30S. The binding reaction is also exothermic but the energy released is less than that for native PmDsbA. Saturation of binding was not achieved in this case. Panels B and C show a representative example from the three replicates.*

Table 4.2. ***Stoichiometry (N), affinity (Kd) and thermodynamic (ΔH, ΔS and ΔG) parameters from ITC for binding of PWATCDS.***

Protein	N	Kd (uM)	ΔH (kcal/mol)	ΔS (cal/mol/deg)	ΔG (kcal/mol)
PmDsbA1 wt	1.0 ± 0.1	8.3 ± 0.4	-13.7 ± 0.3	-22.3 ± 1.1	-6.9 ± 0.1

N, Kd, ΔH and ΔS are reported as means ± standard deviation from 3 titrations of PWATCDS into PmDsbA. ΔG is calculated from ΔG = ΔH –TΔS with T the temperature at which the titration took place

We also investigated the interaction using isothermal titration calorimetry (ITC). An exothermic reaction was observed when titrating PWATCDS into PmDsbA (**Figure 4.2B**). Analysis of the raw data using a 1:1 binding model revealed a binding affinity K_D of 8.3 ± 0.4 µM (**Table 4.2**) with a high enthalpic contribution (ΔH = -13.7 ± 0.3 kcal/mol) and an unfavorable entropy of binding (ΔS = -22.3 ± 1.1 cal/mol/deg). When PmDsbAC30S was used, the energy exchange was much lower (first injection peaks at -0.8 µcal/sec instead of -2.5 µcal/sec) and saturation was not reached (**Figure 4.2C**). Curve-fitting was not optimal and a key enthalpic contribution was lost compared to the binding to native PmDsbA. The Cys30Ser mutation affected peptide binding and

PWATCDS presented a weaker affinity towards PmDsbAC30S. This is consistent with the observations from the thermal shift experiments.

Crystal structure of PmDsbA - To investigate the different binding modes further, we attempted to determine the crystal structures of PmDsbA and PmDsbAC30S, in the presence of the peptide PWATCDS. We were unable to generate a crystal of a stable complex of PmDsbA with PWATCDS. However, crystals of PmDsbA and PmDsbAC30S without peptide, and PmDsbAC30S with peptide yielded high-resolution diffraction data (PmDsbA, 1.77 Å resolution; PmDsbAC30S, 1.98 Å resolution; and PmDsbAC30S-PWATCDS, 1.6 Å resolution).

PmDsbA crystallized in a tetragonal crystal system and was solved (PDB:4OCE) by molecular replacement using the EcDsbA structure (PDB: 1FVK) as a template. One protein chain is present in the asymmetric unit, and this has a typical DsbA-like architecture, comprising a TRX core domain (β1, β 2, α1, β3, C-terminal region of α6, β4, β 5 and α7), interrupted by an α-helical domain (α2- α5, and the N-terminal region of α6). This PmDsbA structure is structurally similar to other *Enterobacteriaciae* DsbAs including EcDsbA (PDB: 1FVK (Guddat *et al.*, 1997)), KpDsbA (PDB: 4MCU (Kurth *et al.*, 2013)) and SeDsbA (PDB: 3L9S (Heras *et al.*, 2010a)) (**Figure 4.3A**). This is reflected in the RMSD of 1.0–1.2 Å comparing 177 Cα atoms from equivalent positions of these enzymes. **Figure 4.3B** shows a structure based sequence alignment of PmDsbA with homologous DsbA proteins from clinically relevant pathogens that share > 59% sequence identity. Sequences are highly conserved, especially at the active site CPHC motif. Sequence identity translates into overall structural similarity between DsbA proteins from these pathogens.

The sequence and structure of the active site motif (CPHC) and the *cis*Pro loop are identical in these DsbA homologues. However, helix α1 and the loops connecting β1 and β2, and α3 and α4 differ in their relative positions. Most importantly loop L3 that connects β3 and helix α7 varies across the structures. The EcDsbA L3 residues D167, T168 and S169 are positioned closer to the active site helix α1 than the equivalent residues (A167, K168, S169) in PmDsbA. This region is relatively hydrophobic in both PmDsbA and EcDsbA, though more basic in PmDsbA than in EcDsbA due to presence of Lys159 in the former and Q160 in the latter. Overall these differences in structure are relatively minor compared to the structures of other DsbA proteins, such as *Pseudomonas aeruginosa* DsbA (25% identity with PmDsbA, RMSD 2.2 Å, 175 Cα, PDB: 3H93 (Shouldice *et al.*, 2010)), and *Wolbachia pipientis* DsbA1 (16% identity with PmDsbA, RMSD 3.6 Å, 151 Cα, PDB: 3F4R (Kurz *et al.*, 2009))

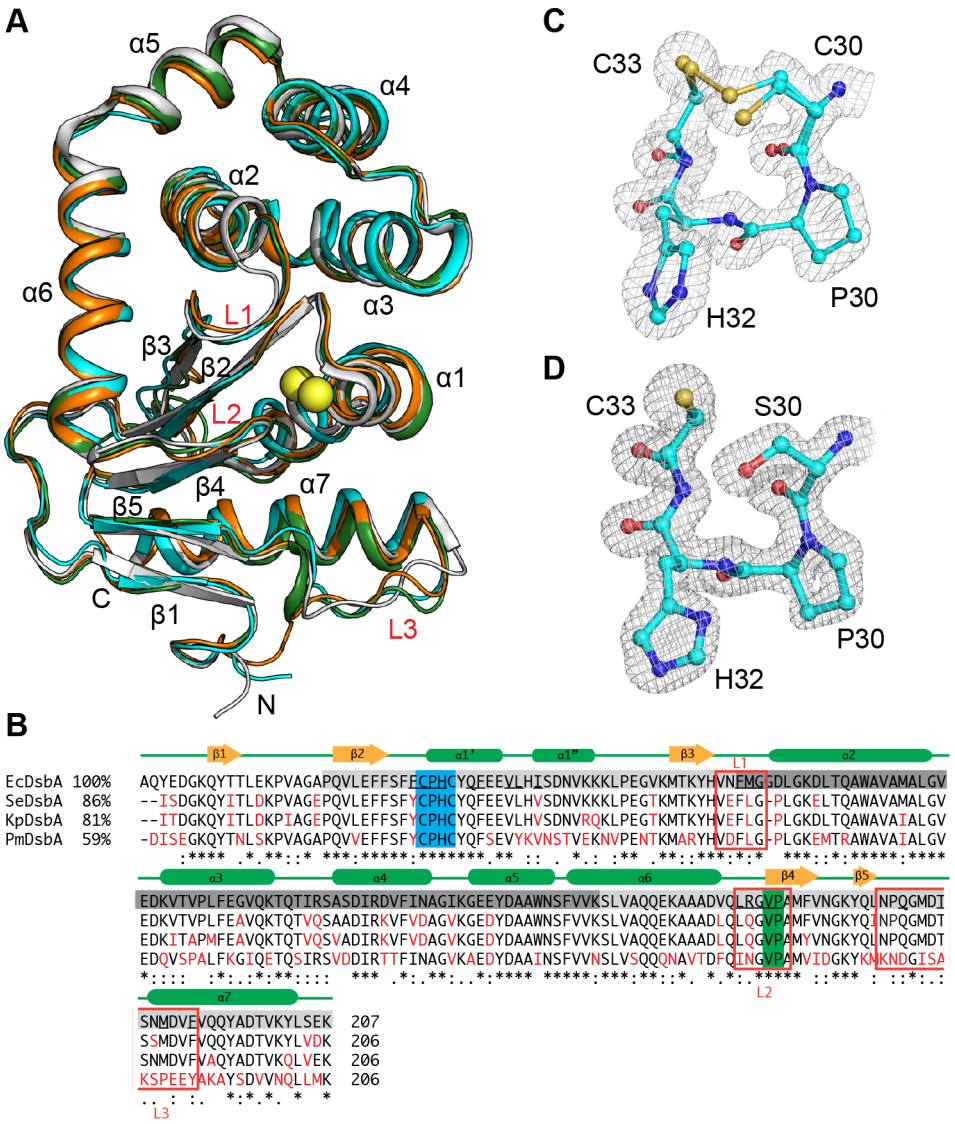

Figure 4.3. ***Crystal structure of PmDsbA and its comparison with close homologues. A.*** *Structural comparison of four closely related DsbA homologues, PmDsbA (4OCE) in cyan, EcDsbA (1FVK protomer B) in white, KpDsbA (4MCU protomer E) in orange and SeDsbA in green. Conserved structural regions are annotated; the catalytic cysteines are shown as yellow spheres.* ***B.*** *Structure based sequence alignment of EcDsbA (1FVK, chain A), SeDsbA (3L9S, chain A), KpDsbA (4MCU, chain F), and PmDsbA (4OCE, chain A). Sequence identity with EcDsbA is shown on the left, conserved residues are black, differing residues are red. The TRX domain is highlighted in light grey, and the helical domain in dark grey. Red squares mark the three loop regions L1/2/3. Amino acid conservation code is shown beneath the sequences. The active site CXXC motif is highlighted in blue, and the cisPro region in green. Secondary structure elements are indicated above the sequences. Residues underlined in EcDsbA bind to the EcDsbB P2 loop peptide (PISA server analysis).* ***C.*** *CXXC active site of PmDsbA.* ***D.*** *CXXC active site of PmDsbAC30S:PWATCDS. For panels C and D, the electron density is from $2F_0$ - F_c FFT maps generated in Phenix (Adams et al., 2010) and contoured at 1.0 σ.*

Crystal structure determination of PmDsbAC30S and PmDsbAC30S:PWATCDS – We solved the structure of the active site mutant PmDsbAC30S (PDB:4OCF). The crystals grew in the presence of peptide, but no bound peptide was evident in the electron density map. We therefore used this structure of PmDsbAC30S to assess whether replacement of Cys30 with Ser30 induced any structural changes. The mutant crystallized in a monoclinic crystal system, containing 4 protomers in the asymmetric unit. The structure was solved by molecular replacement using the coordinates of PmDsbA described above. The average RMSD for comparison of the 6 combinations of the 4 protomers ranges from 0.3–0.7 Å for 177 equivalent Cα atoms (residues 6-181).

PmDsbAC30S in complex with the peptide PWATCDS crystallized in a trigonal crystal system, containing 3 protomers in the asymmetric unit. The complex was solved by molecular replacement using PmDsbA (PDB:4OD7) as the template. All three protomers (A, B and C) reveal strong electron density corresponding to bound PWATCDS. The average RMSD for the 3 comparisons of the protomers in this crystal structure range from 0.4–0.6 Å for 177 equivalent Cα atoms (residues 6-181). The RMSD for comparison of PmDsbAC30S with PmDsbAC30S-PWATCDS range from 0.5–0.9 Å (177 Cα) for the 12 combinations. Similarly, comparison of the wild type PmDsbA structure with PmDsbAC30S and PmDsbAC30S-PWATCDS gave RMSD values of 0.3–0.9 Å (177 Cα). This result indicates there is no major re-organisation of the PmDsbAC30S structure upon interaction with PWATCDS. However, there is evidence of rigid body shifts for helix 1 and side chain adjustments for residues on helix 1 (His32, Tyr34, Gln 35, Phe36, Ser37) and the flexible loop 3 (Ile165, Ser166) that together form part of the peptide binding site.

Active site structure is conserved after peptide binding – A comparison of the active site motifs (CPHC, CPHS) and the Val150/Pro151 residues of the *cis*Pro loop across all the protomers in the PmDsbA, PmDsbAC30S and PmDsbAC30S-PWATCDS crystal structures reveals a high degree of structural conservation. The active site cysteines Cys30 and Cys33 in the native PmDsbA structure were modeled as a mixture of oxidized and reduced (ratio 0.7:0.3). In the oxidized state the two sulfurs (**Figure 4.3C**) are 2.2 Å apart, reflecting the typical length of a covalent disulfide bond found in other oxidized DsbA structures (*eg*. EcDsbA and SeDsbA, S-S distance 2.0 Å) (Martin *et al.*, 1993, Heras *et al.*, 2010a). The dithiol form of the cysteines is likely a consequence of radiation-induced disulfide reduction. The distance between the dithiol sulfurs is 3.4 Å. In the PmDsbAC30S and PmDsbAC30S:PWATCDS structures, the distance between the hydroxyl oxygen of Ser30 and the sulfur atom of Cys33 varies between 3.3–3.5 Å (Figure 3D). These

distances are in agreement with those of other reduced DsbA structures (*eg*. KpDsbA 3.3-3.8 Å) (Kurth *et al.*, 2013). Overall, there is no apparent change in the active site upon binding of the peptide.

Peptide binding mode and interaction with PmDsbAC30S – The binding mode of the peptide (**Figure 4.4A** and **4.4B**) is highly conserved across the three protomers (RMSD 0.1–0.2 Å over all 82 atoms). The electron density from this high-resolution structure provides strong evidence for both the position and conformation of the bound peptide (**Figure 4.4C**). The binding site for PWATCDS (residues 1 to 7) includes the hydrophobic groove and the active site regions (CXXC and *cis*Pro motif) of the enzyme. As expected, the hydrophobic residues *Pro1* and *Trp2* (italics indicate peptide residues) interact with the hydrophobic groove, and the C-terminal residues interact with the *cis*Pro region of the active site.

However, the observed binding mode was not entirely as predicted. On the basis of the EcDsbA:EcDsbB covalent complex, *Cys5* of the peptide should interact with PmDsbAC30S residue 30 (mutated from Cys to Ser). This was not the case. In all three complexes in the asymmetric unit, *Asp6* and not *Cys5* interacts with PmDsbAC30S Ser30 (**Figure 4.4D**). The acidic side chain of *Asp6* is within hydrogen bond contact distance of Ser30 and His32. Moreover, the backbone amide of *Asp6* forms hydrogen bonds with the backbone amide of Val149 of the PmDsbAC30S *cis*Pro loop (Figure 4D).

Comparison of peptide binding mode with DsbA-DsbB complexes – The EcDsbB P2 loop (sequence PSPFATCDF) and the synthetic peptide we used, (PWATCDS), share the same binding location on EcDsbA and PmDsbAC30S, respectively. The EcDsbA-EcDsbB complex (3.7 Å resolution (Inaba *et al.*, 2009a)), revealed one possible hydrogen bond between P2 and the enzyme (backbone oxygen of Arg148 of the EcDsbA *cis*Pro loop with the backbone nitrogen of EcDsbB Phe106). All other interactions with the P2 loop, aside from the covalent disulfide, are hydrophobic (Shouldice *et al.*, 2011).

As indicated above, no interaction was observed between *Cys5* and Ser30 of PmDsbAC30S. Instead, hydrogen bond interactions with *Asp6* and hydrophobic interactions with *Trp2* appear to dominate the PWATCDS binding mode. Residues between these two anchor points - *Cys5, Thr4* and *Ala3* - protrude out of the binding site relative to the equivalent EcDsbB loop residues (**Figure 4.4E, F**).

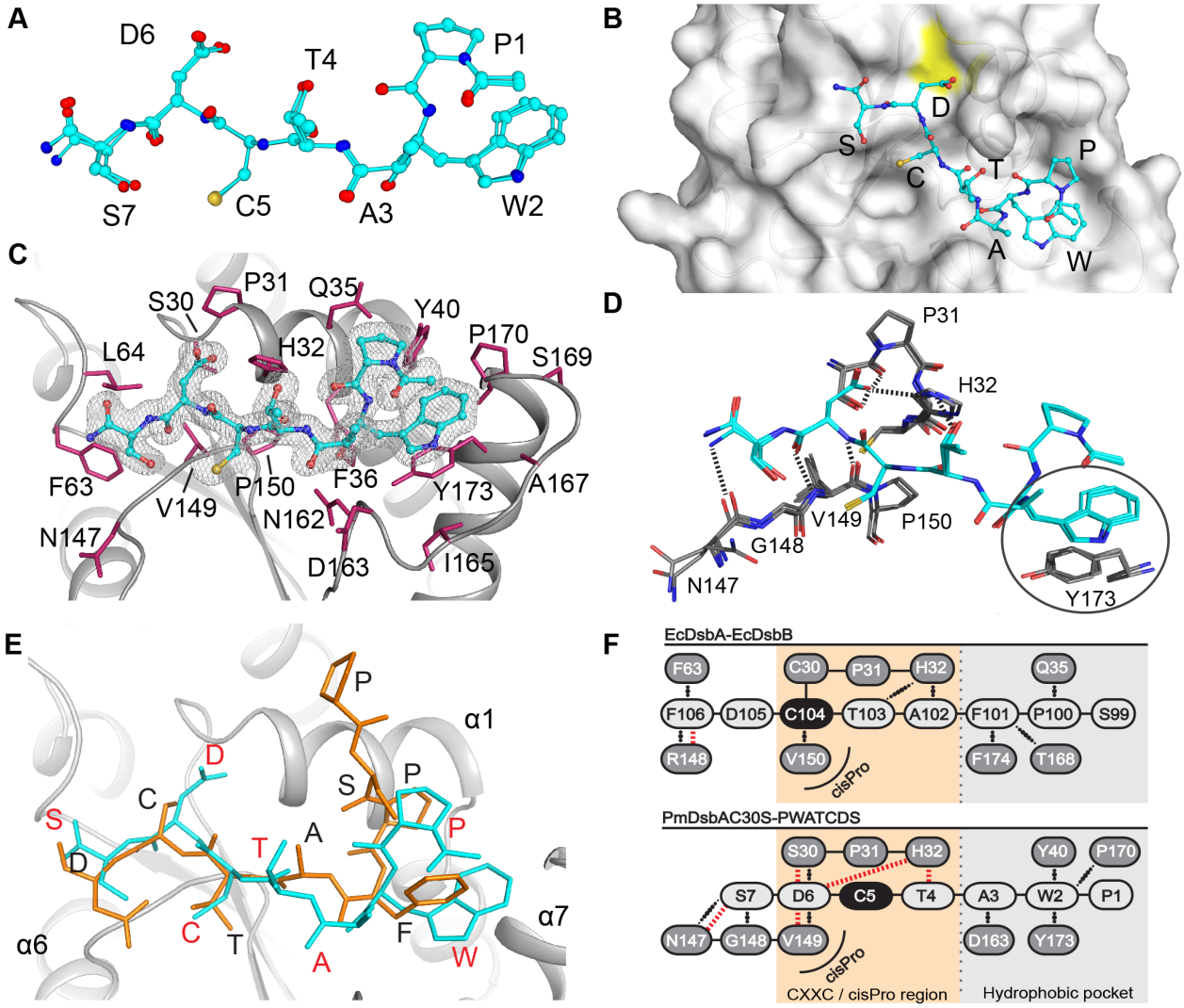

Figure 4.4. ***Analysis of the interaction between peptide PWATCDS and PmDsbAC30S. A.*** *Superposition of the PWATCDS peptides from all three protomer:peptide complexes in the asymmetric unit. Note the peptide includes an N-terminal acetyl and a C-terminal amide group. Carbon atoms are shown in cyan, oxygens in red, nitrogens in blue and sulfurs in yellow.* ***B.*** *Location of the bound PWATCDS peptide on the surface of PmDsbAC30S (protomer A shown, in grey). Peptide residues are labeled and colored as for panel A. The yellow patch indicates the location of Ser30.* ***C.*** *Electron density map of PWATCDS (chain F) at the interface with PmDsbAC30S (chain B). The $2F_0$-F_c map was generated in Phenix (Adams et al., 2010) and is contoured at 1.0 σ. PmDsbAC30S residues forming the binding site are labeled.* ***D.*** *Interactions between the peptide (D-F, in cyan) and protein (chains A-C, in grey) are shown: hydrogen bonds are indicated as black dashed lines; a circle highlights the stacking interaction between Trp2 and PmDsbAC30S Tyr173.* ***E.*** *Superposition of the EcDsbB P2 periplasmic loop (PSPFATCD, orange, black letters, PDB code 2ZUP) with PmDsbAC30S-PWATCDS (red letters, backbone in cyan).* ***F.*** *Schematic representation of the interactions formed between EcDsbB P2 loop binding to EcDsbA (top) in comparison to PWATCDS binding to PmDsbAC30S (bottom), showing the comparative shift in register. Covalent bonds are shown as black lines, hydrogen bonds are indicated with red dashed lines and hydrophobic interactions with black dotted lines.*

The RMSD for comparison of PWATCDS with the EcDsbB P2 loop conformation is relatively high (2.2 Å for 28 backbone atoms), because of the bulge in the peptide conformation. Binding of PWATCDS results in an average buried surface area (*i.e.* surface that becomes inaccessible to solvent) of 955 ± 12 Å or 9.0% ± 0.1% of the total surface of PmDsbAC30S (values are means and S.D. generated from the three molecules in the asymmetric unit). This is similar in area to the EcDsbA buried surface upon binding of the EcDsbB P2 loop (924 $Å^2$) (Inaba *et al.*, 2009a). In both structures a major feature is the binding of an aromatic residue in the hydrophobic groove. EcDsbB P2 loop residue Phe101 forms a T-shaped π-π stacking interaction with EcDsbA Phe174 whereas *Trp2* of the PWATCDS peptide forms a parallel π-π stacking interaction with PmDsbAC30S Tyr173 and possible edge interactions with enzyme residues Pro170 and Tyr40.

Discussion

The increasing incidence of infections caused by multidrug resistant pathogens represents a serious global human health issue. Indeed, the emergence of carbapenem-resistant *Enterobacteriaceae* threatens to make common infections such as UTIs untreatable (Totsika *et al.*, 2012). Antibiotic resistance is spreading rapidly and treatment options are becoming increasingly limited. One possible approach to address the paucity of new antimicrobials in the developmental pipeline lies in the generation of novel anti-virulence drugs (Rasko & Sperandio, 2010, Clatworthy *et al.*, 2007).

The Gram-negative DsbA/B system has been proposed as a target for the development of novel anti-virulence drugs (Heras *et al.*, 2009). Targeting DsbA/B for development of inhibitors could be beneficial in many ways. First DsbA is not essential for bacterial survival (Bardwell *et al.*, 1991) though it plays an essential role in virulence (Heras *et al.*, 2009). Thus, inhibiting DsbA/B would not kill bacteria and this property may reduce the selective pressure to develop resistance. Second, structures of several DsbA homologues have been solved (Kurth *et al.*, 2013, Shouldice *et al.*, 2011, Premkumar *et al.*, 2013) providing a framework for structure-based drug design. Third, DsbA structures and properties are more highly conserved than the structures and sequences of virulence factors across pathogens (Kurth *et al.*, 2013). Therefore, inhibitors that target one DsbA enzyme within a subclass are likely to block DsbAs within the sub-class offering the possibility of medium-spectrum inhibitors (Kurth *et al.*, 2013).

Designing an inhibitor to block a protein-protein interface such as that of a DsbA requires a comprehensive knowledge of its binding interactions. Here we have used an innovative approach to define the interaction surface of PmDsbA by using knowledge from the low resolution crystal structure of EcDsbA-EcDsbB. We characterized a peptide derived from the sequence of DsbB, showed that it bound PmDsbA and co-crystallized it in a non-covalent complex with PmDsbAC30S. This provides the first example of a high-resolution crystal structure of a DsbA in complex with a non-covalently bound peptide. Two previously published structures of DsbA in complex with bound peptides include (i) EcDsbA bound covalently with a substrate SigA derived peptide (Paxman *et al.*, 2009a); and (ii) *Xyfella fastidiosa* DsbA also bound covalently with a peptide that co-crystallized fortuitously (Rinaldi *et al.*, 2009). The SigA peptide was covalently linked to EcDsbA and interestingly showed a binding conformation differing from the DsbB loop or the present peptide, with the binding to EcDsbA Cys30 the only shared feature. For the second structure, the electron density of the peptide bound to XfDsbA was poor, only allowing the fitting of a poly-Ala chain and therefore not suitable for comparison with the present high-resolution structure.

The high resolution of the new PmDsbAC30S-PWATCDS crystal structure allows investigation of finer binding features that can be exploited for inhibitor design. However, due to the alteration in the binding environment around the catalytic site with the Cys to Ser mutation (thus replacing a lipophilic residue with a hydrophilic amino acid), the binding peptide conformation might not be entirely representative of the binding to the wild type DsbA in this region, as hinted by the peptide residue shifts (Figure 4.4.E and 4.4.F) and Cys5 pointing outside of the DsbA suface. Neighboring regions however are very conserved and could be used as template for rational drug design, particularly the hydrophobic pocket.

P. mirabilis associated infections are often difficult to treat due to its propensity to form biofilms (Jacobsen & Shirtliff, 2011). Two cell surface organelles associated with *P. mirabilis* biofilm formation, mannose-resistant Proteus-like (MR/P) fimbriae (Jansen *et al.*, 2004) and flagella (which mediate swarming) (Jacobsen & Shirtliff, 2011), require DsbA for their correct assembly. Taken together, our data show that PmDsbA exhibits redox, functional and structural properties typical of the DsbA class Ia enzymes (McMahon *et al.*, 2014) which extends to all DsbAs characterized to date from *Enterobacteriaceae* (Kurth *et al.*, 2013). We expect that the structural details of the peptide binding mode and the interactions observed will likely hold true for all of these enzymes. Specifically, the hydrophobic groove and the *cis*Pro loop provide key points of interaction that could be exploited further. The high-resolution crystal structure of the non-

covalent complex between PmDsbAC30S and peptide may provide an important platform for the development of peptidomimetic antivirulence compounds targeting PmDsbA and by extension the DsbAs from all *Enterobacteriaceae*.

Acknowledgments

We are grateful to Brett Collins and Makrina Totsika for helpful advice and Stephanie Tay for preparing EcDsbB membranes for the cysteine thiol oxidation assay. We thank the beam-line staff at the Australian Synchrotron for their assistance. We acknowledge use of the UQ ROCX Diffraction Facility. JLM is an Australian Research Council Australian Laureate Fellow (FL0992138) and FK, WD and LP were also supported by this award. JLM is also an Honorary NHMRC Research Fellow (455829). DPF was supported by NHMRC Senior Principal Research Fellowship (1027369). MAS was supported by an Australian Research Council Future Fellowship FT100100662.

CHAPTER V

Evaluation of the first series of peptidomimetics

V.1 Introduction

Peptides were characterized in my PhD project to investigate the potential optimization of the scaffold using natural residues and a few non-natural side chains (see Chapter III), and the highest affinity-to-mass-ratio peptide (PWATCDS) was crystallized with PmDsbAC30S to obtain a high-resolution crystal structure (see Chapter IV) providing insight into the binding features of this sequence. From this work, the next logical step was to develop peptidomimetics as better inhibitors of EcDsbA. This could be done by a broad range of chemical transformations to improve potency, stability, resistance to proteases and bioavailability.

The first goal was to improve the affinity for EcDsbA to the submicromolar or nanomolar range, in order to reach potency closer to typical 'druggable' compounds. The second aim was to develop an inhibitor that did not rely on the formation of a covalent disulfide bond with EcDsbA. Otherwise, the possibility of nucleophilic attack by substrate molecules or EcDsbB onto Cys30 might trigger the release of the disulfide-bond linked inhibitory peptide, hence limiting its efficiency.

Many approaches can be used to develop a peptide sequence into a peptidomimetic scaffold retaining and/or enhancing antimicrobial properties (see section I.3). Substitution with non-natural side chains has briefly been explored in Chapter III, and this chapter focuses on efforts to move away from natural amino acids and peptides, using techniques such as backbone cyclization, addition of covalent 'warheads' and virtual screening to target the hydrophobic pocket neighboring the catalytic cysteines.

Cyclic peptides are already present in the natural reservoir of antibiotics and AMPs. For instance, vancomycin and cyclosporine are all cyclic peptides. Generally, cyclic peptides are divided into three categories: peptides for which cyclization relies on disulfide bridges, such as tachyplesin (Nakamura *et al.*, 1988), peptides that do not include disulfide bonds, such as Gramicidin S (two pentapeptides cyclized head-to-tail (Mogi & Kita, 2009)) and peptides that possess both disulfides bonds and a head-to-tail backbone cyclization, such as cyclotides (Craik *et al.*, 2006). Peptides not including disulfide bonds can be cyclized head-to-tail such as Gramicidin S or through their side chains such as Actinomycin D. In a different approach, engineered cyclic peptides such as D,L-α-residue hybrids are even able to self-assemble into nanotubes with potent bactericidal properties *in vivo* (Dartois *et al.*, 2005). Generally, peptide cyclization confers

additional stability by restraining the peptide conformation in solution and provides proteolytic resistance (Katsara *et al.*, 2006). Another advantage of cyclization is that the restrained conformation decreases the energetic penalty of binding to the target by minimizing entropy losses (Clardy & Walsh, 2004). This way, the preorganization of a peptide into a conformational shape complementing the surface of the target through cyclization might also raise its potency. It was hypothesized that the transformation of DsbA-binding peptides into cyclic peptidomimetics might produce compounds that better complement the EcDsbA hydrophobic pocket. However, cyclization must not be induced by a disulfide bond because of the weak reductase activity of DsbA, and will instead require cross-linking of side chains together.

A second strategy consisted of targeting the domains neighboring the catalytic cysteines that would still prevent EcDsbB periplasmic loop P2 from fitting onto the EcDsbA surface, without forming a disulfide bridge with Cys30. The peptide SAR in chapter III suggested that such a goal would be difficult due to the importance of the disulfide bond formation in the EcDsbA-peptide interaction; the crystal structure of peptide PWATCDS in a non-covalent complex with the PmDsbAC30S mutant in Chapter IV suggested possible clues to develop new binding interactions. Moreover the high resolution of the crystal structure highlighted the molecular features of peptide binding, including the π-stacking interaction between PmDsbAC30S Tyr174 and peptide Trp2 in the hydrophobic pocket. This hydrophobic patch is a feature shared by EcDsbA (see Chapter IV) and the EcDsbB periplasmic loop has been localised within this hydrophobic groove in the three crystal structures available (Inaba, Murakami*, et al.*, 2006, Inaba *et al.*, 2009b, Malojcic *et al.*, 2008). Therefore it was decided that the PmDsbAC30S-PWATCDS crystal structure could be used as a starting point for the development of small peptidomimetic compounds that would be more specific to the hydrophobic groove. The hypothesis was that the presence of such peptidomimetics might decrease the stability of a EcDsbA-EcDsbB complex, or prevent the interaction altogether thus restraining the disulfide bond exchange necessary for EcDsbA activity. As outlined in the following material and methods, a virtual docking of peptidomimetic libraries based on the PmDsbAC30S-bound PWATCDS structure was performed to provide the initial scaffolds. From an initial scaffold, derivatives were synthesized and tested according to the pipeline described in Chapter II.

A third approach relied on the design of irreversible inhibitors of EcDsbA. The peptide SAR in Chapter III revealed the importance of disulfide bond formation in the binding mechanism to EcDsbA. This feature is not favorable in the drug design process as EcDsbA might be able to

release the inhibitor peptide following nucleophilic attack of Cys33 on Cys30, restoring the disulfide bond in the catalytic site and thus re-enabling EcDsbA folding activity. A new strategy would be to switch to a 'suicide' inhibitor strategy, in which the inhibitor is irreversibly linked to the target through a 'warhead' moiety. While this approach might provide better efficiency (the inhibitor is not released from its target and the latter can not resume activity) and lower dosages (the drug can not be out-competed by increasing concentration of substrate), it also presents a strong disadvantage as reactive moieties able to form covalent bonds can potentially bind other off-target proteins (Singh *et al.*, 2011, Potashman & Duggan, 2009, Johnson *et al.*, 2010). Such a compound requires extreme specificity to limit side effects *in vivo*. Nevertheless, previous successful examples of drug molecules following this 'suicide' strategy are available (Guterman, 2011).

In this project, the target for the 'warhead' was the EcDsbA Cys30, as the primary residue involved in the first step of disulfide bond exchange (see Chapter I). There is a broad array of moieties known to react with thiol groups including nitriles (Powers *et al.*, 2002), halomethylketones (Cohen *et al.*, 2005, Cohen *et al.*, 2007), haloacetamides (Sako *et al.*, 2008), vinyl sulfones (Chalker *et al.*, 2009), epoxides (Johnson *et al.*, 2010), maleimides (Kim *et al.*, 2008) and Michael acceptors (Fry *et al.*, 1998).Each of those would form a stable covalent bond with the sulfide atom of a free cysteine (**Figure 5.1**). The first peptidomimetics were synthesized with a nitrile or an aldehyde moiety as a 'warhead' to covalently bind EcDsbA Cys30.

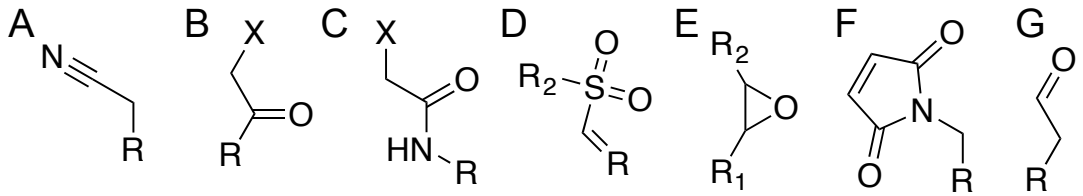

Figure 5.1. ***Examples of reactive functionalities capable of forming irreversible covalent bonds with thiol groups. A.*** *Nitrile.* ***B.*** *Halomethylketone.* ***C.*** *Haloacetamide.* ***D.*** *Vinyl sulfone.* ***E.*** *Epoxide.* ***F.*** *Maleimide.* ***G.*** *An aldehyde group as an example of Michael acceptor.*

These three approaches - macrocyclic peptides, peptidomimetics targeting the hydrophobic pocket and irreversibles binders - are described separately below in their respective material and methods and results sections.

V.2 Material and methods

V.2.1 Macrocyclic peptidomimetics

The initial approach was to synthesize cyclic versions of the sequence PSPWATC. The alanine scanning performed in Chapter III demonstrated that residues Ser2 and Ala5 were not involved in the binding interactions with EcDsbA and thus could be used for other purposes such as cyclization. According to the EcDsbA-EcDsbB and the PmDsbAC30S:PWATCDS structures, a large macrocycle on the peptide N-terminus might occupy most of the hydrophobic pocket and increase hydrophobic contacts with aromatic residues Phe36, Phe174 and Tyr178 and aliphatic residues Leu40 and Ile42 compared to linear PSPWATC.

The usual method for cyclization involves an amine coupling reaction between a free carboxylic acid and a free amine functional groups, in a fashion similar to the usual amino-acid coupling used in solid phase peptide synthesis (see section II.2). This technique requires that all other functional groups on the peptide to be protected to prevent side reactions. To this end, the PSPWATC sequence was modified substituting Ser2 and Ala5 with Lys and Asp residues to give sequences PDPWKTC and PKPWDTC to attempt a 'side chain-to-side chain' macrocyclization. The macrocycle is anticipated to bring structural restraint and alter the conformation of the peptide, potentially adding stability but also limiting the flexibility of the peptide to fit EcDsbA hydrophobic pocket. In order to screen for different conformations, the Lys5 residue (including 4 carbon atoms in the side chain) was replaced with ornithine (Orn) and 2,4-diaminobutyric acid (Dab) presenting shorter side chains leading to different macrocycle sizes (**Figure 5.2**). The length of the side chain might also influence the yield of the cyclization reaction depending on its accessibility by the Asp residue.

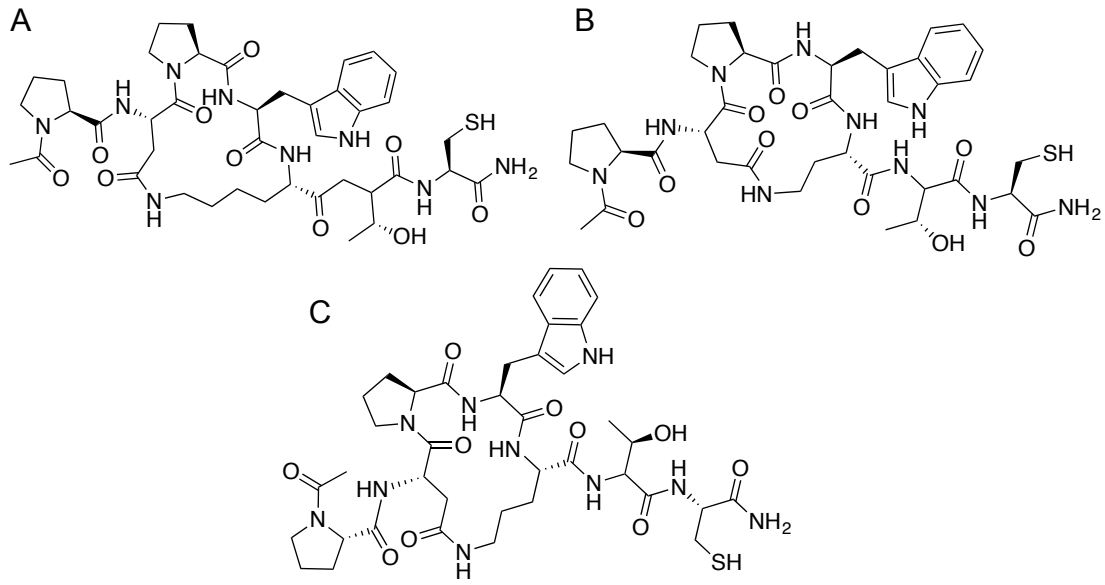

Figure 5.2. ***Structure of different cyclic peptides to be synthesized. A.*** *PDPWKTC as a 17-atom macrocycle.* ***B.*** *PDPW(Dab)TC as a 15-atom macrocycle.* ***C.*** *PDPW(Orn)TC as a 16-atom macrocycle.*

Cyclization was initiated with the classic solid phase synthesis of PDPWKTC, PKPWDTC, PDPW(Orn)TC and PDPW(Dab)TC as described in section II.2, however using Fmoc-Lys, Fmoc-Asp, Fmoc-Orn and Fmoc-Dab residues orthogonally protected by 4-methyltrityl (Mtt) moieties. Peptides still linked on the resin were incubated in TFA 2% in DCM for 30 minutes, which successfully removed the Mtt protection groups while keeping the remaining residues intact (with orthogonal protections resisting up to TFA 90%). The resin was then washed thoroughly with DMF and DCM before incubation with 4 equivalents of Benzotriazol-1-yloxy-tris(dimethylamino)phosphonium hexafluorophosphate (BOP) or otriazol-1-yl-oxytripyrrolidinophosphonium hexafluorophosphate (PyBOP) with excess of DIPEA. Incubation time was screened from 1 hour to 24 hours to identify the time needed for optimal cyclization yield. The resin was then washed again with DMF and DCM before cleaving from the resin and analysis by mass spectrometry.

V.2.2 Targeted peptidomimetics

Virtual Docking – The starting point for the docking study was the 1.6 Å resolution crystal structure of the PmDsbAC30S:PWATCDS peptide complex. The bound peptide was removed and hydrogen atoms were added using the Hermes interface in GoldSuite 5.1 (Verdonk *et al.*, 2003). Additionally

the indole ring system of Trp2 of the bound peptide was separately stored in the same XYZ coordinate space to serve as a template file for the template docking mode within GOLD. The PWA tripeptide was replaced with a small targeted library of 10 compounds based on both D- and L-Tryptophan cores, and both hydrophobic and hydrophilic C- and N-terminal capping groups. These candidate virtual ligands were prepared from 2D ChemDraw (*CS ChemBioDraw Ultra 12.0*) representations via SMILES strings, and minimum energy conformers were prepared using OMEGA2 v2.4.6 (*OMEGA*, Hawkins *et al.*, 2010, Hawkins & Nicholls, 2012) and the mmff94s forcefield. Docking with GOLD 5.1 was performed using the standard precision settings and the default CHEMPLP scoring function. Docking results were visualized in Pymol (Schrodinger, 2010a, b, c). The virtual docking was performed by Dr Martin Stoermer.

Peptidomimetic synthesis – The initial material Boc-Trp-OH (1.00 mmol) was dissolved in 10 mL of dioxane in a nitrogen environment. Carbonyldiimidazole (1.02 mmol) was added in a stepwise manner and the resulting mixture was stirred for 3 h at room temperature followed by heating at 50 $^{\circ}$C for 30 min. Aniline (1.03 mmol) was added to the reaction mixture at room temperature and the solution stirred for 48 h (**Figure 5.3**). The solvent was removed using a rotary evaporator and product was extracted with ethyl acetate (3 x 20ml). The organic extracts were washed with 1 M hydrochloric acid (15 mL), saturated sodium bicarbonate solution (15 mL) and water (15 mL). The extracts were then dried over anhydrous $MgSO_4$ and the solvent was removed using a second rotary evaporator step. The final compound was dissolved in H_2O (1 mL) in which was added aniline (2.00 mmol). The solution was cooled to 0 ^{O}C prior to the addition of TFA (30.00 mmol). After stirring for 1 h at 0 ^{O}C, the reaction mixture was warmed to room temperature and stirring was continued for 12 h. The reaction mixture was then diluted with ethyl acetate (15 mL) and washed with saturated sodium bicarbonate solution (15 mL), water (15 mL) and brine solution (15 mL) and dried over anhydrous $MgSO_4$. The solvent was removed using a rotary evaporator.

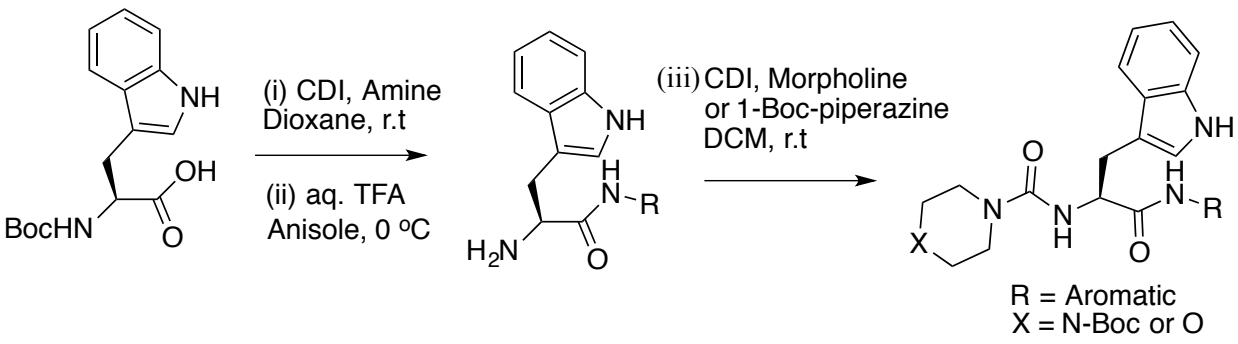

Figure 5.3. ***Synthesis route of the tripeptide peptidomimetics tested in this chapter.***

The compound with the free amine was dissolved in dichloromethane (5 mL) in which was added carbonyldiimidazole (1.2 mmol) in a nitrogen environment. After stirring for 3 h, morpholine or 1-Boc-piperazine (1.55 mmol) was added to the reaction mixture and the solution stirred for another 12 h at room temperature. The solvent was removed using a rotary evaporator, diluted with ethyl acetate (15 mL) and washed with 1 M hydrochloric acid (15 mL), saturated sodium bicarbonate solution (15 mL), brine solution (15 mL) and dried over anhydrous $MgSO_4$. Crude product was then purified by preparative HPLC (Gradient 0 to 100% of 95/5 acetonitrile/water solution over 25 min) and freeze-dried. The 10 compounds presented in this section were synthesized by Dr Prabhakar Bachu.

Differential Scanning Fluorimetry – All protein thermal shift assays were performed on a ViiA™ 7 Real-Time PCR instrument (Life Technologies™, Applied Biosystems™ Division) using 384 well MicroAmp Clear Optical Plates (Life Technologies™, Invitrogen™ Division). Oxidised EcDsbA (25 mM HEPES pH 7.4, 50 mM NaCl) was prepared at a final concentration of 2.5 μM, in the presence of either 5 % (v/v) DMSO (reference) or 2, 1, 0.5, 0.25, 0.125 or 0.0625 mM of the test compound (also in a final concentration of 5% DMSO (v/v.)) A x 5000 stock of SYPRO® Orange Protein Gel Stain (Life Technologies™, Invitrogen™ Division) was diluted to a final concentration of x 5. The final reaction volume was 20 μL. For each condition, five technical replicates were included. Non-protein control reactions (DMSO or compound, and dye in the absence of EcDsbA) were also included to monitor compound-dye interactions respectively. Plates were sealed with Axygen Ultra Clear Pressure Sensitive Sealing Film (Fisher Biotec) and immediately prior to analysis centrifuged (1000 x rpm, 2 min) to draw down all liquid and break any bubbles. A standard melt curve analysis was conducted using a temperature ramp from 25 °C to 99 °C at a rate of 0.05 °C/s. Fluorescence was detected using the in built 'm4' filter set (excitation λ 470±15 nm, emission λ 586±10 nm) and data analysed using Prism Software. *Tm* was determined by fitting a Boltzmann equation to the data. The DSF experiments in this section were performed by Dr Roisin McMahon.

Isothermal titration calorimetry - Oxidized EcDsbA was diluted to 50 μM in 25 mM HEPES pH 7.4, 50 mM NaCl and 5% DMSO. Compounds were dissolved in 100% DMSO, and then diluted to a final concentration of 2 mM into 25mM HEPES pH 7.4 50mM NaCl with a final DMSO concentration of 5%. All experiments were performed using the MicroCal™ Auto-ITC200 instrument (GE Healthcare, USA), loading 200 μL of EcDsbA in the sample cell and 40 μL of compound in the syringe. Titrations were set up at 25 ºC with 19 injections of 2 μL separated by

180 seconds and a constant stirring speed of 1000 rpm. A preliminary injection of 0.5 μL was added to avoid slow leakage of titrant in the sample cell before the first 2 μL injection and the corresponding datapoint excluded from analysis. Every compound was tested with three technical replicates. An additional titration of compound into buffer only (25 mM HEPES pH 7.4, 50 mM NaCl and 5% DMSO) was performed to measure the background heat of dilution. Analysis was performed with the MicroCal™ Origin software (version 7.0552).

Model Substrate Oxidation assay – To prepare the model substrate, lyophilized EcDsbA synthetic substrate (CQQGFDGTQNSCK) which contains a C-terminal methylcoumarin and a N-terminal DOTA functional groups (Anaspec, USA) was dissolved in 100 mM imidazole pH 6.0. 100 mM of europium trifluoromethanesulfonate (Sigma Aldrich, Australia) was added to the synthetic substrate peptide at a molar ratio of 2:1 and incubated for 5 min at room temperature to allow europium chelation. Experiments were performed in a white 384-well plate (Perkin Elmer OptiPlate-384, Part #: 6007290) in 50 mM MES, 50 mM NaCl and 2 mM EDTA pH 5.5 buffer. Each well contained 80 nM EcDsbA, 1.6 μM EcDsbB, one of the tested compounds at concentrations ranging from 16 μM to 2 mM and 10 μM synthetic substrate peptide (added last to initiate the reaction). Positive controls were set up replacing compound by buffer, and negative controls lacked EcDsbA or EcDsbB. Fluorescence emitted by substrate folding was measured with a Synergy H1 multimode plate reader (excitation λ = 340 nm and emission λ = 615 nm). Analysis was performed using the Prism software. To allow plotting the activity of the positive control (the native EcDsbA activity without compound) on a logarithmic scale of compound concentration, a very low compound concentration value was used (100 nM). The substrate oxidation assay experiments presented in this section were performed by Mrs Stephanie Tay.

V.2.3 Irreversible peptidomimetics

Two peptidomimetic molecules were designed from peptide PWATCDS including respectively a nitrile (PWATnitDS) and an aldehyde warhead (PWATaldDS) replacing the Cys5 residue. Synthesis of PWATnitDS was attempted through the direct coupling of an amino acid with a cyanoalanine side chain (**Figure 5.4A**, synthesized by Dr Bachu) and through the dehydration of an Asn α-aminoacid.

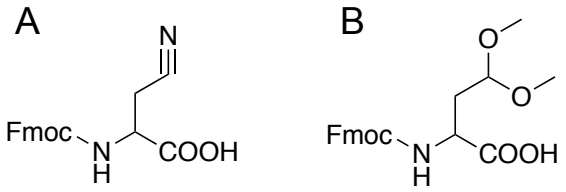

Figure 5.4. ***Residues used in the synthesis of covalent peptide binders. A.*** *Fmoc-beta-cyanoalanine for the synthesis of PWAT(nit)DS.* ***B****. Fmoc-beta-dimethoxyalanine for the synthesis of PWAT(ald)DS, which upon action of TFA will be converted into an aldehyde functionality.*

Synthesis of PWATaldDS was executed using a residue presenting two methoxy groups on the side chain (**Figure 5.4B**, synthesized by Dr Bachu), which was converted into an aldehyde group under the action of TFA during the resin cleaving process. This peptidomimetic was tested in ITC according to section II.2.4.

V.3 Results

V.3.1 Macrocyclic peptidomimetics

The cyclization of four different peptide sequences (PDPWKTC, PKPWDTC, PDPW(Orn)TC, PDPW(Dab)TC) was attempted using amine coupling to form macrocycles of different sizes. Only limited cyclization was detected for peptides PDPWKTC and PKPWDTC despite consecutive coupling rounds in the presence of excess of BOP or PyBOP. Attempts to catalyse the reaction with a series of microwave pulses yielded no improvement. Mostly the final products were of the major non-cyclized peptides. The peptides were also washed with benzene to prevent potential stacking and aggregation, but with no yield improvement. To address the possibility the N-terminal Pro1 was inducing steric hindrance and limiting access of Asp2 to Lys5 (or Lys2 to Asp5), the same synthesis strategy was attempted on sequences Fmoc-DPWKTC and Fmoc-KPWDTC before the final coupling, with no success (**Figure 5.5**). To investigate the hypothesis that a high-loading resin might be encouraging intermolecular coupling and formation of peptide polymers, these experiments were repeated with low-loading MBHA rink-amide resin (0.36 $mmol.g^{-1}$ instead of 0.72 $mmol.g^{-1}$) again with no enhancement in the cyclization yield. The same strategies were applied on peptides PDPW(Orn)TC and PDPW(Dab)TC but no cyclization was observed. Therefore the synthesis of macrocycles was abandoned.

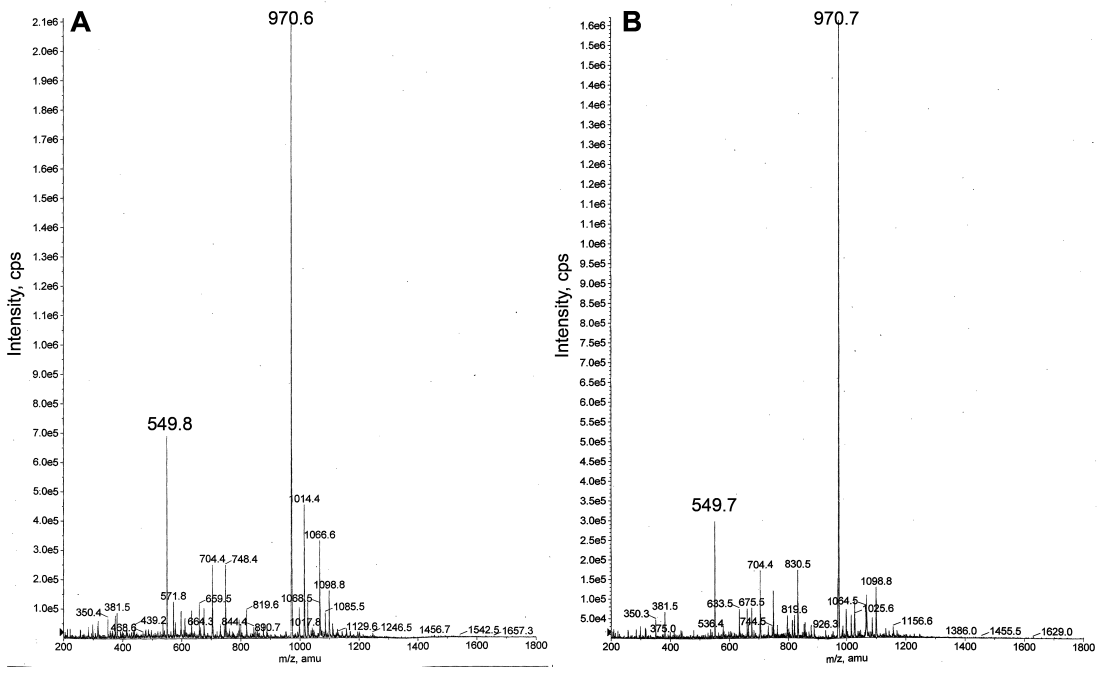

Figure 5.5. ***Mass spectrometry measurements of Fmoc-DPWKTC and Fmoc-KPWDTC peptides.*** *A. The mass spectrometry analysis of Fmoc-DPWKTC showed that the peptide was still linear (M_w = 970 Da) rather than cyclic (M_w =952 Da) despite the cyclization rounds.* ***B.*** *In a similar fashion, peptide PKPWDTC cyclization was not successful and the final synthesis product remained linear (M_w = 970 Da).*

It is known that the linear conformation of L-peptide precursors before cyclization greatly influences the cyclization yield due to allylic strain (White & Yudin, 2011). For 'tail-to-side chain' macrocycles such as DPWKTC (with N-term Asp) and KPWDTC (with N-term Lys), the ring size is known in this case to be important (White & Yudin, 2011) and a potential explanation for the low-yield is the relatively small size of the macrocycle. The linear peptides PDPWKYC and PKPWDTC have been tested with ITC on EcDsbA and presented *K*d values (≈ 30 μM) 8-fold weaker than the original EcDsbB peptide derivative PSPFATCDF (*K*d = 4.0 ± 1.5 μM).

V.3.2 Targeted peptidomimetics

Virtual docking and synthesis. The virtual docking was performed using the PmDsbAC30S-PWATCDS complex as a template, focusing on the interaction of PWATCDS Trp2 with PmDsbAC30S Tyr173 in the hydrophobic pocket. Evaluation of the 10 compounds from the library was based on the PWATCDS Trp2 indole moiety (**Figure 5.6**). The initial docking was

carried out with the template constraint set to the default values, and progressively reduced to allow for better induced fit docking, not to overly bias in favour of the observed crystal structure bound conformation of the Trp. As the backbone amine and carbonyl of the Trp2 residue in the bound full length peptide are not involved with hydrogen bonds to the protein (See Chapter IV), this allowed exploration of whether simpler small molecules could bind in the "opposite" direction to the full length peptide, with only the indole ring of Trp2 being used as a hydrophobic anchor. The steady reduction in the template constraint also allowed subtle changes to arise which may provide additional interactions in the case of smaller molecules which would reasonably be assumed to adopt multiple possible binding conformations. Indeed if the constraint is reduced completely, other conformations were observed (up to 4 out of 10 docking poses), some of which included extra H-bonds with the protein, particularly with the charged molecules. However the dominant interactions in this portion (PWA) of the full (PWATCDS) peptide were the hydrophobic interactions of the Pro and Trp side chains, and these hydrophobic patches are the typical targets of druglike molecules.

The compound that fitted best, here named compound **1**, is a tripeptide consisting of a tryptophan residue flanked by a C-terminal morpholine functional group and a N-terminal benzyl moiety (**Figure 5.7**). Apart from the pi-stacking interaction between the Trp indole and PmDsbAC30S Tyr173, the docking modeled the oxygen atom of the morpholine group at similar distances from the PmDsbAC30S Pro150 backbone amide, His32 imidazole ring amines and Asn162 side chain amide (≈ 4.5 Å). In choosing compound 1 as the favoured compound we took into account several factors. Docking runs were performed with Goldscore, Chemscore and ChemPLP. Compound **1** performed well with all 3 scoring functions. Secondly, consideration was given to medicinal chemistry factors such as regard for a balance between aqueous solubility and "druglike" properties (e.g. compound **1** has a CLogP of 2.6, 6 rotatable bonds, 3 hydrogen bond acceptors, 3 hydrogen bond donors, a molecular weight of 406 Da, and is neutral at physiological pH). Ultimately, however, it was the ability of compound **1** to extend both the indole ring in the Trp-binding pocket, and the benzylamide group to make hydrophobic interactions in the same region as the Proline of the full peptide, as well as the morpholine ring to dock in the groove that made it an attractive synthetic target.

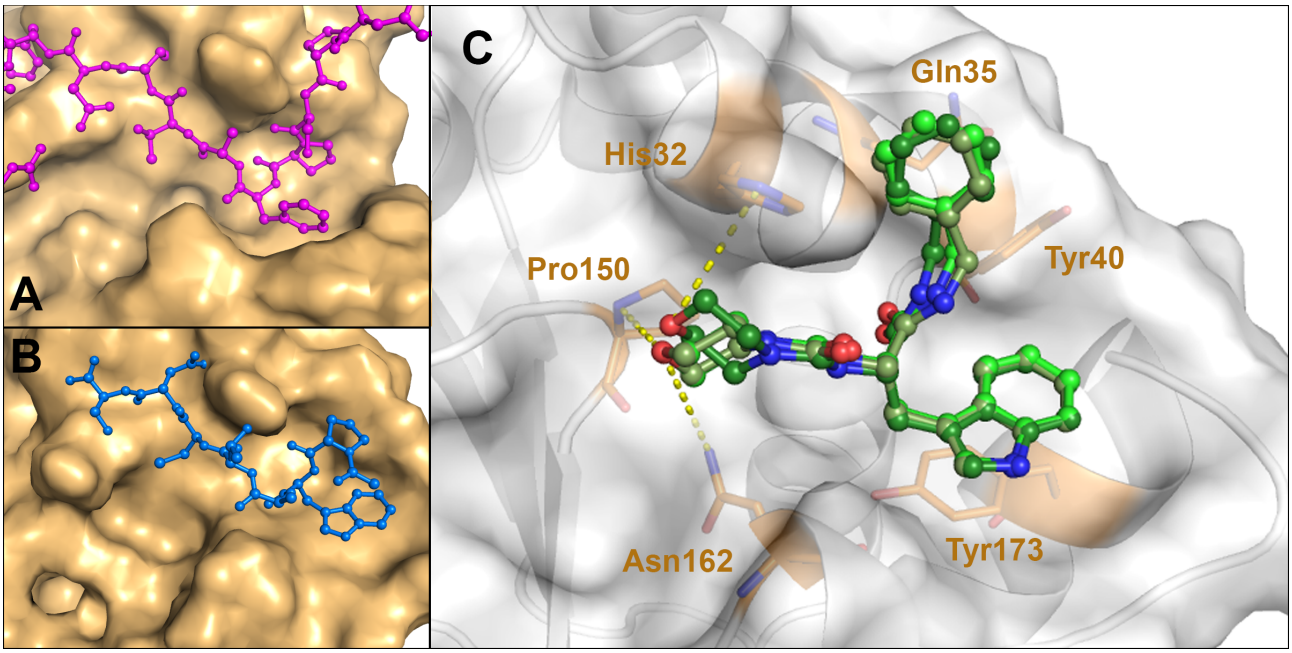

Figure 5.6. ***Comparison of a docked peptidomimetic with the EcDsbA-EcDsbB and PmDsbAC30S-PWATCDS crystal structures.*** ***A.*** *Detail of the EcDsbA-EcDsbB crystal structure (PDB code 2ZUP, (Inaba et al., 2009b)) with EcDsbB Phe101 binding in the EcDsbA hydrophobic pocket.* ***B.*** *Detail of the PmDsbAC30S-PWATCDS crystal structure (PDB code 4OD7, see chapter IV) with Trp2 binding into PmDsbAC30S hydrophobic groove.* ***C.*** *Detail of the virtual docking outcome with the three conformations of compound* ***1*** *shown in shades of green binding to PmDsbAC30S. In orange are shown the PmDsbAC30S residues interacting with compound* ***1.***

From compound **1** nine additional derivatives were synthesized (**Figure 5.7**) to explore the binding groove and exploit potential optimization possibilities. Compound **2** had a piperazine moiety replacing the morpholine group to present a hydrogen bond donor instead of an acceptor in order to bind with EcDsbA Asn142. Compound **3** was similar to compound **2** with an additional tert-butyloxycarbonyl (Boc) group on the piperazine moiety to extend the peptidomimetic in the groove for potential additional interactions with the *cis*Pro loop residues Asn147, Gly148 and Val149. Compounds **4** and **5** investigated the importance of the distance between the benzyl group and the Trp residue by respectively replacing the benzyl by phenyl and phenethyl moieties in compound **1** to effectively expand hydrophobic contacts. Compound **6** presented an extra methyl group for additional hydrophobic interactions. On the benzyl ring of compounds **7** and **8** a trifluoromethyl moiety was attached in the ortho position and a trimethoxyfluoride moiety on the para position respectively; these groups were chosen for their strong electronegativity and their potential as hydrogen bond acceptors. Finally compounds **9** and **10** presented two methoxy moieties

in the ortho/para and meta/para positions respectively to improve the solubility of the scaffold and to further probe for additional hydrogen bonds contacts with EcDsbA.

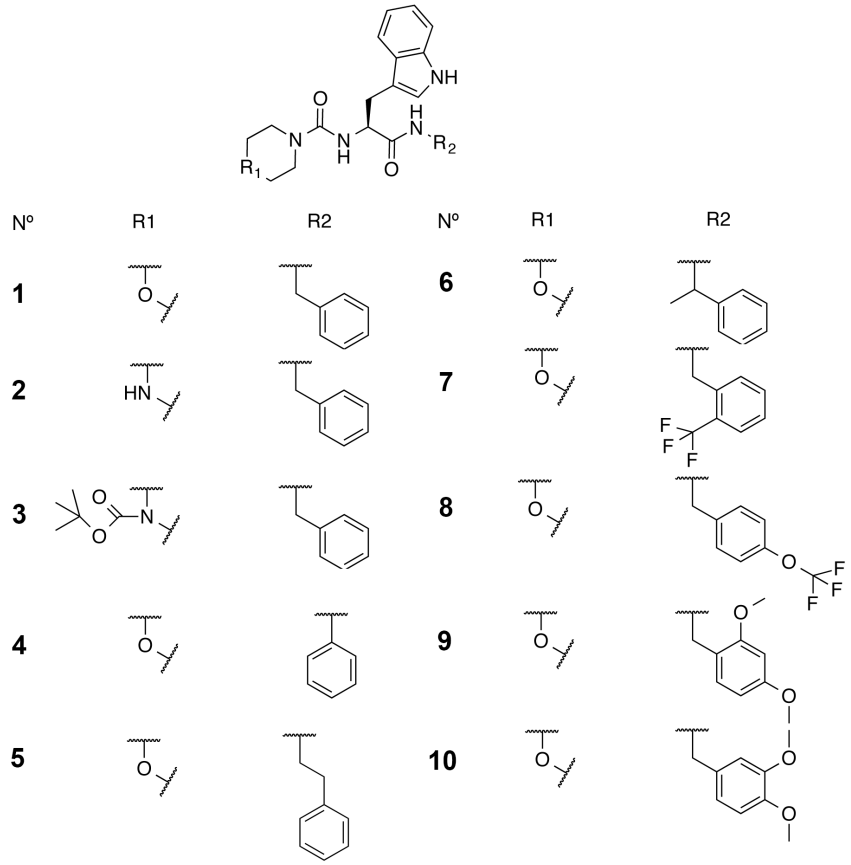

Figure 5.7. ***Structure of the 10 peptidomimetic compounds synthesized and tested in this section.*** *Compound **1** was the initial hit from the virtual docking, from which derivatives **2-10** were designed.*

Differential scanning fluorimetry. The peptidomimetic compounds were first evaluated using DSF to detect any binding through a concentration-dependent increase (ΔTm) of EcDsbA melting temperature *Tm*. The peptidomimetics were tested with a concentration range from 64 µM to 2mM and initially checked for potential compound-dye interferences that could lead to background fluorescence. When mixed with SYPRO orange on a temperature gradient from 25 ºC to 99 ºC, compounds **7** and **8** indicated strong background fluorescence at 0.5 mM, 1 mM and 2 mM concentrations. Compounds **1**, **3**, **4** and **5** showed limited interaction at the highest concentration (2mM) for which fluorescence decreased to background level before the temperature of 50 ºC was reached. Finally, compounds **2**, **6**, **9**, and **10** did not demonstrate substantial fluorescence from interaction with the dye. Measuring the melting temperature of EcDsbA in the presence of each of these compounds did not indicate substantial shift expected from strong ligands (**Figure 5.8**). To be significant, a thermal shift ΔTm has to be at least twice as large as the standard deviation of the

native protein *Tm*, in this case 0.1 ºC. However, most of the measured Δ*Tm* were lower than 0.2 ºC, and the compounds also failed to demonstrate a concentration-dependent effect.

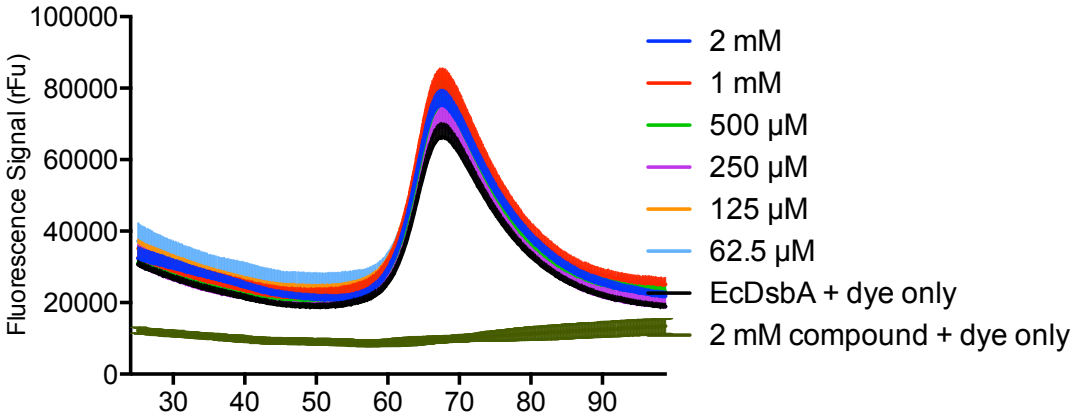

Figure 5.8. ***Measurement of the melting temperature of EcDsbA in presence of compound 6*** *(not interfering with the dye). Each concentration is shown here as an average of 5 technical replicates with their respective standard deviations. No significant differences are observed compared to EcDsbA only, suggesting the compound does not bind strongly to EcDsbA.*

This data suggested that these peptidomimetic compounds do not bind strongly to EcDsbA, but results can be biased by the intrinsic affinity of the compounds for the dye, by virtue of their hydrophobicity. To further identify the potential of this series of peptidomimetic, their affinity was also evaluated by isothermal titration calorimetry, a label-free approach lacking a dye that could interfere in the binding process or the read out.

Isothermal titration calorimetry. The affinity and thermodynamics of the 10 compounds were measured with ITC in order to investigate differences with the original peptide sequence PWATCDS. Titration of EcDsbA with compound **1** revealed poor binding potential with low release of energy (-0.60 µcal.sec^{-1} for the highest peak against -1.6 µcal.sec^{-1} for PWATCDS) and no sign of EcDsbA saturation (**Figure 5.9**).

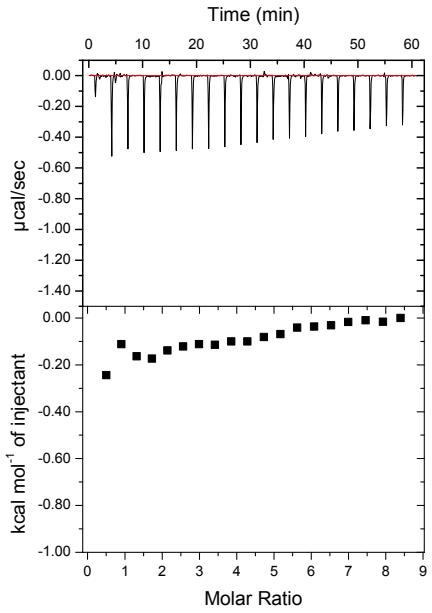

Figure 5.9. ***Isothermal titration calorimetry profile of EcDsbA titrated with compound 1****, showing low energy release and poor EcDsbA saturation suggesting compound* ***1*** *is not a strong binder.*

Similarly for derivatives **2-10** no binding significant enough for accurate curve fitting was detected (**Figure 5.10**). The EcDsbA binding sites in the sample cells are not saturated and the profiles are similar to the negative controls. These data suggest two hypotheses: either EcDsbA demonstrated a very weak (in the millimolar range) affinity for these compounds, or the amount of energy released by the binding reaction was very low and thus difficult to measure with ITC. This second hypothesis is a possibility for binding reactions characterized by a major entropic contribution (Gaisford, 2006). Given that the compounds were designed to target the hydrophobic pocket of EcDsbA and that no atoms were predicted to be in range for the formation of hydrogen bonds, it is likely that ITC is not an optimal screening technique to rank these compounds according to their affinity towards EcDsbA. Screening techniques for hydrophobic binding are scarce, and thus it was decided that compounds to try to rank the compounds by their potential inhibitory activity rather than their binding affinity.

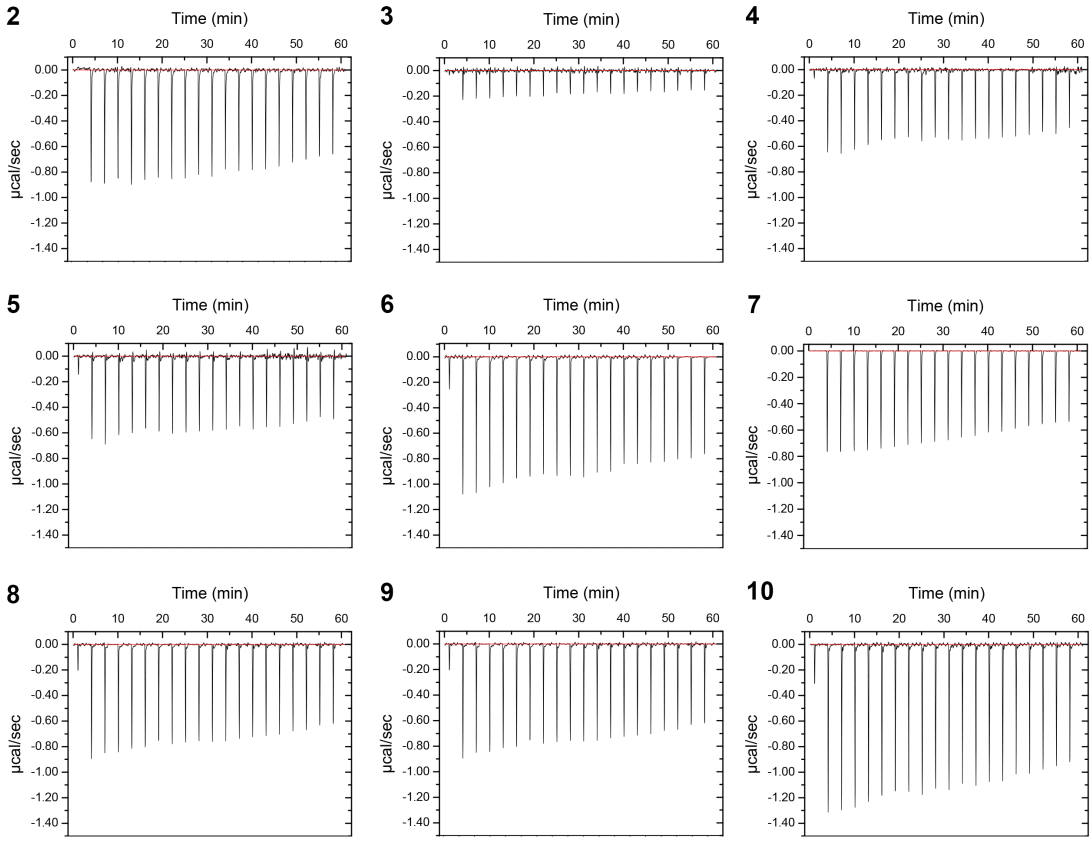

Figure 5.10. ***Raw isothermal titration calorimetry profiles of EcDsbA titrated with compounds 2 to 10,*** *for which none demonstrated binding with the parameters used. This could also be due to the interaction being mainly hydrophobic for which ITC has limited sensitivity.*

Model substrate oxidation assay – The model substrate oxidation assay had the advantage of being independent from the peptide binding mode (unlike ITC) and not using a dye was likely to interact with the compound (unlike thermal shift). Inhibition of the EcDsbA substrate folding activity demonstrated a reduced rate of total fluorescence increase, indicating a diminution in substrate folding. This signified that the peptidomimetic compound was competing either with the EcDsbA-substrate interaction, the EcDsbA-EcDsbB interaction or the EcDsbB-ubiquinone electron exchange. When tested, compounds **1-9** did not have a strong influence on EcDsbA activity at the concentrations used (**Figure 5.11**) whereas compound **10** showed significant reduction in the fluorescence signal at the highest concentrations (1 mM and 2 mM, **Figure 5.12A**). Plotting concentrations against the fluorescence signal increase rate provided an estimated IC_{50} of 1.1 mM for compound **10** (**Figure 5.12B**), which was approximately 200-fold lower than the original EcDsbB sequence (PSPFATCDF, 6.7 ± 1.1 µM) and peptide PWATCDS (5.7 ± 0.4 µM, see Chapter III). Taken together, these peptidomimetic compounds were poor inhibitors of EcDsbA activity with IC_{50} values estimated in the high millimolar range.

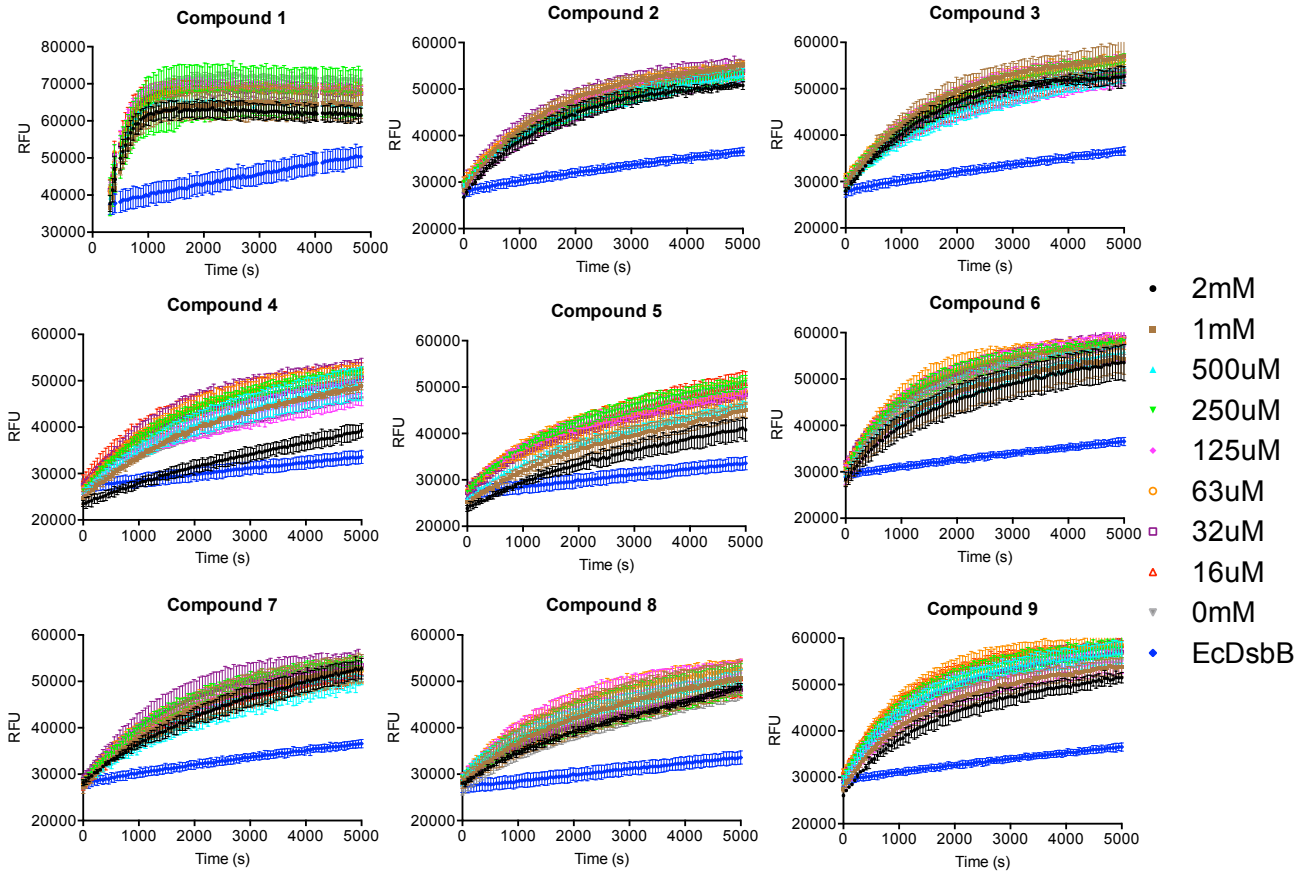

Figure 5.11. ***Raw fluorescence measurements of the substrate folding by EcDsbA in presence of compounds 1 to 9*** *at concentrations ranging from 16 µM to 2 mM. None of these compounds induced a significant reduction in the fluorescence and so had no effect on EcDsbA activity.*

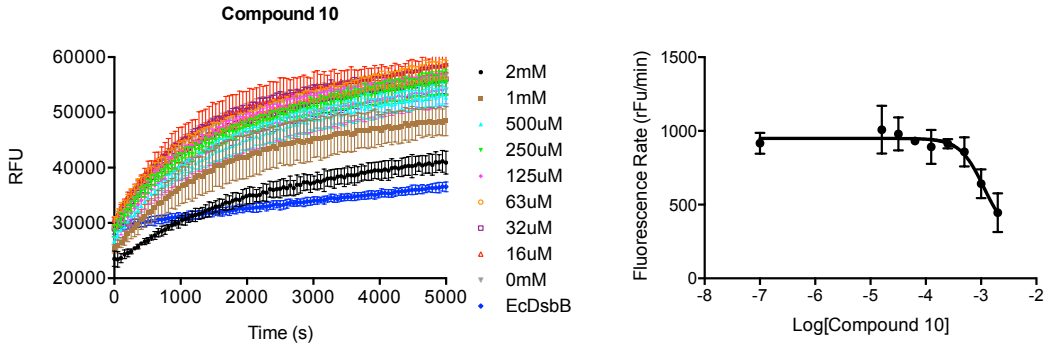

Figure 5.12. ***Compound 10 possessed weak inhibitory activity. A.*** *Compound* ***10*** *was the only peptidomimetic to show detectable inhibition at the concentrations used in this assay with a significantly lower EcDsbA activity at the highest concentration.* ***B.*** *Plotting the log of the concentration against the fluorescence increase rate allowed fitting of a sigmoidal curve and an* IC_{50} *of approximately 1.1 mM was estimated.*

Taken together, a virtual docking of peptidomimetic libraries based on the PmDsbAC30S-PWATCDS structure and focusing on the hydrophobic pocket provided one hit (compound **1**) from which nine derivatives were synthesized (compounds **2**-**10**) to further explore the binding site. We were not able to detect concentration-dependent shifts in the melting temperature of EcDsbA using differential scanning fluorimetry and compounds did not demonstrate strong binding using ITC. The model substrate oxidation assay indicated very weak inhibition with the best compound **10** showing an IC50 of 1.1 mM. Overall, these compounds presented a significant loss in affinity and inhibition compared with the starting peptide PWATCDS used in the virtual docking.

V.3.3 Irreversible inhibitors

The two compounds, PWAT(nit)DS and PWAT(ald)DS were expected to bind irreversibly to EcDsbA. The synthesis of PWAT(nit)DS proved to be difficult; each attempted synthesis experiment showed very low efficiency in the coupling of the nitrile amino acid, even in the presence of large excess (4 equivalents or higher) of the amino acid in multiple consecutive steps. Moreover presence of contaminants that could not be separated by HPLC prevented the production of a purified product (**Figure 5.13A**). The synthesis of PWATnitDS was then outsourced to an external commercial company that was also unable to produce the expected peptidomimetic compound after three months of trials. Therefore efforts towards peptides with a nitrile 'warhead' were abandoned.

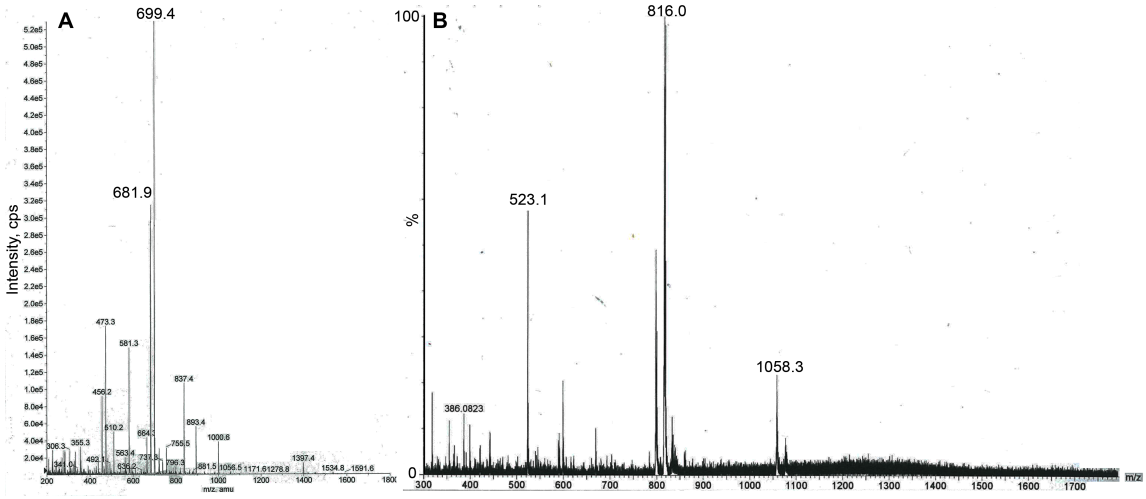

Figure 5.13. ***Mass spectrometry measurements of the final products from PWAT(nit)DS and PWAT(ald)DS synthesis. A.*** *Attempts to synthesize PWAT(nit)DS (of mass 780 Da) mostly resulted in a product of mass 699 Da corresponding to the PWATDS sequence.* ***B.*** *Synthesis of PWAT(ald)DS (of mass 815 Da) proved to be more successful, and the expected product was present in the final cleaved mixture.*

On the other hand, I was able to synthesize PWAT(ald)DS (**Figure 5.13B**). The peptidomimetic was tested using ITC to evaluate the reactivity towards oxidized and reduced EcDsbA. However the titrations demonstrated poor binding with a low signal and no saturation of EcDsbA binding sites (**Figure 5.14**).

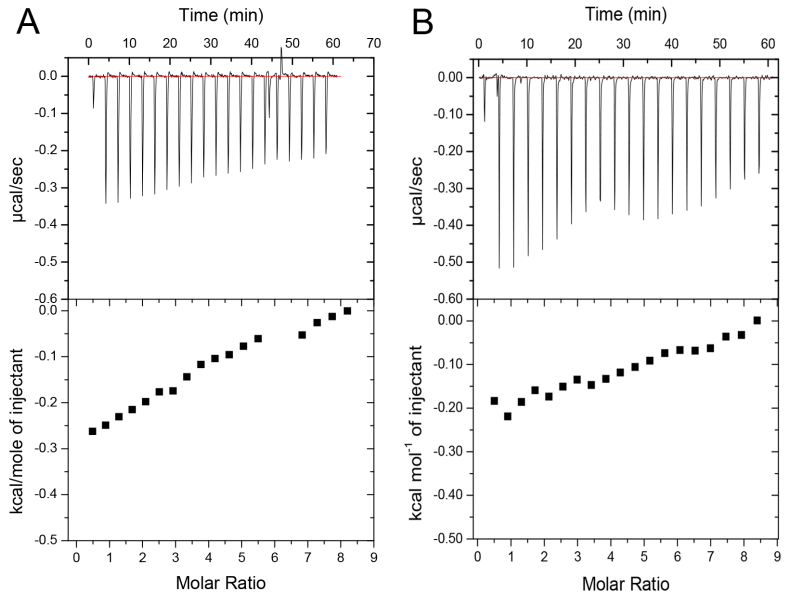

Figure 5.14. ***Isothermal titration calorimetry experiments using covalent binder PWAT(ald)DS*** *to titrate EcDsbA oxidized (**A**) and reduced (**B**) which showed limited affinity.*

NMR experiments performed concomitantly by Dr Brad Doak and Assoc Prof. Martin Scanlon at the Monash Institute of Pharmaceutical Sciences on small molecules targeting EcDsbA showed that most of the reputedly irreversible thiol binders tested (for example fluoromethylketones, acrylamides and maleimide) were in fact turned over and released from EcDsbA (Doak, 2012). The turnover began within 24 hours and EcDsbA was able to restore its former folding activity. In total 42 covalent binders were synthesized and tested but none resulted in irreversible binding onto EcDsbA, demonstrating the unique reactivity of EcDsbA and its ability to break covalent bonds for which no enzyme-mediated resolution has been previously reported. The reactivity of the EcDsbA catalytic cysteines is such that designing a functional group able to form a stable and irreversible bond with Cys30 is a major challenge.

V.4 Discussion

The interactions between peptides and the EcDsbA binding site are quite unusual: 1) the peptide SAR indicated that the disulfide bond was a necessary component for binding but 2) we obtained a structure of a peptide bound in a non-covalent fashion to PmDsbAC30S and 3) deleting the peptide side chains binding to the EcDsbA hydrophobic groove did not alter affinity (See chapter III). However this hydrophobic patch still seems to play an important role as seen in the crystal structure of EcDsbA/EcDsbB and PmDsbAC30S-PWATCDS. Therefore, the development of the first series of peptidomimetics provided the opportunity to investigate the role of this binding site further.

The formation of macrocycles to target the EcDsbA hydrophobic pocket was unsuccessful due to low yields and purity issues, probably due to the small size of the cycle. A solution to this issue would be to cyclize the full peptide sequence using both termini in a similar fashion as cyclopeptides (Craik *et al.*, 2006), although such an approach would substantially increase the molecular mass of the molecule away from 'drug-like' properties.

Targeting the hydrophobic pocket was a strategy aimed at thwarting the disulfide bond formation mechanism in order to develop a reversible binder. The 1.6 Å resolution PmDsbAC30S-PWATCDS structure provided the basis for virtual docking, resulting in an *in silico* hit. However, the evaluation of this hit along with nine derivatives demonstrated limited affinities *in vitro* and these compounds were not able to compete effectively with the EcDsbB periplasmic loop. The inability of these compounds to bind EcDsbA however provides more insight on the role of the EcDsbA hydrophobic pocket and the choice of the drug design strategy. The EcDsbB periplasmic loop binds within this hydrophobic pocket in the three crystal structures solved (Malojcic *et al.*, 2008, Inaba, Murakami*, et al.*, 2006, Inaba *et al.*, 2009a) and EcDsbB-derived peptide PWATCDS also interacts with residues from the PmDsbAC30S hydrophobic pocket (see Chapter IV). However according to the data provided by the peptidomimetic screening above, the hydrophobic pocket by itself is not a target potent enough to prevent DsbA folding activity, which suggests two hypotheses. First, the compounds synthesized in this study can access the binding site, but they might be easily driven out by a substrate molecule or the DsbB loop binding onto the catalytic site. This suggests that the hydrophobic contacts in the groove alone are not strong and specific enough to compete with a substrate molecule or EcDsbB. Second, the peptidomimetic might bind into the groove (and the ITC sensitivity to screen them is limited due to the major entropic component), but the catalytic

disulfide bond transfer between EcDsbA/substrate and EcDsbA/EcDsbB can happen despite this hindrance. In both cases, I suggest that the role of the hydrophobic pocket as a drug target by itself seems limited. Further investigation can lead to the optimization of a future inhibitory scaffold for additional stability of the complex with EcDsbA, but most likely the inhibitor would need to primarily affect the nearby catalytic site. Therefore, the design of the next inhibitors should comprise interactions with the EcDsbA catalytic cysteines to possess inhibitory activity. For example, a reactive moiety specific to the cysteines could be integrated in the peptide design.

The next step was the insertion of a 'warhead' able to form a covalent bond with EcDsbA Cys30, in this case a nitrile and an aldehyde moieties. The synthesis of a nitrile peptide was particularly difficult, and no final purified product was obtained. The peptide presenting the aldehyde moiety indicated a weak affinity for EcDsbA. Moreover the work from Dr Doak and Pr Scanlon showed that moieties known to irreversibly bind thiol groups were turned over and released when binding to EcDsbA *in vitro (Doak, 2012)*. The suggested mechanism involved a nucleophilic attack of Cys33 on the Cys30 linked to the inhibitor scaffold, triggering the restoration of the disulfide bond and the release of the adduct from EcDsbA. An innovative solution would be to target not only Cys30 but engineer a peptidomimetic in such a way that a second 'warhead' would lock onto Cys33 as well, hence preventing any disulfide bond transfer and peptidomimetic release. This would be a delicate process as Cys33 is buried deeper in the thioredoxin fold compared to Cys30. The main drawback is that such a compound including two reactive 'warheads' would be even more likely to trigger side reactions *in vivo*, hence increasing toxicity.

CHAPTER VI

Conclusions

The primary purpose of this PhD was to develop a potent peptide or peptidomimetic scaffold inhibiting the DsbA-DsbB interaction in *Escherichia coli* to impede the bacterial oxidative system *in vivo*. The inhibition of EcDsbA is thought to offer a novel means of preventing maturation of a broad range of virulence factors, leading to an attenuated but viable bacterial phenotype. Such a novel mode of action is expected to provide a new weapon to fight against MDR and pan resistant pathogenic bacterial strains and to limit the appearance of resistance by keeping the bacteria viable (Clatworthy *et al.*, 2007, Rasko & Sperandio, 2010). The only starting point for the structure-based drug design of these inhibitors was the 3.7 Å resolution crystal structure of the EcDsbA-EcDsbB complex (Inaba *et al.*, 2009a).

Outcome of the screening pipeline assembly

The first goal was to develop a robust screening pipeline able to characterize the designed peptides and peptidomimetics by measuring their affinity and their inhibitory activity for EcDsbA. It had to also include crystallographic trials to provide structural data necessary to accurately interpret the biochemical data provided by the pipeline. Such a pipeline was successfully implemented using differential scanning fluorimetry (DSF), isothermal titration calorimetry (ITC) and model substrate oxidation assays as well as crystallography. A major hurdle arose in the development of a surface plasmon resonance assay, and that approach had to be abandoned during my thesis research due to the absence of binding signals. The final optimized pipeline was able to provide all the binding data for a single compound in five days from the beginning of the manual synthesis to the starting of the co-crystallization trials.

A major issue in this pipeline was the lack of a technique for accurate characterization of compounds for which binding involves a major contribution from hydrophobic interactions. DSF would demonstrate a high fluorescence background for the dye because it would bind to the hydrophobic moieties of the inhibitor; hence potentially hiding the fluorescence increase linked to the unfolding of EcDsbA or complexes. Moreover, DSF would not be able to provide a *K*d value. Similarly, ITC would be limited, as the enthalpy contribution would be minimal. Model substrate oxidation assay do not discriminate between binding modes, but would provide an IC_{50} value and not a binding affinity. A suitable assay to overcome this issue would be saturation transfer difference nuclear magnetic resonance (STD NMR), a technique that would identify peptide and peptidomimetic residues involved in the binding process (Viegas *et al.*, 2011). Through a

competition assay with another peptide of known affinity, STD-NMR can also provide a *K*d value (Angulo *et al.*, 2010). A second possibility is microscale thermophoresis, a recently developed assay that relies on the motion of molecules in temperature gradients (Seidel *et al.*, 2013). This label-free assay is able to determine *K*d values independently of the binding mode, thus would suit the screening of hydrophobic compounds. Instruments for both techniques are now available and might be used for follow-up research on EcDsbA inhibitors.

Structure-activity relationship and hypothesis for peptide binding mechanism

The screening pipeline was successfully used to characterize peptide binding (see Chapter III) to identify the key residues in the interaction with EcDsbA. Interestingly the outcome of the alanine scanning showed that only the substitution of the peptide Cys residue resulted in a drastic loss of affinity. It suggested that no other residues are as critical for binding of the peptide to EcDsbA. Concurrently, there was no binding of the same peptides to reduced EcDsbA (thus unable to form disulfide bridges). Therefore, the evidence tends to suggest the formation of a disulfide bond between peptide and DsbA that would be the critical feature for binding. However, it also seems that the disulfide bond might be the only binding force behind the DsbA-DsbB interaction, therefore providing restricted specificity. If this was the case, oxidized active EcDsBA would not be able to differentiate between a substrate to be oxidized and reduced EcDsbB, therefore reduced EcDsbB would be a competitor for EcDsbA folding activity). This scenario is unlikely hence we cannot rule out the possibility that a mechanism intrinsic to EcDsbB prevents the binding of OxEcDsbA, hence responsible for the specificity of the DsbB-DsbA interaction and still remains to be observed (**Figure 6.1A**). This mechanism, that may involve a role from other regions of the perisplasmic loop P2, would not be featured in the peptides tested to date (**Figure 6.1B**).

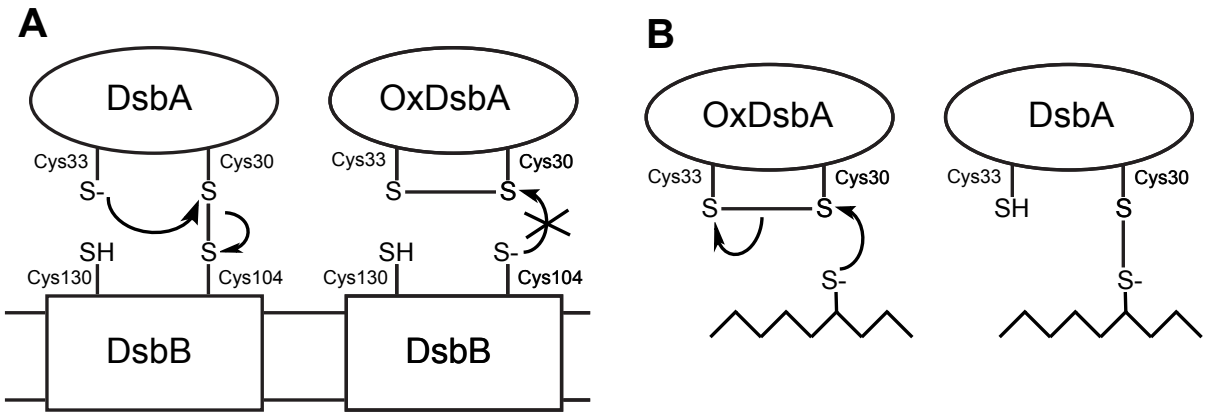

Figure 6.1. ***Difference in the disulfide bond formation between the DsbA/DsbB and the DsbA-peptide complexes. A****. After regeneration of reduced DsbA in its active oxidized state, the reverse reaction with oxidized DsbA binding DsbB would be unproductive; there might be another feature preventing the backward reaction.* ***B.*** *In the proposed peptide binding model, the peptide binds to oxidized DsbA and forms an intramolecular disulfide bond – thus in a different context than the native DsbA-DsbB interaction.*

On the other hand, all peptides tested against oxidized EcDsbA presented a strongly unfavorable entropic contribution, suggesting the peptide conformations do not match the EcDsbA surface. This is consistent with the hypothesis that the disulfide bond is the only force driving the binding mode. It could be suggested that EcDsbB domain might adopt a conformation not present in the short and flexible peptide derivatives tested, but this is also unlikely for a disordered perisplamic loop such as EcDsbB P2. Moreover, the role of the hydrophobic residue (in EcDsbB Phe101) binding into the EcDsbA hydrophobic groove remains unclear as peptide affinity is not altered upon deletion of the hydrophobic side chain. In contrast, the solved structure of peptide PWATCDS binding non-covalently to the mutant PmDsbAC30S (i.e. without intermolecular disulfide bond) demonstrates the hydrophobic Trp2 residue interacting with PmDsbAC30S hydrophobic patch. A technique to evaluate the importance of a residue in soluble proteins is site-directed mutagenesis, mutating the specific residue into a Gly or Ala. However EcDsbB being a membrane protein it would take considerable efforts to engineer a mutant (such as F101A), obtain a quantity of pure protein sufficient for ITC experiments and solve the membrane protein stability issues.

My hypothesis is that the peptide, and possibly the EcDsbB loop, binding mode occurs in two consecutive steps with different kinetics. The first step is the nucleophilic attack of the peptide cysteine thiolate onto DsbA Cys30 (or DsbA Cys30 thiolate onto DsbB Cys104), forming the disulfide bond as per the EcDsbA native mechanism (**Figure 6.2**). This is a rapid reaction measured

by ITC followed by an entropically unfavorable contribution suggesting the peptide is in a disordered state on the surface of the EcDsbA. The peptide now anchored on EcDsbA has limited flexibility and after a period of time the peptide Trp or Phe residue would lock into the EcDsbA hydrophobic pocket. This second phase might be much slower than the first as the peptide might not readily adopt the favorable confirmation that would lead the Trp or Phe residue inside the pocket.

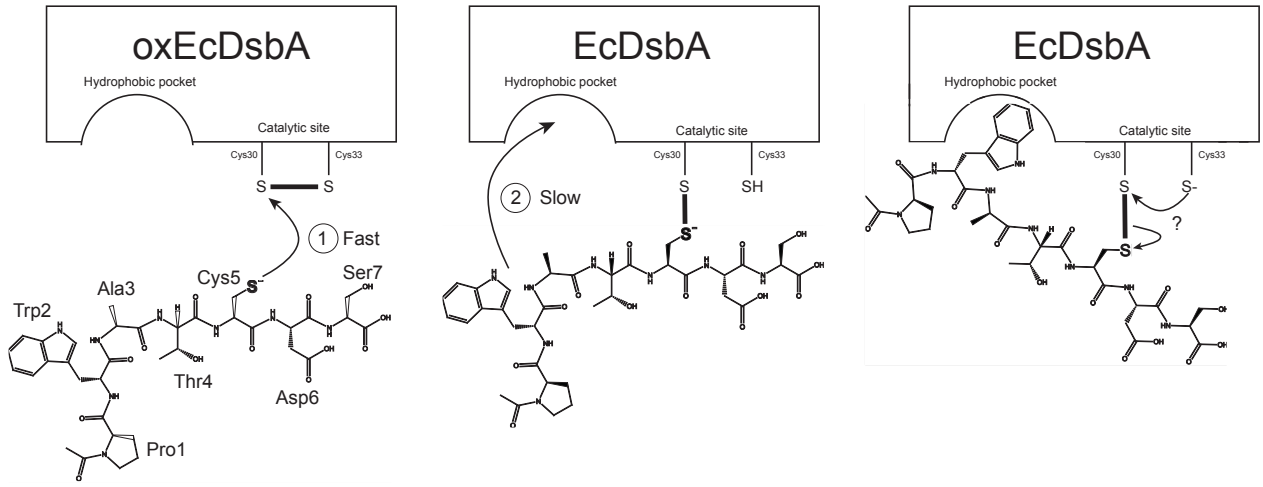

Figure 6.2. ***Suggested binding mechanism of peptide PWATCDS to EcDsbA.*** *The binding is initiated by the nucleophilic attack of Cys5 thiolate onto EcDsbA Cys30 (1), in a fashion similar to substrate binding. This interaction would occur with fast on-rate. Second, the peptide anchored to EcDsbA by the disulfide bond is stabilized by binding to the neighboring hydrophobic pocket (2) through hydrophobic contacts and π-stacking interaction with Phe173. Finally, the nucleophilic attack of EcDsbA Cys33 onto Cys30 might restore the intramolecular disulfide bond and release the peptide (right panel). This last event has been observed only for covalent binders by Doak et al. and has not been investigated in this thesis for peptides (Doak, 2012). However, if EcDsbA is able to turn over irreversible binders, it is very likely that the same phenomenon applies to peptides only bound by a disulfide bridge.*

The different timeframes of the binding experiments - DSF and model substrate oxidation requires over an hour incubation before measurements, ITC is instantaneous and crystallogenesis takes days – made the study of this binding mode difficult, depending on the kinetics of each step. Within this hypothesis, the role of the interaction between the EcDsbB loop Phe101 and the EcDsbA hydrophobic patch might involve additional stability of the complex to allow the disulfide bond exchange to occur. Another possibility presumes that the binding of EcDsbB loop into the EcDsbA hydrophobic groove restrains the flexibility of the periplasmic loop; this event could prevent the unproductive backward reaction in which DsbB Cys130 (on the same loop) attacks the intermolecular disulfide bond, releasing EcDsbA in the inactive state. With the peptide derivatives,

the hydrophobic interaction occurs as well even if the disulfide bond exchange process is never achieved due to the peptide lacking a second cysteine. Molecular dynamics studies might help to shed some light on this hypothesis, but it would require additional complex structures with the peptide anchored to EcDsbA by a disulfide bond, such as EcDsbA-PSPFATCDF and EcDsbA-PWATCDS.

Structural analysis of the DsbA-peptide interaction

The co-crystallization trials performed in this project were successful when a mutant, PmDsbAC30S, was used. No peptides were ever detected in crystals generated with wild type EcDsbA or PmDsbA. This was probably because the peptides were released following restoration of the Cys30-Cys33 disulfide bond before crystallogenesis occurred. Although providing crucial data about peptide binding to DsbA, the conformation of the PWATCDS peptide bound to PmDsbAC30S mutant might not reflect the native interaction as the catalytic cysteine has been substituted. As seen in Chapter IV, the peptide Cys was shifted and the consecutive Asp residue interacted with the catalytic site. Moreover, the inhibitory activity of PWATCDS towards this PmDsbA mutant cannot be evaluated as PmDsbAC30S does not possess a redox potential and cannot fold substrates. Consequently, additional structures of DsbA-peptide complexes with different mutants or the native protein might be needed to understand the peptide conformation on DsbA accurately.

A simple way to cross-link the peptide to DsbA would be to engineer a DsbA mutant with the second cysteine in the catalytic site (Cys33) substituted with an inactive residue such as alanine (C33A). If the peptide indeed forms a disulfide bond with EcDsbA, it would then be trapped to EcDsbA as Cys33 would not be able to restore the disulfide bond and release the peptide. This is a strategy similar to the one applied to the formation of a stable EcDsbA-EcDsbB complex (see section I.2.2), and should be the next step in the structural part of the larger program. Moreover, such a structure might provide the starting point necessary for molecular dynamics experiments to study the peptide binding mechanism hypothesis described above.

Future directions in inhibitor design

During this PhD it appeared that EcDsbA is an extremely potent oxidase, able to turn over all the tested thiol-targeting reactive groups that are thought to form stable and irreversible covalent bonds with cysteine residues. This is a serious hurdle for drug design targeting DsbA as the

interaction with Cys30 seems to be the primary force driving the binding. Consequently, the interest in 'suicide' inhibitors is limited by the timeframe during which the inhibitor stays anchored to EcDsbA before release. Moreover Doak *et al.* suggested that the released 'suicide' inhibitor might lose the 'warhead' in the process, thus being inactivated by EcDsbA (Doak, 2012). If this is correct, these 'suicide' binders would be worse than reversible binders as they could not bind back onto another EcDsbA molecule. Designed peptidomimetics focusing on the nearby hydrophobic pocket had weak potencies. Therefore, a successful inhibitor of the EcDsbA activity must not only bind EcDsbA but also neutralize the interaction between the two catalytic cysteines.

To date, there are no reports in the literature of ligands able to bind two cysteines in the same active site. Such an inhibitor should include two thiol-reactive groups side by side (**Figure 6.3**). These reactive groups must not interact with each other to avoid partial cyclization of the peptide. If both reactive groups connect with Cys30 and Cys33, then theoretically the peptide could be irreversibly bound to EcDbsA.

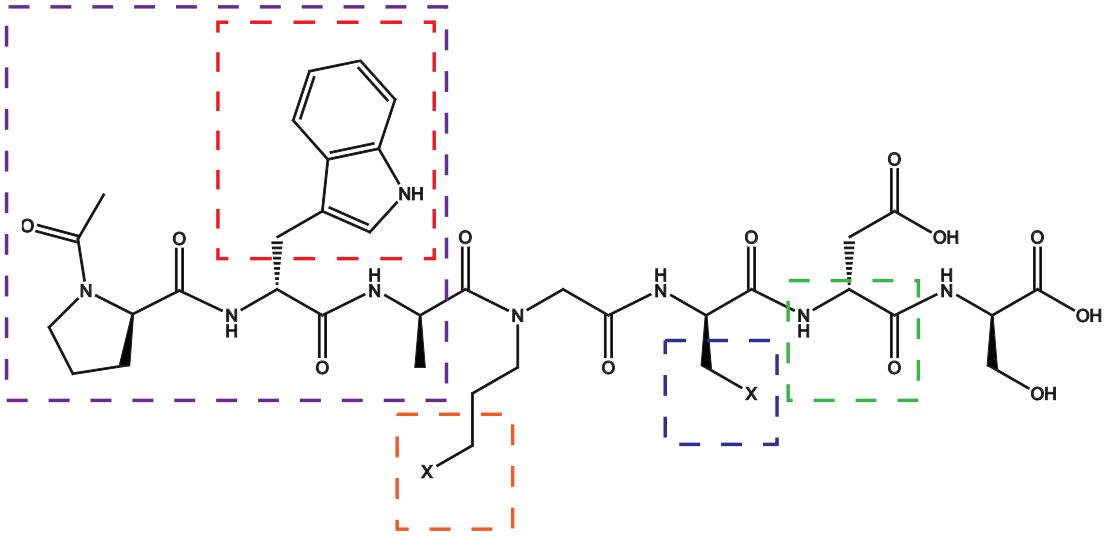

Figure 6.3. ***Suggested peptidomimetic scaffold for future studies of EcDsbA inhibitors.*** *The molecule should include a thiol-reactive group to irreversibly bind EcDsbA Cys30 (in blue) and a second similar moiety to bind EcDsbA Cys33 (in orange), which is buried deeper in the active site. A peptide backbone must be conserved in the residue on the C-terminal side to trigger hydrogen bond(s) with EcDsbA cisPro loop (Arg149, Pro150). On the N-terminus, the peptidomimetic should include at least one phenyl or indole moiety for π-stacking interactions with EcDsbA Phe173 (in red). The entire N-terminus of the peptide can also be replaced by a non-peptidic design that would fit the EcDsbA hydrophobic pocket better (in purple). X represents here an irreversible thiol-reactive group to bind DsbA catalytic cysteines.*

Once we know the structure of such an irreversible peptidomimetic, efforts could then be directed toward the rigidification of the peptide backbone into a conformation that matches EcDsbA binding site interface to improve the thermodynamics of the reaction, and thus the potency, of the peptidomimetic series. Once a potent *in vitro* peptidomimetic is designed, it would need to be tested for membrane permeability and *E. coli* motility inhibition. Assuming that the peptidomimetic efficiently inhibits bacterial swarming, a mouse infection model will then be the obvious next step to evaluate the effect of an antivirulence drug candidate *in vivo.*

Conclusion

Taken together, EcDsbA proved to be a challenging target to inhibit due to the lack of specificity and the high potency of its intrinsic enzymatic mechanism. However, substantial progress has been made in the understanding of the binding mode of peptides on the EcDsbA surface. An optimal inhibitor 7-mer peptide was identified with a K_d 5.7 $\pm$ 0.4 μM (and a binding efficiency index BEI of 6.4) involving the formation of a disulfide bond with EcDsbA Cys30. The same inhibitor showed an inhibitory activity (IC_{50} 8.8 μM) *in vitro*. The first high-resolution structure of a peptide non-covalently bound to a DsbA was obtained, shedding light on the peptide binding mode. The first attempts at designing novel peptidomimetic scaffolds were unsuccessful but paved the way for new approaches.

Overall, this PhD provides the first steps in the design of the first peptide inhibitors targeting a dithiol oxidase, and the acquired knowledge might be applied to other enzymes of similar function. If, based on the preliminary work performed in this thesis, the future design of a peptidomimetic compound bears fruit, it will also offer another argument in favor of the peptidomimetic weaponry in the current effort to relieve the current struggle in the antibiotic pipeline. Moreover, as aimed towards one of the first antivirulence targets, this potentially novel antimicrobial scaffold could be part of a new generation of antibiotics that could limit the appearance of new extremely-drug resistant strains.

Bibliography

The 10 x '20 Initiative: pursuing a global commitment to develop 10 new antibacterial drugs by 2020 (2010). **50**, 1081-1083.

Aarestrup, F. M. (2005). *Basic Clin Pharmacol Toxicol* **96**, 271-281.

Abad-Zapatero, C. & Metz, J. T. (2005). *Drug Discov Today* **10**, 464-469.

Abbenante, G. & Fairlie, D. P. (2005). *Med Chem* **1**, 71-104.

Aberg, V. & Almqvist, F. (2007). *Org Biomol Chem* **5**, 1827-1834.

Aberg, V., Hedenstrom, M., Pinkner, J. S., Hultgren, S. J. & Almqvist, F. (2005). *Org Biomol Chem* **3**, 3886-3892.

Adams, P. D., Afonine, P. V., Bunkoczi, G., Chen, V. B., Davis, I. W., Echols, N., Headd, J. J., Hung, L. W., Kapral, G. J., Grosse-Kunstleve, R. W., McCoy, A. J., Moriarty, N. W., Oeffner, R., Read, R. J., Richardson, D. C., Richardson, J. S., Terwilliger, T. C. & Zwart, P. H. (2010). *Acta Crystallogr D Biol Crystallogr* **66**, 213-221.

Ahn, J. M., Boyle, N. A., MacDonald, M. T. & Janda, K. D. (2002). *Mini Rev Med Chem* **2**, 463-473.

Aitken, A., Learmont, M (2009). *The Protein Protocols Handbook*, pp. 1053-1055: Springer.

Alder, J. D. (2005). *Drugs Today (Barc)* **41**, 81-90.

Aloy, P. & Russell, R. B. (2006). *Nat Rev Mol Cell Biol* **7**, 188-197.

Anderegg, T. R., Biedenbach, D. J. & Jones, R. N. (2003). *Int J Antimicrob Agents* **22**, 84-86.

Anderegg, T. R. & Jones, R. N. (2004). *Diagn Microbiol Infect Dis* **48**, 55-57.

Anderson, A. C. (2003). *Chem Biol* **10**, 787-797.

Anderson, G. G., Palermo, J. J., Schilling, J. D., Roth, R., Heuser, J. & Hultgren, S. J. (2003). *Science* **301**, 105-107.

Andersson, K., Karlsson, R., Lofas, S., Franklin, G. & Hamalainen, M. D. (2006). *Expert Opin Drug Discov* **1**, 439-446.

Andruszkiewicz, R., Chmara, H., Milewski, S. & Borowski, E. (1986). *Int J Pept Protein Res* **27**, 449-453.

Andruszkiewicz, R., Chmara, H., Milewski, S. & Borowski, E. (1987). *J Med Chem* **30**, 1715-1719.

Angulo, J., Enriquez-Navas, P. M. & Nieto, P. M. (2010). *Chemistry* **16**, 7803-7812.

Antibiotics Resistance Threats in the United States, 2013 (2013). Center for Disease Control and prevention, US Department of Health and Human Services.

Antimicrobial Sequences Database, http://www.bbcm.univ.trieste.it/~tossi/amsdb.html.

Aslund, F., Berndt, K. D. & Holmgren, A. (1997). *J Biol Chem* **272**, 30780-30786.

Audie, J. & Swanson, J. (2013). *Chem Biol Drug Des* **81**, 50-60.

Azoulay-Dupuis, E., Mohler, J. & Bedos, J. P. (2004). *Antimicrob Agents Chemother* **48**, 80-85.

The Bacterial Challenge: time to react (2010). European Center for Disease Prevention and Control.

Bader, M., Muse, W., Zander, T. & Bardwell, J. (1998). *J Biol Chem* **273**, 10302-10307.

Baeriswyl, V. & Heinis, C. (2013). *ChemMedChem* **8**, 377-384.

Baker, N. A., Sept, D., Joseph, S., Holst, M. J. & McCammon, J. A. (2001). *Proc Natl Acad Sci U S A* **98**, 10037-10041.

Bals, R., Wang, X., Wu, Z., Freeman, T., Bafna, V., Zasloff, M. & Wilson, J. M. (1998). *J Clin Invest* **102**, 874-880.

Barber, A. E., Norton, J. P., Spivak, A. M. & Mulvey, M. A. (2013). *Clin Infect Dis* **57**, 719-724.

Bardwell, J. C., Lee, J. O., Jander, G., Martin, N., Belin, D. & Beckwith, J. (1993). *Proc Natl Acad Sci U S A* **90**, 1038-1042.

Bardwell, J. C., McGovern, K. & Beckwith, J. (1991). *Cell* **67**, 581-589.

Barnhart, M. M. & Chapman, M. R. (2006). *Annu Rev Microbiol* **60**, 131-147.

Battye, T. G., Kontogiannis, L., Johnson, O., Powell, H. R. & Leslie, A. G. (2011). *Acta Crystallogr D Biol Crystallogr* **67**, 271-281.
Bell, G. & Gouyon, P. H. (2003). *Microbiology* **149**, 1367-1375.
Bengtsson, C., Lindgren, A. E., Uvell, H. & Almqvist, F. (2012). *Eur J Med Chem* **54**, 637-646.
Berg, V., Das, P., Chorell, E., Hedenstrom, M., Pinkner, J. S., Hultgren, S. J. & Almqvist, F. (2008). *Bioorg Med Chem Lett* **18**, 3536-3540.
Berg, V., Sellstedt, M., Hedenstrom, M., Pinkner, J. S., Hultgren, S. J. & Almqvist, F. (2006). *Bioorg Med Chem* **14**, 7563-7581.
Boucher, H. W., Talbot, G. H., Bradley, J. S., Edwards, J. E., Gilbert, D., Rice, L. B., Scheld, M., Spellberg, B. & Bartlett, J. (2009). *Clin Infect Dis* **48**, 1-12.
Bragonzi, A. (2010). *Sci Transl Med* **2**, 21ps29.
Bringer, M. A., Rolhion, N., Glasser, A. L. & Darfeuille-Michaud, A. (2007). *J Bacteriol* **189**, 4860-4871.
Burall, L. S., Harro, J. M., Li, X., Lockatell, C. V., Himpsl, S. D., Hebel, J. R., Johnson, D. E. & Mobley, H. L. (2004). *Infect Immun* **72**, 2922-2938.
Butler, M. S., Blaskovich, M. A. & Cooper, M. A. (2013). *J Antibiot (Tokyo)* **66**, 571-591.
Butler, M. S. & Cooper, M. A. (2012). *Curr Drug Targets* **13**, 373-387.
Casewell, M. W. & Hill, R. L. (1987). *J Antimicrob Chemother* **19**, 1-5.
Cegelski, L., Pinkner, J. S., Hammer, N. D., Cusumano, C. K., Hung, C. S., Chorell, E., Aberg, V., Walker, J. N., Seed, P. C., Almqvist, F., Chapman, M. R. & Hultgren, S. J. (2009). *Nat Chem Biol* **5**, 913-919.
Chalker, J. M., Bernardes, G. J., Lin, Y. A. & Davis, B. G. (2009). *Chem Asian J* **4**, 630-640.
Chan, D. I., Prenner, E. J. & Vogel, H. J. (2006). *Biochim Biophys Acta* **1758**, 1184-1202.
Charbonnier, J. B., Belin, P., Moutiez, M., Stura, E. A. & Quemeneur, E. (1999). *Protein Sci* **8**, 96-105.
Chen, D. Z., Patel, D. V., Hackbarth, C. J., Wang, W., Dreyer, G., Young, D. C., Margolis, P. S., Wu, C., Ni, Z. J., Trias, J., White, R. J. & Yuan, Z. (2000). *Biochemistry* **39**, 1256-1262.
Chen, V. B., Arendall, W. B., 3rd, Headd, J. J., Keedy, D. A., Immormino, R. M., Kapral, G. J., Murray, L. W., Richardson, J. S. & Richardson, D. C. (2010). *Acta Crystallogr D Biol Crystallogr* **66**, 12-21.
Chivers, P. T., Prehoda, K. E. & Raines, R. T. (1997). *Biochemistry* **36**, 4061-4066.
Chmara, H., Andruszkiewicz, R. & Borowski, E. (1986). *Biochim Biophys Acta* **870**, 357-366.
Chmara, H., Milewski, S., Andruszkiewicz, R., Mignini, F. & Borowski, E. (1998). *Microbiology* **144 (Pt 5)**, 1349-1358.
Choi, S., Isaacs, A., Clements, D., Liu, D., Kim, H., Scott, R. W., Winkler, J. D. & DeGrado, W. F. (2009). *Proc Natl Acad Sci U S A* **106**, 6968-6973.
Chongsiriwatana, N. P., Patch, J. A., Czyzewski, A. M., Dohm, M. T., Ivankin, A., Gidalevitz, D., Zuckermann, R. N. & Barron, A. E. (2008). *Proc Natl Acad Sci U S A* **105**, 2794-2799.
Chongsiriwatana, N. P., Wetzler, M. & Barron, A. E. (2011). *Antimicrob Agents Chemother* **55**, 5399-5402.
Chorell, E., Bengtsson, C., Sainte-Luce Banchelin, T., Das, P., Uvell, H., Sinha, A. K., Pinkner, J. S., Hultgren, S. J. & Almqvist, F. (2011). *Eur J Med Chem* **46**, 1103-1116.
Chorell, E., Pinkner, J. S., Bengtsson, C., Banchelin, T. S., Edvinsson, S., Linusson, A., Hultgren, S. J. & Almqvist, F. (2012). *Bioorg Med Chem* **20**, 3128-3142.
Chorell, E., Pinkner, J. S., Phan, G., Edvinsson, S., Buelens, F., Remaut, H., Waksman, G., Hultgren, S. J. & Almqvist, F. (2010). *J Med Chem* **53**, 5690-5695.
Cimmperman, P., Baranauskiene, L., Jachimoviciute, S., Jachno, J., Torresan, J., Michailoviene, V., Matuliene, J., Sereikaite, J., Bumelis, V. & Matulis, D. (2008). *Biophys J* **95**, 3222-3231.
Clardy, J. & Walsh, C. (2004). *Nature* **432**, 829-837.
Clatworthy, A. E., Pierson, E. & Hung, D. T. (2007). *Nat Chem Biol* **3**, 541-548.

Clements, J. M., Beckett, R. P., Brown, A., Catlin, G., Lobell, M., Palan, S., Thomas, W., Whittaker, M., Wood, S., Salama, S., Baker, P. J., Rodgers, H. F., Barynin, V., Rice, D. W. & Hunter, M. G. (2001). *Antimicrob Agents Chemother* **45**, 563-570.

Coetzee, J. N. (1975). *J Gen Microbiol* **87**, 173-176.

Coetzee, J. N. & Sacks, T. G. (1960). *J Gen Microbiol* **23**, 445-455.

Cohen, M. S., Hadjivassiliou, H. & Taunton, J. (2007). *Nat Chem Biol* **3**, 156-160.

Cohen, M. S., Zhang, C., Shokat, K. M. & Taunton, J. (2005). *Science* **308**, 1318-1321.

Cooper, M. A. & Shlaes, D. (2011). *Nature* **472**, 32.

Cox, G. & Wright, G. D. (2013). *Int J Med Microbiol* **303**, 287-292.

Craik, D. J., Cemazar, M., Wang, C. K. & Daly, N. L. (2006). *Biopolymers* **84**, 250-266.

Credito, K., Lin, G., Ednie, L. M. & Appelbaum, P. C. (2004). *Antimicrob Agents Chemother* **48**, 4033-4036.

Crow, A., Lewin, A., Hecht, O., Carlsson Moller, M., Moore, G. R., Hederstedt, L. & Le Brun, N. E. (2009). *J Biol Chem* **284**, 23719-23733.

CS ChemBioDraw Ultra 12.0. (2011). Version 12.0.

Dailey, F. E. & Berg, H. C. (1993). *Proc Natl Acad Sci U S A* **90**, 1043-1047.

Danley, D. E. (2006). *Acta Crystallogr D Biol Crystallogr* **62**, 569-575.

Dartois, V., Sanchez-Quesada, J., Cabezas, E., Chi, E., Dubbelde, C., Dunn, C., Granja, J., Gritzen, C., Weinberger, D., Ghadiri, M. R. & Parr, T. R., Jr. (2005). *Antimicrob Agents Chemother* **49**, 3302-3310.

Davies, J. (1994). *Science* **264**, 375-382.

Davies, S. J., Ayscough, A. P., Beckett, R. P., Bragg, R. A., Clements, J. M., Doel, S., Grew, C., Launchbury, S. B., Perkins, G. M., Pratt, L. M., Smith, H. K., Spavold, Z. M., Thomas, S. W., Todd, R. S. & Whittaker, M. (2003). *Bioorg Med Chem Lett* **13**, 2709-2713.

Davies, S. J., Ayscough, A. P., Beckett, R. P., Clements, J. M., Doel, S., Pratt, L. M., Spavold, Z. M., Thomas, S. W. & Whittaker, M. (2003). *Bioorg Med Chem Lett* **13**, 2715-2718.

Deshpande, P., Rodrigues, C., Shetty, A., Kapadia, F., Hedge, A. & Soman, R. (2010). *J Assoc Physicians India* **58**, 147-149.

Doak, B. (2012). PhD thesis, Monash University.

Dutton, R. J., Boyd, D., Berkmen, M. & Beckwith, J. (2008). *Proc Natl Acad Sci U S A* **105**, 11933-11938.

East, S. P., Beckett, R. P., Brookings, D. C., Clements, J. M., Doel, S., Keavey, K., Pain, G., Smith, H. K., Thomas, W., Thompson, A. J., Todd, R. S. & Whittaker, M. (2004). *Bioorg Med Chem Lett* **14**, 59-62.

ECDC/EMEA

Ednie, L. M., Pankuch, G. & Appelbaum, P. C. (2004). *Antimicrob Agents Chemother* **48**, 4027-4032.

Ellman, G. L. (1959). *Arch Biochem Biophys* **82**, 70-77.

Elsea, S. H., Osheroff, N. & Nitiss, J. L. (1992). *J Biol Chem* **267**, 13150-13153.

Emsley, P., Lohkamp, B., Scott, W. G. & Cowtan, K. (2010). *Acta Crystallogr D Biol Crystallogr* **66**, 486-501.

Emtenas, H., Ahlin, K., Pinkner, J. S., Hultgren, S. J. & Almqvist, F. (2002). *J Comb Chem* **4**, 630-639.

Emtenas, H., Taflin, C. & Almqvist, F. (2003). *Mol Divers* **7**, 165-169.

Epand, R. M., Rotem, S., Mor, A., Berno, B. & Epand, R. F. (2008). *J Am Chem Soc* **130**, 14346-14352.

Ericsson, U. B., Hallberg, B. M., Detitta, G. T., Dekker, N. & Nordlund, P. (2006). *Anal Biochem* **357**, 289-298.

Eschenfeldt, W. H., Lucy, S., Millard, C. S., Joachimiak, A. & Mark, I. D. (2009). *Methods Mol Biol* **498**, 105-115.

Evans, P. (2006). *Acta Crystallogr D Biol Crystallogr* **62**, 72-82.

Falla, T. J., Karunaratne, D. N. & Hancock, R. E. (1996). *J Biol Chem* **271**, 19298-19303.
Fernandes, P. A. & Ramos, M. J. (2004). *Chemistry* **10**, 257-266.
Fernandez-Lopez, S., Kim, H. S., Choi, E. C., Delgado, M., Granja, J. R., Khasanov, A., Kraehenbuehl, K., Long, G., Weinberger, D. A., Wilcoxen, K. M. & Ghadiri, M. R. (2001). *Nature* **412**, 452-455.
Fischer, L., Claudon, P., Pendem, N., Miclet, E., Didierjean, C., Ennifar, E. & Guichard, G. (2010). *Angew Chem Int Ed Engl* **49**, 1067-1070.
Ford, C. W., Zurenko, G. E. & Barbachyn, M. R. (2001). *Curr Drug Targets Infect Disord* **1**, 181-199.
Foreman, D. T., Martinez, Y., Coombs, G., Torres, A. & Kupersztoch, Y. M. (1995). *Mol Microbiol* **18**, 237-245.
Fox, J. L. (2013). *Nat Biotechnol* **31**, 379-382.
Franklin, T. J. & Rownd, R. (1973). *J Bacteriol* **115**, 235-242.
Frech, C., Wunderlich, M., Glockshuber, R. & Schmid, F. X. (1996). *EMBO J* **15**, 392-398.
Fry, D. W., Bridges, A. J., Denny, W. A., Doherty, A., Greis, K. D., Hicks, J. L., Hook, K. E., Keller, P. R., Leopold, W. R., Loo, J. A., McNamara, D. J., Nelson, J. M., Sherwood, V., Smaill, J. B., Trumpp-Kallmeyer, S. & Dobrusin, E. M. (1998). *Proc Natl Acad Sci U S A* **95**, 12022-12027.
Gaisford, S., O'Neill, M (2006). *Pharmaceutical Isothermal Calorimetry*. Informa healthcare.
Gasteiger E., H. C., Gattiker A., Duvaud S., Wilkins M.R., Appel R.D., Bairoch A. (2005). *The Proteomics Protocols Handbook*, edited by J. M. Walker, pp. pp. 571-607 New York, USA: Humana Press.
Giuliani, A. & Rinaldi, A. C. (2011). *Cell Mol Life Sci* **68**, 2255-2266.
Goldberg, K., Sarig, H., Zaknoon, F., Epand, R. F., Epand, R. M. & Mor, A. (2013). *FASEB J* **27**, 3818-3826.
Goldman, M. J., Anderson, G. M., Stolzenberg, E. D., Kari, U. P., Zasloff, M. & Wilson, J. M. (1997). *Cell* **88**, 553-560.
Gordon, J. J., Kelly, B. K. & Miller, G. A. (1962). *Nature* **195**, 701-702.
Gordon, K. A., Rhomberg, P. R. & Jones, R. N. (2003). *J Clin Microbiol* **41**, 3967-3969.
Gray, J. J. (2006). *Curr Opin Struct Biol* **16**, 183-193.
Grigoryan, L., Monnet, D. L., Haaijer-Ruskamp, F. M., Bonten, M. J., Lundborg, S. & Verheij, T. J. (2010). *Curr Drug Saf* **5**, 329-332.
Gross, M., Clements, J., Beckett, R. P., Thomas, W., Taylor, S., Lofland, D., Ramanathan-Girish, S., Garcia, M., Difuntorum, S., Hoch, U., Chen, H. & Johnson, K. W. (2004). *J Antimicrob Chemother* **53**, 487-493.
Guay, D. R. (2008). *Drugs* **68**, 1169-1205.
Guddat, L. W., Bardwell, J. C., Glockshuber, R., Huber-Wunderlich, M., Zander, T. & Martin, J. L. (1997). *Protein Sci* **6**, 1893-1900.
Guilhot, C., Jander, G., Martin, N. L. & Beckwith, J. (1995). *Proc Natl Acad Sci U S A* **92**, 9895-9899.
Guterman, L. (2011). *Chemical and engineering news* **89**, 19-26.
Guzman, L. M., Belin, D., Carson, M. J. & Beckwith, J. (1995). *J Bacteriol* **177**, 4121-4130.
Ha, U. H., Wang, Y. & Jin, S. (2003). *Infect Immun* **71**, 1590-1595.
Hammond, M. C., Harris, B. Z., Lim, W. A. & Bartlett, P. A. (2006). *Chem Biol* **13**, 1247-1251.
Hancock, R. E. & Chapple, D. S. (1999). *Antimicrob Agents Chemother* **43**, 1317-1323.
Haney, E. F., Hunter, H. N., Matsuzaki, K. & Vogel, H. J. (2009). *Biochim Biophys Acta* **1788**, 1639-1655.
Hassell, A. M., An, G., Bledsoe, R. K., Bynum, J. M., Carter, H. L., 3rd, Deng, S. J., Gampe, R. T., Grisard, T. E., Madauss, K. P., Nolte, R. T., Rocque, W. J., Wang, L., Weaver, K. L., Williams, S. P., Wisely, G. B., Xu, R. & Shewchuk, L. M. (2007). *Acta Crystallogr D Biol Crystallogr* **63**, 72-79.

Hatahet, F. & Ruddock, L. W. (2009). *Curr Pharm Des* **15**, 2488-2507.
Hawkins, P. C. & Nicholls, A. (2012). *J Chem Inf Model* **52**, 2919-2936.
Hawkins, P. C., Skillman, A. G., Warren, G. L., Ellingson, B. A. & Stahl, M. T. (2010). *J Chem Inf Model* **50**, 572-584.
Hedenstrom, M., Emtenas, H., Pemberton, N., Aberg, V., Hultgren, S. J., Pinkner, J. S., Tegman, V., Almqvist, F., Sethson, I. & Kihlberg, J. (2005). *Org Biomol Chem* **3**, 4193-4200.
Heras, B., Kurz, M., Jarrott, R., Shouldice, S. R., Frei, P., Robin, G., Cemazar, M., Thony-Meyer, L., Glockshuber, R. & Martin, J. L. (2008a). *J Biol Chem* **283**, 4261-4271.
Heras, B., Kurz, M., Jarrott, R., Shouldice, S. R., Frei, P., Robin, G., Cemazar, M., Thony-Meyer, L., Glockshuber, R. & Martin, J. L. (2008b). *J Biol Chem* **283**, 4261-4271.
Heras, B., Shouldice, S. R., Totsika, M., Scanlon, M. J., Schembri, M. A. & Martin, J. L. (2009). *Nat Rev Microbiol* **7**, 215-225.
Heras, B., Totsika, M., Jarrott, R., Shouldice, S. R., Guncar, G., Achard, M. E., Wells, T. J., Argente, M. P., McEwan, A. G. & Schembri, M. A. (2010a). *J Biol Chem* **285**, 18423-18432.
Heras, B., Totsika, M., Jarrott, R., Shouldice, S. R., Guncar, G., Achard, M. E. S., Wells, T. J., Argente, M. P., McEwan, A. G. & Schembri, M. A. (2010b). *J Biol Chem* **285**, 18423-18432.
Hitchings, G. H. (1973). *J Infect Dis* **128**, Suppl:433-436 p.
Holdgate, G. A. (2001). *Biotechniques* **31**, 164-166, 168, 170 passim.
Holmgren, A. (1979). *J Biol Chem* **254**, 9627-9632.
Holt, A. & Killian, J. A. (2010). *Eur Biophys J* **39**, 609-621.
Homola, J., Yee, S. & Gauglitz, G. (1999). *Sensors and Actuators B: Chemical* **54**, 3-15.
Hu, X., Nguyen, K. T., Verlinde, C. L., Hol, W. G. & Pei, D. (2003). *J Med Chem* **46**, 3771-3774.
Huang, M. L., Shin, S. B., Benson, M. A., Torres, V. J. & Kirshenbaum, K. (2012). *ChemMedChem* **7**, 114-122.
Huber-Wunderlich, M. & Glockshuber, R. (1998). *Fold Des* **3**, 161-171.
Hultgren, S. J., Abraham, S., Caparon, M., Falk, P., St Geme, J. W., 3rd & Normark, S. (1993). *Cell* **73**, 887-901.
Huntington, K. M., Yi, T., Wei, Y. & Pei, D. (2000). *Biochemistry* **39**, 4543-4551.
IDSA Report 1537-6591 (Electronic) 1058-4838 (Linking).
Imura, Y., Choda, N. & Matsuzaki, K. (2008). *Biophys J* **95**, 5757-5765.
Inaba, K. & Ito, K. (2008). *Biochimica Et Biophysica Acta-Molecular Cell Research* **1783**, 520-529.
Inaba, K., Murakami, S., Nakagawa, A., Iida, H., Kinjo, M., Ito, K. & Suzuki, M. (2009a). *EMBO J* **28**, 779-791.
Inaba, K., Murakami, S., Nakagawa, A., Iida, H., Kinjo, M., Ito, K. & Suzuki, M. (2009b). *EMBO J* **28**, 779-791.
Inaba, K., Murakami, S., Suzuki, M., Nakagawa, A., Yamashita, E., Okada, K. & Ito, K. (2006). *Cell* **127**, 789-801.
Inaba, K., Takahashi, Y., Ito, K. & Hayashi, S. (2006). *Proc Nat Acad Sci USA* **103**, 287-292.
Inaba, K., Takahashi, Y. H., Fujieda, N., Kano, K., Miyoshi, H. & Ito, K. (2004). *J Biol Chem* **279**, 6761-6768.
Inaba, K., Takahashi, Y. H. & Ito, K. (2005). *J Biol Chem* **280**, 33035-33044.
Ireland, P. M., McMahon, R. M., Marshall, L. E., Halili, M., Furlong, E., Tay, S., Martin, J. L. & Sarkar-Tyson, M. (2014). *Antioxid Redox Signal* **20**, 606-617.
Jacob-Dubuisson, F., Pinkner, J., Xu, Z., Striker, R., Padmanhaban, A. & Hultgren, S. J. (1994). *Proc Natl Acad Sci U S A* **91**, 11552-11556.
Jacobsen, S. M. & Shirtliff, M. E. (2011). *Virulence* **2**, 460-465.
Jacobsen, S. M., Stickler, D. J., Mobley, H. L. & Shirtliff, M. E. (2008). *Clin Microbiol Rev* **21**, 26-59.

Jahnsen, R. D., Frimodt-Moller, N. & Franzyk, H. (2012). *J Med Chem* **55**, 7253-7261.
Jansen, A. M., Lockatell, V., Johnson, D. E. & Mobley, H. L. (2004). *Infect Immun* **72**, 7294-7305.
Jason-Moller, L., Murphy, M. & Bruno, J. (2006). *Curr Protoc Protein Sci* **Chapter 19**, Unit 19 13.
Johnson, A. P. & Wilcox, M. H. (2012). *J Antimicrob Chemother* **67**, 2788-2792.
Johnson, D. S., Weerapana, E. & Cravatt, B. F. (2010). *Future Med Chem* **2**, 949-964.
Jones, R. N., Fritsche, T. R. & Sader, H. S. (2004). *Diagn Microbiol Infect Dis* **49**, 63-65.
Jones, R. N., Moet, G. J., Sader, H. S. & Fritsche, T. R. (2004). *J Antimicrob Chemother* **53**, 804-807.
Kabsch, W. (2010). *Acta Crystallogr D Biol Crystallogr* **66**, 125-132.
Kadokura, H. & Beckwith, J. (2002). *Embo Journal* **21**, 2354-2363.
Kadokura, H. & Beckwith, J. (2009). *Cell* **138**, 1164-1173.
Kaneti, G., Sarig, H., Marjieh, I., Fadia, Z. & Mor, A. (2013). *FASEB J*.
Karala, A. R., Lappi, A. K. & Ruddock, L. W. (2010). *J Mol Biol* **396**, 883-892.
Karlsson, K. F., Walse, B., Drakenberg, T., Roy, S., Bergquist, K. E., Pinkner, J. S., Hultgren, S. J. & Kihlberg, J. (1998). *Bioorg Med Chem* **6**, 2085-2101.
Karlsson, R. (2004). *J Mol Recognit* **17**, 151-161.
Katsara, M., Tselios, T., Deraos, S., Deraos, G., Matsoukas, M. T., Lazoura, E., Matsoukas, J. & Apostolopoulos, V. (2006). *Curr Med Chem* **13**, 2221-2232.
Keseru, G. M. & Makara, G. M. (2006). *Drug Discov Today* **11**, 741-748.
Kim, Y., Ho, S. O., Gassman, N. R., Korlann, Y., Landorf, E. V., Collart, F. R. & Weiss, S. (2008). *Bioconjug Chem* **19**, 786-791.
Kishigami, S., Kanaya, E., Kikuchi, M. & Ito, K. (1995). *J Biol Chem* **270**, 17072-17074.
Kokryakov, V. N., Harwig, S. S., Panyutich, E. A., Shevchenko, A. A., Aleshina, G. M., Shamova, O. V., Korneva, H. A. & Lehrer, R. I. (1993). *FEBS Lett* **327**, 231-236.
Kortemme, T., Darby, N. J. & Creighton, T. E. (1996). *Biochemistry* **35**, 14503-14511.
Kourtesi, C., Ball, A. R., Huang, Y. Y., Jachak, S. M., Vera, D. M., Khondkar, P., Gibbons, S., Hamblin, M. R. & Tegos, G. P. (2013). *Open Microbiol J* **7**, 34-52.
Kranz, J. K. & Schalk-Hihi, C. (2011). *Methods Enzymol* **493**, 277-298.
Kraus, D. & Peschel, A. (2006). *Curr Top Microbiol Immunol* **306**, 231-250.
Kraus, D. & Peschel, A. (2008). *Future Microbiol* **3**, 437-451.
Krissinel, E. & Henrick, K. (2007). *J Mol Biol* **372**, 774-797.
Kuehn, M. J., Ogg, D. J., Kihlberg, J., Slonim, L. N., Flemmer, K., Bergfors, T. & Hultgren, S. J. (1993). *Science* **262**, 1234-1241.
Kurth, F., Rimmer, K., Premkumar, L., Mohanty, B., Duprez, W., Halili, M. A., Shouldice, S. R., Heras, B., Fairlie, D. P., Scanlon, M. J. & Martin, J. L. (2013). *PLoS One* **8**, e80210.
Kurz, M., Iturbe-Ormaetxe, I., Jarrott, R., Shouldice, S. R., Wouters, M. A., Frei, P., Glockshuber, R., O'Neill, S. L., Heras, B. & Martin, J. L. (2009). *Antioxid Redox Signal* **11**, 1485-1500.
Kustanovich, I., Shalev, D. E., Mikhlin, M., Gaidukov, L. & Mor, A. (2002). *J Biol Chem* **277**, 16941-16951.
Ladbury, J. E. (2010). *Biochem Soc Trans* **38**, 888-893.
Lafaye, C., Iwema, T., Carpentier, P., Jullian-Binard, C., Kroll, J. S., Collet, J. F. & Serre, L. (2009). *J Mol Biol* **392**, 952-966.
Laine, D. I. & Busch-Petersen, J. (2010). *Expert Opin Ther Pat* **20**, 497-506.
Lambert, T. (2012). *Rev Sci Tech* **31**, 57-64.
Latham, P. W. (1999). *Nat Biotechnol* **17**, 755-757.
Leader, B., Baca, Q. J. & Golan, D. E. (2008). *Nat Rev Drug Discov* **7**, 21-39.
Leavitt, S. & Freire, E. (2001). *Curr Opin Struct Biol* **11**, 560-566.
Lee, I. H., Cho, Y. & Lehrer, R. I. (1997). *Infect Immun* **65**, 2898-2903.
Li, B., Wendlandt, S., Yao, J., Liu, Y., Zhang, Q., Shi, Z., Wei, J., Shao, D., Schwarz, S., Wang, S. & Ma, Z. (2013). *J Antimicrob Chemother* **68**, 1251-1255.
Li, X. Z. & Nikaido, H. (2009). *Drugs* **69**, 1555-1623.

Lin, D., Rao, C. V. & Slauch, J. M. (2008). *J Bacteriol* **190**, 87-97.
Lipinski, C. A., Lombardo, F., Dominy, B. W. & Feeney, P. J. (2001). *Adv Drug Deliv Rev* **46**, 3-26.
Liskamp, R. M., Rijkers, D. T., Kruijtzer, J. A. & Kemmink, J. (2011). *Chembiochem* **12**, 1626-1653.
Liu, D., Choi, S., Chen, B., Doerksen, R. J., Clements, D. J., Winkler, J. D., Klein, M. L. & DeGrado, W. F. (2004). *Angew Chem Int Ed Engl* **43**, 1158-1162.
Liu, D. & DeGrado, W. F. (2001). *J Am Chem Soc* **123**, 7553-7559.
Livermore, D. M. (2002). *Clin Infect Dis* **34**, 634-640.
Livne, L., Epand, R. F., Papahadjopoulos-Sternberg, B., Epand, R. M. & Mor, A. (2010). *FASEB J* **24**, 5092-5101.
Lo, M. C., Aulabaugh, A., Jin, G., Cowling, R., Bard, J., Malamas, M. & Ellestad, G. (2004). *Anal Biochem* **332**, 153-159.
Lomovskaya, O. & Bostian, K. A. (2006). *Biochem Pharmacol* **71**, 910-918.
Lomovskaya, O. & Watkins, W. (2001). *J Mol Microbiol Biotechnol* **3**, 225-236.
Mahamoud, A., Chevalier, J., Alibert-Franco, S., Kern, W. V. & Pages, J. M. (2007). *J Antimicrob Chemother* **59**, 1223-1229.
Malojcic, G., Owen, R. L., Grimshaw, J. P. & Glockshuber, R. (2008). *FEBS Lett* **582**, 3301-3307.
Mandal, S., Moudgil, M. & Mandal, S. K. (2009). *Eur J Pharmacol* **625**, 90-100.
Marshall, N. J., Andruszkiewicz, R., Gupta, S., Milewski, S. & Payne, J. W. (2003). *J Antimicrob Chemother* **51**, 821-831.
Martin, J. L., Bardwell, J. C. & Kuriyan, J. (1993). *Nature* **365**, 464-468.
Marynka, K., Rotem, S., Portnaya, I., Cogan, U. & Mor, A. (2007). *Chem Biol* **14**, 75-85.
Mazel, D., Pochet, S. & Marliere, P. (1994). *EMBO J* **13**, 914-923.
McCoy, A. J., Grosse-Kunstleve, R. W., Adams, P. D., Winn, M. D., Storoni, L. C. & Read, R. J. (2007). *J App Crystallogr* **40**, 658-674.
McMahon, R. M., Premkumar, L. & Martin, J. L. (2014). *Biochim Biophys Acta*.
McPhee, J. B. & Hancock, R. E. (2005). *J Pept Sci* **11**, 677-687.
McPhillips, T. M., McPhillips, S. E., Chiu, H. J., Cohen, A. E., Deacon, A. M., Ellis, P. J., Garman, E., Gonzalez, A., Sauter, N. K., Phizackerley, R. P., Soltis, S. M. & Kuhn, P. (2002). *J Synchrotron Radiat* **9**, 401-406.
Mehtar, S., Tsakris, A. & Pitt, T. L. (1991). *J Antimicrob Chemother* **28**, 612-615.
Meinnel, T. & Blanquet, S. (1994). *J Bacteriol* **176**, 7387-7390.
Meinnel, T., Patiny, L., Ragusa, S. & Blanquet, S. (1999). *Biochemistry* **38**, 4287-4295.
Mensa, B., Kim, Y. H., Choi, S., Scott, R., Caputo, G. A. & DeGrado, W. F. (2011). *Antimicrob Agents Chemother* **55**, 5043-5053.
Miki, T., Okada, N., Kim, Y., Abe, A. & Danbara, H. (2008). *Microbial Pathogenesis* **44**, 151-158.
Milewski, S. (2002). *Biochim Biophys Acta* **1597**, 173-192.
Miller, C., Kong, J., Tran, T. T., Arias, C. A., Saxer, G. & Shamoo, Y. (2013). *Antimicrob Agents Chemother* **57**, 5373-5383.
Miller, C. P. & Bohnhoff, M. (1945). *Proc Soc Exp Biol Med* **60**, 354-356.
Mogi, T. & Kita, K. (2009). *Cell Mol Life Sci* **66**, 3821-3826.
Nakamura, T., Furunaka, H., Miyata, T., Tokunaga, F., Muta, T., Iwanaga, S., Niwa, M., Takao, T. & Shimonishi, Y. (1988). *J Biol Chem* **263**, 16709-16713.
Navon-Venezia, S., Feder, R., Gaidukov, L., Carmeli, Y. & Mor, A. (2002). *Antimicrob Agents Chemother* **46**, 689-694.
Nelson, J. W. & Creighton, T. E. (1994). *Biochemistry* **33**, 5974-5983.
Nguyen, K. T., Hu, X. & Pei, D. (2004). *Bioorganic chemistry* **32**, 178-191.
Nguyen, L. T., Haney, E. F. & Vogel, H. J. (2011). *Trends Biotechnol* **29**, 464-472.
Niesen, F. H., Berglund, H. & Vedadi, M. (2007). *Nat Protoc* **2**, 2212-2221.

Nikkola, M., Gleason, F. K., Saarinen, M., Joelson, T., Bjornberg, O. & Eklund, H. (1991). *J Biol Chem* **266**, 16105-16112.
Niu, Y., Wang, R. E., Wu, H. & Cai, J. (2012). *Future Med Chem* **4**, 1853-1862.
Novak, R. & Shlaes, D. M. (2010). *Curr Opin Investig Drugs* **11**, 182-191.
Nunez, S., Venhorst, J. & Kruse, C. G. (2012). *Drug Discov Today* **17**, 10-22.
O'Shea, R. & Moser, H. E. (2008). *Journal of medicinal chemistry* **51**, 2871-2878.
Ohnishi, K., Homma, M., Kutsukake, K. & Iino, T. (1987). *J Bacteriol* **169**, 1485-1488.
Okeke, I. N., Lamikanra, A. & Edelman, R. (1999). *Emerg Infect Dis* **5**, 18-27.
Olsen, C. A., Ziegler, H. L., Nielsen, H. M., Frimodt-Moller, N., Jaroszewski, J. W. & Franzyk, H. (2010). *Chembiochem* **11**, 1356-1360.
OMEGA. Version 2.4.6.
Osborne, C. S., Neckermann, G., Fischer, E., Pecanka, R., Yu, D., Manni, K., Goldovitz, J., Amaral, K., Dzink-Fox, J. & Ryder, N. S. (2009). *Antimicrob Agents Chemother* **53**, 3777-3781.
Palomino, J. C. & Martin, A. (2013). *Future Microbiol* **8**, 1071-1080.
Patch, J. A. & Barron, A. E. (2002). *Curr Op Chem Biol* **6**, 872-877.
Paul, S. M., Mytelka, D. S., Dunwiddie, C. T., Persinger, C. C., Munos, B. H., Lindborg, S. R. & Schacht, A. L. (2010). *Nat Rev Drug Discov* **9**, 203-214.
Paxman, J. J., Borg, N. A., Horne, J., Thompson, P. E., Chin, Y., Sharma, P., Simpson, J. S., Wielens, J., Piek, S., Kahler, C. M., Sakellaris, H., Pearce, M., Bottomley, S. P., Rossjohn, J. & Scanlon, M. J. (2009a). *J Biol Chem* **284**, 17835-17845.
Paxman, J. J., Borg, N. A., Horne, J., Thompson, P. E., Chin, Y., Sharma, P., Simpson, J. S., Wielens, J., Piek, S., Kahler, C. M., Sakellaris, H., Pearce, M., Bottomley, S. P., Rossjohn, J. & Scanlon, M. J. (2009b). *J Biol Chem* **284**, 17835-17845.
Pearson, M. M., Sebaihia, M., Churcher, C., Quail, M. A., Seshasayee, A. S., Luscombe, N. M., Abdellah, Z., Arrosmith, C., Atkin, B., Chillingworth, T., Hauser, H., Jagels, K., Moule, S., Mungall, K., Norbertczak, H., Rabbinowitsch, E., Walker, D., Whithead, S., Thomson, N. R., Rather, P. N., Parkhill, J. & Mobley, H. L. (2008). *J Bacteriol* **190**, 4027-4037.
Peek, J. A. & Taylor, R. K. (1992). *Proc Natl Acad Sci U S A* **89**, 6210-6214.
Pemberton, N., Aberg, V., Almstedt, H., Westermark, A. & Almqvist, F. (2004). *J Org Chem* **69**, 7830-7835.
Perozzo, R., Folkers, G. & Scapozza, L. (2004). *J Recept Signal Transduct Res* **24**, 1-52.
Peschel, A. & Sahl, H. G. (2006). *Nat Rev Microbiol* **4**, 529-536.
Piddock, L. J. (2006). *Clin Microbiol Rev* **19**, 382-402.
Plough, H. H. (1945). *Am J Clin Pathol* **15**, 446-451.
Pogliano, J., Lynch, A. S., Belin, D., Lin, E. C. & Beckwith, J. (1997). *Genes Dev* **11**, 1169-1182.
Pogliano, J., Pogliano, N. & Silverman, J. A. (2012). *J Bacteriol* **194**, 4494-4504.
Pollaro, L. & Heinis, C. (2010). *Medchemcomm* **1**, 319-324.
Porter, E. A., Wang, X., Lee, H. S., Weisblum, B. & Gellman, S. H. (2000). *Nature* **404**, 565.
Potashman, M. H. & Duggan, M. E. (2009). *J Med Chem* **52**, 1231-1246.
Poulin, R., Lu, L., Ackermann, B., Bey, P. & Pegg, A. E. (1992). *J Biol Chem* **267**, 150-158.
Powers, J. C., Asgian, J. L., Ekici, O. D. & James, K. E. (2002). *Chem Rev* **102**, 4639-4750.
Powers, J. P. & Hancock, R. E. (2003). *Peptides* **24**, 1681-1691.
Premkumar, L., Heras, B., Duprez, W., Walden, P., Halili, M., Kurth, F., Fairlie, D. P. & Martin, J. L. (2013). *Acta Crystallogr D Biol Crystallogr* **69**, 1981-1994.
Qin, J., Clore, G. M., Kennedy, W. P., Kuszewski, J. & Gronenborn, A. M. (1996). *Structure* **4**, 613-620.
Radzishevsky, I. S., Kovachi, T., Porat, Y., Ziserman, L., Zaknoon, F., Danino, D. & Mor, A. (2008). *Chem Biol* **15**, 354-362.
Radzishevsky, I. S., Rotem, S., Bourdetsky, D., Navon-Venezia, S., Carmeli, Y. & Mor, A. (2007). *Nat Biotechnol* **25**, 657-659.

Rasko, D. A. & Sperandio, V. (2010). *Nat Rev Drug Discov* **9**, 117-128.
Raveh, B., London, N., Zimmerman, L. & Schueler-Furman, O. (2011). *PLoS One* **6**, e18934.
Regeimbal, J. & Bardwell, J. C. A. (2002). *Journal of Biological Chemistry* **277**, 32706-32713.
Renau, T. E., Leger, R., Filonova, L., Flamme, E. M., Wang, M., Yen, R., Madsen, D., Griffith, D., Chamberland, S., Dudley, M. N., Lee, V. J., Lomovskaya, O., Watkins, W. J., Ohta, T., Nakayama, K. & Ishida, Y. (2003). *Bioorg Med Chem Lett* **13**, 2755-2758.
Renau, T. E., Leger, R., Flamme, E. M., Sangalang, J., She, M. W., Yen, R., Gannon, C. L., Griffith, D., Chamberland, S., Lomovskaya, O., Hecker, S. J., Lee, V. J., Ohta, T. & Nakayama, K. (1999). *J Med Chem* **42**, 4928-4931.
Renau, T. E., Leger, R., Flamme, E. M., She, M. W., Gannon, C. L., Mathias, K. M., Lomovskaya, O., Chamberland, S., Lee, V. J., Ohta, T., Nakayama, K. & Ishida, Y. (2001). *Bioorg Med Chem Lett* **11**, 663-667.
Rinaldi, F. C., Meza, A. N. & Guimaraes, B. G. (2009). *Biochemistry* **48**, 3508-3518.
Robinson, J. A. (2008). *Acc Chem Res* **41**, 1278-1288.
Robinson, J. A., Shankaramma, S. C., Jetter, P., Kienzl, U., Schwendener, R. A., Vrijbloed, J. W. & Obrecht, D. (2005). *Bioorg Med Chem* **13**, 2055-2064.
Rodriguez-Rojas, A., Rodriguez-Beltran, J., Couce, A. & Blazquez, J. (2013). *Int J Med Microbiol* **303**, 293-297.
Rolan, P., Sun, H., Macleod, C., Bracken, K. & Evans, T. G. (2011). *Clin Pharmacol Ther* **90**, 256-262.
Ronald, A. (2003). *Dis Mon* **49**, 71-82.
Rotem, S. & Mor, A. (2009). *Biochim Biophys Acta* **1788**, 1582-1592.
Rotem, S., Radzishevsky, I. S., Bourdetsky, D., Navon-Venezia, S., Carmeli, Y. & Mor, A. (2008). *FASEB J* **22**, 2652-2661.
Ruddock, L. W., Hirst, T. R. & Freedman, R. B. (1996). *Biochem J* **315 (Pt 3)**, 1001-1005.
Ruiz, N., Chng, S. S., Hiniker, A., Kahne, D. & Silhavy, T. J. (2010). *Proc Nat Acad Sci USA* **107**, 12245-12250.
Rydlo, T., Rotem, S. & Mor, A. (2006). *Antimicrob Agents Chemother* **50**, 490-497.
Sabath, L. D. (1969). *N Engl J Med* **280**, 91-94.
Sako, Y., Morimoto, J., Murakami, H. & Suga, H. (2008). *J Am Chem Soc* **130**, 7232-7234.
Sarig, H., Goldfeder, Y., Rotem, S. & Mor, A. (2011). *Antimicrob Agents Chemother* **55**, 688-695.
Sarig, H., Livne, L., Held-Kuznetsov, V., Zaknoon, F., Ivankin, A., Gidalevitz, D. & Mor, A. (2010). *FASEB J* **24**, 1904-1913.
Satyanarayanajois, S. D. & Hill, R. A. (2011). *Future Med Chem* **3**, 1765-1786.
Schellman, J. A. (1997). *Biophys J* **73**, 2960-2964.
Schlichting, I. (2005). *Methods Mol Biol* **305**, 155-166.
Schmidt, J., Patora-Komisarska, K., Moehle, K., Obrecht, D. & Robinson, J. A. (2013). *Bioorg Med Chem* **21**, 5806-5810.
Schroder, J. M. (1999). *Biochem Pharmacol* **57**, 121-134.
Schrodinger, LLC (2010a). The AxPyMOL Molecular Graphics Plugin for Microsoft PowerPoint, Version 1.0.
Schrodinger, LLC (2010b). The JyMOL Molecular Graphics Development Component, Version 1.0.
Schrodinger, LLC (2010c). The PyMOL Molecular Graphics System, Version 1.3r1.
Schweizer, H. P. (2003). *Genet Mol Res* **2**, 48-62.
Scott, R. W., DeGrado, W. F. & Tew, G. N. (2008). *Curr Opin Biotechnol* **19**, 620-627.
Seidel, S. A., Dijkman, P. M., Lea, W. A., van den Bogaart, G., Jerabek-Willemsen, M., Lazic, A., Joseph, J. S., Srinivasan, P., Baaske, P., Simeonov, A., Katritch, I., Melo, F. A., Ladbury, J. E., Schreiber, G., Watts, A., Braun, D. & Duhr, S. (2013). *Methods* **59**, 301-315.
Senisterra, G. A., Markin, E., Yamazaki, K., Hui, R., Vedadi, M. & Awrey, D. E. (2006). *J Biomol Screen* **11**, 940-948.

Shalev, D. E., Mor, A. & Kustanovich, I. (2002). *Biochemistry* **41**, 7312-7317.
Shankaramma, S. C., Athanassiou, Z., Zerbe, O., Moehle, K., Mouton, C., Bernardini, F., Vrijbloed, J. W., Obrecht, D. & Robinson, J. A. (2002). *Chembiochem* **3**, 1126-1133.
Sharma, A., Khuller, G. K. & Sharma, S. (2009). *Expert Opin Ther Targets* **13**, 753-765.
Shaw, K. J. & Barbachyn, M. R. (2011). *Ann N Y Acad Sci* **1241**, 48-70.
Shouldice, S. R., Heras, B., Jarrott, R., Sharma, P., Scanlon, M. J. & Martin, J. L. (2010). *Antioxid Redox Signal* **12**, 921-931.
Shouldice, S. R., Heras, B., Walden, P. M., Totsika, M., Schembri, M. A. & Martin, J. L. (2011). *Antioxid Redox Signal* **14**, 1729-1760.
Singh, J., Petter, R. C., Baillie, T. A. & Whitty, A. (2011). *Nat Rev Drug Discov* **10**, 307-317.
Smith, H. K., Beckett, R. P., Clements, J. M., Doel, S., East, S. P., Launchbury, S. B., Pratt, L. M., Spavold, Z. M., Thomas, W., Todd, R. S. & Whittaker, M. (2002). *Bioorg Med Chem Lett* **12**, 3595-3599.
Song, C., Weichbrodt, C., Salnikov, E. S., Dynowski, M., Forsberg, B. O., Bechinger, B., Steinem, C., de Groot, B. L., Zachariae, U. & Zeth, K. (2013). *Proc Natl Acad Sci U S A* **110**, 4586-4591.
Spellberg, B., Powers, J. H., Brass, E. P., Miller, L. G. & Edwards, J. E., Jr. (2004). *Clin Infect Dis* **38**, 1279-1286.
Sperling, L. J., Tang, M., Berthold, D. A., Nesbitt, A. E., Gennis, R. B. & Rienstra, C. M. (2013). *J Phys Chem B* **117**, 6052-6060.
Srinivas, N., Jetter, P., Ueberbacher, B. J., Werneburg, M., Zerbe, K., Steinmann, J., Van der Meijden, B., Bernardini, F., Lederer, A., Dias, R. L., Misson, P. E., Henze, H., Zumbrunn, J., Gombert, F. O., Obrecht, D., Hunziker, P., Schauer, S., Ziegler, U., Kach, A., Eberl, L., Riedel, K., DeMarco, S. J. & Robinson, J. A. (2010). *Science* **327**, 1010-1013.
Steinberg, D. A., Hurst, M. A., Fujii, C. A., Kung, A. H., Ho, J. F., Cheng, F. C., Loury, D. J. & Fiddes, J. C. (1997). *Antimicrob Agents Chemother* **41**, 1738-1742.
Stenson, T. H. & Weiss, A. A. (2002). *Infection and Immunity* **70**, 2297-2303.
Stephens, C. & Shapiro, L. (1997). *Chem Biol* **4**, 637-641.
Studier, F. W. (2005). *Protein Expr Purif* **41**, 207-234.
Su, Y., DeGrado, W. F. & Hong, M. (2010). *J Am Chem Soc* **132**, 9197-9205.
Svensson, A., Larsson, A., Emtenas, H., Hedenstrom, M., Fex, T., Hultgren, S. J., Pinkner, J. S., Almqvist, F. & Kihlberg, J. (2001). *Chembiochem* **2**, 915-918.
Tally, F. P. & DeBruin, M. F. (2000). *J Antimicrob Chemother* **46**, 523-526.
Tang, H., Doerksen, R. J., Jones, T. V., Klein, M. L. & Tew, G. N. (2006). *Chem Biol* **13**, 427-435.
Tang, M. & Hong, M. (2009). *Mol Biosyst* **5**, 317-322.
Temussi, P. A., Picone, D., Castiglione-Morelli, M. A., Motta, A. & Tancredi, T. (1989). *Biopolymers* **28**, 91-107.
Tew, G. N., Liu, D., Chen, B., Doerksen, R. J., Kaplan, J., Carroll, P. J., Klein, M. L. & DeGrado, W. F. (2002). *Proc Natl Acad Sci U S A* **99**, 5110-5114.
Thomas, C. M., Hothersall, J., Willis, C. L. & Simpson, T. J. (2010). *Nat Rev Microbiol* **8**, 281-289.
Tibbetts, R., Frye, J. G., Marschall, J., Warren, D. & Dunne, W. (2008). *J Clin Microbiol* **46**, 3080-3083.
Tossi, A., Sandri, L. & Giangaspero, A. (2000). *Biopolymers* **55**, 4-30.
Totsika, M., Heras, B., Wurpel, D. J. & Schembri, M. A. (2009a). *J Bacteriol* **191**, 3901-3908.
Totsika, M., Heras, B., Wurpel, D. J. & Schembri, M. A. (2009b). *J Bacteriol* **191**, 3901-3908.
Totsika, M., Moriel, D. G., Idris, A., Rogers, B. A., Wurpel, D. J., Phan, M. D., Paterson, D. L. & Schembri, M. A. (2012). *Curr Drug Targets* **13**, 1386-1399.
Turnbull, A. P. & Emsley, P. (2013). *Methods Mol Biol* **1008**, 457-477.
Tzeng, Y. L., Ambrose, K. D., Zughaier, S., Zhou, X., Miller, Y. K., Shafer, W. M. & Stephens, D. S. (2005). *J Bacteriol* **187**, 5387-5396.
Ung, P. & Winkler, D. A. (2011). *J Med Chem* **54**, 1111-1125.

Vaara, M. (2009). *Curr Opin Pharmacol* **9**, 571-576.
Vallance, B. A. & Finlay, B. B. (2000). *Proc Natl Acad Sci U S A* **97**, 8799-8806.
Vangone, A., Spinelli, R., Scarano, V., Cavallo, L. & Oliva, R. (2011). *Bioinformatics* **27**, 2915-2916.
Vedadi, M., Niesen, F. H., Allali-Hassani, A., Fedorov, O. Y., Finerty, P. J., Jr., Wasney, G. A., Yeung, R., Arrowsmith, C., Ball, L. J., Berglund, H., Hui, R., Marsden, B. D., Nordlund, P., Sundstrom, M., Weigelt, J. & Edwards, A. M. (2006). *Proc Natl Acad Sci U S A* **103**, 15835-15840.
Verdonk, M. L., Cole, J. C., Hartshorn, M. J., Murray, C. W. & Taylor, R. D. (2003). *Proteins* **52**, 609-623.
Verlinde, C. L. & Hol, W. G. (1994). *Structure* **2**, 577-587.
Viegas, A., Manso, J., Nobrega, F. & Cabrita, E. (2011). *J Chem Educ* **88**, 990-994.
Vieth, M., Siegel, M. G., Higgs, R. E., Watson, I. A., Robertson, D. H., Savin, K. A., Durst, G. L. & Hipskind, P. A. (2004). *J Med Chem* **47**, 224-232.
Vivian, J. P., Scoullar, J., Rimmer, K., Bushell, S. R., Beddoe, T., Wilce, M. C., Byres, E., Boyle, T. P., Doak, B., Simpson, J. S., Graham, B., Heras, B., Kahler, C. M., Rossjohn, J. & Scanlon, M. J. (2009). *J Mol Biol* **394**, 931-943.
Waksman, G. & Hultgren, S. J. (2009). *Nat Rev Microbiol* **7**, 765-774.
Walden, P. M., Heras, B., Chen, K. E., Halili, M. A., Rimmer, K., Sharma, P., Scanlon, M. J. & Martin, J. L. (2012). *Acta Crystallogr D Biol Crystallogr* **68**, 1290-1302.
Walker, K. W., Lyles, M. M. & Gilbert, H. F. (1996). *Biochemistry* **35**, 1972-1980.
Wang, M., Guo, Q., Xu, X., Wang, X., Ye, X., Wu, S., Hooper, D. C. & Wang, M. (2009). *Antimicrob Agents Chemother* **53**, 1892-1897.
Weinstock, M. T., Francis, J. N., Redman, J. S. & Kay, M. S. (2012). *Biopolymers* **98**, 431-442.
Wellington, E. M., Boxall, A. B., Cross, P., Feil, E. J., Gaze, W. H., Hawkey, P. M., Johnson-Rollings, A. S., Jones, D. L., Lee, N. M., Otten, W., Thomas, C. M. & Williams, A. P. (2013). *Lancet Infect Dis* **13**, 155-165.
White, C. J. & Yudin, A. K. (2011). *Nat Chem* **3**, 509-524.
Winn, M. D., Ballard, C. C., Cowtan, K. D., Dodson, E. J., Emsley, P., Evans, P. R., Keegan, R. M., Krissinel, E. B., Leslie, A. G., McCoy, A., McNicholas, S. J., Murshudov, G. N., Pannu, N. S., Potterton, E. A., Powell, H. R., Read, R. J., Vagin, A. & Wilson, K. S. (2011). *Acta Crystallogr D Biol Crystallogr* **67**, 235-242.
Wulfing, C. & Rappuoli, R. (1997). *Arch Microbiol* **167**, 280-283.
Wunderlich, M. & Glockshuber, R. (1993). *Protein Sci* **2**, 717-726.
Ye, Y. & Godzik, A. (2003). *Bioinformatics* **19 Suppl 2**, ii246-255.
Yu, J. (1998). *Infect Immun* **66**, 3909-3917.
Yu, J., Webb, H. & Hirst, T. R. (1992). *Mol Microbiol* **6**, 1949-1958.
Yuan, B., Cheng, A. & Wang, M. (2013). *Future Microbiol* **8**, 525-535.
Zapun, A., Bardwell, J. C. & Creighton, T. E. (1993). *Biochemistry* **32**, 5083-5092.
Zasloff, M. (2002). *Nature* **415**, 389-395.
Zhao, W. H. & Hu, Z. Q. (2013). *Crit Rev Microbiol* **39**, 79-101.
Zhou, Y., Cierpicki, T., Jimenez, R. H., Lukasik, S. M., Ellena, J. F., Cafiso, D. S., Kadokura, H., Beckwith, J. & Bushweller, J. H. (2008). *Mol Cell* **31**, 896-908.
Zuckermann, R. N., Martin, E. J., Spellmeyer, D. C., Stauber, G. B., Shoemaker, K. R., Kerr, J. M., Figliozzi, G. M., Goff, D. A., Siani, M. A., Simon, R. J. & et al. (1994). *J Med Chem* **37**, 2678-2685.
Zurenko, G. E., Ford, C. W., Hutchinson, D. K., Brickner, S. J. & Barbachyn, M. R. (1997). *Expert Opin Investig Drugs* **6**, 151-158.

APPENDIX

The following appendices includes two additional publications to which I contributed during the course of this PhD for the better understanding of the DsbA protein family and to investigate the possibility of designing a broad-spectrum antibiotic that might bind DsbA in different pathogenic species. Appendix A presents the characterization of *Klebsiella pneumoniae* DsbA and the outline of a first subclass of DsbA proteins in *Enterobacteriaceae* (including EcDsBA), for which a common inhibitor scaffold might be designed. I performed peptide binding experiments (ITC) using sequences I synthesized both against EcDsBA and specifically against KpDsbA. Appendix B characterizes a DsbA from a different subclass, originating from *Mycobacterium tuberculosis*, and shows that significant structural differences compared with EcDsbA suggest a different inhibitory scaffold would have to be designed. Here again, I synthesized and tested (with ITC) a series of specific peptides that were proved to bind and inhibit MtbDsbA.

Second, Appendix C presents all the supplementary information provided with the manuscript of the EcDsbA-peptides SAR publication (Chapter III). This includes the peptide characterization data as well as additional ITC and DSF graphs.

APPENDIX A

OPEN ACCESS Freely available online

PLOS ONE

Comparative Sequence, Structure and Redox Analyses of *Klebsiella pneumoniae* DsbA Show That Anti-Virulence Target DsbA Enzymes Fall into Distinct Classes

Fabian Kurth[1], Kieran Rimmer[2], Lakshmanane Premkumar[1], Biswaranjan Mohanty[2], Wilko Duprez[1], Maria A. Halili[1], Stephen R. Shouldice[1¤a], Begoña Heras[1¤b], David P. Fairlie[1], Martin J. Scanlon[2,3*], Jennifer L. Martin[1*]

1 Division of Chemistry and Structural Biology, Institute for Molecular Bioscience, The University of Queensland, Brisbane, Queensland, Australia, **2** Faculty of Pharmacy and Pharmaceutical Sciences, Medicinal Chemistry, Monash Institute of Pharmaceutical Sciences, Monash University, Parkville, Victoria, Australia, **3** ARC Centre of Excellence for Coherent X-ray Science, Monash University, Parkville, Victoria, Australia

Abstract

Bacterial DsbA enzymes catalyze oxidative folding of virulence factors, and have been identified as targets for antivirulence drugs. However, DsbA enzymes characterized to date exhibit a wide spectrum of redox properties and divergent structural features compared to the prototypical DsbA enzyme of *Escherichia coli* DsbA (EcDsbA). Nonetheless, sequence analysis shows that DsbAs are more highly conserved than their known substrate virulence factors, highlighting the potential to inhibit virulence across a range of organisms by targeting DsbA. For example, *Salmonella enterica typhimurium* (SeDsbA, 86 % sequence identity to EcDsbA) shares almost identical structural, surface and redox properties. Using comparative sequence and structure analysis we predicted that five other bacterial DsbAs would share these properties. To confirm this, we characterized *Klebsiella pneumoniae* DsbA (KpDsbA, 81 % identity to EcDsbA). As expected, the redox properties, structure and surface features (from crystal and NMR data) of KpDsbA were almost identical to those of EcDsbA and SeDsbA. Moreover, KpDsbA and EcDsbA bind peptides derived from their respective DsbBs with almost equal affinity, supporting the notion that compounds designed to inhibit EcDsbA will also inhibit KpDsbA. Taken together, our data show that DsbAs fall into different classes; that DsbAs within a class may be predicted by sequence analysis of binding loops; that DsbAs within a class are able to complement one another *in vivo* and that compounds designed to inhibit EcDsbA are likely to inhibit DsbAs within the same class.

Citation: Kurth F, Rimmer K, Premkumar L, Mohanty B, Duprez W, et al. (2013) Comparative Sequence, Structure and Redox Analyses of *Klebsiella pneumoniae* DsbA Show That Anti-Virulence Target DsbA Enzymes Fall into Distinct Classes. PLoS ONE 8(11): e80210. doi:10.1371/journal.pone.0080210

Editor: Vladimir N. Uversky, University of South Florida College of Medicine, United States of America

Received August 25, 2013; **Accepted** September 30, 2013; **Published** November 14, 2013

Funding: This work was supported by an ARC (www.arc.gov.au) Australian Laureate Fellowship (FL0992138) to JLM—which also supported PhD scholarships to FK and WD—and an NHMRC (www.nhmrc.gov.au) Project Grant (APP1009785) to MJS and BH. JLM is also an Honorary NHMRC Research Fellow (455829). The funders had no role in study design, data collection and analysis, decision to publish, or preparation of the manuscript.

Competing interests: The authors have declared that no competing interests exist.

* E-mail: j.martin@imb.uq.edu.au (JLM); martin.scanlon@monash.edu (MJS)

¤a Current address: Janssen-Cilag Pty Ltd., Macquarie Park, New South Wales, Australia
¤b Current address: Institute for Molecular Science, Latrobe University, Melbourne, Victoria, Australia

Introduction

Antibiotic resistance has increased dramatically over the last decade and the consequent lack of treatment options poses a major threat for public health [1]. One approach to develop new chemical classes of antibacterials is to target virulence factors that cause disease in antibiotic resistant organisms [2]. Most pathogenic *Enterobacteriaceae* encode an oxidative folding pathway essential for virulence factor production [2-5]. Typically, the oxidative folding machinery includes a soluble thioredoxin-fold protein, DsbA, and an integral membrane protein partner, DsbB [6-8]. The disulfide form of DsbA is highly oxidizing and donates its disulfide bond to unfolded substrate proteins [9], leaving DsbA in the inactive reduced form. The inner membrane protein DsbB, in concert with its cofactor ubiquinone, interacts with reduced DsbA to oxidize the active site cysteines and convert DsbA to its functionally competent disulfide form [10]. Inhibition of the interaction between DsbA and substrate proteins or between DsbA and its partner DsbB could constitute a means of blocking virulence factor formation and thereby of inhibiting virulence of bacterial pathogens. Supporting this notion, deletion of DsbA homologues in

Table 1. Comparison of structures and redox properties of DsbAs.

	Seq id to EcDsbA	RMSD (Å)	RMSD #Cα	E°' (mV)	pK_a "Cys30"	T_m (K) (red/ox)
Other DsbAs [a]	10 - 40 %	1.3 - 2.9	122 - 167	-80/-163	3.0 - 5.1	337-357 / 331-341
EcDsbA[b]	100 %	0.6	176	-122	3.3	350 / 341
SeDsbA[c]	86 %	0.9	176	-126	3.3	351 / 343
KpDsbA	81 %	0.8	176	-116	3.2	347 / 335
VcDsbA[d]	40 %	1.8	168	- 116	5.1	357 / 346
NmDsbA1[e]	23 %	2.6	163	- 80	3.0	348 / 333

a. [14] , redox potential range for NmDsbA1 (-80 , WpDsbA (- 163); pK_a range, NmDsbA1 (3.0), VcDsbA (5.1); T_m oxidised (min) NmDsbA3, (max) VcDsbA and reduced (min) NmDsbA3, (max) VcDsbA.

b. [6] [14],, RMSD of EcDsbA derived from the overlay of molecules A and B from the asymmetric unit in 1FVK.

c. [43] and [14]

d. [54]

e. [51]

doi: 10.1371/journal.pone.0080210.t001

pathogenic organisms results in diminished virulence in infection models [2,11] and deletion of *dsbA* or *dsbB* in uropathogenic *E. coli* (UPEC) severely attenuated its ability to colonize the bladder [11,12].

The characteristic properties of EcDsbA include: an active site CPHC motif that forms a destabilizing disulfide (T_m reduced EcDsbA 350 K; T_m oxidized EcDsbA 342 K) [13]; the more N-terminal of the two cysteines is nucleophilic and highly acidic, pK_a 3.3 (usual value for a cysteine is 8-9) [9]; and EcDsbA is highly oxidizing (redox potential -122 mV) [9]. The past 5 years has seen the characterization of DsbA enzymes from many other bacteria including DsbAs with varying degrees of sequence identity to EcDsbA such as *Neisseria meningitidis* DsbA1 (NmDsbA1, 23% identity), *Pseudomonas aeruginosa* DsbA (PaDsbA, 30%) and *Vibrio cholerae* DsbA (VcDsbA, or TcpG, 40%). These DsbAs share a similar structural fold with EcDsbA though their surface properties vary [14] and they exhibit a wide range of redox properties (Table **1**). Importantly, the EcDsbA hydrophobic groove that interacts with its essential partner EcDsbB is considerably truncated in NmDsbA1, PaDsbA and VcDsbA [15-17]. This modification and other surface changes in these DsbAs indicate that they fall into a separate class, distinct from EcDsbA, and that inhibitors designed against EcDsbA may not inhibit members of this class of DsbA. Conversely, DsbAs closely related to EcDsbA should be susceptible to the same mode of chemical inhibition.

Here we tested how close the sequence relationship must be to produce similar redox properties and binding interactions. We investigated two well-characterised DsbAs sharing 86% sequence identity, from *E. coli* K-12 strain (EcDsbA) and *S. enterica Typhimurium* DsbA strain SL1344 (SeDsbA), by applying comparative structural, sequence and redox analyses to identify properties conserved across these two enzymes. The results allow us to place DsbAs of five other Gram-negative bacteria *Enterobacteriaceae*, namely *Shigella flexneri* 8401 (SfDsbA, 100% sequence identity to EcDsbA), *Enterobacter cloacae* SCF-1 (EnDsbA, 84%), *Citrobacter koseri* ATCC BAA-895 (CkDsbA, 84%), *Cronobacter sakazakii* SP291 (CsDsbA, 82%) and *K. pneumonia* 342 (KpDsbA, 81%) into the same DsbA cluster as SeDsbA and EcDsbA. To assess whether the redox and structural properties are maintained in this DsbA group we focused on KpDsbA, which shares the lowest sequence identity with EcDsbA. We determined the high resolution crystal structure of reduced KpDsbA and the NMR solution structure of oxidized KpDsbA, and we measured the redox properties of this enzyme. As expected, the redox properties, surface characteristics and binding properties of KpDsbA are similar to those of EcDsbA suggesting that inhibitors developed against EcDsbA are likely to also be effective against other members of this DsbA subclass.

Materials and Methods

Protein production

Codon-optimized *K. pneumoniae dsbA* (GenBank® accession number ACI08793), lacking the sequence coding for the predicted signal sequence (19 aa), was cloned into a modified pMCSG7 (Midwest Center for Structural Genomics) vector compatible with ligation-independent cloning. This modified vector encoded a leader sequence consisting of an N-terminal His_6-tag followed by a linker containing the tobacco-etch virus protease (TEV) recognition sequence. KpDsbA was expressed in BL21(DE3)pLys cells using autoinduction medium [18] and purified with Talon® resin (Clontech, Australia). The His_6-tag was removed by TEV protease, leaving the engineered KpDsbA with two additional amino acids (S–1 and N0) at the N-terminus. A final size-exclusion chromatography step using a Superdex75 column (GE Healthcare, USA) yielded highly purified KpDsbA, as judged by SDS-PAGE. Oxidized or reduced KpDsbA was prepared using a 25-fold molar excess of copper-(II)-1,10-phenanthroline or DTT, respectively. Oxidizing/reducing agent was then removed and the protein buffer-exchanged into 10 mM HEPES, pH 7.4 in one step using GE-25 Sephadex desalting resin for crystallization and biochemical experiments.

Preparation of *E. coli* DsbA (CAA56736), *S. enterica Typhimurium* DsbA (AAB81592) and *E. coli* DsbC (AAA83074), lacking the periplasmic leader signal were purified as described for KpDsbA. For peptide oxidation experiments, *E. coli* DsbB (AAC74269) membrane extracts were prepared as described previously [19] and re-suspended in phosphate buffered saline (PBS, 137 mM NaCl, 2.7 mM KCl, Na_2HPO_4 10 mM and KH_2PO_4, pH 7.4) containing 10 % glycerol.

KpDsbA Complementation of EcDsbA

The ability of KpDsbA to rescue non-motile *E. coli dsbA*$^-$ null (JCB817) and *dsbA*$^-$/*dsbB*$^-$ double-null (JCB818) strains was assessed in a cell-swarming assay as described previously [16]. The mature KpDsbA coding sequence was cloned into pBAD33 under an arabinose inducible promotor with the EcDsbA periplasmic signal sequence. A wild-type EcDsbA cloned into pBAD33 vector was used as a positive control.

Non-motile *E. coli dsbA*$^-$ deficient (JCB817) or *dsbA*$^-$ / *dsbB*$^-$ double-mutant (JCB818) [3] cells ($2x10^6$) transformed with a KpDsbA or EcDsbA pBAD33 inducible vector were spotted onto the center of a soft M63 minimal agar plate containing 40 mg/mL of each amino acid (except L-cysteine). Plates were incubated at 37 °C and motility of cells monitored using a Molecular Imager® Gel Doc™ system from BIO-RAD (CA 94547, USA) after 3-7 h. Complementation experiments were repeated as biological triplicates.

KpDsbA Disulfide Reductase Activity

Under mild reducing conditions, DsbA proteins can reduce the intermolecular disulfide bonds formed between insulin chains A and B [3]. The rate of disulfide bond reduction can be spectroscopically followed at OD_{650nm} by an increase in turbidity resulting from production of the insoluble insulin chain B [20]. Samples were prepared in 1 cm cuvettes containing 10 µM of protein (KpDsbA, EcDsbA or EcDsbC), 0.33 mM DTT and 2 mM EDTA in 100 mM NaH_2PO_4 / Na_2HPO_4 titrated to pH 7.0. Catalysis was initiated by the addition of 0.131 mM insulin (I0516, Sigma-Aldrich, Australia) to the sample mixture. The assay was repeated three times and data were plotted showing standard deviations.

Measurement of KpDsbA Redox Potential

The standard redox potential of KpDsbA was measured using its intrinsic tryptophan fluorescence, as described previously for EcDsbA [6]. Oxidized KpDsbA was incubated for 12 h at 25 °C in degassed 100 mM NaH_2PO_4 / Na_2HPO_4 buffer (pH 7.0, 1 mM EDTA, 298K), containing 1 mM oxidized glutathione (GSSG) and varying concentrations of reduced glutathione (GSH) (0–2 mM). KpDsbA (200 µL) from each redox condition was dispensed into a 96-well plate (TPP AG, Switzerland #92096) and tryptophan fluorescence was measured (excitation at 280 nm, emission set to 332 nm) using a microplate reader (Synergy H1 and Gen5 2.0 software, Biotek, USA). Data were normalized and the redox potential was calculated as described for EcDsbA [6]. In brief, the equilibrium constant K_{eq} was calculated using the equation: $Y = ([GSH]^2 / [GSSH])/(K_{eq} + ([GSH]^2 / [GSSH]))$, where Y is the fraction of reduced protein at equilibrium. The redox potential for KpDsbA was calculated from the Nernst equation: $E^{0'}_{KpDsbA} = E^{0'}_{GSH/GSSH} - (RT/nF)\ln K_{eq}$ where $E^{0'}_{GSH/GSSH} = -240$ mV, R is the ideal gas constant 8.314 $JK^{-1}mol^{-1}$, T is the absolute temperature in K, n is the number of electrons transferred (n = 2), F is the Faraday constant 9.648x104 $Cmol^{-1}$ and K_{eq} is the equilibrium constant derived from the binding equation. All measurements were performed as biological triplicates. The graph shows a plot of the average values including error bars representing the standard deviation for the replicates.

KpDsbA Thiolate Anion pK_a Determination

The pH-dependent absorbance of the catalytic thiolate anion of KpDsbA was followed at 240 nm [21] using a CARY 50 UV/VIS spectrophotometer (Agilent Technologies, USA). The pH titration measurements of oxidized or reduced KpDsbA (40 µM) in 2 mL composite buffer (10 mM Tris, 10 mM sodium citrate, 10 mM K_2HPO_4, 10 mM KH_2PO_4, 200 mM KCl, and 1 mM EDTA) were conducted at 22 °C. Absorbance (λ = 240 and 280 nm) was measured between pH 6.5 and 2.0 in 0.25 increments. The pK_a value was calculated from the fitted curves of three replicates using the Henderson-Hasselbalch equation ($pH = pK_a - \log([A240/A280]red/[A240/A280]oxid)$). Experiments were repeated at least three times. Plotted data represent average values and error bars represent the standard deviations across the replicates.

Relative Stability of Oxidized and Reduced Forms of DsbA Enzymes

Temperature-induced unfolding of native SeDsbA and KpDsbA was determined as described previously [13] using a Jasco J-810 circular dichroism (CD) spectropolarimeter (Jasco, USA). The redox state of the protein was confirmed using Ellman's reagent [22]. The largest difference in molar ellipticity for oxidized or reduced enzymes was calculated from initial far-UV CD spectra (from 250 nm to 190 nm) recorded at 25 °C and 95 °C, respectively. The unfolding of oxidized and reduced protein ($SeDsbA_{ox}$ = 220 nm, $SeDsbA_{red}$ = 220.5 nm and $KpDsbA_{ox}$ = 211 nm, $KpDsbA_{red}$ = 209.5 nm) was monitored at a heat rate of 1 K / min from 298 K to 368 K in a 1 mm quartz cuvette. All measurements were carried out with 10 µM protein in 100 mM NaH_2PO_4 / Na_2HPO_4, 1 mM EDTA at pH 7.0. Samples for measurement of reduced enzyme contained 0.75 mM DTT. Raw data were analyzed in Prism and fitted to a two-state unfolding model as described previously [23]. The standard deviation was measured from three replicates.

KpDsbA Dithiol Oxidation Activity

A peptide (CQQGFDGTQNSCK) with a 1,4,7,10-tetraazacyclododecane-1,4,7,10-tetraacetic acid (DOTA) group amide-coupled to the N-terminus, and a methylcoumarin amide-coupled to the ε-amino group of the C-terminal lysine, was purchased from AnaSpec (Fremont, CA). Lyophilized peptide was re-suspended in 100 mM imidazole, pH 6, at a concentration of 2 mM. Europium trifluoromethanesulfonate (Sigma Aldrich, Australia) solution (100 mM) was added to the peptide at a molar ratio of 2:1 and incubated for 5 min at room temperature, to allow europium chelation. The peptide solution was then immediately aliquoted, flash frozen in liquid nitrogen and stored at -80°C. An increase in fluorescence occurs upon oxidation of the peptide cysteines to form a disulfide. Thus, fluorescence can be used to monitor the capacity of DsbA enzymes to catalyse dithiol oxidation.

Assays were conducted using a Synergy H1 multimode plate reader (BioTek, USA) with the excitation wavelength set to 340 nm and emission to 615 nm. A 150 µs delay before reading and 100 µs reading time were used for time-resolved fluorescence. The assay was performed in a white 384-well plate (Perkin Elmer OptiPlate-384, Part #: 6007290). The buffer consisted of 50 mM MES, 50 mM NaCl and 2 mM EDTA at pH 5.5. The reaction consisted of a 50 µL solution in each well, containing 160 nM EcDsbA, KpDsbA or SeDsbA, 1.6 µM EcDsbB (crude membrane extracts, containing ubiquinone) and 8 µM peptide substrate added last to initiate the reaction. Samples containing buffer and DsbA or buffer and peptide were used as controls. Data were measured for three

replicates and are presented as mean values, with the standard error of the mean indicated by error bars.

KpDsbA Crystallization and Crystal Structure Determination

After initial screening using the UQ ROCX facilities, crystals of reduced KpDsbA were grown at 20 °C in VDXm 24-well plates (Hampton Research) using the hanging-drop vapor diffusion method. Screening plates were imaged and incubated in a RockImager 1000 (Formulatrix, MA, USA). Drops contained 0.5 µL of 180 mg/mL reduced KpDsbA and 0.5 µL of crystallization solution (0.1 M succinic acid pH 5.3, 25 % (w/v) polyethylene glycol 1500 and 15 % (v/v) 2-methyl-2,4-pentanediol). For diffraction data measurement, crystals were frozen in liquid nitrogen without additional cryo-protectant. Diffraction data were measured at the Australian Synchrotron micro-focus MX2 beamline using BlueIce software [24]. Reflections were processed in Mosflm [25] and XDS [26], analyzed and converted to MTZ in Pointless [27] and scaled in SCALA [27]. Phases were obtained by molecular replacement (MR) using PHASER [28] with EcDsbA as template (PDB code: 1DSB) . The initial model was improved by iterative model building in COOT [29] and refinement in PHENIX [30]. However, the progress of refinement was stalled with a high R-factor/Rfree of 25.7 % / 29.3 %. Diffraction data analysis in Phenix.xtriage indicated that the crystal was merohedrally twinned with a twinning fraction of 0.42. Further refinement cycles were performed using the twin target function as implemented in PHENIX with the twinning operator h,-h-k,-l. Two fold non-crystallographic symmetry (NCS) is present (which does not align with space group axes), though NCS was not used at any stage of refinement. The refinement finally converged after several TLS refinement cycles. No atoms were modeled into additionally spherical density located between chain D (L133) and chain B (T57) because it was not obvious what was bound. The stereochemical quality of the final model was assessed using MolProbity [31]. A summary of the data processing and refinement statistics are provided in Table 2.

Molecular figures were generated in PyMOL (The PyMOL Molecular Graphics System, Version 1.5.0.4 Schrödinger, LLC) and figures of the electrostatic potential were generated using APBS [32]. The surface, including the proportion of carbon atoms lining the hydrophobic groove in KpDsbA, was calculated using the CastP server [33], by averaging over all six molecules within the asymmetric unit. RMSD calculations and structural alignments were conducted using PyMOL as well as FATCAT [34].

NMR Structure Determination of Oxidized KpDsbA

A sample of uniformly ^{13}C,^{15}N labeled oxidized KpDsbA (1.3 mM) was prepared in 50 mM MES (pH 6.5, 10% $^{2}H_2O$ and 90 % $^{1}H_2O$). NMR experiments were conducted at 303 K on either 600 MHz or 800 MHz spectrometers equipped with cryogenically cooled probes. All spectra were acquired with standard pulse sequences and processed using TOPSPIN3.1 (Bruker BioSpin). H^N, N, C^α, $C^{\alpha-1}$, C^β, $C^{\beta-1}$ peak lists were generated manually in CARA using 2D [^{15}N,^{1}H]-HSQC, 3D HNCA, 3D CBCA(CO)NH and 3D HNCACB spectra and used as the input for automated backbone assignments using UNIO-MATCH. These assignments were refined manually and extended using 3D ^{15}N-resolved [^{1}H,^{1}H]-NOESY. H^β, H^α assignments were obtained using a 3D HBHA(CBCACO)NH spectrum. H^N, N, C^α and C^β assignments together with H^β, H^α were provided as input for UNIO-ATNOS/ASCAN for automated side-chain assignments using 3D ^{15}N-, $^{13}C_{ali}$ - and $^{13}C_{aro}$ - resolved [^{1}H,^{1}H] NOESY datasets [35,36]. Upper limits for distance restraints used in structure calculations were automatically generated from NOESY datasets using UNIO-ATNOS/CANDID and the structure of oxidized KpDsbA was determined using the torsion angle dynamics program CYANA3.0 [37]. Conformers with lowest CYANA target function values were energy minimized using OPALp and validated using structure validation tools (http:/www.pdb.org/ and http:/www.nihserver.mbi.ucla.edu/). Structures were inspected and

Table 2. X-ray data measurement and refinement statistics for KpDsbA.

Data collection	Value
Space group	P 32
Unit cell dimensions	
a (Å)	91.5
b (Å)	91.5
c (Å)	147.2
α, β, γ (°)	90, 90, 120
Wavelength (Å)	0.95369
Resolution (Å)	53.94 - 1.99 (2.10 - 1.99)
Number measured reflections	527,166
Number of unique reflections	94,694
R_{merge}[a]	0.091 (0.566)
$R_{p.i.m.}$	0.043 (0.264)
<I>/<σI>	11.1 (2.9)
Redundancy	5.6 (5.5)
Completeness (%)	99.9 (99.9)
Refinement statistics	
Number of Reflections	94,693
Resolution (Å)	53.9-1.99 (2.02 -1.99)
R_{free} (%)	19.6 (31.9)
R_{work} (%)	16.1 (27.8)
Number of monomers in a.u.	6
Number of protein atoms	16622
Number of waters	371
B factors (Å^2)	
Wilson	29.6
Protein atoms	39.4
Waters	41.4
RMSD Bond length (Å)	0.004
RMSD Bond angles (°)	0.740
Ramachandran favored / outlier (%)	97.4 / 0
Molprobity clashscore / score[b]	2.23 [99th(712)] / 1.12 [100th(12290)]

a. The values in parentheses refer to the highest resolution shell.

b. 100th Molprobity [31] percentile is the best among structures of comparable resolution; 0th percentile is the worst. The number of structures included in the comparison is given in parentheses within square brackets.

doi: 10.1371/journal.pone.0080210.t002

Table 3. Parameters for structure calculation and characterization of 20 lowest energy minimized NMR conformers of oxidised KpDsbA (1–188).

Quantity[a]	Value
NOE upper distance limits	3859
intraresidual	813
short-range	1052
medium-range	969
long-range	1025
Residual target function value [Å^2]	3.3 ± 0.2
Residual NOE violations	
number ≥ 0.1 Å	36.8 ± 7.5
maximum [Å]	0.16 ± 0.11
Residual dihedral angle violations	
number ≥ 2.5°	1.1 ± 0.6
maximum [°]	4.2 ± 3.2
AMBER energies [kcal/mol]	
total	-7513 ± 381
van der Waals	-562 ± 213
electrostatic	-8402 ± 159
RMSD from mean coordinates[b] [Å]	
For well-defined regions (1-15,24-187)	
backbone	0.67 ± 0.17
heavy atoms	1.03 ± 0.13
For TRX domain (1-15, 24-62,146-187)	
backbone	0.55 ± 0.12
heavy atoms	0.99 ± 0.11
For helical domain (67-142)	
backbone	0.44 ± 0.08
heavy atoms	0.81 ± 0.09
Ramachandran plot statistics[c]	
most favoured regions [%]	77.7
additional allowed regions [%]	19.6
generously allowed regions [%]	1.2
disallowed regions [%]	1.5

[a] Except for the top five entries (those relating to NOEs), average values and standard deviations for the 20 energy-minimized conformers are given. The top six entries represent the output generated in the final cycle of the UNIO-ATNOS/CANDID-CYANA3.0 calculation. [b] The numbers in parentheses indicate the residues for which the RMSD was calculated. [c] As determined by PROCHECK.

doi: 10.1371/journal.pone.0080210.t003

analyzed with MOLMOL [38]. Table 3 summarizes the NMR statistics.

Binding Affinity of DsbA-Interacting Peptides

Crystal structures of the EcDsbA:EcDsbB complex revealed that the P2 loop region of EcDsbB interacts with EcDsbA [39,40]. Two peptides derived from the P2 loop sequences of EcDsbB and KpDsbB (*Ec* – PSPFATCD and *Kp* – PSPFQTCD) were synthesized by solid-phase methods using Fmoc deprotection on rink-amide MBHA resin (leading to C-terminal amidation) and capped by N-terminal acetylation. Amidation and acetylation ensure that there are no charges on the peptide termini, as these are not present in the native DsbB loop sequence. Binding affinity was measured using a MicroCal™ Auto-iTC$_{200}$ from (GE Healthcare, USA) at 25 °C. The sample cell was loaded with 200 µL of 100 µM KpDsbA or EcDsbA in 25 mM HEPES, 50 mM NaCl, pH 7.4, and DMSO 0.8 %. The peptide (3 mM) diluted in the same buffer was titrated with an initial injection of 0.5 µL into DsbA, followed by 19 consecutive injections (2.0 µL) offset by 180 s, while the solution was constantly stirred (1000 rpm). Data were fitted to a single-site binding model using MicroCal™ Origin 7.0 software (Origin 7 SR4 v7.0552). Experiments were conducted in triplicate and affinity and thermodynamic parameters are reported as means and standard deviations (Table 4).

Table 4. Affinity and enthalpy for DsbB-derived peptides binding to DsbA proteins[1].

DsbA	DsbB-peptide	Stoichiometry	K_d (µM)	ΔH (kcal/mol)
EcDsbA	PSPFATCD	1.0	16.1 ± 1.8	-8.4 ± 0.1
	PSPFQTCD	0.99	10.9 ± 0.6	-9.1 ± 0.2
KpDsbA	PSPFATCD	0.93	17.9 ± 1.5	-9.5 ± 0.7
	PSPFQTCD	0.97	16.7 ± 0.6	-11.1 ± 0.2

1. Apparent dissociation constant (K_d) and enthalpy of binding (ΔH) at 20 °C obtained from three independent ITC experiments. See Figure S3 for representative ITC traces.

doi: 10.1371/journal.pone.0080210.t004

Comparative Sequence and Structural Analyses

The sequence conservation of ten virulence factors previously identified [2] as substrates of DsbA were analyzed here. Sequences from published and validated DsbA substrate virulence factors were taken from the original literature and used to search the publicly available UniProt database [41] for potential homologues in *E. coli*, *S.* enterica *Typhimurium* and *K. pneumoniae*. Most of the 10 factors were originally identified in those three organisms except YscC and Caf1M, which were initially reported in *Yersinia pestis*. A protein-protein BLAST search was performed using the UniProt bacterial genome database with a threshold of P < 0.0001. Unless stated otherwise, homologues were identified in pathogenic strains, i.e. *E. coli* UPEC O6:K15:H31 and EPEC O127:H6 / O55:H7, *S. enterica Typhimurium* SL1344 and non-motile *K. pneumonieae* (hvKP1 / MGH 78578 / NTUH-K2044). Sequence identity between homologues was extracted from the UniProt protein BLAST results. All other sequence alignments reported herein (e.g. for Table 1) were conducted using ClustalW2 [42].

Results

Binding Residues of EcDsbA are conserved in SeDsbA and DsbAs of Five Other *Enterobacteriaciae*

EcDsbA and SeDsbA share 86 % sequence identity and both have been characterized previously [14,43]. SeDsbA can complement EcDsbA [44] in a null mutant motility assay, indicating that SeDsbA is able to interact with the EcDsbA binding partner EcDsbB and with the EcDsbA substrate *E. coli* FlgI [45]. Both are weak disulfide reductants in the standard

insulin reduction assay for redox enzymes [43]. Both are similarly oxidizing enzymes: the redox potentials of EcDsbA and SeDsbA are -122 and -126 mV, respectively [9,43], whereas the range for all DsbAs is -80 to -163 mV (Table **1**). In both EcDsbA and SeDsbA the measured pK_a of the nucleophilic cysteine is 3.3 [7,43], though values vary across all DsbAs from 3.0 to 5.1 (Table **1**). Although disulfide bonds generally stabilize folded proteins, the disulfide form of DsbA enzymes is destabilizing [6,7]. The melting temperatures of the oxidized and reduced forms of EcDsbA and SeDsbA are almost identical (reduced 350 K and 351 K; oxidized 341 K and 342 K, respectively) [13] (Figure **S1**), whereas the range of melting temperatures across all DsbAs varies considerably (Table **1**). Importantly, the crystal structures of EcDsbA and SeDsbA can be superimposed with an RMSD of 0.8 Å for 176 Cα atoms, whereas across all structurally characterized DsbAs the RMSD with EcDsbA varies from 1.3 Å to 2.9 Å (for 122-167 Cα atoms) (Table **1**) [14].

Two catalytically relevant EcDsbA complex structures have been described, a complex between EcDsbA and EcDsbB [39,40,46] and one between EcDsbA and a peptide segment of SigA, an autotransporter protein from *Shigella flexneri* [47]. Analysis of these structures revealed that the binding interface comprises the N-terminal regions of the active site helix H1, as well as loops L1 (the first of two loops connecting the thioredoxin and helical domains), L2 (the second of two loops connecting the thioredoxin and helical domains, also referred to as the *cis*Pro loop) and L3-H7 (residues in the loop preceding and at the N-terminal region of helix H7) (Figure **1A**). A hypothesis is that DsbAs sharing overall high sequence identity with EcDsbA and with highly conserved loop lengths and residues in these regions will share similar binding activities. As shown in Figure **1B**, SeDsbA falls into this cluster as does *Shigella flexneri* (SfDsbA, P52235), *Enterobacter cloacae* (EnDsbA. E3G5L9), *Citrobacter koseri* (CkDsbA, A8AL80) and *Cronobacter sakazakii* (CsDsbA, I2ED40) and *K. pneumoniae* (KpDsbA) (Figure **1B**). Of these, the DsbA with lowest sequence identity to EcDsbA is KpDsbA (81 %) encoded by an important human pathogen responsible for many antibiotic-resistant nosocomial infections [1,48,49]. To determine whether KpDsbA falls within the same class as EcDsbA, we investigated its structure, surface, redox and binding properties and compared them with EcDsbA.

KpDsbA Complements EcDsbA *in vivo*

The *E. coli* protein FlgI is required for *E. coli* motility and, in turn, FlgI requires the DSB machinery of *E. coli* to function. FlgI function is impaired in *E. coli dsbA*$^-$ deficient (JCB817) and *dsbA*$^-$/*dsbB*$^-$ double-mutant (JCB818) strains due to the absence of EcDsbA mediated dithiol oxidase activity [50]. As a consequence, these *E. coli* strains are non-motile. Intriguingly, *K. pneumoniae* is non-motile and does not encode a FlgI homologue. We tested whether KpDsbA was able to catalyse disulfide bond formation of *E. coli* FlgI using an *in vivo* complementation strategy [3]. We demonstrated that KpDsbA – like SeDsbA [44] – can fully restore the motility of *dsbA*$^-$ deficient strains, but not in the double *dsbA*$^-$/*dsbB*$^-$ mutant cells (Figure **S2**). This experiment shows that KpDsbA is able to oxidize FlgI cysteines and this requires the presence of EcDsbB.

Some distantly related DsbAs do not complement EcDsbA in this assay, including Gram-negative *Wolbachia pipientis* α-DsbA1 [23] and Gram-positive *Staphylococcus aureus* DsbA [13]. However, rescue or partial rescue of motility has been observed for a wide range of DsbA homologues, some sharing quite low sequence identity with EcDsbA, such as VcDsbA (40 %), PaDsbA (30 %) and NmDsbA1 (23 %) [15-17,51]. Consequently, EcDsbA complementation may not be a suitable guide for categorizing DsbA enzymes into distinct classes.

KpDsbA has redox properties almost identical to those of EcDsbA and SeDsbA

EcDsbA exhibits weak insulin reductase activity in the presence of dithiothreitol [52] whereas the *E. coli* disulfide isomerase EcDsbC is highly active in this assay. Reduction of the intermolecular disulfide bonds between the A and B chains of insulin results in precipitation of the B chain and this can be monitored by measuring the OD_{650nm}. We found that purified recombinant KpDsbA has the same weak insulin reductase activity as EcDsbA (Figure **2A**) and SeDsbA [43]. The activity of other characterized DsbA enzymes varies. NmDsbA1, for example, has a much weaker activity than that of EcDsbA [15], and DsbA from *Mycobacterium tuberculosis* (MtbDsbA) is inactive in this assay [53]. In contrast, TcpG (VcDsbA) from *Vibrio cholerae* catalyses insulin reduction much faster than EcDsbA [54].

We next determined the standard redox potential of KpDsbA relative to glutathione ($[GSH]^2$/GSSG, $E^{0'}$ = -240 V). The equilibrium constant for KpDsbA was estimated from the $[GSH]^2$/GSSG titration experiment to be 61.4 ± 0.1 μM (Figure **2B**), which corresponds to a standard redox potential of -116 mV. This value falls very close to the values reported for EcDsbA (-122 mV [9]) and SeDsbA (-126 mV [43]) considering the wide range of values reported across all DsbA enzymes (-80 to -163 mV) [14].

The pK_a value of the nucleophilic cysteine in the active site CXXC motif is a key determinant of DsbA reactivity towards substrate proteins. We measured the pK_a value for the nucleophilic cysteine of KpDsbA using pH-dependent thiolate absorbance at λ = 240 nm (Figure **2C**). The pK_a^{Cys30} for KpDsbA was found to be 3.2, nearly identical to that of EcDsbA and SeDsbA (3.3) compared with the observed range for other DsbAs (3.0-5.1).

We also confirmed that reduced KpDsbA (T_m^{red} 347.1 ± 0.2 K) is more stable than oxidized KpDsbA (T_m^{ox} 335.8 ± 0.3 K) (Figure **2D**). The melting temperatures fall between values reported previously for EcDsbA (T_m^{red} 350.9 ± 0.2 K, T_m^{ox} 341.7 ± 0.2 K [7]) and those for SeDsbA (T_m^{red} 351.2 ± 0.2 K, T_m^{ox} 342.8 ± 0.4 K) reported here (Figure **S1**). Again, the range reported for all DsbAs is much wider (T_m^{red} 337-357 / T_m^{ox} 331-341 K) [51,54].

We then tested the dithiol oxidase activity of KpDsbA using a fluorescently labeled peptide substrate. The activity was monitored by the increase in europium fluorescence resulting from cyclization of the substrate peptide through formation of an intramolecular disulfide bond. In the presence of EcDsbB,

A

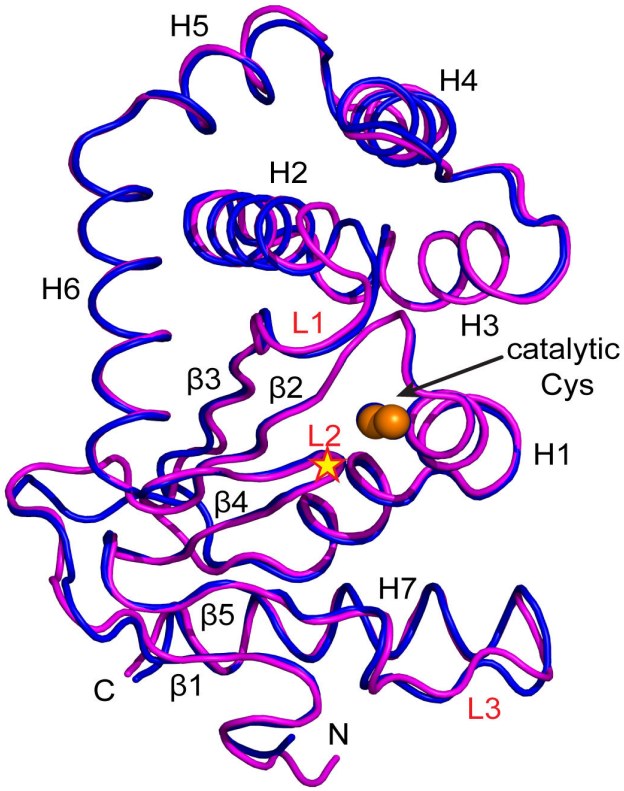

B

	Seq.ID	H1 active site helix	L1	L2	L3 to N-ter-H7
EcDsbA	100	FCPHCYQFEEVLHI	VNFMG	LRGVPA	NPQGMDTSNMDVF
SfDsbA	100	FCPHCYQFEEVLHI	VNFLG	LRGVPA	NPQGMDTSNMDVF
SeDsbA	86	YCPHCYQFEEVLHV	VEFLG	LQGVPA	NPQGMDTSSMDVF
CkDsbA	84	YCPHCYQFEEVLHV	VEFLG	LQGVPA	NPQGMDTSSMDIF
EnDsbA	84	YCPHCYQFEEVLHV	VEFLG	LQGVPA	NPQGMDTSNMDAF
CsDsbA	82	YCPHCYQFEEVLHV	VEFLG	LQGVPA	NPQGMDTSNMDVF
KpDsbA	81	YCPHCYQFEEVLHV	VEFLG	LQGVPA	NPQGMDTSNMDVF

Figure 1. Comparison of EcDsbA and SeDsbA. **A**. Structural superposition of EcDsbA (magenta, PDB id: 1FVK) and SeDsbA (blue, PDB Id: 3L9S). N- and C-termini, helices (H1 - 7) and strands (β1-5) are indicated. In addition, surface loops (L1 – L3) predicted to be involved in binding EcDsbB periplasmic loop P2 or substrate are labeled in red. Active site cysteines are shown as orange spheres and the *cis*Pro motif in the L2 loop is indicated by a yellow star. **B**. Sequences of EcDsbA loops that bind DsbB (blue/red) or SigA substrate (blue). Homologues with highly conserved loop sequences are shown: *S. flexneri* (SfDsbA, P52235), *S. enterica Typhimurium* (SeDsbA E1WE53), *C. koseri* (CkDsbA, A8AL80), *E. cloacae* (EnDsbA, E3G5L9), *C. sakazakii* (CsDsbA, I2ED40) and *K. pneumoniae* (KpDsbA B5XZJ6). Conserved residues are shown in grey, and variable residues in black.
doi: 10.1371/journal.pone.0080210.g001

we found that the rate for KpDsbA and SeDsbA catalyzed disulfide bond formation was almost indistinguishable from that of EcDsbA measured at the same concentration of enzyme (Figure **3**). This result suggests that KpDsbA (and SeDsbA) is able to interact in the same way as EcDsbA with the peptide substrate and with EcDsbB. TcpG has a similar activity to EcDsbA in this assay [54], whereas MtbDsbA is inactive in the presence of EcDsbB [53].

Crystal structure of reduced KpDsbA

We determined the crystal structure of reduced KpDsbA (PDB: 4MCU) at 1.99 Å resolution by molecular replacement, using EcDsbA as the template. As expected, the structure is very similar to that of EcDsbA (Figure **4A**). The asymmetric unit contains six KpDsbA molecules each adopting the typical DsbA fold. Structural superposition of these six independent copies yielded a root mean square deviation (RMSD) < 0.45 Å for 176 Cα atoms between residues Gly6 - Val181. Likewise, structural

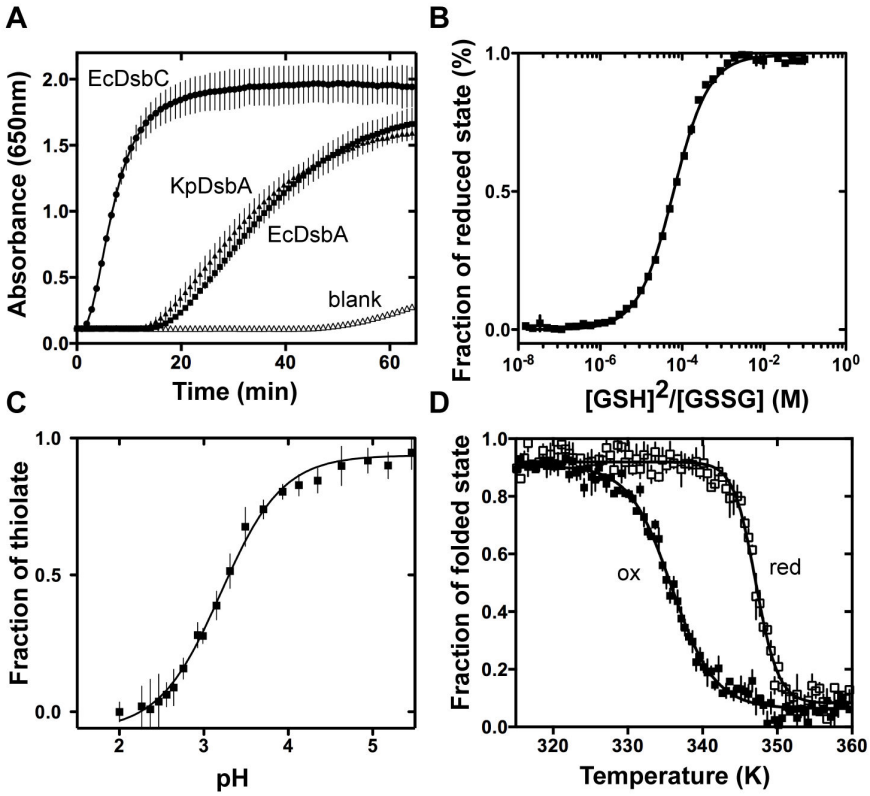

Figure 2. KpDsbA redox properties. **A**. Disulfide bond reduction activity of KpDsbA (▲), EcDsbA (■) EcDsbC (●) and a control without enzyme (△) was monitored spectrophotometrically. SeDsbA activity has been published elsewhere [43]. **B**. Redox equilibria of KpDsbA with glutathione (GSH/GSSG). **C**. Determination of the nucleophilic Cys33 (CXXC) pK_a. The pH-dependent absorbance of the thiolate anion at 240 nm was fitted to the Henderson-Hasselbach equation **D**. Temperature induced unfolding of oxidized (ox, ■) and reduced (red, □) KpDsbA was determined by far-UV CD spectroscopy, showing that the reduced form is more stable than the oxidized form.

doi: 10.1371/journal.pone.0080210.g002

alignment of KpDsbA with EcDsbA (1FVK, 1.7 Å, molecule B) and SeDsbA (3L9S, 1.6 Å) gave RMSD values < 0.9 Å for the identical range of 176 Cα atoms. By comparison, high resolution crystal structures of distantly related DsbAs have much higher RMSDs covering a smaller range of equivalent Cα atoms (e.g. PaDsbA (PDB code 3H93) and EcDsbA (1FVK, molecule B), 161 Cα atoms RMSD of 2.4 Å) [16]. These higher values are a consequence of structural deviations including a truncated helix H7 and a shortened hydrophobic groove.

The structure of the catalytic site of KpDsbA is strictly conserved with that of EcDsbA, comprising the active site motif ^{30}Cys-Pro-His-Cys^{33} located at the N-terminal end of helix H1 and the adjacent *cis*Pro (Val-Pro^{151}) L2 loop (Figure **4B**). The cysteine residues (Cys30 and Cys33) are present in the reduced state in the crystal structure. A hydrophobic patch and a large groove surrounds the nucleophilic Cys30, as also occurs in EcDsbA and SeDsbA (Figure **4C**). As expected, these surface features are lined with residues contributed from the L1, L2 and L3 loops.

The six independent copies of KpDsbA in the crystal structure allow an analysis of conformational variability of the loop residues forming the binding surface. This revealed that the side chains of His32, Phe63, Leu64, Gln147, Thr167 and Met170 adopt various rotamer conformations, whereas there is no evidence of conformational variability in Tyr29, Cys30, Pro31, Val149, Pro150, and Phe173 (Figure **5A**). The side chain variations do not influence the surface accessibility of the hydrophobic groove, which was calculated to be 371 ± 32 Å^2 by CastP [33] across the 6 molecules. Moreover, the hydrophobic nature of the groove is unaffected by the side chain conformational variability as indicated by the proportion of carbon atoms lining this groove (69 ± 3 %) [33].

NMR Solution Structure of KpDsbA is Similar to the Crystal Structure

Previous studies have demonstrated that there are minimal differences between reported structures (crystal and NMR) of oxidized and reduced EcDsbA. To determine if this was also

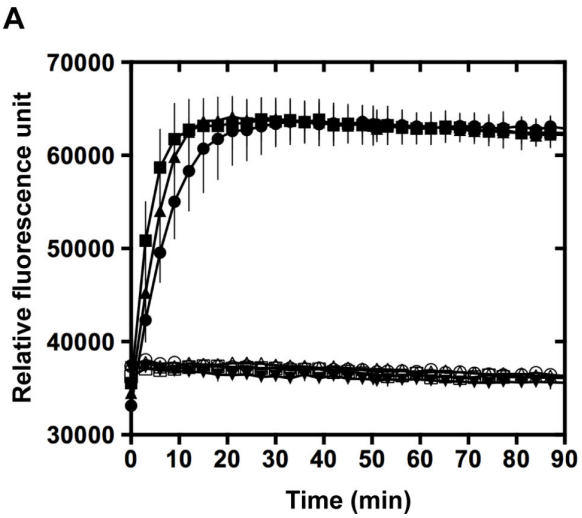

Figure 3. ***In vitro*** **peptide dithiol oxidation.** **A**. Dithiol oxidase activities of EcDsbA (■), SeDsbA (●) and KpDsbA (⑩) were monitored using a fluorescently labeled peptide substrate. Samples lacking the partner protein EcDsbB (KpDsbA/peptide △), EcDsbA/peptide □, SeDsbA/peptide ○, or buffer alone ▼) showed no increase in signal over the same time period.
doi: 10.1371/journal.pone.0080210.g003

the case for KpDsbA, a semi-automated NMR approach was used to determine the structure of oxidized KpDsbA (PDB ID: 2MBS, BMRB ID: 19413). Following UNIO-ATNOS/ASCAN, manual verification and refinement enabled assignment of 89.2 % of the non-labile proton resonances in KpDsbA. These were used to generate the NOE-based distance constraints for final structure calculation. Twenty conformers with lowest target function and least violations of input restraints were chosen to represent the structure of oxidized KpDsbA (Figure **S4 A/B**). It was not possible to assign several backbone amide resonances corresponding to residues in the β1- β2 loop (Ile16, Gly18, Glu19, Gln21, Val22, Leu23), so that this region appears to be largely disordered in the NMR ensemble compared with the rest of the structure. The backbone (N, Cα, C') and all-heavy atom RMSD for the 179 well-defined residues (1–15, 24-187) of the 20 KpDsbA conformers were 0.67 ± 0.17 Å and 1.03 ± 0.13 Å, respectively. Structural statistics are summarized in Table 3. As observed for other DsbA structures, the individual thioredoxin and helical domains can be superimposed with higher precision than the entire structure. This is most likely due to inter-domain motion, which has also been reported in the structures of EcDsbA [55] and VcDsbA [56]. Residues which fall into disallowed Ramachandran regions include the unassigned residues Glu19, Gln21, Val22, and His32, and residues in loop regions, i.e. Lys55, Phe63, Leu64, Asn155 and Met170.

The overall conformation of the NMR structure of oxidized KpDsbA is similar to that of the crystal structure of reduced KpDsbA (Figure 5C). For example, superposition of molecule A in the crystal structure of reduced KpDsbA with the first structure in the NMR ensemble of oxidized KpDsbA, yields an RMSD of 1.09 Å over 169 Cα atoms. To make a similar comparison, the crystal structures of oxidized (1FVK, molecule B) and reduced (1A2L, molecule B) EcDsbA have an RMSD of 0.45 Å (over 186 Cα atoms) and the crystal structure of oxidized EcDsbA (1FVK, molecule B) and the first structure in the NMR ensemble of reduced EcDsbA (1A24) have an RMSD of 1.95 Å over 181 Cα atoms [57,58].

The structures of the catalytic sites and hydrophobic surface features are similar, considering that the cysteines of the CXXC motif are oxidized in the NMR structure and reduced in the crystal structure (Figure **S4C**). As has been noted previously for other DsbA solution and crystal structures [56,59], L3 of KpDsbA is a relatively flexible part of the protein in both NMR and crystal structures (Figure **5B and C**). Thus, overall the structures of oxidized and reduced KpDsbA are similar, notwithstanding the different conditions and approaches used for structure determination.

Binding Affinity of DsbB peptides is similar for KpDsbA and EcDsbA

The similar surface features and similar predicted binding residues of KpDsbA and EcDsbA suggested that these enzymes would interact with binding partners with similar affinity. The crystal structures of the EcDsbA:EcDsbB complex showed that the second periplasmic loop P2 of EcDsbB binds directly to EcDsbA [39,40]. The binding residues are 98-PSPFATCD-104 and these are highly conserved in KpDsbB (98-PSPFQTCD-104). These two P2 peptides were synthesized and isothermal titration calorimetry (ITC) was used to assess their binding affinity for both enzymes. KpDsbA and EcDsbA were found to bind to PSPFATCD and PSPFQTCD with similar affinities (K_d 11-18 μM, Table **4**, Figure **S3A**). We investigated the interaction of KpDsbA with PSPFQTCD by structural superposition of KpDsbA onto the structure of EcDsbA in the EcDsbA:EcDsbB complex structure. Residue Ala of EcDsbB PSPFATCD was mutated *in silico* to PSPFQTCD, using the most commonly observed rotamer for glutamine. The superimposed model showed that the P2 loop matched the surface of KpDsbA very well, with no clashes apparent between the P2 residues and KpDsbA (Figure **S3B**).

Discussion

We have shown that the structural, surface, redox and binding properties of EcDsbA, SeDsbA and KpDsbA enzymes are highly conserved, and that these three DsbAs and four other DsbAs (from *Enterobacter cloacae*, *Citrobacter koseri*, *Shigella flexneri* and *Cronobacter sakazakii*) might be considered an *Enterobacteriaceae* subclass of DsbA. Carbapenem-resistant *Enterobacteriaceae* are responsible for a large proportion of difficult to treat community- and hospital-acquired infections [60] and there is an urgent need to develop novel therapeutic strategies to tackle these so-called 'super bugs' [61].

One approach to generate new classes of antibacterials is to target virulence rather than viability of bacteria. An antivirulence approach is predicted to lead to less selective

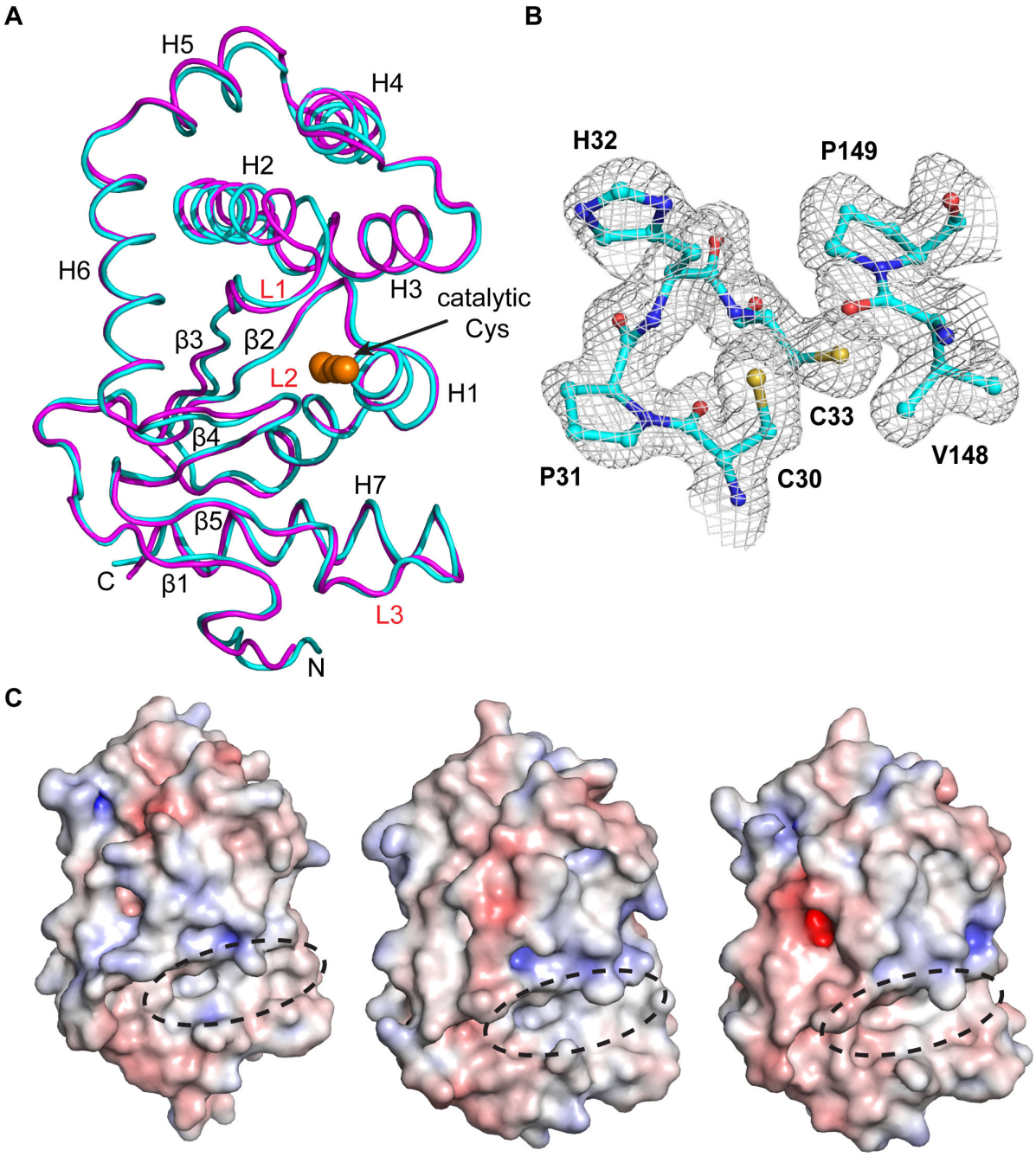

Figure 4. Crystal structure of KpDsbA. **A**. Superposition of crystal structures of KpDsbA (cyan, PDB Id: 4MCU) and EcDsbA (magenta, PDB id: 1FVK). The N- and C-termini, helices (H1 - 7) and strands (β1-5) are indicated. Surface loops L1 – L3 are labeled in red, and active site cysteines are shown as orange spheres. **B**. Electron density in the active site region of KpDsbA indicates that the cysteines are reduced. The 2Fo - Fc map was created using Phenix (model-map correlations) [30] and is contoured at 1.0 σ C. Electrostatic surface representation of EcDsbA, SeDsbA and KpDsbA (left, middle, right). Positive and negative electrostatic potentials are contoured from blue (+7.5 kT/e) to red (-7.5 kT/e). The hydrophobic grooves of all three enzymes are indicated by a dashed oval [8,43].

doi: 10.1371/journal.pone.0080210.g004

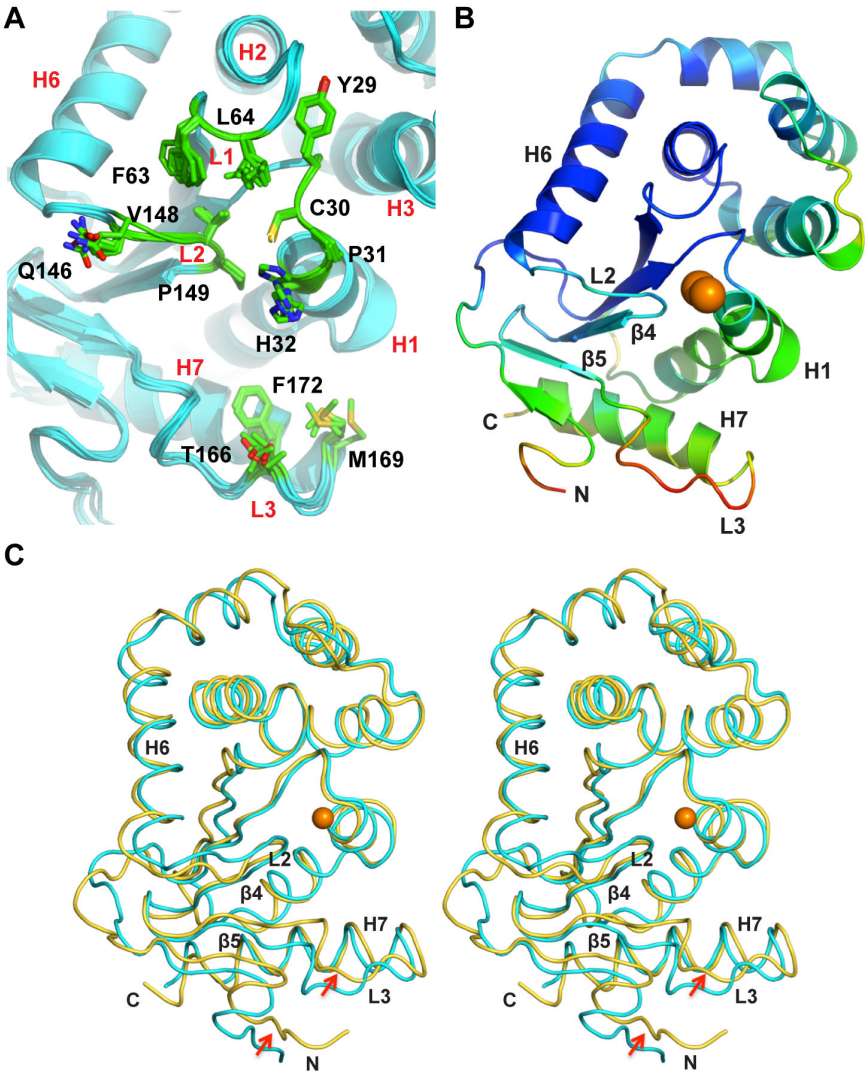

Figure 5. Conformational variability in X-ray and NMR structures of KpDsbA. A Superimposition of the six KpDsbA molecules (blue) in the asymmetric unit shows the limited conformational variability in the side chains of active site and L1, L2, and L3 loop residues (stick representation). **B**. Cartoon representation of the KpDsbA crystal structure (Molecule D), with C_α atoms colored by temperature factor (B-factor). Molecule D was selected as its temperature factor distribution is the most pronounced due to minimal crystallographic contacts. In particular, the high B-factor of loop L3 indicates mobility in that region, consistent with the NMR data **C**. Stereo diagram of representative states of reduced (X-ray, cyan) and oxidized (NMR, yellow) structures of KpDsbA. Red arrows highlight differences in the structures at N-terminal and L3 loop regions.

doi: 10.1371/journal.pone.0080210.g005

pressure for resistance development, since most virulence traits are not essential for survival [62]. Targeting virulence may also expand the repertoire of antimicrobial targets, preserve the endogenous host microbiome and extend the lifespan of conventional antibiotics [61]. Most antivirulence strategies developed to date target individual virulence factors [61-65] and this has yielded some successes [66,67]. However, the armory of DsbA substrate virulence factors expressed in different *Enterobacteriaceae* varies (Figure **6**), so that drugs targeting specific virulence factors may not be effective against all *Enterobacteriaceae*. On the other hand, DsbA itself catalyzes assembly of many virulence factors [68-70] and DsbA knockouts severely attenuate virulence in infection models [12]. Targeting DsbA is therefore a compelling approach for the development of anti-virulence agents, because DsbA inhibitors should inhibit a range of virulence traits. Significantly, our findings point to the opportunity to

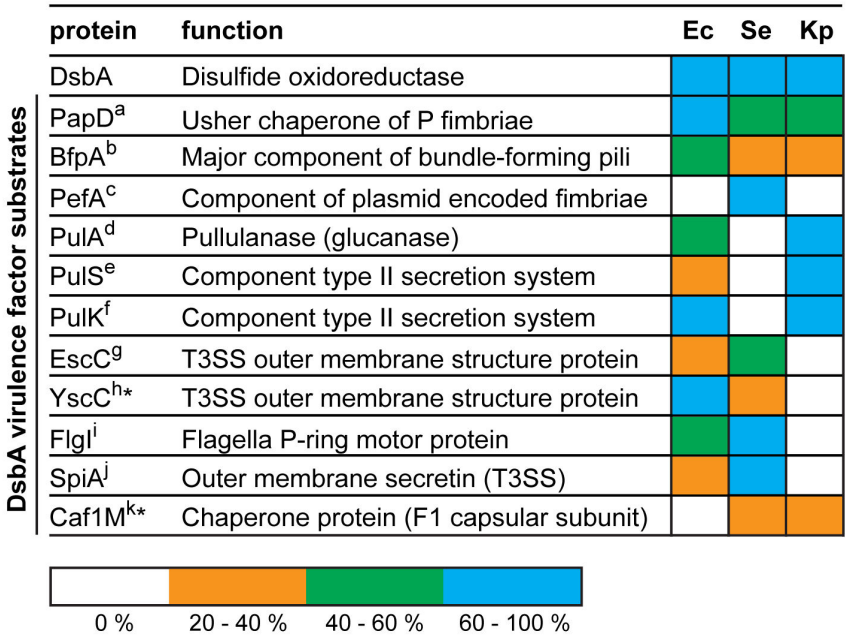

Figure 6. Conservation of DsbA substrate virulence factors. Comparison of the sequence conservation of DsbA oxidoreductases from *E. coli* (Ec), *S. enterica Typhimurium* (Se) and *K. pneumonia* (Kp) and of characterized DsbA substrate virulence factors. Sequence identities relative to the characterized substrate protein are represented in different colours, as shown in the key. White squares indicate the lack of a sequence homologue in the specific bacteria. *YscC and Caf1M were identified as DsbA substrate proteins in *Yersinia pestis* [71,72]. [a] [68], [b] [73], [c] [44], [d] [74], [e,f] [75], [g] [5], [h,k] [71,72], [i] [45], [j] [69].
doi: 10.1371/journal.pone.0080210.g006

develop a single antivirulence drug effective against DsbAs encoded by at least seven *Enterobacteriaceae* pathogens.

The crystal structure and NMR solution structure of KpDsbA (the latter derived by semi-automated approaches) reported here are in excellent agreement. The availability of structural data for KpDsbA opens up the possibility of using structure-based approaches to generate DsbA inhibitors. Moreover, the close similarity of the crystal and NMR structures, and the use of semi-automated NMR, highlights how NMR can be used as an efficient first screen in e.g. drug-like fragment campaigns. By contrast, the six molecules in the asymmetric unit of KpDsbA crystal structure is far from ideal for rapid fragment-screening, but is nevertheless advantageous for follow up analysis.

Taken together, our data show that DsbA enzymes sharing >80% sequence identity with EcDsbA also share almost identical redox and surface properties and can thus be categorized as a distinct DsbA subclass. Further analyses will be required to determine how many subclasses of DsbA exist, and whether DsbAs with lower than 80% sequence identity will fall into the EcDsbA-like class. Importantly, our results suggest that compounds designed to inhibit EcDsbA will likely inhibit all DsbAs within the same class. Finally, we propose that compounds that bind KpDsbA might be identified rapidly using semi-automated NMR approaches, and that development of 'hits' to optimise potency can be achieved using a pipeline comprising biochemical and structural assays similar to those outlined herein.

Supporting Information

Figure S1. Thermal unfolding of SeDsbA. A. Temperature-induced unfolding of oxidized (ox, ν) and reduced (red, θ) SeDsbA was monitored by far-UV CD spectroscopy. Unfolding was monitored in 1 K steps from 298 K to 368 K. Normalized average data points of three measurements were fitted to a two-state folding model. The reduced state of SeDsbA (351.2 +/- 0.2 K) is 9 K more stable than its oxidized (342.8 +/- 0.4 K) form.
(TIF)

Figure S2. Summary of *in vivo* complementation of KpDsbA and EcDsbA (A). *E. coli* cells lacking *dsbA*$^-$ (JCB817) or *dsbA*$^-$ */dsbB*$^-$ (JCB818) are non-motile. Expression of KpDsbA or EcDsbA can rescue the swarming of *E. coli dsbA*$^-$ (JCB817) but not of *dsbA*$^-$ */dsbB*$^-$ cells. Expression of KpDsbA or EcDsbA is induced by inclusion of arabinose (arab).
(TIF)

Figure S3. Binding studies of PSPFQTCD to KpDsbA. A. Representative ITC profile for PSPFQTCD peptide binding to EcDsbA. For all combinations tested see Table 4. **B**. Model of

the interaction of the KpDsbA (molecule A) with PSPFQTCD generated by structural superposition on the EcDsbA:EcDsbB complex [76].
(TIF)

Figure S4. NMR structure of oxidized KpDsbA. A. Overlay of the 20 NMR models; disordered region highlighted in blue. **B**. lowest energy NMR conformer. c. magnification of the active site region showing the disulfide bond formed between the cysteines in the averaged NMR solution structure of oxidized KpDsbA.
(TIF)

Acknowledgements

We thank the Australasian Crystallography School, especially Prof. Eleanor Dodson FRS for her advice and support to FK in solving the molecular replacement problem for KpDsbA. We thank the beam-line support team at the Australian Synchrotron for data collection advice and acknowledge use of the University of Queensland Remote Operation Crystallization and X-ray (UQ ROCX) Diffraction Facility and thank Mr Karl Byriel and Mr Gordon King for their expert assistance.

Author Contributions

Conceived and designed the experiments: FK KR MJS JLM. Performed the experiments: FK KR LP BM WD MH SRS BH. Analyzed the data: FK KR LP BM WD MH BH MJS JLM. Contributed reagents/materials/analysis tools: FK KR SRS DPF MJS JLM. Wrote the manuscript: FK KR LP MJS JLM. Provided critical comment on the manuscript: JLM FK KR LP BM WD MH SRS BH DPF MJS.

References

1. Souli M, Galani I, Giamarellou H (2008) Emergence of extensively drug-resistant and pandrug-resistant Gram-negative bacilli in Europe. Euro Surveill 13(47): 19045. PubMed: 19021957.
2. Heras B, Shouldice SR, Totsika M, Scanlon MJ, Schembri MA et al. (2009) DSB proteins and bacterial pathogenicity. Nat Rev Microbiol 7: 215-225. doi:10.1038/nrmicro2087. PubMed: 19198617.
3. Bardwell JC, McGovern K, Beckwith J (1991) Identification of a protein required for disulfide bond formation in vivo. Cell 67: 581-589. doi: 10.1016/0092-8674(91)90532-4. PubMed: 1934062.
4. Dutton RJ, Boyd D, Berkmen M, Beckwith J (2008) Bacterial species exhibit diversity in their mechanisms and capacity for protein disulfide bond formation. Proc Natl Acad Sci U S A 105: 11933-11938. doi: 10.1073/pnas.0804621105. PubMed: 18695247.
5. Miki T, Okada N, Kim Y, Abe A, Danbara H (2008) DsbA directs efficient expression of outer membrane secretin EscC of the enteropathogenic Escherichia coli type III secretion apparatus. Microb Pathog 44: 151-158. doi:10.1016/j.micpath.2007.09.001. PubMed: 17933489.
6. Wunderlich M, Glockshuber R (1993) Redox properties of protein disulfide isomerase (DsbA) from Escherichia coli. Protein Sci 2: 717-726. doi:10.1002/pro.5560020503. PubMed: 8495194.
7. Zapun A, Bardwell JC, Creighton TE (1993) The reactive and destabilizing disulfide bond of DsbA, a protein required for protein disulfide bond formation in vivo. Biochemistry 32: 5083-5092. doi: 10.1021/bi00070a016. PubMed: 8494885.
8. Martin JL, Bardwell JC, Kuriyan J (1993) Crystal structure of the DsbA protein required for disulphide bond formation in vivo. Nature 365: 464-468. doi:10.1038/365464a0. PubMed: 8413591.
9. Huber-Wunderlich M, Glockshuber R (1998) A single dipeptide sequence modulates the redox properties of a whole enzyme family. Fold Des 3: 161-171. doi:10.1016/S1359-0278(98)00024-8. PubMed: 9562546.
10. Kobayashi T, Kishigami S, Sone M, Inokuchi H, Mogi T et al. (1997) Respiratory chain is required to maintain oxidized states of the DsbA-DsbB disulfide bond formation system in aerobically growing Escherichia coli cells. Proc Natl Acad Sci U S A 94: 11857-11862. doi: 10.1073/pnas.94.22.11857. PubMed: 9342327.
11. Ireland PM, McMahon RM, Marshall LE, Halili M, Furlong et al. (: Sep 202013) Disarming Burkholderia pseudomallei: Structural and functional characterisation of a disulfide oxidoreductase (DsbA) required for virulence in vivo. Antioxid Redox Signal: Sep 20 Epub.
12. Totsika M, Heras B, Wurpel DJ, Schembri MA (2009) Characterization of two homologous disulfide bond systems involved in virulence factor biogenesis in uropathogenic Escherichia coli CFT073. J Bacteriol 191: 3901-3908. doi:10.1128/JB.00143-09. PubMed: 19376849.
13. Heras B, Kurz M, Jarrott R, Shouldice SR, Frei P et al. (2008) Staphylococcus aureus DsbA does not have a destabilizing disulfide. A new paradigm for bacterial oxidative folding. J Biol Chem 283: 4261-4271. PubMed: 18077463.
14. Shouldice SR, Heras B, Walden PM, Totsika M, Schembri MA et al. (2011) Structure and function of DsbA, a key bacterial oxidative folding catalyst. Antioxid Redox Signal 14: 1729-1760. doi:10.1089/ars.2010.3344. PubMed: 21241169.
15. Vivian JP, Scoullar J, Rimmer K, Bushell SR, Beddoe T et al. (2009) Structure and function of the oxidoreductase DsbA1 from Neisseria meningitidis. J Mol Biol 394: 931-943. doi:10.1016/j.jmb.2009.09.065. PubMed: 19815019.
16. Shouldice SR, Heras B, Jarrott R, Sharma P, Scanlon MJ et al. (2010) Characterization of the DsbA oxidative folding catalyst from Pseudomonas aeruginosa reveals a highly oxidizing protein that binds small molecules. Antioxid Redox Signal 12: 921-931. doi:10.1089/ars.2009.2736. PubMed: 19788398.
17. Hu SH, Peek JA, Rattigan E, Taylor RK, Martin JL (1997) Structure of TcpG, the DsbA protein folding catalyst from Vibrio cholerae. J Mol Biol 268: 137-146. doi:10.1006/jmbi.1997.0940. PubMed: 9149147.
18. Studier FW (2005) Protein production by auto-induction in high density shaking cultures. Protein Expr Purif 41: 207-234. doi:10.1016/j.pep.2005.01.016. PubMed: 15915565.
19. Bader M, Muse W, Zander T, Bardwell J (1998) Reconstitution of a protein disulfide catalytic system. J Biol Chem 273: 10302-10307. doi: 10.1074/jbc.273.17.10302. PubMed: 9553083.
20. Holmgren A (1979) Thioredoxin catalyzes the reduction of insulin disulfides by dithiothreitol and dihydrolipoamide. J Biol Chem 254: 9627-9632. PubMed: 385588.
21. Nelson JW, Creighton TE (1994) Reactivity and ionization of the active site cysteine residues of DsbA, a protein required for disulfide bond formation in vivo. Biochemistry 33: 5974-5983. doi:10.1021/bi00185a039. PubMed: 8180227.
22. Ellman GL (1959) Tissue sulfhydryl groups. Arch Biochem Biophys 82: 70-77. doi:10.1016/0003-9861(59)90090-6. PubMed: 13650640.
23. Kurz M, Iturbe-Ormaetxe I, Jarrott R, Shouldice SR, Wouters MA et al. (2009) Structural and functional characterization of the oxidoreductase alpha-DsbA1 from Wolbachia pipientis. Antioxid Redox Signal 11: 1485-1500. doi:10.1089/ars.2008.2420. PubMed: 19265485.
24. McPhillips TM, McPhillips SE, Chiu HJ, Cohen AE, Deacon AM et al. (2002) Blu-Ice and the Distributed Control System: software for data acquisition and instrument control at macromolecular crystallography beamlines. J Synchrotron Radiat 9: 401-406. doi:10.1107/S0909049502015170. PubMed: 12409628.
25. Battye TG, Kontogiannis L, Johnson O, Powell HR, Leslie AG (2011) iMOSFLM: a new graphical interface for diffraction-image processing with MOSFLM. Acta Crystallogr D Biol Crystallogr 67: 271-281. doi: 10.1107/S0907444910048675. PubMed: 21460445.
26. Kabsch W (2010) Xds. Acta Crystallogr D Biol Crystallogr 66: 125-132. doi:10.1107/S0907444909047337. PubMed: 20124692.
27. Evans P (2006) Scaling and assessment of data quality. Acta Crystallogr D Biol Crystallogr 62: 72-82. doi:10.1107/S0108767306098564. PubMed: 16369096.
28. McCoy AJ, Grosse-Kunstleve RW, Adams PD, Winn MD, Storoni LC et al. (2007) Phaser crystallographic software. J Appl Crystallogr 40: 658-674. doi:10.1107/S0021889807021206. PubMed: 19461840.

29. Emsley P, Lohkamp B, Scott WG, Cowtan K (2010) Features and development of Coot. Acta Crystallogr D Biol Crystallogr 66: 486-501. doi:10.1107/S0907444910007493. PubMed: 20383002.
30. Adams PD, Afonine PV, Bunkóczi G, Chen VB, Davis IW et al. (2010) PHENIX: a comprehensive Python-based system for macromolecular structure solution. Acta Crystallogr D Biol Crystallogr 66: 213-221. doi: 10.1107/S0907444909052925. PubMed: 20124702.
31. Chen VB, Arendall WB 3rd, Headd JJ, Keedy DA, Immormino RM et al. (2010) MolProbity: all-atom structure validation for macromolecular crystallography. Acta Crystallogr D Biol Crystallogr 66: 12-21. doi: 10.1107/S1744309109042018. PubMed: 20057044.
32. Baker NA, Sept D, Joseph S, Holst MJ, McCammon JA (2001) Electrostatics of nanosystems: application to microtubules and the ribosome. Proc Natl Acad Sci U S A 98: 10037-10041. doi:10.1073/pnas.181342398. PubMed: 11517324.
33. Dundas J, Ouyang Z, Tseng J, Binkowski A, Turpaz Y et al. (2006) CASTp: computed atlas of surface topography of proteins with structural and topographical mapping of functionally annotated residues. Nucleic Acids Res 34: W116-W118. doi:10.1093/nar/gkl601. PubMed: 16844972.
34. Li Z, Ye Y, Godzik A (2006) Flexible Structural Neighborhood - a database of protein structural similarities and alignments. Nucleic Acids Res 34: D277-D280. doi:10.1093/nar/gkj124. PubMed: 16381864.
35. Fiorito F, Herrmann T, Damberger FF, Wuthrich K (2008) Autom Automated amino acid side-chain NMR assignment of proteins using (13)C- and (15)N-resolved 3D [(1)H, (1)H]-NOESY. J Biomol NMR 42: 23-33
36. Mohanty B, Serrano P, Pedrini B, Jaudzems K, Geralt M et al. (2010) Comparison of NMR and crystal structures for the proteins TM1112 and TM1367. Acta Crystallogr Sect F Struct Biol Cryst Commun 66: 1381-1392. doi:10.1107/S1744309110020956. PubMed: 20944235.
37. Güntert P (2004) Automated NMR structure calculation with CYANA. Methods Mol Biol 278: 353-378. PubMed: 15318003.
38. Koradi R, Billeter M, Wüthrich K (1996) MOLMOL: a program for display and analysis of macromolecular structures. J Mol Graph 14: 29-55. 8744573.
39. Inaba K, Murakami S, Suzuki M, Nakagawa A, Yamashita E et al. (2006) Crystal structure of the DsbB-DsbA complex reveals a mechanism of disulfide bond generation. Cell 127: 789-801. doi: 10.1016/j.cell.2006.10.034. PubMed: 17110337.
40. Malojcić G, Owen RL, Grimshaw JP, Glockshuber R (2008) Preparation and structure of the charge-transfer intermediate of the transmembrane redox catalyst DsbB. FEBS Lett 582: 3301-3307. doi:10.1016/j.febslet.2008.07.063. PubMed: 18775700.
41. UniProt Consortium (2012) Reorganizing the protein space at the Universal Protein Resource (UniProt). Nucleic Acids Res 40: D71-D75. doi:10.1093/nar/gkr981. PubMed: 22102590.
42. Larkin MA, Blackshields G, Brown NP, Chenna R, McGettigan PA et al. (2007) Clustal W and Clustal X version 2.0. Bioinformatics 23: 2947-2948. doi:10.1093/bioinformatics/btm404. PubMed: 17846036.
43. Heras B, Totsika M, Jarrott R, Shouldice SR, Guncar G et al. (2010) Structural and functional characterization of three DsbA paralogues from Salmonella enterica serovar typhimurium. J Biol Chem 285: 18423-18432. doi:10.1074/jbc.M110.101360. PubMed: 20233716.
44. Bouwman CW, Kohli M, Killoran A, Touchie GA, Kadner RJ et al. (2003) Characterization of SrgA, a Salmonella enterica serovar Typhimurium virulence plasmid-encoded paralogue of the disulfide oxidoreductase DsbA, essential for biogenesis of plasmid-encoded fimbriae. J Bacteriol 185: 991-1000. doi:10.1128/JB.185.3.991-1000.2003. PubMed: 12533475.
45. Hiniker A, Bardwell JC (2004) In vivo substrate specificity of periplasmic disulfide oxidoreductases. J Biol Chem 279: 12967-12973. PubMed: 14726535.
46. Inaba K, Ito K (2008) Structure and mechanisms of the DsbB-DsbA disulfide bond generation machine. Biochim Biophys Acta 1783: 520-529. doi:10.1016/j.bbamcr.2007.11.006. PubMed: 18082634.
47. Paxman JJ, Borg NA, Horne J, Thompson PE, Chin Y et al. (2009) The structure of the bacterial oxidoreductase enzyme DsbA in complex with a peptide reveals a basis for substrate specificity in the catalytic cycle of DsbA enzymes. J Biol Chem 284: 17835-17845. doi:10.1074/jbc.M109.011502. PubMed: 19389711.
48. Boucher HW, Talbot GH, Bradley JS, Edwards JE, Gilbert D et al. (2009) Bad bugs, no drugs: no ESKAPE! An update from the Infectious Diseases Society of America. Clin Infect Dis 48: 1-12. doi: 10.1086/591855. PubMed: 19035777.
49. Keynan Y, Rubinstein E (2007) The changing face of Klebsiella pneumoniae infections in the community. Int J Antimicrob Agents 30: 385-389. doi:10.1016/j.ijantimicag.2007.06.019. PubMed: 17716872.
50. Dailey FE, Berg HC (1993) Mutants in disulfide bond formation that disrupt flagellar assembly in Escherichia coli. Proc Natl Acad Sci U S A 90: 1043-1047. doi:10.1073/pnas.90.3.1043. PubMed: 8503954.
51. Lafaye C, Iwema T, Carpentier P, Jullian-Binard C, Kroll JS et al. (2009) Biochemical and structural study of the homologues of the thiol-disulfide oxidoreductase DsbA in Neisseria meningitidis. J Mol Biol 392: 952-966. doi:10.1016/j.jmb.2009.07.056. PubMed: 19631659.
52. Hillson DA, Lambert N, Freedman RB (1984) Formation and isomerization of disulfide bonds in proteins: protein disulfide-isomerase. Methods Enzymol 107: 281-294. doi:10.1016/0076-6879(84)07018-X. PubMed: 6503714.
53. Premkumar L, Heras B, Duprez W, Walden P, Halili M et al. (2013) Rv2969c, essential for optimal growth in Mycobacterium tuberculosis, is a DsbA-like enzyme that interacts with VKOR-derived peptides and has atypical features of DsbA-like disulfide oxidases. Acta Crystallogr D Biol Crystallogr 69: 1981-1994. doi:10.1107/S0907444913017800. PubMed: 24100317.
54. Walden PM, Heras B, Chen KE, Halili MA, Rimmer K et al. (2012) The 1.2 Å resolution crystal structure of TcpG, the Vibrio cholerae DsbA disulfide-forming protein required for pilus and cholera-toxin production. Acta Crystallogr D Biol Crystallogr 68: 1290-1302. doi:10.1107/S0907444912026388. PubMed: 22993083.
55. Guddat LW, Bardwell JC, Zander T, Martin JL (1997) The uncharged surface features surrounding the active site of Escherichia coli DsbA are conserved and are implicated in peptide binding. Protein Sci 6: 1148-1156. doi:10.1002/pro.5560060603. PubMed: 9194175.
56. Horne J, d'Auvergne EJ, Coles M, Velkov T, Chin Y et al. (2007) Probing the flexibility of the DsbA oxidoreductase from Vibrio cholerae - a 15N - 1H heteronuclear NMR relaxation analysis of oxidized and reduced forms of DsbA. J Mol Biol 371: 703-716. doi:10.1016/j.jmb.2007.05.067. PubMed: 17585933.
57. Guddat LW, Bardwell JC, Glockshuber R, Huber-Wunderlich M, Zander T et al. (1997) Structural analysis of three His32 mutants of DsbA: support for an electrostatic role of His32 in DsbA stability. Protein Sci 6: 1893-1900. doi:10.1002/pro.5560060910. PubMed: 9300489.
58. Schirra HJ, Renner C, Czisch M, Huber-Wunderlich M, Holak TA et al. (1998) Structure of reduced DsbA from Escherichia coli in solution. Biochemistry 37: 6263-6276. doi:10.1021/bi980136y. PubMed: 9572841.
59. Guddat LW, Bardwell JC, Martin JL (1998) Crystal structures of reduced and oxidized DsbA: investigation of domain motion and thiolate stabilization. Structure 6: 757-767. doi:10.1016/S0969-2126(98)00077-X. PubMed: 9655827.
60. Ho J, Tambyah PA, Paterson DL (2010) Multiresistant Gram-negative infections: a global perspective. Curr Opin Infect Dis 23: 546-553. doi: 10.1097/QCO.0b013e32833f0d3e. PubMed: 20802331.
61. Clatworthy AE, Pierson E, Hung DT (2007) Targeting virulence: a new paradigm for antimicrobial therapy. Nat Chem Biol 3: 541-548. doi: 10.1038/nchembio.2007.24. PubMed: 17710100.
62. Rasko DA, Sperandio V (2010) Anti-virulence strategies to combat bacteria-mediated disease. Nat Rev Drug Discov 9: 117-128. doi: 10.1038/nrd3013. PubMed: 20081869.
63. Alksne LE, Projan SJ (2000) Bacterial virulence as a target for antimicrobial chemotherapy. Curr Opin Biotechnol 11: 625-636. doi: 10.1016/S0958-1669(00)00155-5. PubMed: 11102800.
64. Lee YM, Almqvist F, Hultgren SJ (2003) Targeting virulence for antimicrobial chemotherapy. Curr Opin Pharmacol 3: 513-519. doi: 10.1016/j.coph.2003.04.001. PubMed: 14559097.
65. Barczak AK, Hung DT (2009) Productive steps toward an antimicrobial targeting virulence. Curr Opin Microbiol 12: 490-496. doi:10.1016/j.mib.2009.06.012. PubMed: 19631578.
66. Pinkner JS, Remaut H, Buelens F, Miller E, Aberg V et al. (2006) Rationally designed small compounds inhibit pilus biogenesis in uropathogenic bacteria. Proc Natl Acad Sci U S A 103: 17897-17902. doi:10.1073/pnas.0606795103. PubMed: 17098869.
67. Felise HB, Nguyen HV, Pfuetzner RA, Barry KC, Jackson SR et al. (2008) An inhibitor of gram-negative bacterial virulence protein secretion. Cell Host Microbe 4: 325-336. doi:10.1016/j.chom.2008.08.001. PubMed: 18854237.
68. Jacob-Dubuisson F, Pinkner J, Xu Z, Striker R, Padmanhaban A et al. (1994) PapD chaperone function in pilus biogenesis depends on oxidant and chaperone-like activities of DsbA. Proc Natl Acad Sci U S A 91: 11552-11556. doi:10.1073/pnas.91.24.11552. PubMed: 7972100.
69. Miki T, Okada N, Danbara H (2004) Two periplasmic disulfide oxidoreductases, DsbA and SrgA, target outer membrane protein SpiA, a component of the Salmonella pathogenicity island 2 type III secretion system. J Biol Chem 279: 34631-34642. doi:10.1074/jbc.M402760200. PubMed: 15169785.

70. Lin D, Rao CV, Slauch JM (2008) The Salmonella SPI1 type three secretion system responds to periplasmic disulfide bond status via the flagellar apparatus and the RcsCDB system. J Bacteriol 190: 87-97. doi:10.1128/JB.01323-07. PubMed: 17951383.
71. Jackson MW, Plano GV (1999) DsbA is required for stable expression of outer membrane protein YscC and for efficient Yop secretion in Yersinia pestis. J Bacteriol 181: 5126-5130. PubMed: 10438793.
72. Zav'yalov VP, Chernovskaya TV, Chapman DA, Karlyshev AV, MacIntyre S et al. (1997) Influence of the conserved disulphide bond, exposed to the putative binding pocket, on the structure and function of the immunoglobulin-like molecular chaperone Caf1M of Yersinia pestis. Biochem J 324 (2): 571-578. PubMed: 9182720.
73. Zhang HZ, Donnenberg MS (1996) DsbA is required for stability of the type IV pilin of enteropathogenic escherichia coli. Mol Microbiol 21: 787-797. doi:10.1046/j.1365-2958.1996.431403.x. PubMed: 8878041.
74. Sauvonnet N, Pugsley AP (1998) The requirement for DsbA in pullulanase secretion is independent of disulphide bond formation in the enzyme. Mol Microbiol 27: 661-667. doi:10.1046/j.1365-2958.1998.00722.x. PubMed: 9489677.
75. Pugsley AP, Bayan N, Sauvonnet N (2001) Disulfide bond formation in secreton component PulK provides a possible explanation for the role of DsbA in pullulanase secretion. J Bacteriol 183: 1312-1319. doi:10.1128/JB.183.4.1312-1319.2001. PubMed: 11157944.
76. Inaba K, Murakami S, Nakagawa A, Iida H, Kinjo M et al. (2009) Dynamic nature of disulphide bond formation catalysts revealed by crystal structures of DsbB. EMBO J 28: 779-791. doi:10.1038/emboj.2009.21. PubMed: 19214188.

APPENDIX B

Acta Crystallographica Section D
Biological Crystallography
ISSN 0907-4449

Rv2969c, essential for optimal growth in *Mycobacterium tuberculosis*, is a DsbA-like enzyme that interacts with VKOR-derived peptides and has atypical features of DsbA-like disulfide oxidases

Lakshmanane Premkumar,* Begoña Heras,‡ Wilko Duprez, Patricia Walden, Maria Halili, Fabian Kurth, David P. Fairlie and Jennifer L. Martin*

Institute for Molecular Bioscience, Division of Chemistry and Structural Biology, University of Queensland, St Lucia, QLD 4067, Australia

‡ Current address: La Trobe Institute for Molecular Sciences, La Trobe University, Melbourne, Victoria 3086, Australia.

Correspondence e-mail: p.lakshmanane@imb.uq.edu.au, j.martin@imb.uq.edu.au

Received 23 April 2013
Accepted 28 June 2013

PDB Reference: Rv2969c, 4k6x

The bacterial disulfide machinery is an attractive molecular target for developing new antibacterials because it is required for the production of multiple virulence factors. The archetypal disulfide oxidase proteins in *Escherichia coli* (Ec) are DsbA and DsbB, which together form a functional unit: DsbA introduces disulfides into folding proteins and DsbB re-oxidizes DsbA to maintain it in the active form. In *Mycobacterium tuberculosis* (Mtb), no DsbB homologue is encoded but a functionally similar but structurally divergent protein, MtbVKOR, has been identified. Here, the Mtb protein Rv2969c is investigated and it is shown that it is the DsbA-like partner protein of MtbVKOR. It is found that it has the characteristic redox features of a DsbA-like protein: a highly acidic catalytic cysteine, a highly oxidizing potential and a destabilizing active-site disulfide bond. Rv2969c also has peptide-oxidizing activity and recognizes peptide segments derived from the periplasmic loops of MtbVKOR. Unlike the archetypal EcDsbA enzyme, Rv2969c has little or no activity in disulfide-reducing and disulfide-isomerase assays. The crystal structure of Rv2969c reveals a canonical DsbA fold comprising a thioredoxin domain with an embedded helical domain. However, Rv2969c diverges considerably from other DsbAs, including having an additional C-terminal helix (H8) that may restrain the mobility of the catalytic helix H1. The enzyme is also characterized by a very shallow hydrophobic binding surface and a negative electrostatic surface potential surrounding the catalytic cysteine. The structure of Rv2969c was also used to model the structure of a paralogous DsbA-like domain of the Ser/Thr protein kinase PknE. Together, these results show that Rv2969c is a DsbA-like protein with unique properties and a limited substrate-binding specificity.

1. Introduction

The devastating disease tuberculosis (TB) caused by the bacterium *Mycobacterium tuberculosis* (Mtb) is responsible for approximately two million deaths annually. The loss of effectiveness of the only available TB vaccine, Bacillus Calmette–Guérin (BCG), for people of economically productive age (15–59 years) has created an enormous drain on the world economy (World Health Organization, 2011). A major hurdle to eradicating TB is the requirement for multi-antibiotic therapy administered over a period of six to nine months (Connolly *et al.*, 2007). Multidrug-resistant (MDR) and extensively drug-resistant (XDR) Mtb strains have evolved for which therapeutic options are limited to toxic and expensive second-line and third-line reserved drugs (Phillips, 2013). Aside from MDR and XDR strains, Mtb has evolved mechanisms to succeed as an intracellular pathogen by

manipulating the host immune signalling responses (Kumar & Narayanan, 2012; Pieters, 2008). Mtb virulence factors can avert host-cell apoptosis, phagosome maturation and autophagy to gain intracellular persistence, hence restricting the adaptive immune response (Vergne *et al.*, 2004; Welin *et al.*, 2011; Songane *et al.*, 2012; Kim *et al.*, 2012). Considering that one third of the world's population is infected with TB, there is a compelling need to identify new molecular targets for the development of antituberculosis drugs as alternatives or additions to the current broad-spectrum traditional antibiotics (Raman *et al.*, 2012; Murillo *et al.*, 2007; Lou & Zhang, 2010).

Mtb cell-surface and secretory proteins are known virulence components for mycobacterial growth during infection and for continued survival in host cells (Zhou *et al.*, 2010; Scherr *et al.*, 2007; Feltcher *et al.*, 2010; DiGiuseppe Champion & Cox, 2007). Consequently, antivirulence approaches targeting individual proteins responsible for mycobacterial virulence are being intensively investigated (Feltcher *et al.*, 2010). While these approaches offer some advantages, there is also a case to be made for a therapeutic strategy that interferes with the early stages of Mtb infection and that affects multiple virulence targets.

Periplasmic disulfide-bond forming (Dsb) enzymes catalyze the oxidative folding and maturation of many toxins and surface proteins required for virulence in a range of pathogenic bacteria (Heras *et al.*, 2009). Typically, Dsb proteins include a soluble thioredoxin (Trx) fold protein DsbA, which introduces disulfide bonds into newly translocated proteins in the periplasm (Heras *et al.*, 2009; Kadokura *et al.*, 2003; Inaba, 2009), and its cognate inner membrane partner protein DsbB that keeps DsbA in the functionally active oxidized form (Inaba & Ito, 2008; Inaba *et al.*, 2006). Deletion of DsbA or DsbB has pleiotropic effects on virulence-factor production and in some cases can provide a marginal increase in sensitivity to conventional antibiotics (Hayashi *et al.*, 2000). Both DsbA and DsbB have therefore been identified as potential antibacterial targets to combat virulence of pathogenic bacteria (Heras *et al.*, 2009; Yu, 1998). DsbA and DsbB enzymes are not always conserved across bacterial species, although the oxidative-folding pathway seems to be widely required for bacterial virulence (Dutton *et al.*, 2008).

Approximately 60% of Mtb exported proteins are estimated to require a disulfide bond for activity, stability and protease resistance (Chim *et al.*, 2011; Goulding *et al.*, 2004). However, the mycobacterial genome is deficient in a DsbB sequence homologue. Moreover, a DsbA-like protein responsible for disulfide oxidase activity has not been confirmed in *Mycobacterium*, although the Mtb gene product of Rv2969c (annotated as uncharacterized) has been identified as a potential candidate DsbA (Wang *et al.*, 2011). DsbA enzymes typically comprise two domains: a noncontiguous Trx domain, which has a characteristic redox-active C*XX*C motif and a *cis*-Pro motif, and a helical domain inserted into the Trx domain. Aside from the Trx domain motifs, sequence conservation among DsbA enzymes is very low. The Mtb genome contains two genes encoding remote DsbA homologues, Rv2969c and a transmembrane serine/threonine protein kinase protein incorporating a DsbA-like domain (PknE; Rv1743; I6YBI4).

A gene adjacent to the *dsbA*-like Rv2969c gene encodes a mammalian homologue of vitamin K epoxide reductase (VKOR; Rv2968c; Dutton *et al.*, 2008). In humans, deficiency of VKOR or administration of its antagonist warfarin inhibits reduction of vitamin K 2,3-epoxide that is otherwise required for blood clotting. In an elegant series of studies, the Beckwith group proposed that MtbVKOR may represent the functional equivalent of *E. coli* DsbB (EcDsbB) and showed that MtbVKOR rescues motility of *E. coli dsbB* null cells (Dutton *et al.*, 2008; Wang *et al.*, 2011). This notion was further supported by the observation that some plants and bacteria encode a Trx-VKOR fusion protein. A crystal structure of a *Cyanobacterium* Trx-VKOR fusion confirmed that VKOR and DsbB are functionally similar but structurally divergent (Li *et al.*, 2010).

Throughout *Mycobacterium*, Rv2969c and VKOR are genetically linked. This may indicate that they are functionally related genes. Genome-wide transposon-insertion mutagenesis studies showed that these two genes are essential for the optimal growth of Mtb (Sassetti *et al.*, 2003). This is in agreement with the observation that deletion of VKOR in *M. smegmatis* confers severe growth defects (Wang *et al.*, 2011). Moreover, the anticoagulant medication warfarin can inhibit growth of Mtb in a VKOR-dependent manner (Dutton *et al.*, 2010).

Here, we present a detailed structural and functional characterization of Rv2969c, the remote DsbA homologue encoded by Mtb (which we refer to as MtbDsbA). The structure of MtbDsbA reveals a number of modifications to the archetypal EcDsbA structure and to the binding surface surrounding the active-site cysteine. The *in vitro* activity of MtbDsbA indicates that it is a mycobacterial disulfide oxidase and its ability to bind peptides derived from MtbVKOR supports the notion that MtbDsbA and MtbVKOR form a functional redox pair. MtbDsbA may therefore represent an important target for the development of antituberculosis drugs that block oxidative folding of exported Mtb proteins necessary for mycobacterial infection and survival within host macrophages. The structure that we report may serve as a starting point for rational drug design towards this end.

2. Experimental procedures

2.1. Cloning, expression and protein production

The N-terminal region of MtbDsbA is predicted to be a secretion signal (*SignalP*; Emanuelsson *et al.*, 2007) or transmembrane anchor (TMHMM; Krogh *et al.*, 2001). A codon-optimized synthetic gene corresponding to the soluble MtbDsbA enzyme lacking this region (*M. tuberculosis* H37Rv, residues 46–255) was inserted into the bacterial expression vector pMCSG7 by ligation-independent cloning (Eschenfeldt *et al.*, 2009). An amino-terminal His_6-tagged MtbDsbA was expressed in *E. coli* BL21(DE3) cells using auto-induction medium (Studier, 2005). Protein was purified using TALON

cobalt resin (Clontech) and the His_6 tag was removed by TEV protease leaving three vector-derived residues (Ser-Asn-Ala) at the N-terminus. For crystallization experiments, the protein was incubated with 100 m*M* oxidized glutathione to generate the oxidized enzyme, prior to final purification on a Superdex 75 gel-filtration column (GE Healthcare). Site-directed mutagenesis was performed using the QuikChange method and the mutation was confirmed by DNA sequencing. A noncatalytic double cysteine mutant $MtbDsbA^m$ (Cys140Ala, Cys192Ala) and an active-site single cysteine mutant MtbDsbA (Cys92Ala) were expressed and purified in the same way as for wild-type MtbDsbA.

2.2. Crystallization and diffraction data collection

MtbDsbA crystals were grown by the hanging-drop vapour-diffusion method at 293 K; drops were set up using a Mosquito crystallization robot (TTP Labtech) and were incubated and imaged in a RockImager 1000 (Formulatrix). 250 nl MtbDsbA solution concentrated to 55 mg ml^{-1} in 25 m*M* HEPES pH 7.4, 100 m*M* NaCl was mixed with 250 nl reservoir solution consisting of 2.4 *M* sodium malonate pH 5.5, 3.7% 1,4-dioxane, 0.08% polyvinylpyrrolidone. Crystals grew as long thin rods (~30 × 500 µm) in 3–4 weeks and were flash-cooled in liquid nitrogen after brief rinsing in 3.4 *M* sodium malonate pH 5.5. Diffraction data were collected on the MX2 beamline at the Australian Synchrotron at a wavelength of 0.9537 Å and were recorded using an ADSC Quantum 315r detector controlled by *Blu-Ice* (McPhillips *et al.*, 2002). Data were integrated in *XDS* (Kabsch, 2010), space-group possibilities were analyzed using *POINTLESS* (Evans, 2006) and data were scaled in *SCALA* from the *CCP*4 suite (Winn *et al.*, 2011).

2.3. Structure determination and refinement

Molecular-replacement (MR) searches for MtbDsbA with *Phaser* (McCoy *et al.*, 2007) using intact DsbA templates (less than 21% sequence identity) were unsuccessful. Regions contributing to DsbA structural divergence were identified by superposition of DsbA structures currently available in the PDB and the structurally divergent regions were trimmed to generate a collection of DsbA 'Poly Ser' MR templates (nonglycine and non-alanine residues that were not conserved were changed to serine) for MR trials in *Phaser*. A Poly Ser conserved structural core search model derived from *Staphylococcus aureus* DsbA (SaDsbA) (PDB entry 3bci; Heras *et al.*, 2008) gave an MR solution (TFZ = 8.0) with two copies in the asymmetric unit. This trimmed MR search model provided 39% coverage with 48% identity to the MtbDsbA sequence (Supplementary Fig. S1[1]). Iterative manual building, density modification and refinement in *PHENIX* (Adams *et al.*, 2010) and *Coot* (Emsley & Cowtan, 2004) allowed tracing of almost the entire MtbDsbA sequence. Final refinement cycles involving TLS were carried out in *phenix.refine*.

[1] Supplementary material has been deposited in the IUCr electronic archive (Reference: TZ5033). Services for accessing this material are described at the back of the journal.

Table 1
Summary of data-collection and refinement statistics.

Values in parentheses are for the highest resolution shell.

Space group	$I4_122$
Unit-cell parameters (Å)	a = 92.05, b = 92.05, c = 232.76
Data-collection wavelength (Å)	0.9537
Resolution range (Å)	85.6–1.97 (2.08–1.97)
No. of observations	286100 (39641)
No. of unique reflections	35185 (5080)
Mean $I/\sigma(I)$	14.9 (3.3)
R_{merge}	0.096 (0.66)
$R_{p.i.m.}$	0.036 (0.246)
Multiplicity	8.1 (7.8)
Wilson B factor (Å^2)	26.1
Model and refinement statistics	
Resolution range (Å)	59.3–1.97
No. of unique reflections	35175
Completeness	98.4
R_{work} (%)	14.5 (20.3)
R_{free}† (%)	19.2 (28.4)
No. of non-H atoms	
Protein	2996
Ligand	17
Water	415
R.m.s.d., bond lengths (Å)	0.011
R.m.s.d., bond angles (°)	1.27
Ramachandran favoured/allowed (%)	97.5/99.5
Average B factor (Å^2)	
Protein	23.7
Ligand	24.6
Water	34.6

† R_{free} is calculated as for R_{work} but for 5% of the total reflections chosen at random and omitted from refinement.

Electron density was absent for the three vector-derived residues and the N-terminal 11 residues of the MtbDsbA construct in both molecules in the asymmetric unit. At the interface of the two MtbDsbA molecules in the asymmetric unit, two additional regions of electron density were observed in the difference Fourier map contoured at 3.0σ. These were interpreted as 1,4-dioxane and HEPES, both of which were present in the crystallization condition. A summary of the data-processing and refinement statistics is presented in Table 1. The stereochemical quality of the final model was assessed using *AutoDep Input Tool* (Yang *et al.*, 2004), *MolProbity* (Chen *et al.*, 2010) and *SFCHECK* (Vaguine *et al.*, 1999). The coordinates and structure factors have been deposited in the Protein Data Bank (PDB entry 4k6x).

2.4. Isothermal titration calorimetry (ITC)

Experiments were carried out on a Microcal Auto-iTC200 (GE Healthcare). Peptides with N-terminal acetylation and C-terminal amidation were chemically synthesized manually by classic solid-phase peptide synthesis using rink amide MBHA resin (ChemImpex International, loading 0.65 mmol g^{-1}) and Fmoc-protected amino acids (ChemImpex International). Peptides were purified by reversed-phase HPLC (C18, Phenomenex) and characterized by retention times, electrospray mass spectrometry and ^{1}H NMR spectroscopy. Each ITC titration involved an initial 0.5 µl injection (not included in the subsequent analysis) followed by 19 injections of 2 µl of 2–4 m*M* peptide into cells containing 100 µ*M* MtbDsbA in 25 m*M* HEPES pH 7.4, 100 m*M* NaCl at

298 K. Thermodynamic parameters were obtained from nonlinear curve fitting using a single-site binding mode in *Origin* 7.0 (SR4 v7.0552 beta, Microcal).

2.5. Thermal stability measurement

Temperature-induced unfolding of MtbDsbA was recorded by far-UV circular dichroism (CD), with the temperature increasing from 298 to 368 K at a rate of 1 K min^{-1} using a Jasco J-810 spectropolarimeter. The normalized CD signal for oxidized (219 nm) and reduced (220.5 nm) MtbDsbA in 100 m*M* phosphate buffer, 1 m*M* ethylenediaminetetraacetic acid (EDTA) pH 7.0 was fitted to a two-state unfolding model as described previously (Kurz *et al.*, 2009). The redox status of the oxidized and reduced protein preparation with oxidized glutathione and DTT (dithiothreitol), respectively, was verified with Ellman's reagent.

2.6. Insulin-reduction assay

The catalytic ability of MtbDsbA to reduce insulin in the presence of DTT was monitored by the increase in absorbance at 650 nm over 80 min as described previously (Heras *et al.*, 2008). Briefly, the reaction mixture contained 131 µ*M* insulin and 10 µ*M* of oxidized MtbDsbA or EcDsbA in 100 m*M* phosphate buffer pH 7.0, 2 m*M* EDTA. The reaction was initiated by adding DTT to a final concentration of 0.35 m*M*. The noncatalyzed aggregation of insulin by DTT was monitored in a control reaction without enzyme.

2.7. Isomerization of scrambled RNaseA

In vitro disulfide isomerase activity of MtbDsbA, EcDsbC and EcDsbA was monitored using a scrambled RNaseA refolding assay (Hillson *et al.*, 1984). Scrambled RNaseA was produced as previously described (Heras *et al.*, 2008). Isomerization of scrambled RNaseA (40 µ*M*) was conducted in 100 m*M* sodium phosphate buffer containing 1 m*M* EDTA pH 7.0, 10 m*M* DTT and 10 µ*M* DsbA or DsbC at 298 K (750 µl). At various time intervals, 50 µl of refolded RNase sample was taken to monitor the hydrolysis activity of cytidine 3′,5′-cyclic monophosphate (3 m*M*) using a BioTek H1 plate reader at 296 nm. Native RNaseA and scrambled RNaseA in the absence of DsbA or DsbC served as positive and negative controls, respectively.

2.8. Ubiquinone-reduction assay

DsbB-catalyzed oxidation of DsbA can be monitored by following the decrease in ubiquinone absorbance at 275 nm (Bader *et al.*, 2000). The reaction mixture (70 µl) contained 30 µ*M* reduced MtbDsbA or EcDsbA, 30 µ*M* ubiquinone-1 (UQ1) in 50 m*M* Tris pH 7.0, 100 m*M* NaCl and 0.01% *n*-dodecyl β-D-maltoside. The decrease in absorbance was recorded for 3 min at 303 K after addition of 57 n*M* EcDsbB using a Varian Cary 50 UV–visible spectrophotometer.

2.9. Determination of redox potential

Oxidized $MtbDsbA^{m}$ (2 µ*M*) was incubated in 200 µl degassed buffer consisting of 100 m*M* phosphate buffer, 1 m*M* EDTA pH 7.0, 1 m*M* oxidized glutathione (GSSG) for 1 h at room temperature. The protein was then incubated in buffers with a range of reduced glutathione (GSH) concentrations (0.01 µ*M*–1 m*M*) for 24 h at 298 K (10 µl per reaction containing 2 µ*M* protein concentration). After incubation, the reactions were stopped with 10% trichloroacetic acid and the precipitated protein pellets were collected by centrifugation at 14 000 rev min^{-1} for 10 min at 277 K. The pellets were washed with 100% ice-cold acetone and dissolved in buffer consisting of 50 m*M* Tris pH 7.0, 1% SDS, 4 m*M* 4-acetamido-4′-maleimidylstilbene-2,2′-disulfonate (AMS) to label the free thiols. Separation of reduced and oxidized forms was performed on a NuPAGE 12% bis-tris gel (1.0 mm thick, 12 well; Invitrogen, Australia). The gel was stained with Coomassie, scanned (Perfection V700 Scanner, Epson) and intensities of the reduced protein were analyzed using *ImageJ* v.1.42q (Schneider *et al.*, 2012). The fraction of the reduced protein was plotted against the ratio $[GSH]^2/[GSSG]$ and the equilibrium constant K_{eq} was calculated using the binding equation $Y = ([GSH]^2/[GSSH])/\{K_{eq} + ([GSH]^2/[GSSH])\}$, where Y is the fraction of reduced protein at equilibrium. The redox potential was calculated using the Nernst equation $E^{0'} = E^{0'}_{GSH/GSSG} - (RT/nF)\ln K_{eq}$, where $E^{0'}_{GSH/GSSG}$ is the standard potential of −240 mV (Gilbert, 1995), R is the universal gas constant 8.314 J K^{-1} mol^{-1}, T is the absolute temperature in K, n is the number of electrons transferred, F is the Faraday constant 9.648×10^4 C mol^{-1} and K_{eq} is the equilibrium constant.

2.10. Determination of pK_a

The pH-dependent UV absorbance of the nucleophilic cysteine thiol was followed at 240 nm (Nelson & Creighton, 1994). Measurements of oxidized or reduced $MtbDsbA^{m}$ (lacking the second disulfide) of 24 or 16 µ*M* in a total volume of 200 µl buffer comprising 10 m*M* dipotassium phosphate, 10 m*M* monopotassium phosphate, 10 m*M* sodium citrate, 10 m*M* Tris, 1 m*M* EDTA, 200 m*M* KCl were performed at pH values ranging from 2.2 to 7.5 using Greiner 96-well UV-Star microplates. The redox status of the protein preparation was verified with Ellman's reagent. The absorbance at 240 and 280 nm was recorded on a BioTek Synergy H1 microplate reader and corrected for blank absorbance. The pH-dependent thiolate-specific absorbance signal $[(A_{240}/A_{280})_{reduced}/(A_{240}/A_{280})_{oxidized}]$ was fitted to the Henderson–Hasselbach equation as described previously (Kurz *et al.*, 2009).

2.11. Complementation assay

Complementation of EcDsbA by MtbDsbA was monitored in a cell-swarming assay as described previously (Kurz *et al.*, 2009). A chimeric gene encoding an EcDsbA signal peptide fused to the mature form of MtbDsbA was cloned into the arabinose-inducible pBAD33 vector (Guzman *et al.*, 1995). A nonmotile *E. coli dsbA*$^-$ mutant (JCB817) strain transformed

Table 2
Survey of Trx-related proteins in *M. tuberculosis* strain H37Rv.

Summary of the 15 Trx-related proteins found using keyword and *BLASTP* searches. Only Rv2969c and Rv1743 could be considered similar to DsbA-like proteins. Structural similarities to Trx-related proteins were identified using *BLASTP* and *Fold and Function Assignment* (*FFAS*; http://ffas.burnham.org/) searches against PDB codes or % identity to reported structure (PDB code in parentheses) are given. The functional annotation, presence and location of signal peptide/membrane-spanning region and operon are derived information from Target TB annotation (http://genome.tbdb.org/). The presence of signal sequence and transmembrane region were also confirmed using *SignalP*3.0 and transmembrane prediction using hidden Markov models (*TMHMM*). DsbA-like (Rv2969c) is predicted to have an N-terminal transmembrane (TM) helix or signal peptide (SP).

Protein	Length	Functional annotation	Signal peptide	Structural representative	Operon
PknE-DsbA (Rv1743)	566	Ser/Thr kinase	Integral membrane	2h34 (kinase; Gay *et al.*, 2006), 31% (DsbA-like)	Ser-Thr protein kinase, fused DsbA-like
DsbA-like (Rv2969c)	255	Conserved, unknown	TM or SP	Present work	Pyruvate carboxylase-like, VKOR, Dsb-like
DsbE (Rv2878c)	173	Unknown	Yes	1lu4 (Goulding *et al.*, 2004)	Rv2877c, DsbE
DsbF (Rv1677)	182	Unknown	Yes	3ios (Chim *et al.*, 2010)	Rv1676, DsbF
ResA-like (Rv3673c)	227	Unknown	Yes	30% (DsbE/F)	Rv3673c, endonuclease III
Trx-related (Rv0526)	216	Unknown	Yes	47% (3lwa; Midwest Center for Structural Genomics, unpublished work)	HemeL, Rv0525, Rv0526, ccdA, Rv0528, ccsA
TrxC (Rv3914)	116	Disulfide exchange	No	3o6t (Hall *et al.*, 2011)	TrxB2, TrxC
TrxB2 (Rv3913)	335	Disulfide reductase	No	2a87 (Akif *et al.*, 2005)	TrxB2, TrxC
TrxB1 (Rv1471)	123	Disulfide exchange	No	36% (3hhv; Ruggiero *et al.*, 2009)	TrxA, TrxB1
TrxA (Rv1470)	124	Disulfide exchange	No	32% (3hhv; Ruggiero *et al.*, 2009)	TrxA, TrxB1
Trx-like (Rv0816c)	140	Disulfide exchange	??	28% (3ilu; Ptak *et al.*, 2009)	Rv0816c, Rv0817c
Trx-like (Rv2183c)	131	Conserved, unknown	??	14% (3raz; New York SGX Research Center for Structural Genomics, unpublished work)	Rv2183c, Rv2184c
Trx-fusion protein (Rv1324)	304	Disulfide exchange	No	24% (3qdn; Center for Structural Genomics of Infectious Diseases, unpublished work)	Rv1324
Trx-related (Rv2286c)	230	Conserved, unknown	No	20% (3fz5; Midwest Center for Structural Genomics, unpublished work)	Rv2286c
Trx-related (Rv2466c)	207	Unknown	No	14% (3fz5; Midwest Center for Structural Genomics, unpublished work)	Rv2466c

with this chimera construct was stabbed into a minimal agar (M63) plate supplemented with 40 mg ml^{-1} of each amino acid and 1 mg ml^{-1} arabinose. The swarming of *E. coli* cells was analyzed after incubating the plate for 4–6 h at 303 K. JCB817 cells transformed with pBAD33::EcDsbA were used as a positive control. A nonmotile *dsbA*$^{-}$/*dsbB*$^{-}$ double-mutant strain (JCB818) served as a negative control. Plates without arabinose were used to monitor background complementation.

2.12. Peptide-oxidation assay

A synthetic peptide substrate CQQGFDGTQNSCK with a europium DOTA (1,4,7,10-tetraazacyclododecane-1,4,7,10-tetraacetic acid europium) chelate at the N-terminus and a methylcoumarin amide at the ε-amino group of the lysine was obtained from Anaspec, USA (for further details of the peptide, see Vivian *et al.*, 2009). Disulfide-bond formation of the peptide was fluorometrically followed using time-resolved fluorescence with excitation at 340 nm and emission at 615 nm, a delay of 150 µs and a reading time of 100 µs in a Synergy H1 multimode plate reader (BioTek, USA). The assay was performed in a 384-well white plate (PerkinElmer OptiPlate) containing EcDsbA or MtbDsbA and 2 m*M* GSSG in 50 m*M* MES, 50 m*M* NaCl, 2 m*M* EDTA at pH 5.5. The reaction was initiated by the addition of substrate peptide at 4–8 µ*M* in a total volume of 50 µl. The reaction was performed in triplicate and repeated at various concentrations of EcDsbA or MtbDsbA. The reaction in the absence of enzyme was used as a control.

3. Results

3.1. Putative Mtb DsbA-like proteins

To identify potential Mtb DsbA-like oxidases, we searched the genome of the virulent strain Mtb H37Rv by using keyword and *BLASTP* searches. 15 Trx-related gene products were identified (Table 2) and nine of these were eliminated as potential DsbA-like proteins as they are likely to be located in the cytoplasm (on the basis of literature reports, the absence of sorting signal/transmembrane region and sequence-to-structure relationships). Of the remaining six predicted to be extracytoplasmic Trx-related proteins, only the sequences of hypothetical Rv2969c and the DsbA-like domain of PknE (Rv1743) remotely resembled DsbA homologues. The sequence identity of the nearest structurally characterized neighbour, *Bacillus subtilis* DsbA (BsDsbA), is less than 19% (by sequence-based alignment) to these two Mtb DsbA paralogues. Rv2969c and Rv1743 share ∼50% sequence similarity (31% identity) and both contain four conserved cysteine residues. The sequence positions of two of the four cysteines are similar to that of the characteristic redox-active C*XX*C motif of the Trx fold, whereas the other two cysteines are consistent with the structural (noncatalytic) cysteines found in *Wolbachia pipientis* α-DsbA1 (Wpα-DsbA1; Kurz *et al.*, 2009).

The presence of a predicted sorting signal or trans membrane helix in Rv2969c (currently annotated as uncharacterized) indicates it is either secreted into, or membrane-anchored with the catalytic domain facing, the recently characterized mycobacterial periplasm (Patarroyo *et*

al., 2008; Sani *et al.*, 2010) and may therefore represent a potential candidate for a DsbA-like protein. Hereafter, we refer to it as MtbDsbA. Its paralogue PknE is a single-pass transmembrane Ser/Thr protein kinase that comprises an extracytoplasmic DsbA-like domain and a cytoplasmic kinase domain (Gay *et al.*, 2006). PknE has been shown to regulate cellular events in response to host-mediated apoptotic stimuli such as nitric oxide (Jayakumar *et al.*, 2008). As such, PknE appears to promote the survival of Mtb in the latent state by suppressing host apoptosis (Kumar & Narayanan, 2012).

3.2. MtbDsbA is highly oxidizing

Typically, DsbA enzymes have a highly acidic catalytic cysteine and a highly oxidizing redox potential that enable its participation in thiol–disulfide exchange reactions. To study the redox characteristics of MtbDsbA, we created a double noncatalytic cysteine mutant MtbDsbA^{m} (Cys140Ala, Cys192Ala). Similar to Wpα-DsbA1, this mutation did not affect the solubility and integrity of MtbDsbA. Using a pH-titration experiment (Fig. 1*a*), we found that the measured pK_a of the catalytic cysteine Cys89 is 4.2 $\pm$ 0.2, which falls between the previously reported values for EcDsbA (pK_a = 3.3) and *Vibrio cholerae* DsbA (VcDsbA, pK_a = 5.1). The redox potentials of DsbA proteins also vary among characterized DsbAs; the most reducing and oxidizing DsbAs reported to date are Wpα-DsbA1 (−163 mV) and neisserial NmDsbA3 (−80 mV), respectively. We measured the standard redox potential by equilibration of MtbDsbA^{m} with glutathione at 298 K and pH 7.0 (Fig. 1*b*). We found that the oxidizing power of MtbDsbA (−99 mV) is comparable to that of *Pseudomonas aeruginosa* DsbA (PdDsbA) (−94 mV; Shouldice *et al.*, 2010), somewhat more oxidizing than EcDsbA (−122 m*M*; Wunderlich & Glockshuber, 1993) and a little less oxidizing than BsDsbA (−80 m*M*; Crow *et al.*, 2009).

Another characteristic feature common to DsbA enzymes is that the catalytic cysteine disulfide bond reduces the stability of the protein (Heras *et al.*, 2008). A thermal unfolding experiment comparing the stability of the redox forms showed that the oxidized (disulfide) form of MtbDsbA is less stable than its reduced form by 13 K (Fig. 1*c*), which is in agreement with the findings for other DsbA enzymes.

Taken together, these results show that the putative DsbA protein encoded by *M. tuberculosis* has the redox hallmarks of a DsbA disulfide oxidoreductase.

3.3. MtbDsbA is a disulfide oxidase

An *in vivo* complementation experiment has been developed to demonstrate that the expression of a DsbA enzyme can rescue the motility of *E. coli* cells deficient in EcDsbA (Kurz *et al.*, 2009; Paxman *et al.*, 2009). However, MtbDsbA does not restore the motility of *E. coli* DsbA null cells as shown by the results of the cell-swarming assay (Fig. 2*a*). To establish whether this might be a consequence of a lack of interaction between MtbDsbA and EcDsbB (the essential redox partner of EcDsbA), we monitored the ability of EcDsbB to oxidize MtbDsbA in an EcDsbB-catalyzed ubiquinone reduction assay (Fig. 2*b*). This experiment showed as expected that EcDsbB can oxidize EcDsbA, but it failed to redox couple with MtbDsbA. This could explain why MtbDsbA does not complement EcDsbA in the motility assay, but we cannot rule out the possibility that MtbDsbA is inactive because it also does not recognize the P-ring protein (FlgI) substrate of EcDsbA in the assay (Dailey & Berg, 1993).

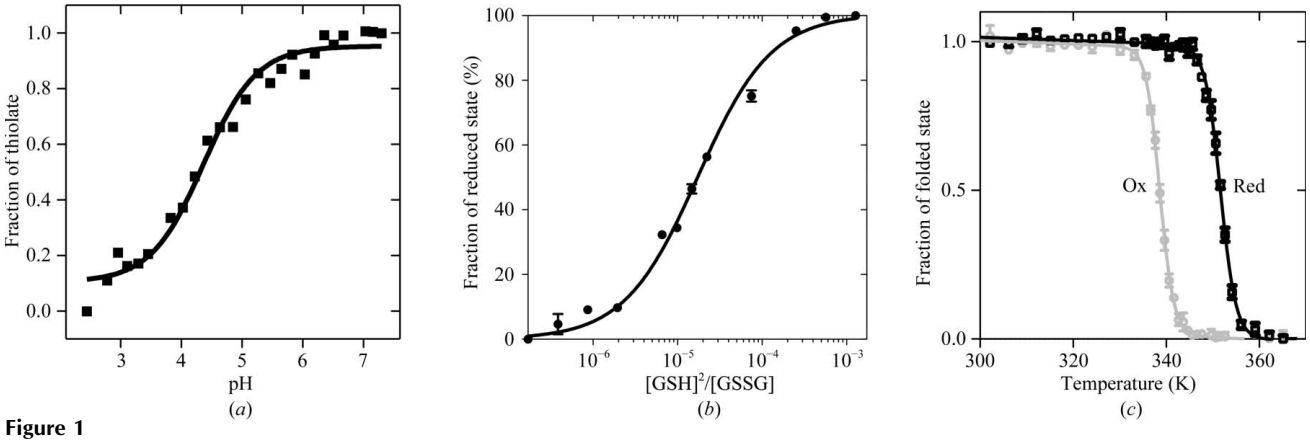

Figure 1
Characterization of the redox properties of MtbDsbA. (*a*) pK_a determination of the nucleophilic cysteine of MtbDsbA. This is a representative plot of three independent measurements of the pH-dependent thiolate-specific absorbance of the catalytic cysteine. The pK_a was obtained from the nonlinear fit to the Henderson–Hasselbach equation. (*b*) Determination of the redox equilibria of MtbDsbA with glutathione at pH 7.0 and 298 K. The plot shows the averaged fraction (three replicates) of reduced MtbDsbA at various ratios of reduced:oxidized glutathione. The resulting equilibrium constant K_{eq} (17.37 $\pm$ 0.1 μM) from the nonlinear curve fit for a one-site binding equation was used to calculate the redox potential of MtbDsbA relative to the glutathione (GSH/GSSG) standard potential of −240 mV (Gilbert, 1995). (*c*) Relative thermal stability of oxidized (grey) and reduced (black) MtbDsbA at pH 7.0. The normalized average far-UV CD signal from three measurements was fitted to a two-state unfolding model as described previously (Kurz *et al.*, 2009). The resulting melting temperature (T_m) of MtbDsbA shows that its reduced form (351.7 $\pm$ 0.1 K) is more stable than its oxidized form (338.6 $\pm$ 0.1 K).

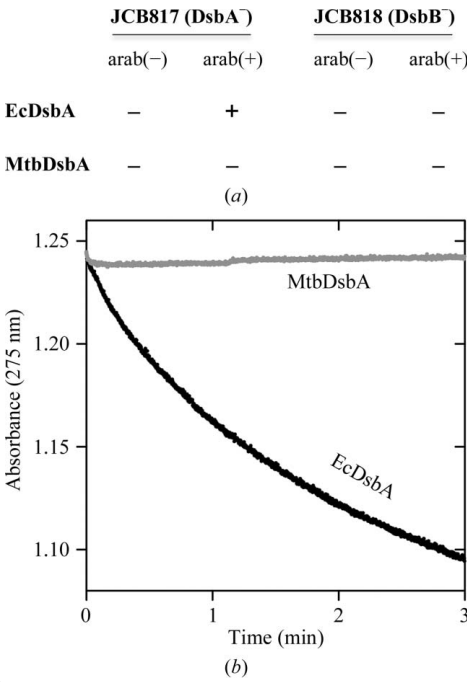

Figure 2
Ability of MtbDsbA to recognize EcDsbB. (*a*) Restoration of *E. coli* motility. Constructs expressing MtbDsbA or EcDsbA (control) were transformed into *E. coli* DsbA null (JCB817) and DsbA/DsbB double null (JCB818) mutant cells. FlgI function is impaired in the absence of EcDsbA or EcDsbB owing to the absence of disulfide-bonding activity (Dailey & Berg, 1993). The ability to recognize EcDsbB and EcDsbA substrates *in vivo* by MtbDsbA was evaluated by restoration of *E. coli* motility in the agar, as seen in the induced EcDsbA control. Shown is the summary of three replicates of induced (containing arabinose) and uninduced bacterial swarming plates (not containing arabinose, as a negative control). See Supplementary Fig. S2 for bacterial plate images. (*b*) Ubiquinone reduction of EcDsbB–UQ1 by MtbDsbA. The data presented here are the normalized mean absorbance of UQ1 from three independent measurements. EcDsbB was added to the EcDsbA/UQ1 mixture to initiate the reaction.

We then set out to determine the redox-activity profile of MtbDsbA in standard disulfide oxidase, reductase and isomerase assays.

The disulfide oxidase activity of MtbDsbA was investigated using an *in vitro* peptide-oxidation assay with a fluorescently labelled peptide substrate (CQQGFDGTQNSCK), using GSSG as the electron donor to regenerate the oxidized DsbA (Fig. 3*a*). MtbDsbA catalyzed peptide oxidation well above the background rate [in the absence of enzyme or in the presence of the catalytic cysteine mutant MtbDsbA (Cys92Ala)]. However, EcDsbA-mediated peptide oxidation was found to be faster than MtbDsbA as it required five times more MtbDsbA to match the catalytic rate of EcDsbA. This suggests the possibility that MtbDsbA and EcDsbA recognize the substrate peptide with differing affinities or kinetics.

The reductase activity of MtbDsbA was assessed spectrophotometrically by analyzing the ability of the enzyme to reduce the interchain disulfides of insulin (measured as an increase in turbidity through precipitation of the insulin B chain; Fig. 3*c*). In contrast to EcDsbA, MtbDsbA did not show any disulfide reductase activity against insulin, supporting the possibility that the two enzymes have different substrate-binding surfaces.

Finally, we tested the ability of MtbDsbA to isomerize, or shuffle, the incorrect disulfides of scrambled RNaseA to form the correctly folded RNaseA. Under the conditions of the assay, MtbDsbA was able to generate just 10% of the activity of fully folded RNaseA after 5 h (Fig. 3*c*). By comparison, EcDsbA and EcDsbC (a disulfide isomerase enzyme) produced ∼60 and ∼90%, respectively, of the activity of correctly folded RNase over the same time period. These observations are consistent with the view that MtbDsbA has the characteristic redox properties of a disulfide oxidase but differs functionally in other redox assays compared with the prototypical EcDsbA oxidase.

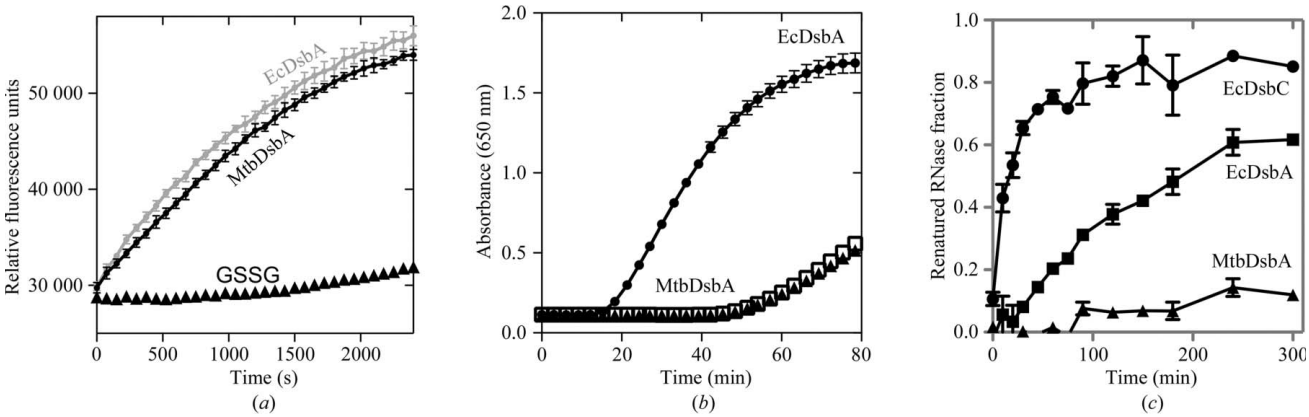

Figure 3
Disulfide oxidoreductase activities. (*a*) Disulfide oxidase activity. Representative fluorescence curves of peptide cysteine oxidation by MtbDsbA and EcDsbA in the presence of glutathione as the electron donor. Enzyme-catalyzed peptide oxidation is significantly faster than the glutathione-mediated reaction. Peptide oxidation in the buffer control or by the catalytically inactive MtbDsbA (Cys89Ala) or EcDsbA (Cys33Ala) was insignificant over the duration of the assay (not shown for clarity). (*b*) Insulin disulfide-reduction assay. The precipitation of insulin by MtbDsbA or EcDsbA or DTT (trace overlaps that of EcDsbA) was monitored as described in §2. (*c*) Scrambled RNase disulfide isomerization assay. Disulfide isomerization activity of MtbDsbA, EcDsbA and EcDsbC was monitored using scrambled RNase as the substrate.

3.4. The crystal structure of MtbDsbA reveals unique features

To explore the atomic details of MtbDsbA, we determined its structure at 2.0 Å resolution. The structure was solved by MR searches using trimmed 'Poly Ser' templates derived from remote DsbA homologues (see §2 and Supplementary Fig. S1). Two independent MtbDsbA molecules were well resolved in the asymmetric unit (residues 57–255; 199 residues for each monomer) and were refined to R_{work} and R_{free} values of 14.5 and 19.2%, respectively (Table 1). The MtbDsbA structure has a canonical DsbA-like architecture comprising a Trx domain with a helical domain inserted into the middle of the Trx domain (Fig. 4*a*). The two MtbDsbA molecules in the asymmetric unit are very similar (r.m.s. deviation of 0.26 Å for all C^{α} atoms). However, the structure of MtbDsbA differs significantly from the prototypical EcDsbA with an r.m.s. deviation of 3.7 Å for 149 C^{α} atoms (PDB entry 1fvk chain *A*; 3.7 Å for 148 C^{α} atoms for 1fvk chain *B*; Guddat *et al.*, 1997). Notable differences from EcDsbA include the folding topology of the central β-sheet, an additional helix H8 at the C-terminus and a much shorter connecting loop between β5 and H7 (Fig. 4*a*) that forms part of the binding interface between EcDsbA and its redox partner EcDsbB. As in all thioredoxin-like proteins, the catalytic C*XX*C motif is located at the N-terminus of helix H1 in MtbDsbA.

A structural comparison of MtbDsbA against all structures in the PDB using *DALI* (Holm *et al.*, 2008) revealed similarities to other DsbA structures, albeit with relatively large r.m.s. deviations (2.1–4.0 Å for 148–168 C^{α} atoms) and weak sequence conservation (Supplementary Fig. S3). The closest structural similarity occurs with DsbAs from Gram-positive organisms: BsDsbA (r.m.s. deviation 2.6 Å for 168 C^{α} atoms; 21% identity) and SaDsbA (r.m.s. deviation 2.1 Å for 154 C^{α} atoms; 21% identity). The central four strands of the core β-sheet have the same topology (3–2–4–5) in the Trx domains of this group of DsbAs. However, a topological difference is noted in the arrangement of strand β1 (Figs. 4 and 5*a*): in MtbDsbA, BsDsbA and WpDsbA1 β1 forms hydrogen bonds to β5 (3–2–4–5–1), whereas in the majority of DsbA structures β1 forms hydrogen bonds to β3 on the opposite edge of the β-sheet (1–3–2–4–5).

A unique feature of MtbDsbA compared with all other structurally characterized DsbAs is the C-terminal extension that forms an additional helix, H8, that packs against helices H1 and H7 (Figs. 4*b* and 5*a*). Crystallographic *B* factors plotted onto these helices suggest the possibility that the H8 helix may reduce

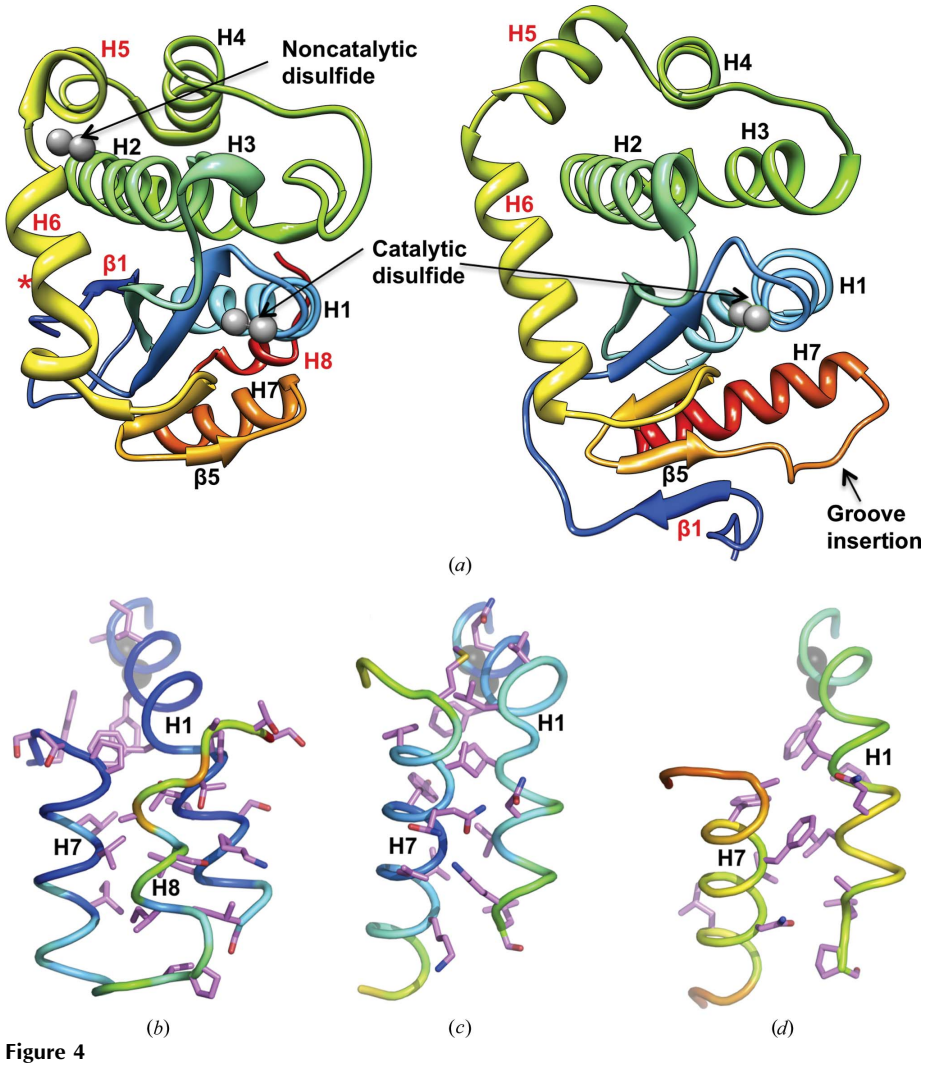

Figure 4
Structural comparison of MtbDsbA. (*a*) The crystal structure of MtbDsbA (left) is compared with the prototypical EcDsbA (right; PDB entry 1fvk; Guddat *et al.*, 1998). Catalytic/noncatalytic cysteine residues are shown as light grey spheres. The noncatalytic structural disulfide of MtbDsbA is absent in EcDsbA. Helix H8 appears to be unique to MtbDsbA. The orientation of helix H5 dramatically varies in these two proteins. Gly204 breaks the hydrogen-bonding pattern in the middle of helix H6 of MtbDsbA (helix H6 is kinked in MtbDsbA compared with EcDsbA). MtbDsbA appears to be much smaller in size than EcDsbA in this orientation. However, the molecular surface areas of MtbDsbA (8208 $Å^2$) and EcDsbA (8670 $Å^2$) are comparable. The intramolecular interaction of helix H1 with the C-terminal region of (*b*) MtbDsbA, (*c*) EcDsbA (PDB entry 1fvk; Guddat *et al.*, 1998) and (*d*) VcDsbA (PDB entry 1bed; Hu *et al.*, 1997) is also shown. For (*b*), (*c*) and (*d*) the backbone colour is set to the temperature factor from the PDB. The side chains of interfacing residues identified by *PISA* (*Protein Interfaces, Surfaces and Assemblies*; Krissinel & Henrick, 2007) analysis are shown as sticks. Catalytic and noncatalytic cysteines are shown as grey spheres.

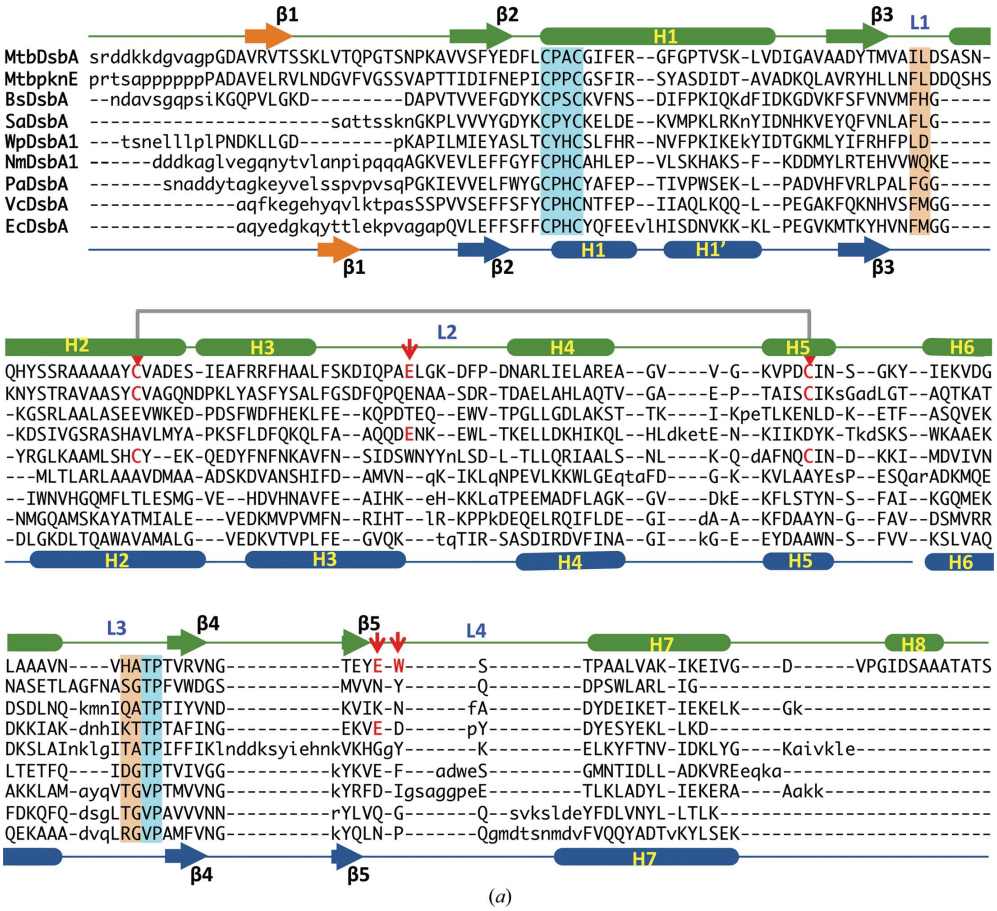

(*a*)

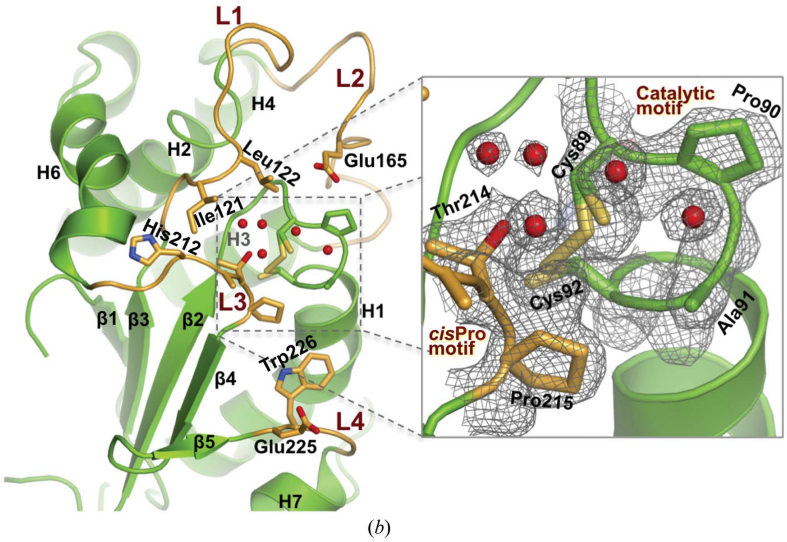

(*b*)

Figure 5
Structural elements of DsbAs and the catalytic site of MtbDsbA. (*a*) Structure-based sequence alignment of DsbAs. Structurally equivalent positions (upper case), variable regions (lower case) and insertions (dashes) are shown. PknE DsbA sequence alignment is based on MtbDsbA and BsDsbA (see Supplementary Fig. S6 for the PknE hypothetical model). Secondary-structure assignments for MtbDsbA (top green), EcDsbA (bottom blue) and topological variations originating at strand $\beta1$ in MtbDsbA and EcDsbA (orange) are presented. The catalytic motif and *cis*-Pro motif are highlighted in cyan and the equivalent EcDsbA residues involved in partner/substrate interaction are highlighted in orange. A negatively charged residue (Glu165) in the vicinity of the catalytic cysteine, a residue blocking the hydrophobic groove (Trp226) and a noncatalytic structural disulfide bond are marked with red arrows (see text for details). (*b*) The structure of the catalytic face of MtbDsbA. Residues forming the putative binding surface and negatively charged residues neighbouring the catalytic cysteine are shown. The inset displays the $2mF_o - DF_c$ electron-density map around the catalytic motif, the *cis*-Pro loop and ordered active-site water molecules (1.0σ contour level).

the mobility of the catalytic helix H1 in comparison to EcDsbA and VcDsbA (Figs. 4*b*–4*d*). We then analyzed the interface between helix H1 and the C-terminal H8 region (Table 3). Compared with other structurally characterized DsbAs, the presence of helix H8 in MtbDsbA buries a greater proportion of helix H1 (buried surface area of 592 *versus* 401–260 Å^2). The H8 helix interaction may restrict the conformational flexibility of helices H1 and H7. Similarly, the second disulfide bond (Cys140–Cys192) of MtbDsbA that links helices H2 and H5 may also restrict flexibility of the four-helix bundle (Figs. 4 and 5*a*). The functional effects of these conformational restrictions are unclear but might explain at least in part the differences that we observe in the functional assays for MtbDsbA and EcDsbA.

The highly conserved structural regions in these DsbAs are the catalytic motif and *cis*-proline (*cis*-Pro) loop, both of which are known to be critical for activity in other DsbA enzymes (Kadokura *et al.*, 2004). However, the catalytic motif (Cys89-Pro90-Ala91-Cys92) in MtbDsbA differs from other structurally characterized DsbAs, which are generally Cys-Pro-His/Tyr/Ser-Cys. The catalytic cysteines Cys89 and Cys92 display alternative side-chain conformations corresponding to oxidized and reduced states (estimated approximately 50 and 65% for reduced states on the basis of crystallographic occupancy), despite the fact that oxidized protein was used for crystal growth (Fig. 5*b*). The active-site disulfides of DsbA proteins are susceptible to radiation damage in the crystal (Guddat *et al.*, 1998) and the broken disulfide bond in MtbDsbA is therefore likely to be a result of the synchrotron radiation used to measure the diffraction data. In its reduced form in the crystal, Cys89 of MtbDsbA is likely to exist as the thiolate (pK_a 4.2, pH in the crystal drop 5.5). Ordered active-site water molecules are present in the crystal structure at positions consistent with formation of stabilizing hydrogen bonds to the Cys89 thiolate and to Thr214, a residue preceding the *cis*-Pro loop. This hydrogen-bonding network differs from that in EcDsbA, which has a Val at the equivalent position to Thr214, but is similar to that in SaDsbA, which also has a Thr prior to the *cis*-Pro residue (Heras *et al.*, 2008).

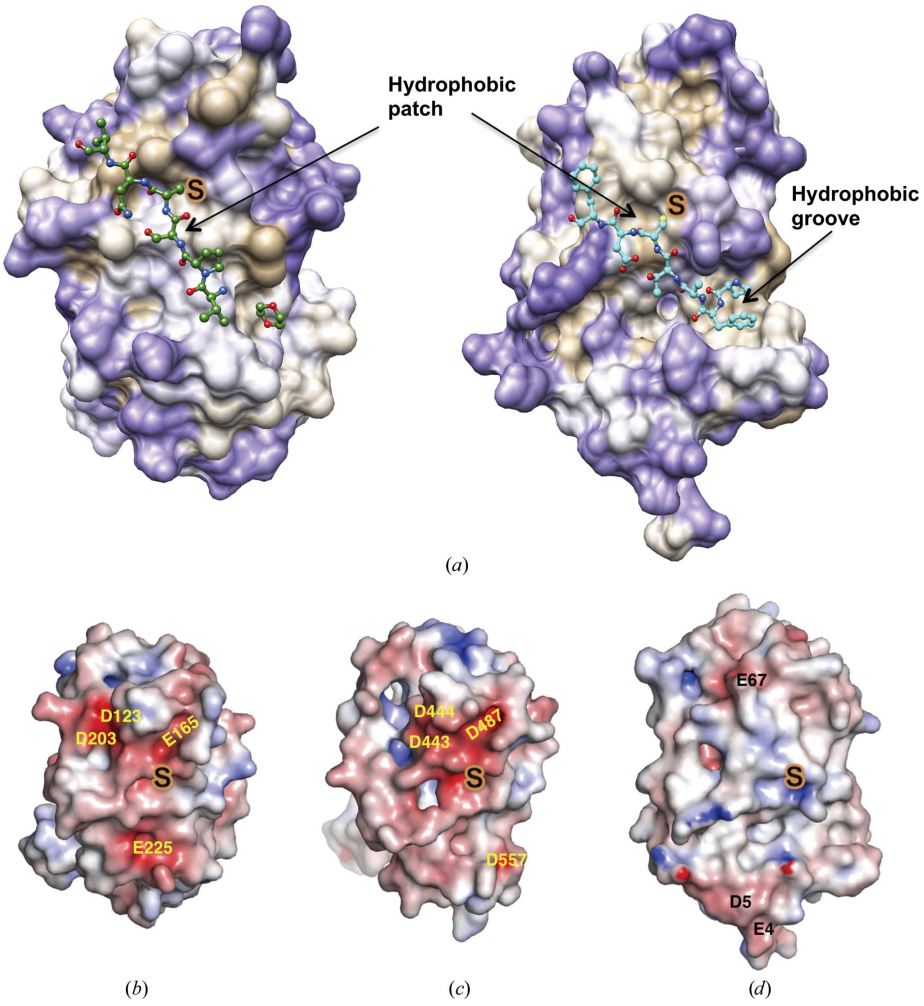

Figure 6
Comparison of surface properties. (*a*) Hydrophobicity surface presentations for MtbDsbA and EcDsbA. Surface colourings are mapped to the Kyte–Doolittle hydrophobicity scale from purple (most hydrophilic) to white to tan (most hydrophobic). The MtbDsbA structure is shown (left) with the modelled VKOR peptide (VPSCNV) and crystallographically identified artificial ligand 1,4-dioxane (see text and Supplementary Fig. S4 for details). The EcDsbA–EcDsbB complex structure is shown on the right (PDB entry 3e9j; Malojcić *et al.*, 2008). For clarity only the periplasmic loop segment 'PFATCDF' of EcDsbB is shown. Electrostatic surface comparisons of (*b*) MtbDsbA, (*c*) the hypothetical model of PknE DsbA and (*d*) EcDsbA. Electrostatic surface potential is contoured between −6 (red) and +6 (blue) *kT*/e. The homology model of PknE (template based on MtbDsbA and BsDsbA) was prepared in *MODELLER* (Eswar *et al.*, 2006) and atomic clashes were minimized in *Chiron* (Ramachandran *et al.*, 2011).

3.5. The surface surrounding the active site of MtbDsbA differs from that of EcDsbA

The conformation and amino-acid composition of the loop connecting the Trx domain and the helical domain (β3–H2, L1), an inter-helix loop (H3–H4, L2), the *cis*-Pro loop (H6–β4, L3) and the connecting loop β5–H7 (L4) create the surface features surrounding the catalytic cysteine (Cys89) of MtbDsbA (Fig. 5).

Table 3
Analysis of the interface between helix H1 and the C-terminal region of DsbA structures.

The buried surface area (BSA) in helix H1 (column 3) was determined using *PISA* analysis (Krissinel & Henrick, 2007). DsbAs, their PDB codes (column 1, in parentheses) and the residue ranges in helix H1 (column 2, in parentheses) and the C-terminal region (column 4, in parentheses) included in the *PISA* analysis are listed. The percentage of surface area buried in helix H1 relative to its total accessible surface area (∼2000 Å^2) is given in column 3 (in parentheses). For MtbDsbA and EcDsbA, BSA and the values reported for the percentage of surface area buried are an average of two MtbDsbA chains (molecule 1 and molecule 2 in the asymmetric unit) and nine EcDsbA chains [PDB entries 1dsb (two chains; Martin *et al.*, 1993), 1fvk (two chains; Guddat *et al.*, 1997), 1a2m (two chains; Guddat *et al.*, 1998), 1a2l (two chains; Guddat *et al.*, 1998) and 1a2j (one chain; Guddat *et al.*, 1998)].

Protein (PDB code)	No. of interfacing residues in helix H1	Helix H1 BSA (Å^2)	No. of interfacing residues in C-terminal region
MtbDsbA	13 (89–109)	592 ± 4 (29.6)	18 (226–255)
EcDsbA	9 (30–50)	401 ± 42 (18.9)	10 (168–188)
BsDsbA (3eu3; Crow *et al.*, 2009)	8 (69–91)	355 (15.9)	8 (205–222)
SaDsbA (3bci; Heras *et al.*, 2008)	9 (26–46)	370 (15.8)	7 (167–178)
PaDsbA (3h93; Shouldice *et al.*, 2010)	7 (37–55)	282 (14.3)	9 (166–192)
VcDsbA (1bed; Hu *et al.*, 1997)	8 (30–48)	261 (13.7)	6 (164–181)
WpDsbA (3f4r; Kurz *et al.*, 2009)	9 (51–71)	363 (16.5)	9 (196–218)
NmDsbA1 (3a3t; Vivian *et al.*, 2009)	7 (57–74)	290 (15.5)	7 (189–212)

Crystal structures of EcDsbA in complex with protein partners have shown that the hydrophobic patch created by loops L1 and L3, the active-site motif and the hydrophobic groove formed by loop L4 and helix H1 contribute to interactions with partner proteins (Paxman *et al.*, 2009; Inaba *et al.*, 2006). The length and amino-acid identity of these loops are generally not conserved among DsbAs (Fig. 5*a*). The relatively long L4 loop in EcDsbA creates a large hydrophobic groove compared with the short loop found in MtbDsbA, SaDsbA and BsDsbA (Fig. 6). In MtbDsbA, the side chain of Trp226 (L4 loop) sits in a shallow groove formed by Ile94, Phe95, Gly98, Phe99, Ser227, Thr228 and Pro229 (Fig. 5*b*). The hydrophobic nature of the surrounding catalytic residues is largely preserved in MtbDsbA (Fig. 6). Unexpectedly, a ligand, 1,4-dioxane from the crystallization solution, was bound in this shallow groove, forming contacts with Ile94, Gly98, Phe99 and Pro229 (Supplementary Fig. S4). MtbDsbA also has two negatively charged residues near the catalytic Cys89, similar to those observed in SaDsbA (Glu165 and Glu225, see Fig. 5*b*). The SaDsbA glutamate equivalent to Glu165 has been shown to influence the pK_a of the catalytic cysteine (Heras *et al.*, 2008).

3.6. MtbDsbA binds a peptide derived from VKOR

Although the binding surface of MtbDsbA does not have the distinct binding groove of EcDsbA that interacts with a periplasmic loop of its membrane partner EcDsbB, we investigated whether a fragment of a periplasmic loop from the putative binding partner MtbVKOR would interact with MtbDsbA. We used ITC to assess the binding of MtbDsbA to several peptides derived from MtbVKOR (see Supplementary Fig. S5 for the quality of the ITC data). Topological prediction indicated that MtbVKOR is comprised of five transmembrane helices connected by two periplasmic loops. Cys57 from the first periplasmic loop has been shown to form a mixed disulfide bond with EcDsbA (Wang *et al.*, 2011), although a direct interaction of MtbVKOR with any mycobacterial protein has not been reported. We found that the MtbVKOR 11-residue peptide segment surrounding Cys57 (^{51}PIYVPSCNVNP^{61}) binds to MtbDsbA with an apparent K_d of 3.8 µ*M* (Table 4). Trimming from either end of this peptide showed that a minimal hexapeptide (^{54}VPSCNV^{59}) binds to MtbDsbA with $K_{d,app}$ = 6.7 µ*M*. Further, modelling of the ^{54}VPSCNV^{59} peptide onto MtbDsbA suggested that Tyr53 of the VKOR sequence might bind to the site occupied by 1,4-dioxane in the crystal structure (Fig. 6*a*). Indeed, this heptapeptide ^{53}YVPSCNV^{59} showed improved binding ($K_{d,app}$ =2.9 µ*M*) to MtbDsbA. Binding of this VKOR peptide to MtbDsbA is cysteine-dependent, as substitution of Cys with Ala or Leu or mutation of the MtbDsbA catalytic Cys89 to Ala abolished binding under the conditions tested.

3.7. Comparison with the predicted mycobacterial DsbA-like domain of PknE

Aside from MtbDsbA, the H37Rv strain encodes five other putative extracytoplasmic Trx-related proteins: DsbE (Rv2878c), DsbF (Rv1677), Rv3673c, Rv0526 and the transmembrane protein kinase PknE (Rv1743). PknE is a clear structural homologue of MtbDsbA and also contains a kinase domain. Curiously, sequence searches suggest that PknE orthologues are restricted to pathogenic mycobacteria and PknE appears to be the only Mtb protein kinase fused to a DsbA homologous domain. The PknE predicted DsbA domain (residues 377–566) is linked to the intracellular protein kinase domain (residues 1–289) through a single-pass transmembrane helix (residues 337–359). Sequence comparison and secondary-structure prediction are consistent with the notion that PknE DsbA shares the same overall fold as that of MtbDsbA. We generated a homology model for PknE DsbA based on the MtbDsbA structure to compare the sequence variation in the context of the three-dimensional structure (Supplementary Fig. S6). Predicted differences from MtbDsbA in the PknE DsbA domain include the absence of helix H8 and a short helix H7 at the C-terminus. There are also sequence variations in loops L1, L3 and L4 (Fig. 5*a*). Predicted similarities in PknE DsbA include conservation of the Thr-*cis*-

Table 4
Thermodynamic parameters for VKOR-derived peptides binding to MtbDsbA.

$K_{d,app}$, apparent dissociation constant; ΔH, enthalpy change; $T\Delta S$, temperature (K) × entropy change; N is the apparent stoichiometry. $T\Delta S$ is calculated from the free energy equation ($\Delta H - T\Delta S = -RT\ln K_{d,app}$). Values reported are the mean and standard deviation of the curve fits from two ITC runs in each case. Representative ITC profiles are provided in Supplementary Fig. S5. n.b., no binding detected. 1 cal = 4.184 J.

	N	$K_{d,app}$ (μM)	ΔH (kcal mol^{-1})	$-T\Delta S$ (kcal mol^{-1})
PIYVPSCNVNP	1.0	3.8 ± 0.2	−10.9 ± 0.0	3.5
VPSCNVNP	1.0	5.9 ± 2.6	−7.1 ± 4.0	2.5
VPSCNV	1.0	6.7 ± 0.0	−6.8 ± 0.2	−0.1
VPSLNV		n.b.		
YVPSCNV	1.1	2.9 ± 0.3	−7.0 ± 0.4	−0.5
YVPSANV		n.b.		

Pro motif, a glutamate equivalent of Glu225 and a tyrosine equivalent of Trp226. The calculated electrostatic potential surfaces are negative in the region surrounding the catalytic site in both proteins (Figs. 6*c* and 6*d*). However, the CPPC catalytic motif in PknE DsbA differs from that of CPAC of MtbDsbA. These differences may contribute to a difference in redox characteristics. In EcDsbA, mutation of CPHC to CPPC dramatically increased its reducing potential (−122 mV to −220 mV; Bessette *et al.*, 2001). The native CPPC active site in a DsbA homologue from *Salmonella enterica* (SeSrgA) has also been linked to a more strongly reducing potential (−154 mV). Indeed, the insulin reductase activity of SeSrgA was shown to be similar to that of the disulfide isomerase EcDsbC (Heras *et al.*, 2010).

4. Discussion

Novel drug targets are desperately needed to combat tuberculosis. Mycobacterial proteins exported across the cytoplasmic membrane play important roles in Mtb adhesion, invasion, virulence, pathogenesis and survival inside host cells. Drugs targeting export systems in Gram-negative bacteria have been tested for their ability to block delivery of effector proteins required for virulence (Moir *et al.*, 2011). Likewise, there are intensive efforts to develop antituberculosis drugs that target the major mycobacterial protein-export systems: the Sec pathway, the Tat pathway and the ESX pathways (Feltcher *et al.*, 2010; McCann *et al.*, 2011).

Another approach is to target the disulfide pathways that mediate disulfide-bond formation and correct folding of exported proteins in Mtb (Chim *et al.*, 2010, 2011; Goulding *et al.*, 2004). In bacteria, disulfide-bond formation in newly exported proteins is commonly mediated through mechanisms that rely on electron transfer between redox proteins. The best-studied protein redox pair, DsbA/DsbB, is found in most aerobic α-, β- and γ-proteobacteria. However, in mycobacteria and other actinobacteria, cyanobacteria and δ- and ε-proteobacteria, it has been proposed that DsbA/VKOR forms a functional redox pair to catalyze disulfide-bond formation (Dutton *et al.*, 2008; Li *et al.*, 2010; Wang *et al.*, 2011). The currently accepted mechanism is that the cysteine-containing periplasmic loop of transmembrane protein DsbB or VKOR is transiently drawn into the binding groove of DsbA (Fig. 6) to drive the flow of electrons (Inaba & Ito, 2008). Oxidized DsbA then exchanges its catalytic disulfide bond with newly exported proteins by transiently interacting with them through its catalytic cysteine and binding surface (Inaba & Ito, 2008; Inaba *et al.*, 2006; Kadokura *et al.*, 2003). Thus, compounds targeting the protein–protein interaction surface responsible for interaction between DsbA and its substrate proteins or between DsbA and DsbB/VKOR may inhibit virulence-factor maturation in pathogens.

The data we present here show that Rv2969c has disulfide oxidase activity, a highly acidic active-site cysteine, a destabilizing active-site disulfide and a highly oxidizing potential. Structurally, MtbDsbA has a canonical DsbA architecture with a C*XX*C active-site motif. We therefore conclude that Mtb Rv2969c is an authentic DsbA enzyme. Our data also show that MtbDsbA is able to interact tightly with a seven-residue peptide corresponding to the periplasmic loop of MtbVKOR and these data support the notion that MtbDsbA and MtbVKOR are a functional redox pair that could catalyze disulfide-bond formation in newly translocated substrates.

Helix H8 at the C-terminus of MtbDsbA and its interaction with active-site helix H1 are unique to MtbDsbA among structurally characterized DsbAs. This feature appears to be absent in the DsbA-like domain of PknE. Substrate binding and mobility of DsbAs has been linked to the catalytic activity of DsbA (Horne *et al.*, 2007). In this context, restraint of helix H1 by helix H8 in MtbDsbA may contribute to the catalytic activity of MtbDsbA. Moreover, the relatively negative surface potential surrounding the catalytic site of MtbDsbA compared with EcDsbA suggests that these two enzymes have very different substrate-binding specificities. This is supported by our assay data showing the relative activities of these two enzymes in assays for reductase (MtbDsbA no activity), oxidase (MtbDsbA slower activity) and isomerase (MtbDsbA marginal activity) activity. EcDsbA is known to be a promiscuous enzyme that interacts with many substrates. Our structural and functional data suggest that MtbDsbA may have a more limited number of specific substrates.

Previous work has shown that the anticoagulant warfarin that inhibits human VKOR can also inhibit MtbVKOR and it interferes with the growth of Mtb in cell studies (Dutton *et al.*, 2010). Inhibiting MtbVKOR is an appealing strategy for treating Mtb, but will require the design of selective inhibitors that target MtbVKOR and not its human counterpart. Our results suggest that MtbDsbA may represent an alternative target for inhibiting disulfide oxidation in Mtb and for preventing the production of virulence factors.

We thank the outstanding beamline support team at the Australian Synchrotron for data-collection facilities. We also acknowledge use of the University of Queensland Remote Operation Crystallization and X-ray (UQROCX) Diffraction Facility and the assistance of Mr Karl Byriel and Dr Gordon King. This work was supported by an Australian Laureate

Fellowship (FL0992138) to JLM. JLM is also an Honorary NHMRC Research Fellow (455829).

References

Adams, P. D. *et al.* (2010). *Acta Cryst.* D**66**, 213–221.
Akif, M., Suhre, K., Verma, C. & Mande, S. C. (2005). *Acta Cryst.* D**61**, 1603–1611.
Bader, M. W., Xie, T., Yu, C.-A. & Bardwell, J. C. A. (2000). *J. Biol. Chem.* **275**, 26082–26088.
Bessette, P. H., Qiu, J., Bardwell, J. C. A., Swartz, J. R. & Georgiou, G. (2001). *J. Bacteriol.* **183**, 980–988.
Chen, V. B., Arendall, W. B., Headd, J. J., Keedy, D. A., Immormino, R. M., Kapral, G. J., Murray, L. W., Richardson, J. S. & Richardson, D. C. (2010). *Acta Cryst.* D**66**, 12–21.
Chim, N. *et al.* (2011). *Tuberculosis*, **91**, 155–172.
Chim, N., Riley, R., The, J., Im, S., Segelke, B., Lekin, T., Yu, M., Hung, L.-W., Terwilliger, T., Whitelegge, J. P. & Goulding, C. W. (2010). *J. Mol. Biol.* **396**, 1211–1226.
Connolly, L. E., Edelstein, P. H. & Ramakrishnan, L. (2007). *PLoS Med.* **4**, e120.
Crow, A., Lewin, A., Hecht, O., Carlsson Möller, M., Moore, G. R., Hederstedt, L. & Le Brun, N. E. (2009). *J. Biol. Chem.* **284**, 23719–23733.
Dailey, F. E. & Berg, H. C. (1993). *Proc. Natl Acad. Sci. USA*, **90**, 1043–1047.
DiGiuseppe Champion, P. A. & Cox, J. S. (2007). *Cell. Microbiol.* **9**, 1376–1384.
Dutton, R. J., Boyd, D., Berkmen, M. & Beckwith, J. (2008). *Proc. Natl Acad. Sci. USA*, **105**, 11933–11938.
Dutton, R. J., Wayman, A., Wei, J.-R., Rubin, E. J., Beckwith, J. & Boyd, D. (2010). *Proc. Natl Acad. Sci. USA*, **107**, 297–301.
Emanuelsson, O., Brunak, S., von Heijne, G. & Nielsen, H. (2007). *Nature Protoc.* **2**, 953–971.
Emsley, P. & Cowtan, K. (2004). *Acta Cryst.* D**60**, 2126–2132.
Eschenfeldt, W. H., Lucy, S., Millard, C. S., Joachimiak, A. & Mark, I. D. (2009). *Methods Mol. Biol.* **498**, 105–115.
Eswar, N., Webb, B., Marti-Renom, M. A., Madhusudhan, M. S., Eramian, D., Shen, M.-Y., Pieper, U. & Sali, A. (2006). *Curr. Protoc. Bioinformatics*, Unit 5.6. doi:10.1002/0471250953.bi0506s15.
Evans, P. (2006). *Acta Cryst.* D**62**, 72–82.
Feltcher, M. E., Sullivan, J. T. & Braunstein, M. (2010). *Future Microbiol.* **5**, 1581–1597.
Gay, L. M., Ng, H.-L. & Alber, T. (2006). *J. Mol. Biol.* **360**, 409–420.
Gilbert, H. F. (1995). *Methods Enzymol.* **251**, 8–28.
Goulding, C. W., Apostol, M. I., Gleiter, S., Parseghian, A., Bardwell, J., Gennaro, M. & Eisenberg, D. (2004). *J. Biol. Chem.* **279**, 3516–3524.
Guddat, L. W., Bardwell, J. C. A., Glockshuber, R., Huber-Wunderlich, M., Zander, T. & Martin, J. L. (1997). *Protein Sci.* **6**, 1893–1900.
Guddat, L. W., Bardwell, J. C. A. & Martin, J. L. (1998). *Structure*, **6**, 757–767.
Guzman, L. M., Belin, D., Carson, M. J. & Beckwith, J. (1995). *J. Bacteriol.* **177**, 4121–4130.
Hall, G., Bradshaw, T. D., Laughton, C. A., Stevens, M. F. & Emsley, J. (2011). *Protein Sci.* **20**, 210–215.
Hayashi, S., Abe, M., Kimoto, M., Furukawa, S. & Nakazawa, T. (2000). *Microbiol. Immunol.* **44**, 41–50.
Heras, B., Kurz, M., Jarrott, R., Shouldice, S. R., Frei, P., Robin, G., Cemazar, M., Thöny-Meyer, L., Glockshuber, R. & Martin, J. L. (2008). *J. Biol. Chem.* **283**, 4261–4271.
Heras, B., Shouldice, S. R., Totsika, M., Scanlon, M. J., Schembri, M. A. & Martin, J. L. (2009). *Nature Rev. Microbiol.* **7**, 215–225.
Heras, B., Totsika, M., Jarrott, R., Shouldice, S. R., Guncar, G., Achard, M. E., Wells, T. J., Argente, M. P., McEwan, A. G. & Schembri, M. A. (2010). *J. Biol. Chem.* **285**, 18423–18432.
Hillson, D. A., Lambert, N. & Freedman, R. B. (1984). *Methods Enzymol.* **107**, 281–294.
Holm, L., Kääriäinen, S., Rosenström, P. & Schenkel, A. (2008). *Bioinformatics*, **24**, 2780–2781.
Horne, J., d'Auvergne, E. J., Coles, M., Velkov, T., Chin, Y., Charman, W. N., Prankerd, R., Gooley, P. R. & Scanlon, M. J. (2007). *J. Mol. Biol.* **371**, 703–716.
Hu, S.-H., Peek, J. A., Rattigan, E., Taylor, R. K. & Martin, J. L. (1997). *J. Mol. Biol.* **268**, 137–146.
Inaba, K. (2009). *J. Biochem.* **146**, 591–597.
Inaba, K. & Ito, K. (2008). *Biochim. Biophys. Acta*, **1783**, 520–529.
Inaba, K., Murakami, S., Suzuki, M., Nakagawa, A., Yamashita, E., Okada, K. & Ito, K. (2006). *Cell*, **127**, 789–801.
Jayakumar, D., Jacobs, W. R. & Narayanan, S. (2008). *Cell. Microbiol.* **10**, 365–374.
Kabsch, W. (2010). *Acta Cryst.* D**66**, 133–144.
Kadokura, H., Katzen, F. & Beckwith, J. (2003). *Annu. Rev. Biochem.* **72**, 111–135.
Kadokura, H., Tian, H., Zander, T., Bardwell, J. C. & Beckwith, J. (2004). *Science*, **303**, 534–537.
Kim, J. J. *et al.* (2012). *Cell Host Microbe*, **11**, 457–468.
Krissinel, E. & Henrick, K. (2007). *J. Mol. Biol.* **372**, 774–797.
Krogh, A., Larsson, B., von Heijne, G. & Sonnhammer, E. L. (2001). *J. Mol. Biol.* **305**, 567–580.
Kumar, D. & Narayanan, S. (2012). *Infect. Genet. Evol.* **12**, 737–747.
Kurz, M., Iturbe-Ormaetxe, I., Jarrott, R., Shouldice, S. R., Wouters, M. A., Frei, P., Glockshuber, R., O'Neill, S. L., Heras, B. & Martin, J. L. (2009). *Antioxid. Redox Signal.* **11**, 1485–1500.
Li, W., Schulman, S., Dutton, R. J., Boyd, D., Beckwith, J. & Rapoport, T. A. (2010). *Nature (London)*, **463**, 507–512.
Lou, Z. & Zhang, X. (2010). *Protein Cell*, **1**, 435–442.
McCann, J. R., McDonough, J. A., Sullivan, J. T., Feltcher, M. E. & Braunstein, M. (2011). *J. Bacteriol.* **193**, 854–861.
McCoy, A. J., Grosse-Kunstleve, R. W., Adams, P. D., Winn, M. D., Storoni, L. C. & Read, R. J. (2007). *J. Appl. Cryst.* **40**, 658–674.
McPhillips, T. M., McPhillips, S. E., Chiu, H.-J., Cohen, A. E., Deacon, A. M., Ellis, P. J., Garman, E., Gonzalez, A., Sauter, N. K., Phizackerley, R. P., Soltis, S. M. & Kuhn, P. (2002). *J. Synchrotron Rad.* **9**, 401–406.
Malojcić, G., Owen, R. L., Grimshaw, J. P. & Glockshuber, R. (2008). *FEBS Lett.* **582**, 3301–3307.
Martin, J. L., Bardwell, J. C. & Kuriyan, J. (1993). *Nature (London)*, **365**, 464–468.
Moir, D. T., Di, M., Wong, E., Moore, R. A., Schweizer, H. P., Woods, D. E. & Bowlin, T. L. (2011). *J. Biomol. Screen.* **16**, 694–705.
Murillo, A. C. *et al.* (2007). *Infect. Disord. Drug Targets*, **7**, 127–139.
Nelson, J. W. & Creighton, T. E. (1994). *Biochemistry*, **33**, 5974–5983.
Patarroyo, M. A., Plaza, D. F., Ocampo, M., Curtidor, H., Forero, M., Rodriguez, L. E. & Patarroyo, M. E. (2008). *Biochem. Biophys. Res. Commun.* **372**, 935–940.
Paxman, J. J., Borg, N. A., Horne, J., Thompson, P. E., Chin, Y., Sharma, P., Simpson, J. S., Wielens, J., Piek, S., Kahler, C. M., Sakellaris, H., Pearce, M., Bottomley, S. P., Rossjohn, J. & Scanlon, M. J. (2009). *J. Biol. Chem.* **284**, 17835–17845.
Phillips, L. (2013). *Nature (London)*, **493**, 14–16.
Pieters, J. (2008). *Cell Host Microbe*, **3**, 399–407.
Ptak, C. P., Ahmed, A. H. & Oswald, R. E. (2009). *Biochemistry*, **48**, 8594–8602.
Ramachandran, S., Kota, P., Ding, F. & Dokholyan, N. V. (2011). *Proteins*, **79**, 261–270.
Raman, M. P., Singh, S., Devi, P. R. & Velmurugan, D. (2012). *Bioinformation*, **8**, 403–406.
Ruggiero, A., Masullo, M., Marasco, D., Ruocco, M. R., Grimaldi, P., Arcari, P., Zagari, A. & Vitagliano, L. (2009). *Proteins*, **77**, 1004–1008.
Sani, M., Houben, E. N., Geurtsen, J., Pierson, J., de Punder, K., van Zon, M., Wever, B., Piersma, S. R., Jiménez, C. R., Daffé, M.,

Appelmelk, B. J., Bitter, W., van der Wel, N. & Peters, P. J. (2010). *PLoS Pathog.* **6**, e1000794.
Sassetti, C. M., Boyd, D. H. & Rubin, E. J. (2003). *Mol. Microbiol.* **48**, 77–84.
Scherr, N., Honnappa, S., Kunz, G., Mueller, P., Jayachandran, R., Winkler, F., Pieters, J. & Steinmetz, M. O. (2007). *Proc. Natl Acad. Sci. USA*, **104**, 12151–12156.
Schneider, C. A., Rasband, W. S. & Eliceiri, K. W. (2012). *Nature Methods*, **9**, 671–675.
Shouldice, S. R., Heras, B., Jarrott, R., Sharma, P., Scanlon, M. J. & Martin, J. L. (2010). *Antioxid. Redox Signal.* **12**, 921–931.
Songane, M., Kleinnijenhuis, J., Netea, M. G. & van Crevel, R. (2012). *Tuberculosis*, **92**, 388–396.
Studier, F. W. (2005). *Protein Expr. Purif.* **41**, 207–234.
Vaguine, A. A., Richelle, J. & Wodak, S. J. (1999). *Acta Cryst.* D**55**, 191–205.
Vergne, I., Chua, J., Singh, S. B. & Deretic, V. (2004). *Annu. Rev. Cell Dev. Biol.* **20**, 367–394.
Vivian, J. P., Scoullar, J., Rimmer, K., Bushell, S. R., Beddoe, T., Wilce, M. C., Byres, E., Boyle, T. P., Doak, B., Simpson, J. S., Graham, B., Heras, B., Kahler, C. M., Rossjohn, J. & Scanlon, M. J. (2009). *J. Mol. Biol.* **394**, 931–943.
Wang, X., Dutton, R. J., Beckwith, J. & Boyd, D. (2011). *Antioxid. Redox Signal.* **14**, 1413–1420.
Welin, A., Raffetseder, J., Eklund, D., Stendahl, O. & Lerm, M. (2011). *J. Innate Immun.* **3**, 508–518.
Winn, M. D. *et al.* (2011). *Acta Cryst.* D**67**, 235–242.
World Health Organization (2011). *Global Tuberculosis Control.* Geneva: World Health Organization. http://whqlibdoc.who.int/publications/2011/9789241564380_eng.pdf.
Wunderlich, M. & Glockshuber, R. (1993). *Protein Sci.* **2**, 717–726.
Yang, H., Guranovic, V., Dutta, S., Feng, Z., Berman, H. M. & Westbrook, J. D. (2004). *Acta Cryst.* D**60**, 1833–1839.
Yu, J. (1998). *Infect. Immun.* **66**, 3909–3917.
Zhou, B., He, Y., Zhang, X., Xu, J., Luo, Y., Wang, Y., Franzblau, S. G., Yang, Z., Chan, R. J., Liu, Y., Zheng, J. & Zhang, Z.-Y. (2010). *Proc. Natl Acad. Sci. USA*, **107**, 4573–4578.

APPENDIX C

Peptide inhibitors of the *Escherichia coli* DsbA/DsbB interface

Wilko Duprez, Maria Halili, Fredrik Lindahl, Robert C. Reid, David P. Fairlie and Jennifer L. Martin.

SUPPORTING INFORMATION

Table of contents:

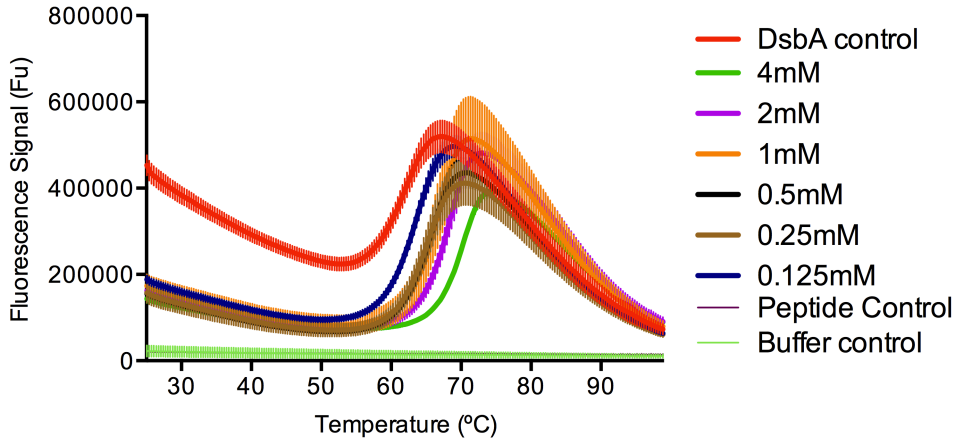

Supplementary figure S1. Thermal shift assay raw fluorescence measurements of oxidized EcDsbA in presence of different concentrations of peptide PSPFATCDF (peptide **1**). Positive control with no peptide is shown in red, negative control with no EcDsbA in pink (along the baseline), and dye only as a light green (also along the baseline).

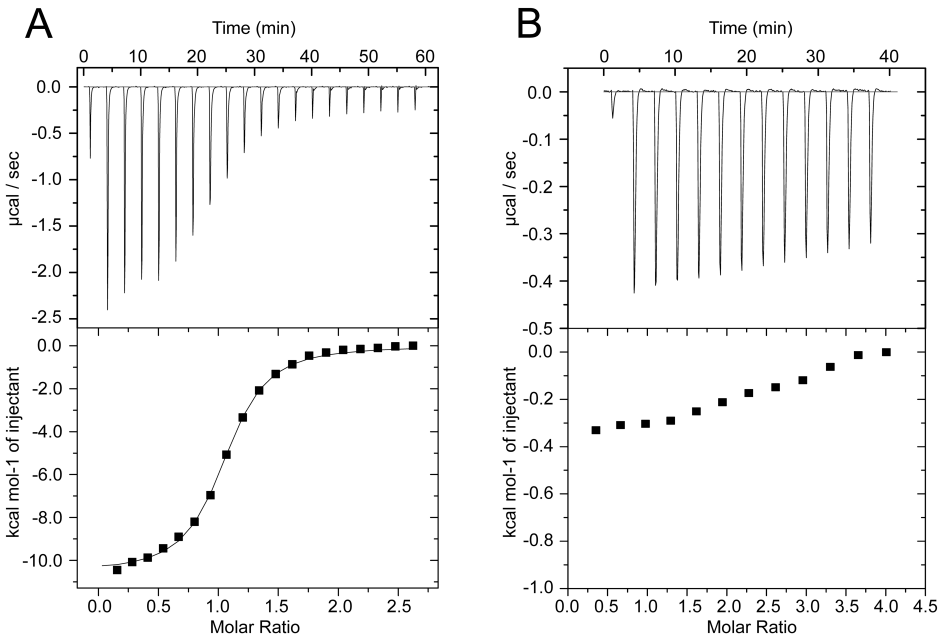

Supplementary figure S2. Isothermal Titration Calorimetry profiles and curve-fitting of EcDsbA titration with peptide PSPFATCDF. A. Titration using oxidized EcDsbA. B. Titration using reduced EcDsbA. Graph is representative of three independent experiments.

Supplementary figure S3. *Characterization of synthetic peptides*

N°	Sequence	RT (min)[A]	Calculated mass MH+	Calculated mass M2H+/2	Measured LCMS 2020	Measured Q-STAR HRMS
1	PSPFATCDF	4.4	1025.4397	513.2235	1025.5	N.D.*
2	PSPFATCD	3.7	878.3713	439.6893	878.5	878.3717
3	PSPWATCDF	4.5	1064.4506	532.7289	1064.6	532.7289
4	PSPWATCD	3.7	917.3822	459.1947	917.5	459.1946
5	PSPWATC	3.8	802.3552	401.6812	802.5	802.3548
6	PSP(hF)ATC	4.0	777.3600	389.1836	777.5	777.3602
7	PSP(1Dip)ATC	4.6	839.3756	420.1914	839.2	839.3754
8	PS(pip)WATC	4.1	816.3709	408.6891	816.5	807.3705
9	PS(thiq)WATC	4.6	864.3709	432.6891	864.5	864.3711
10	ASPWATCDF	4.3	1038.4349	519.7211	1038.5	519.7207
11	PAPWATCDF	4.6	1048.4557	524.7315	1048.6	524.7134
12	PSAWATCDF	4.4	1038.4349	519.7211	1038.5	519.7207
13	PSPAATCDF	3.7	949.4084	475.20785	949.5	949.4081
14	PSPWAACDF	4.5	1034.4400	517.7237	1034.5	517.7239
15	PSPWATADF	4.3	1032.4785	516.7429	1032.5	516.7429
16	PSPWATCAF	4.6	1020.4608	510.734	1020.5	N.D.*
17	PSPWATCDA	3.7	988.4193	494.7133	988.5	494.7131
18	PSPWATCDFMV	5.0	1294.5595	647.7834	1294.7	677.7832
19	PSPWATCDFM	4.8	1195.4911	598.2492	1195.6	598.2492
20	SPWATCDF	4.3	967.3978	484.2026	967.5	484.2026
21	PWATCDF	4.7	880.3658	440.6866	880.5	880.3659
22	PWATCDS	3.9	820.3294	410.6684	820.4	820.3296
23	P(hF)ATCDS	3.5	795.3342	398.1708	795.3	795.3344
24	PSPWATSDF	4.1	1048.4734	524.7404	1048.6	N.D.*

25	PSPWAT(hS)	3.5	800.3937	408.6891	800.5	800.3863
26	PSPWATN	3.5	813.3890	407.1981	813.5	813.3847
27	PSPWATVDF	5.0	1060.5098	530.7585	1060.6	N.D.*
28	PSPWATIDF	4.7	1074.5255	537.7664	1074.6	537.7668
29	PSPWAT(Nve)	3.1	798.4145	399.7109	798.6	798.4149
30	PSPWATM	4.0	830.3865	415.6969	830.5	830.3865
31	PWATSDS	3.6	804.3523	402.6798	804.5	804.3524

[A]retention time in minutes using a 0-100% gradient of 90/9.9/0.1 acetonitrile/H_2O/trifluoroacetic acid over 10 min. N.D.* the peptide mass was not detected in high resolution mass spectrometry.

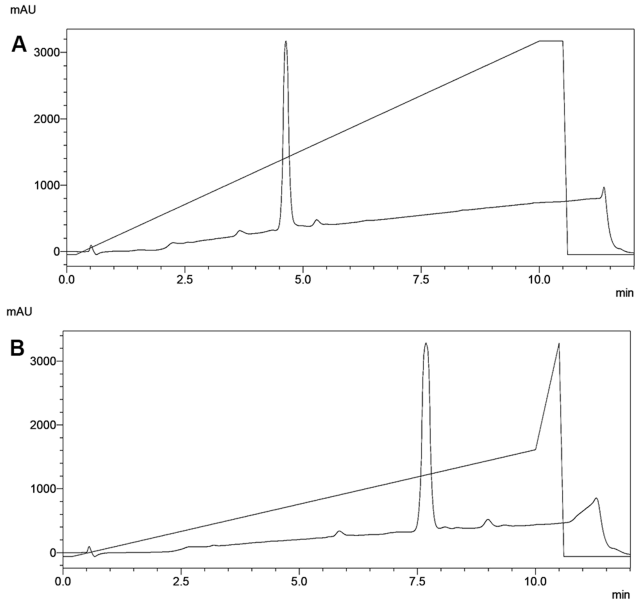

Supplementary figure S4. HPLC profiles of peptide **21** PWATCDF. UV measurements at 214nm are shown along with gradient of solvent over time. **A.** Elution profile on a 0-100% gradient of 90/9.9/0.1 acetonitrile/H_2O/trifluoroactic acid over 10 minutes. **B.** Elution profile on a 0-50% gradient of 90/9.9/0.1 acetonitrile/H_2O/trifluoroactic acid over 10 minutes.

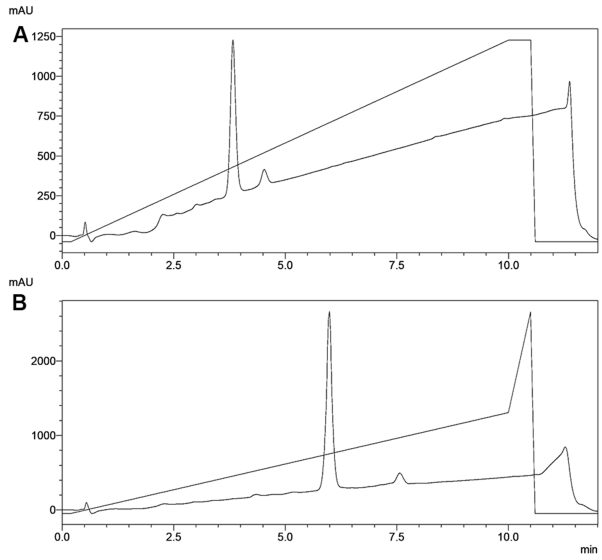

Supplementary figure S5. HPLC profiles of peptide 22 PWATCDS. UV measurements at 214nm are shown along with gradient of solvent over time. **A.** Elution profile on a 0-100% gradient of 90/9.9/0.1 acetonitrile/H_2O/trifluoroactic acid over 10 minutes. **B.** Elution profile on a 0-50% gradient of 90/9.9/0.1 acetonitrile/H_2O/trifluoroactic acid over 10 minutes.